

RRFM

EUROPEAN RESEARCH
REACTOR CONFERENCE **2015**



Conference Proceedings

Bucharest, Romania
19-23 April 2015



ENS CONFERENCE

RRFM 2015 Silver Sponsor



organised in collaboration with:



IAEA

International Atomic Energy Agency



ASOCIAȚIA ROMÂNĂ
"ENERGIA NUCLEARĂ"

© 2015
European Nuclear Society
Avenue des Art 56
1000 Brussels, Belgium
Phone + 32 2 505 30 54
Fax +32 2 502 39 02
E-mail ens@euronuclear.org
Internet www.euronuclear.org

ISBN 978-92-95064-23-2

The content of contributions published in this book reflects solely the opinions of the authors concerned. The European Nuclear Society is not responsible for details published and the accuracy of data presented.

Poster

RRFM2015-A0021	MULTI-CHANNEL THERMAL HYDRAULIC ANALYSIS OF PLATE TYPE RESEARCH REACTOR	Albati', M. (1); Alkhafaji, S. (1); Abusaleem, K. (2); Jo, D. (3); Alfandi, A. (1) 1 - Jordan Atomic Energy Commission (JAEC), Jordan 2 - The University of Jordan, Jordan 3 - Kyungpook National University, Korea, Republic of
RRFM2015-A0022	DEVELOPMENT OF PERFORMANCE ANALYSIS CODE FOR RESEARCH REACTOR FUEL	jeong, G. Y. (1); Sohn, D.-S. (1); Lee, K. H. (2); Park, J. M. (2) 1 - Ulsan National Institute of Science and Technology, 50 UNIST-gil, Eonyang-eup, Korea, Republic of 2 - Korea Atomic Energy Research Institute, Korea, Republic of
RRFM2015-A0027	EVALUATION OF PERFORMED EXPERIMENTS ON FAST MULTIPLYING SYSTEMS WITH HEU FUEL FOR RECEIVING BENCHMARK DATA ON CRITICALITY	Sikorin, S. (1); Mandzik, S. (1); Polazau, S. (1); Kuzmin, A. (1); Damarad, Y. (1); Soltan, I. (1) 1 - The Joint Institute for Power and Nuclear Research – Sosny of the National Academy of Sciences of Belarus, Belarus
RRFM2015-A0034	JRTR INITIAL CRITICALITY CALCULATIONS AND NUCLEAR COMMISSIONING TESTS	Jaradat, M. (1); Alkhafaji, S. (1); Abu saleem, K. (1); Park, C. J. (2) 1 - Jordan Atomic Energy Commission, Jordan 2 - Korea Atomic Energy Research Institute, Korea, Republic of

RRFM2015-A0047	A COMPREHENSIVE ANALYSIS OF THE TECHNICAL FEASIBILITY OF THE MIR RESEARCH REACTOR CONVERSION TO LOW-ENRICHED URANIUM FUEL	Izhutov, A. (1); Starkov, V. (1); Pimenov, V. (1); Maynskov, S. (2); Osipova, T. (2); Uzikov, V. (1); Fedoseev, V. (1) 1 - JSC "SSC Research Institute of Atomic Reactors", Russian federation 2 - National Nuclear University MEPhI (Moscow Engineering Physics Institute), Russian Federation
RRFM2015-A0053	NEUTRONIC COMPARISON OF HIGH DENSITY FUELS (U-MO-AL AND U3SI2-AL) FOR RESEARCH REACTORS	Oliveira rondon muniz, R. (1); Teixeira e silva, A. (1); Borges domingos, D. (1); Dos santos, A. (1); Yamaguchi, M. (1) 1 - IPEN/CNEN-SP, Brazil
RRFM2015-A0057	COMPARISON OF LOW ENRICHED URANIUM (UALX-AL AND U-NI) TARGETS WITH DIFFERENT GEOMETRIES FOR THE PRODUCTION OF MOLYBDENUM-99	Teixeira e silva, A. (1); Borges domingos, D. (1); Garcia joão, T. (1); Oliveira rondon muniz, R. (1) 1 - IPEN/CNEN-SP, Brazil

RRFM2015-A0059	NEUTRONIC AND THERMAL-HYDRAULICS CALCULATIONS FOR THE PRODUCTION OF MOLYBDENUM-99 BY FISSION IN LOW ENRICHED URANIUM UALX-AL TARGETS	borges dominigos, D. B. D. (1); Teixeira e silva, A. (1); Garcia joão, T. (1); J.B. de o. Nishiyama, P. (2); Giovedi, C. (2) 1 - IPEN-CNEN/SP, Brazil 2 - CTMSP, Brazil
RRFM2015-A0060	LOW ENRICHED URANIUM FOIL TARGETS WITH DIFFERENT GEOMETRIES FOR THE PRODUCTION OF MOLYBDENUM-99	Borges Domingos, D. (1); Teixeira e Silva, A. (1); Garcia João, T. (1) 1 - IPEN/CNEN-SP, Brazil

RRFM2015-A0063	HORUS3D NEUTRON CALCULATION TOOL DEDICATED TO JHR DESIGN AND SAFETY STUDIES – DEVELOPMENT, VALIDATION, BIASES AND UNCERTAINTIES QUANTIFICATION	Vaglio-gaudard, C. (1); Jeury, F. (1); D'aletto, C. (1); Vidal, J.-F. (1); Vidal, J.-M. (1); Gaubert, L. (1); Politello, J. (1) 1 - CEA, France
----------------	--	--

RRFM2015-A0066	UNCERTAINTY ASSESSMENT FOR REACTIVITY INDUCED ACCIDENT OF 5-MW POOL-TYPE RESEARCH REACTOR	Yum, S. (1); Park, S. (1) 1 - Korea Atomic Energy Research Institute, Korea, Republic of
RRFM2015-A0072	CONTRIBUTIONS TO PROBABILISTIC SAFETY ASSESSMENT STUDIES FOR TRIGA RESEARCH REACTORS	Mladin, D. (1); Mladin, M. (1) 1 - Institute for Nuclear Research, Romania
RRFM2015-A0073	INVESTIGATING THE SETUP FOR IRRADIATION OF MATERIAL SAMPLES IN TRIGA ROMANIA	Mladin, M. (1); Dulugeac, S. (1); Budriman, G. (1); Barbos, D. (1); Ciocanescu, M. (1) 1 - Institute for Nuclear Research, Romania
RRFM2015-A0075	STUDY OF MOLYBDENUM-99 PRODUCTION POSSIBILITIES IN TRIGA 14 MW REACTOR	Dulugeac, S. (1); Mladin, M. (1); Budriman, G. (1) 1 - Institute for Nuclear Research, Romania
RRFM2015-A0076	THE 14 MEV NEUTRON IRRADIATION FACILITY IN MARIA REACTOR	Prokopowicz, R. (1); Pytel, K. (1); Dorosz, M. (1); Zawadka, A. (1); Lechniak, J. (1); Lipka, M. (1); Marcinkowska, Z. (1); Wierzchnicka, M. (1); Małkiewicz, A. (1); Wilczek, I. (1); Krok, T. (1); Migdal, M. (1); Kozieł, A. (1) 1 - National Centre for Nuclear Research, Poland

RRFM2015-A0094	OVERVIEW ON A RRSF REPROCESSING, FROM SPENT FUEL EVACUATION TO VITRIFIED RESIDUES STORAGE	Domingo, X. (1); Valery, J.-F. (1); Landau, P. (1); Dupeyrat, A. (1); Deschamps, P. (1); Pechard, C. (1); Laloy, V. (2); Kalifa, M. (2) 1 - AREVA NC, France 2 - AREVA TN, France
----------------	---	---

RRFM2015-A0104	COMPARISON BETWEEN U(Mo)/Al(Si) MINIPLATE AND U ₃ Si ₂ /Al MINIPLATE AFTER THE SAME FABRICATION PROCESS.	Mirandou, M. (1); Aricó, S. (1); Balart, S. (1); Fabro, J. (1); Podestá, D. (1) 1 - Comisión Nacional de Energía Atómica , Argentina
----------------	--	---

RRFM2015-A0130	ANALYSIS OF MICROSTRUCTURE AND PRECIPITATIONS IN THE U-ZR METALLIC FUEL	Lee, C.-T. (1); Kim, H. L. (1) 1 - Korea Atomic Energy Research Institutes (KAERI), Korea, Republic of
----------------	---	---

RRFM2015-A0145	NEUTRONIC COMPARISON OF RELAP5-3D AND MCNP5 MODELS FOR THE TRIGA IPR-R1	A. F. Mesquita, P. (1); L. Costa, A. (1); A. M. Silva, C. (1); A. I. Reis, P. (1); Pereira, C. (1); F. Veloso, M. A. (1); V. Soares, H. (1) 1 - UNIVERSIDADE FEDERAL DE MINAS GERAIS, Brazil
RRFM2015-A0166	TRANSPORT OF IRRADIATED FUEL RODS AND SEGMENTS OF IRRADIATED FUEL RODS	Boeckx, W. (1) 1 - Transnubel, Belgium

RRFM2015-A0173	Y-12 NATIONAL SECURITY COMPLEX U-MO FABRICATION	Gambrell, M. (1); Langham, C. (1); Moore, A. (1); Demint, A. (1); Henkel, J. (1); Longmire, H. (1) 1 - Y-12 National Security Complex, United States
----------------	---	---



Poster

MULTI-CHANNEL THERMAL HYDRAULIC ANALYSIS OF PLATE TYPE RESEARCH REACTOR

MOHAMMAD ALBATI, ASHRAF ALFANDI, KHALIFEH ABUSALEEM, SALIH ALKHAFAJI

Jordan Atomic Energy Commission (JAEC), Amman 11934, Jordan.

The University of Jordan, Amman 11942, Jordan

DAESEONG JO

Korea Atomic Energy Research Institute, 1045 Daeduk-daero, Dukjin-dong, Yuseong-gu, Daejeon, 305-353, Republic of Korea

ABSTRACT

An introduction of the multi-channel systems is introduced. The geometry of the multi-channel systems is described. The basic conditions used in the multi-channel analysis are introduced. The methodology of the multi-channels analysis is explained. An explanation of the different iterations used in the analysis is described. A description of the methodology used in the calculation of the temperature profiles of a multi-plate system is introduced. A multi-channels Thermal hydraulic analysis code is developed using the MATLAB programming software. A verification of the mass and energy conservation equation models and the basic conditions applied to the multi-channel analysis is conducted through the run of multiple test cases. The code is used to calculate the mass flow distribution and the temperature profile radially and axially for the China Advanced Research Reactor (CARR). The code results are validated against the results of (Tian et al., 2005). The developed code is applied to a 5 MW MTR reactor and the results for the mass flow distributions and temperature profiles are validated against the PLTEMP V3.7 code. A conclusion and suggestion for future work is introduced.

Keywords: TMAP, COOLOD-N2, thermal margin, forced convection, natural convection, research reactor

1.0 Introduction

Research reactors are nuclear reactors that are used primarily as a neutron source. These neutrons are utilized for many applications such as neutron transmutation doping (NTD), radioisotope production, material testing, and research and education. Research reactors are used all around the world. There are around 764 research reactors around the world from which 246 are operational, 5 under construction, and 8 planned. Research reactors are simpler than power reactors and operate at lower pressure and temperatures than power reactors. Although the fuel needed in the research reactor is less than power reactor, the uranium enrichment is much higher and in these days is limited to 20 percent enrichment as stated by the U.S. Department of energy in its program that was initiated to develop the means to convert research reactor from the use of highly enriched uranium to the low enriched uranium. This program was then called the Reduced Enrichment Research and Test Reactor (RERTR) project. There are many types of Fuel that are used in research reactors such as MTR type, TRIGA type, VVR, and many others. The most common type of fuel is MTR type. Almost 25% of the operational reactors around the world (65 research reactors) use the MTR type fuel, which constitutes the largest percent of the different fuel types used in research reactors (IAEA, 2009). The thermal power generated in research reactors have a very wide range starting from almost Zero power to the highest power of 250 MW in the ATR reactor in the United States (IAEA, 2009). The research reactor produces neutrons by uranium fission process. Each fission process produces about 200 MeV of energy. Most of This energy is carried out by fission products as kinetic energy and the rest goes as neutron or radiation energy. This energy is transferred to a heat form generated in the fuel and then transferred through cladding to the coolant. In the design process of research reactors, many limitations control the way of design. One of the most important steps in the design of research reactors is to ensure their safety against nuclear and thermal hydraulics margins. The insurance of reactor safety against these limits is very important to prevent any failure in the fuel plate that can lead to a release of radioactive materials into the environment. These limitations are divided into nuclear limitations and thermal limitations. The nuclear limitations includes reactivity control, power density, etc. the thermal limitations includes fuel, cladding, and coolant temperatures, along with many safety limiting parameters such as Onset of Nucleate Boiling (ONB), Onset of Flow Instability (OFI), and Departure from Nucleate Boiling (DNB). In general, computer codes are used to evaluate the thermal hydraulic margins of research reactors, but unfortunately most of the developed and commercialized codes are originally designed for power reactors such as RELAP and RETRAN. Although more recent versions of these codes include modifications capable of simulating the operational conditions of research reactors, the use of these codes requires a lot of effort in the input preparation and program simulation. For this reason, many attempts had been made to develop simpler thermal hydraulics codes to design, license, and evaluate the performance of research reactors under various conditions. For example, JAERI (Japan Atomic Energy Research Institute) developed COOLOD-N2, which was applied to evaluate the steady state thermal hydraulic analyses for JRR-3. In 2011, KAERI (Korea Atomic Energy Research Institute) developed a computer code, TMAP, to evaluate the thermal hydraulic margins of a plate type fuel research reactor. Although there are many computer codes, they cannot be directly applied to a newly designed research reactor owing to the unique features of the research reactor or the different methodology adopted by the regulatory body. Most of these designed thermal hydraulic codes are used for single channel analysis, in which the mass flow rate and heat flux are provided as input parameters. In single channel codes, it is assumed that the heat generated in a fuel plate is distributed equally to the two adjacent channels. This assumption may not be true for the case where different cooling conditions exist on the two sides of the fuel plate. In some cases, the mass flow distribution and the heat distribution between the different types of flow paths in the reactor should be calculated rather than assumed.

Most of these are designed for single channel analysis, in which the mass flow rate and heat flux are provided as input parameters. The following study is conducted to develop a thermal hydraulic code that is capable of calculating the mass flow distribution between different flow paths in parallel with each other and connected to a shared upper and lower plenum. The code is also capable of calculating the coolant, cladding, and fuel temperature profiles radially and axially.

2.0 Geometry model

The geometry of the parallel coolant mass flow paths are shown in Figure II-1. The system is composed of (np) number of parallel flow paths that is connected only at the upper and lower plenums. It is assumed that each flow path is composed of different axial regions. Each axial region in a flow path has its own, geometry and properties. There are two main types of flow paths which are:

1. Heated flow paths (Fuel assemblies).
2. Un-heated flow paths (different types of bypasses).

In the heated flow paths there is a parallel fuel plates, and so more calculation efforts are needed to obtain the mass flow distribution in the flow channels parallel to the fuel plates. Figure II-2 shows the geometrical model for single fuel assembly which is considered as single flow path in the system shown in Figure II-1. The fuel assembly is composed of different axial regions. Each region has its own shape and dimensions. Axial Regions are numbered from $J=1$ to $J=np$ including the region between fuel plates. The pressure drop in the fuel assembly is the sum of the pressure drops in each of the axial regions.

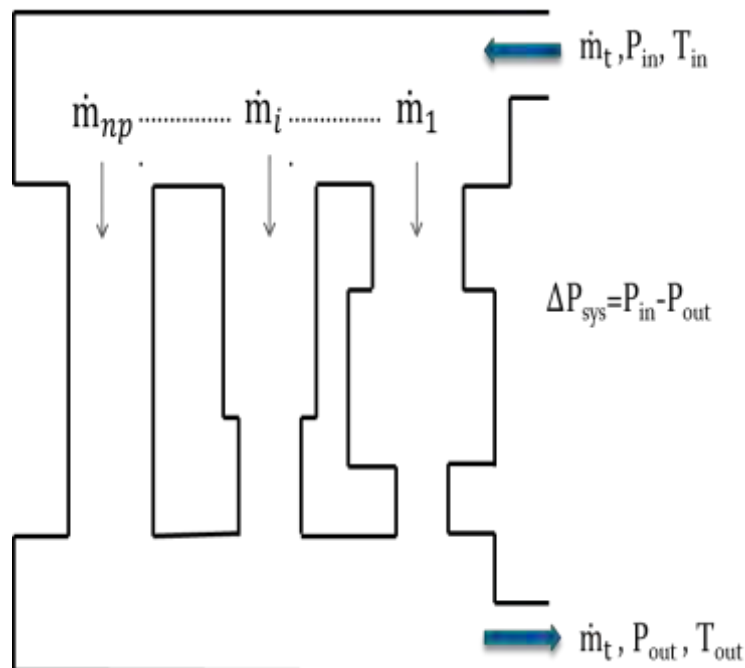


Figure 1: Parallel flow paths system.

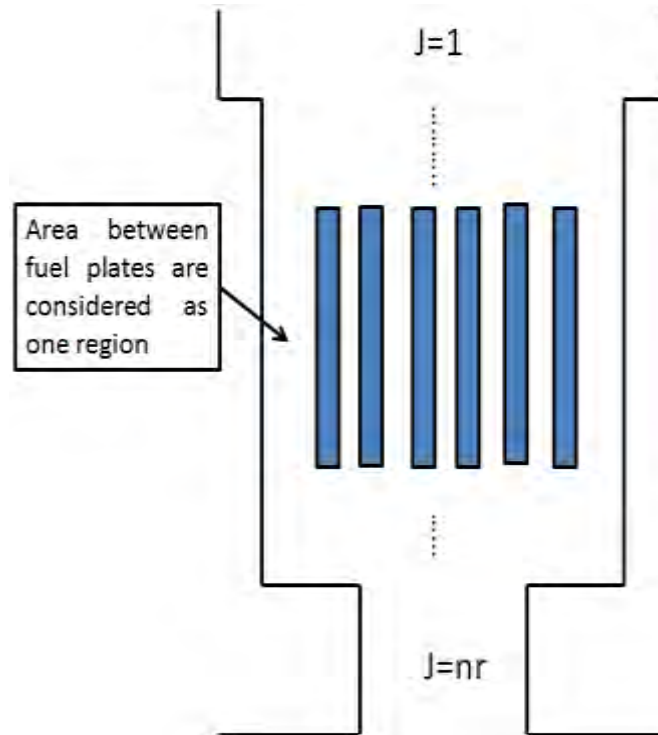


Figure 2: Assembly geometry.

3.0 Governing equations:

In this section, the general governing equations for mass, momentum, and energy are introduced. The assumptions used in the derivation of the final version of these equations are described.

3.1 Mass conservation equation:

The mass conservation equation (continuity equation) is

$$\frac{\partial \rho}{\partial t} + \frac{\partial}{\partial z}(G) = 0$$

Where ρ is the coolant density in kg/m^3 , G is the coolant mass flux in $kg/m^2.s$, t is time in s , and z is the axial location in m . Assuming steady state conditions, the equation reduces to

$$\frac{\partial}{\partial z}(G) = 0$$

Integrating along the axial length of the channel and multiply by the constant flow area yields

$$G * A_{flow} = Constant$$

This constant is the mass flow where $G * A_{flow} = \dot{m}$.

3.2 Momentum equation

The momentum equation is

$$\frac{\partial G}{\partial t} + \frac{\partial}{\partial z} \left(\frac{G^2}{\rho} \right) = -\frac{\partial p}{\partial z} - \frac{f G |G|}{2D_h \rho} - \rho g \cos \theta$$

Where G is the coolant mass flux in $kg/m^2.s$, t is the time in s , z is the axial location in m , ρ is the coolant density in kg/m^3 , p is the pressure in $kg/m.s^2$ (Pascal), f is the dimensionless friction factor, D_h is the hydraulic diameter in m , g is the gravity acceleration in m/s^2 , θ is the angle from the vertical position ($\theta = 0$) for vertical channels. Assuming steady state condition yields to

$$\frac{\partial}{\partial z} \left(\frac{G^2}{\rho} \right) = -\frac{\partial p}{\partial z} - \frac{f G |G|}{2D_h \rho} - \rho g \cos \theta$$

Assuming a vertical channel ($\theta=0$) of length L , and integrating yields to the total pressure drop in the channel as

$$\Delta p = \int_0^L \rho g dz + \int_0^L \left(\frac{f G |G|}{2D_h \rho} \right) dz + \sum \left(\frac{K G |G|}{2\rho} \right) dz + G^2 \left(\frac{1}{\rho(L)} - \frac{1}{\rho(0)} \right)$$

3.3 Energy equation

The energy equation used in the analysis is

$$\dot{m} C_p \frac{dT}{dz} = q'' * P_h$$

Where \dot{m} is the mass flow rate in kg/s , C_p is the specific heat of coolant in $kJ/kg.^{\circ}C$, T is the temperature in $^{\circ}C$, z is the axial length in m , q'' is the heat flux in kW , and P_h is the heated perimeter in m .

4.0 Analysis methodology:

4.1 Multi-Channels basic applied condition:

In this section, a description of the two main conditions that should be satisfied in the analyses of Multi-channel systems is described. These two conditions are used in the multi-channel thermal hydraulic codes to obtain the mass flow distribution in the system. The two conditions are:

1. Equal pressure drop in all flow paths.
2. Conservation of the total mass flow rate.

Pressure drop condition

Since the parallel flow paths are connected to the shared upper and lower plenums, they all share the same coolant pressures at the inlet and outlet. This means that all the flow paths shares the same amount of pressure drop given as

$$\Delta P_1 = \Delta P_2 = \Delta P_3 = \dots = \Delta P_i = \dots = \Delta P_N = P_{in} - P_{out}$$

Where ΔP_i is the total pressure drop through the i -th flow path, P_{in} is the inlet pressure to the system (shared for all flow paths), P_{out} is the outlet pressure to the system (shared for all flow paths).

Conservation of the total mass flow rate

The total mass flow rate is equal to the summation of all the flow rates in the different flow paths. This provides us with

$$\dot{m}_t = \sum_i \dot{m}_i$$

Where \dot{m}_t is the total mass flow rate in the system in *kg/s* and \dot{m}_i is the mass flow rate in the *i*-th flow path in *kg/s*.

4.2 Calculation methodology:

The calculation methodology of the thermal hydraulic analysis is summarized by the following three main functions:

1. Iteration on pressure drop.
2. Iteration on mass flow (subroutine FLOW).
3. Solution of the multi-plate temperature profile.

Each of the previous main functions is explained separately.

4.2.1 Iteration on pressure drop

In this section the solution procedure to obtain the mass flow distribution is described. The inputs needed for the calculations are the total mass flow rate, the inlet pressure and temperature to the system, the geometry of all the flow paths, and the heat generation in each flow path. The unknowns are:

1. The mass flow rates distribution in the system.
2. Pressure drop through the system.

The known parameters are:

1. Total mass flow rate.
2. Inlet pressure and temperature to the system.
3. Geometry of all flow paths.
4. Heat generation in each fuel plate.

Iteration on the pressure drop in the system is the main body of calculation procedure, and it is the outer iteration of the calculation code.

4.2.2 Iteration mass flow rate (subroutine FLOW)

The subroutine **FLOW** is used to calculate the mass flow in a single flow path for a given pressure drop. The known variables are:

1. Pressure drop in the flow path (from the pressure drop iteration).
2. Geometry of the flow path.
3. Heating condition of the flow path.

The unknown variable is the mass flow rate in the flow path. There are two procedures used in subroutine flow depending on the heating condition of the flow path:

1. Procedure for the un-heated flow path (different types of bypasses).
2. Procedure for the heated flow path (fuel assemblies).

4.2.3 Multi-plate temperature profile solution:

In The single channel thermal hydraulic analysis, it is always assumed that the heat is distributed symmetrically from the fuel plate to the two adjacent channels and that the maximum fuel temperature is located in the middle of fuel plate thickness. This assumption is valid only for the case where exact cooling conditions are applied to the two sides of the fuel plate. In some cases the cooling conditions from the two sides differ from each other. This happens if a different channels thickness and so different mass flow rates exists on both sides of the fuel plate. In this analysis, it is assumed that each channel have different flow area and wetted perimeter and also it is assumed that each fuel plate have different dimensions, thicknesses, and heat generation rates. First, a differentiation of the heat and energy transfer equations is conducted on a system composed of only two plates and 3 channels. Then the solution is extended to a system composed of N plates separated by N+1 Channels. The description of the solution requires a large amount of explanation and derivation so it was dismissed in this paper.

5.0 Results:

The China Advanced Research Reactor (CARR) is located at the china institute of atomic energy. It is multi-purposes research reactor used for neutron scattering measurements, radioisotope production, neutron transmutation doping, etc. the CARR is a tank in pool reactor with nuclear power of 60 MW. Slightly pressurized light water is used as the primary coolant. The top of the reactor core is located 16 m below the surface of the pool. The core is about 0.85 m in height and 0.451 m in diameter. Under the normal operation of CARR, the coolant is pumped to flow through the cold leg, downward through the active core, then through the decay tank, the hot leg, the heat exchanger, and re-circulated to the main pump ([Tian et al., 2005](#)).

In 2005, a thermal hydraulic study is conducted on the CARR by ([Tian et al., 2005](#)). In the study, the whole reactor core is analysed to find the mass flow distribution in reactor assemblies, and the temperature profile of coolant, cladding, and fuel in each fuel element. In the following sections, the CARR reactor is analysed using the developed Multi-Channel Code. And the results are compared and verified against the results shown by ([Tian et al., 2005](#)).

Design parameters of CARR:

The main design parameters of CARR are shown in [Table 1](#). The core is composed of 17 standard fuel assemblies and 4 follower fuel assemblies. Each standard fuel assembly is composed of 20 fuel plates separated by 21 coolant channels. All the standard fuel assemblies have the same geometry. All the fuel plates in the standard fuel assembly have the same shape and geometry. The channels in the assemblies vary in thicknesses and are symmetrical around the centre channel. The channels thickness variations are shown in [Figure 3](#) ([Xian et. al](#)) below. As can be seen, there are 5 different channel thicknesses. In the code, the channels are numbered from left to right starting from 1 to 21 as shown in [Figure 4](#). The geometry of fuel plates and coolant channels are summarized in [Table 2](#)

Table 5: Main design parameters of CARR.

Design parameters	Input
Core diameter (m)	0.399
Core height (m)	0.85
Elevation of reactor pool water surface (m)	13.2
Core inlet temperature (°C)	35
Core inlet pressure	0.89
Core nuclear power (MW)	60
Core thermal power (MW)	56.4
Mass flow rate in primary loop (kg/s)	600
Number of standard fuel assembly	17
Number of follower fuel assembly	4
Type of fuel elements	Plate

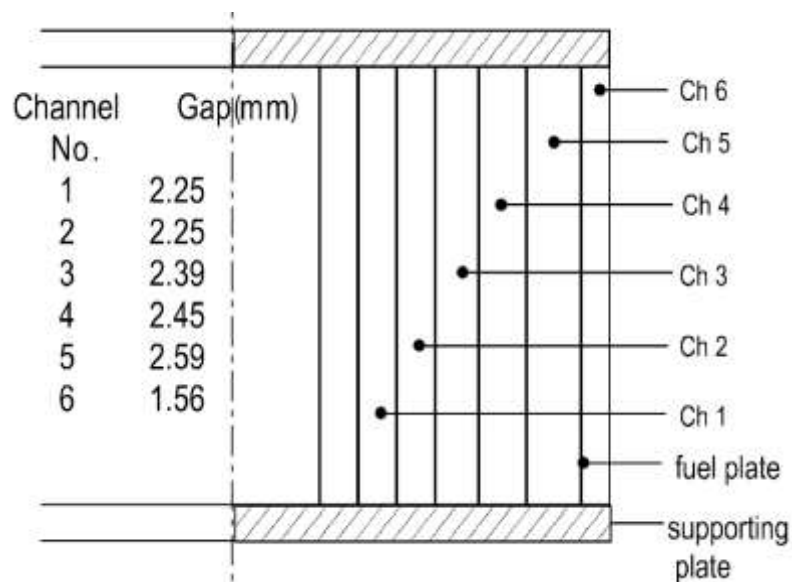


Figure 3: Detailed structure of CARR standard assembly.

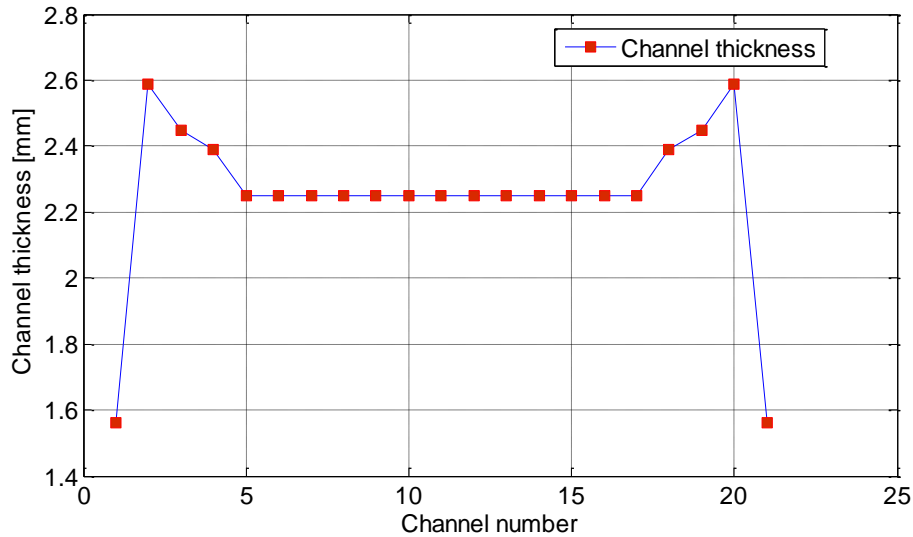


Figure 4: Channels thickness variation of the standard fuel assembly.

Table 2: Fuel plate and coolant channels geometries.

Geometry parameter	Input
Fuel plate	
Fuel thickness[mm]	0.6
Fuel width [mm]	61.6
Fuel length [mm]	850
Cladding thickness [mm]	0.38
Fuel thermal conductivity [W/m.oC]	32
Cladding thermal conductivity	180
Coolant Channel	
Channel width [mm]	71
Channel thickness [mm]	Figure 4
Channel length [mm]	880

The power distribution in the fuel assemblies is represented by the radial power peaking factor distribution that is shown in Figure 5. The power generated in one assembly is assumed to be distributed equally between the different fuel plates in the assembly. The axial length of the active core is divided into 17 control volumes. Each control volume has its axial weighted power factor. The axial weighted power distribution used in the analysis is shown in Figure 6.

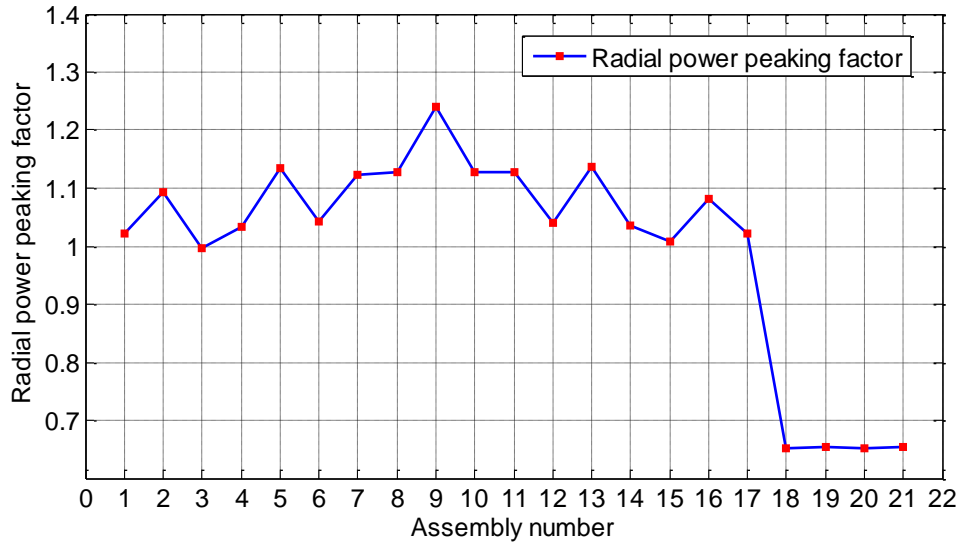


Figure 5: Radial power peaking factor distribution.

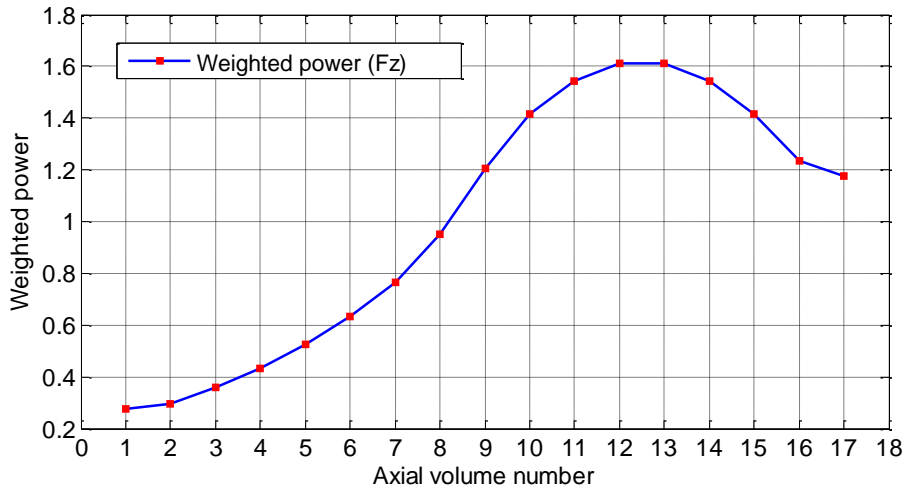


Figure 6: Axial weighted power distribution.

The results of thermal hydraulic analysis of CARR show a good agreement between the developed code and the results published by (Tian et al., 2005). The mass flow distribution in the standard fuel assemblies is shown in Figure 7. The results shows a good agreement with a maximum relative error of 0.3% which could be neglected. As can be seen from Figure 7, the assembly mass flow rates distribution follows the same trend in both results. The assembly with the highest power generation requires more mass flow rate in order to keep the same pressure drop. This phenomenon is studied in detail and the reason is found to be the effect of temperature on the density and viscosity of water. As it is already described the pressure drop is calculated using The Equation below

$$\Delta P_{friction} = \frac{1}{2} \rho V^2 \frac{fL}{D_h}$$

The friction factor used is calculated as

$$f = 0.316 Re^{-0.25}$$

Where Re is given by

$$Re = \frac{\rho V D}{\mu}$$

And the velocity V is given by

$$V = \frac{\dot{m}}{\rho A}$$

This gives the following equation for pressure drop

$$\Delta P_{friction} = \left(\frac{0.316}{2}\right) \left(\frac{D_h^{-1.25} L}{A^{1.75}}\right) \left(\frac{\mu^{0.25}}{\rho}\right) \dot{m}$$

The first and second terms on the right hand side are independent of heat flux, and only the third term in parentheses is to be studied. The change in μ , ρ , and $\frac{\mu^{0.25}}{\rho}$ with temperature is shown in Figures 7, 8, and 9 respectively. As can be seen from Figures 7 to 9, the effect of increasing the heat flux is to decrease the value of $(\mu^{0.25}/\rho)$, which in turn decreases the frictional pressure drop and so the total pressure drop.

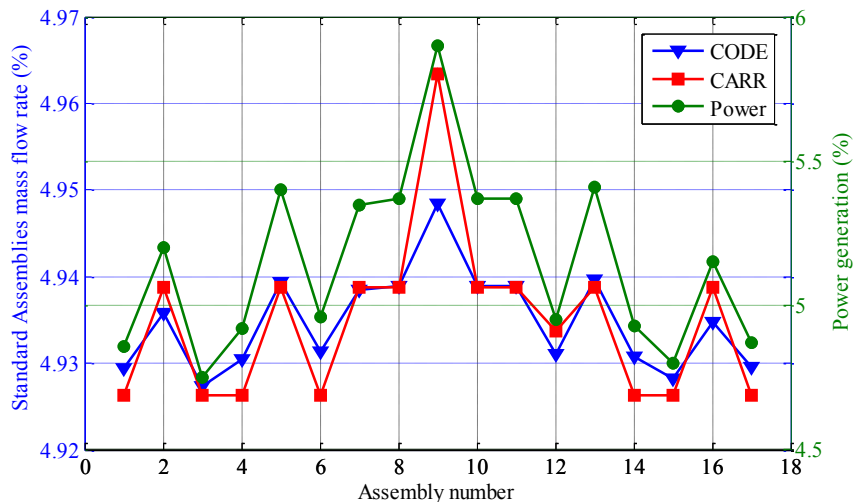


Figure 7: Assemblies Mass flow rate distribution.

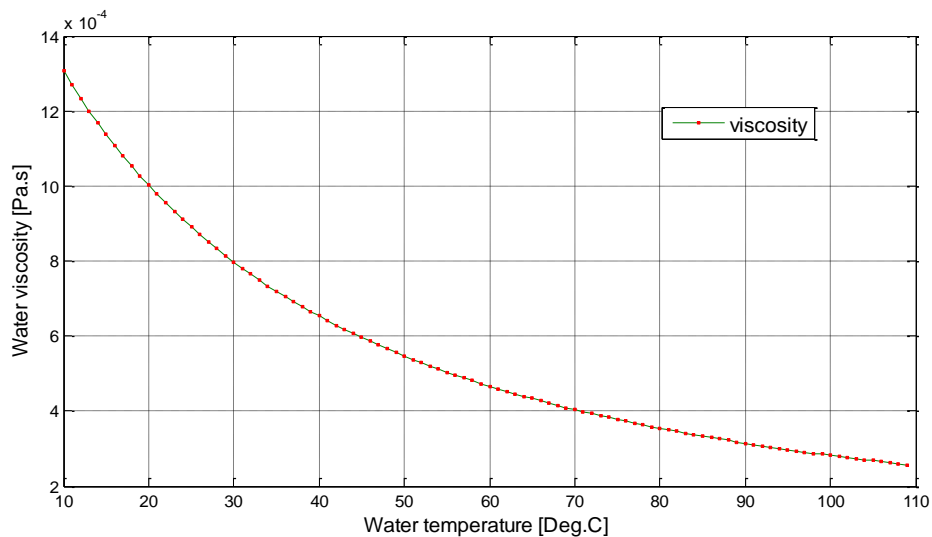


Figure 5-1: The change in water viscosity μ with temperature under a fixed pressure of 0.17 MPa.

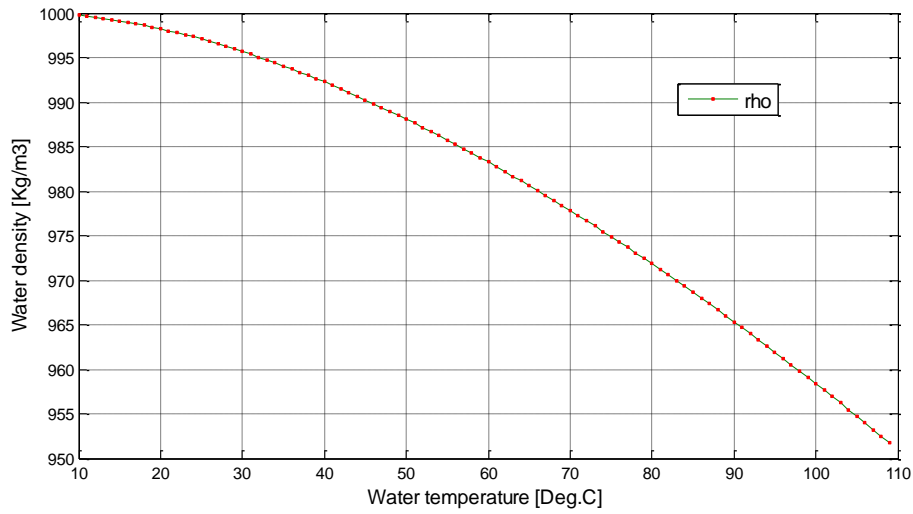


Figure 8: The change in water density ρ with temperature under a fixed pressure of 0.17 MPa.

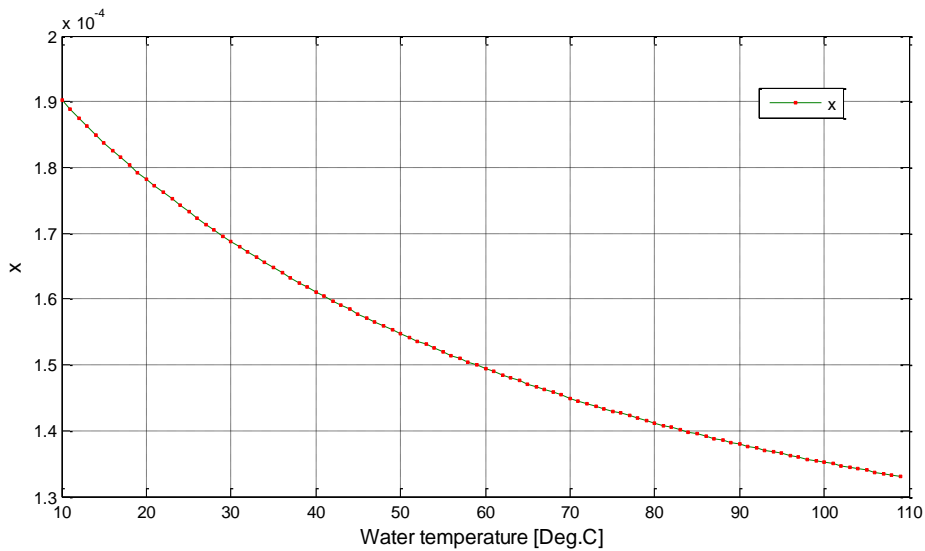


Figure 9: The change in $x = \frac{\mu^{0.25}}{\rho}$ with temperature under a fixed pressure of 0.17 MPa.

The channels mass flow distribution is shown in Figure 10 below. As can be seen, the results show a good agreement. The maximum error in the channels flow rates is calculated to be 3.7%.

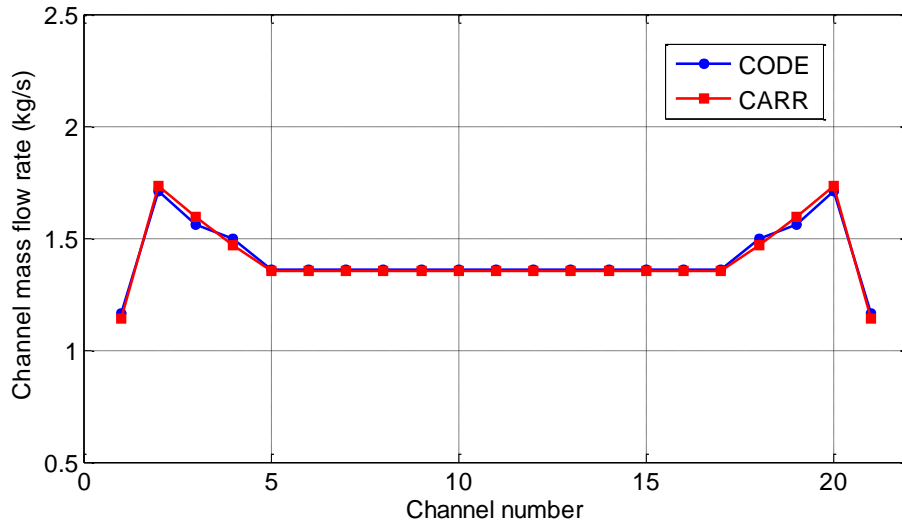


Figure 10: Channels mass flow distribution in the hot assembly (Assembly No.9).

The axial coolant temperature profiles in Channels types numbered from 1 to 6 are shown in Figure 11 below. Figure 12 shows the zoom out view for channels 1 and 2. The coolant channels outlet temperatures for all the 21 channels (numbered 1 to 21 starting from left to right) of the hot assembly in CARR reactor are shown in Figure 13. The maximum difference is 0.7 °C.

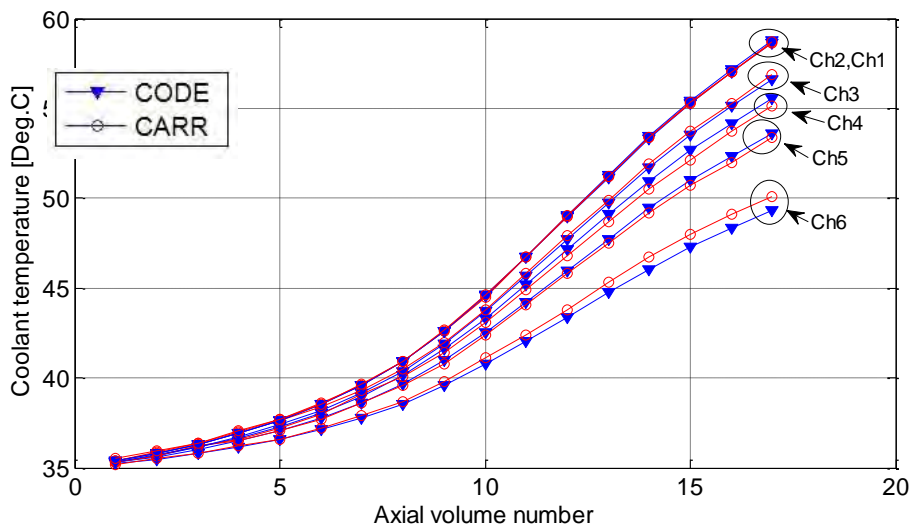


Figure 11: Axial coolant temperature profile along the hot assembly for channels 1 to 6.

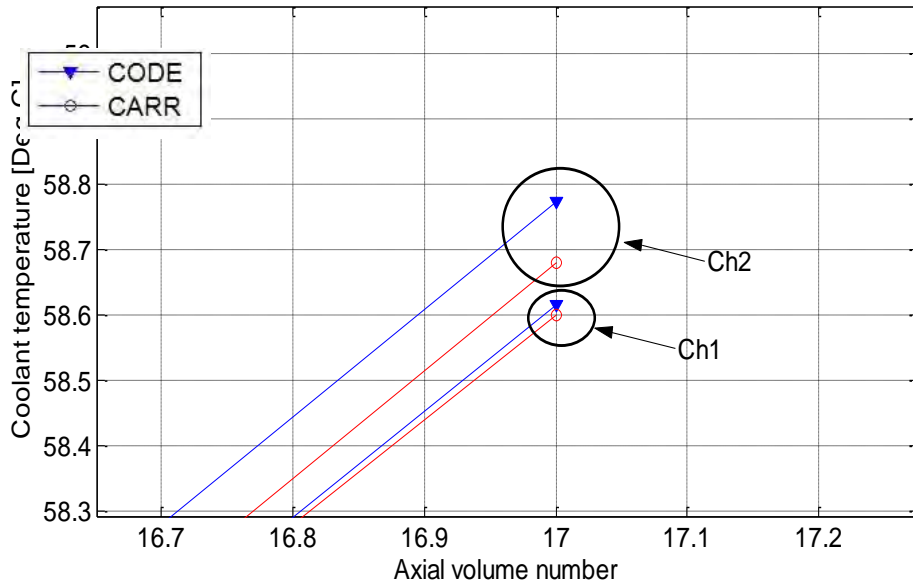


Figure 12: Zoom out of Figure III-11 around channels 1 and 2.

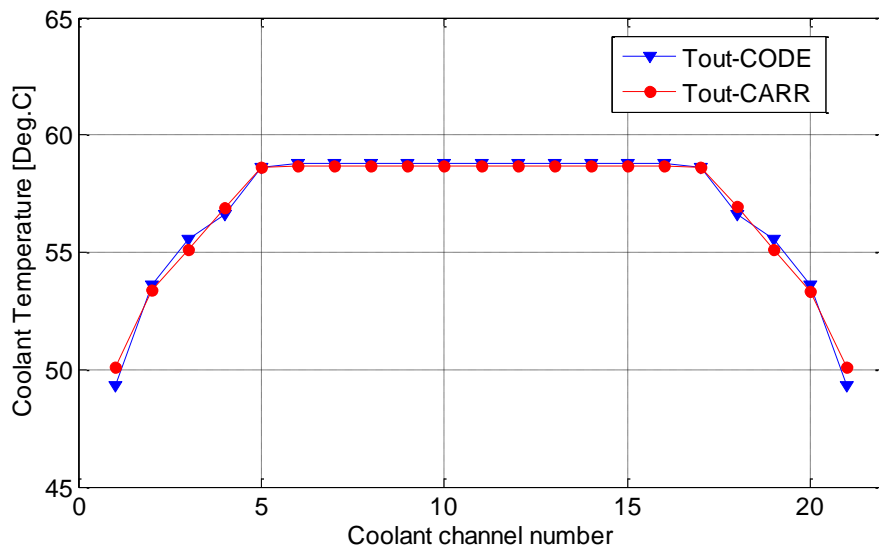


Figure 13: Channels coolant outlet temperatures in the hot assembly in CARR.

As can be seen from Figures 10 to 13, the mass flow rates and coolant temperature shows a very good agreement.

Development of performance analysis code for research reactor fuel

G.Y. JEONG, D-S. SOHN

UNIST, 50 UNIST-gil, Eonyang-eup, Ulju-gun, Ulsan 689-798 – Republic of Korea

Kyu Hong Lee, Jong Man Park

*Korea Atomic Energy Research Institute, 989-111 Daedeokdaero, Yuseong, Daejeon 305-353,–
Republic of Korea*

ABSTRACT

Thermo-mechanical code dedicated to the modeling of U-Mo dispersion fuel plates is being under development in Korea to satisfy a demand for advanced performance analysis and safe assessment of the plates. The major physical phenomena during irradiation are considered in the code such that interaction layer formation by fuel-matrix interdiffusion, fission induced swelling of fuel particle, mass relocation by fission induced stress, and pore formation at the interface between the reaction product and Al matrix.

The framework of performance analysis code for U-Mo dispersion fuel has been established with newly updated models.

1. INTRODUCTION

The need to develop an advanced performance and safety analysis code for research reactor fuel grows in Korea. A performance analysis modeling applicable to research reactor fuel is being developed with available models describing fuel performance phenomena observed from in-pile tests. We established the calculation algorithm and scheme to best predict fuel performance using radio-thermo-mechanically coupled system to consider fuel swelling, interaction layer growth, pore formation in the fuel meat, and creep fuel deformation and mass relocation.

In this paper, we present a general structure of the performance analysis code for typical research reactor fuel and advanced features such as a model to predict fuel failure induced by combination of breakaway swelling and pore growth in the fuel meat.

2. CODE FRAMEWORK

Accurate prediction of fuel temperature and states of stresses induced by fission is essential for research reactor fuel performance code. It is necessary to employ proper and sufficient models that are applicable evaluate in-pile behaviors such as a dimensional change, stress-strain variation, and material degradation by fission and neutron irradiation.

Drastic microstructure changes in the dispersion fuel meat have been observed and investigated including interaction layer (IL) formation by fuel-Al matrix interdiffusion, fuel-Al

matrix consumption, and large pore formation, particularly at the interface of IL and Al matrix. It is necessary to take into consideration of the coupling between thermal and mechanical response to predict those microstructure variation of the meat.

In this section, a general fuel performance model implemented in the code such as temperature calculation, stress-strain analysis, fission induced swelling are described.

2.1. PERFORMANCE MODEL

The coupling among thermal, mechanical, and irradiation-related performance issues is critical to fuel performance modeling. Typical operation temperature for U-Mo/Al dispersion fuel meat for plate type is below 200 °C, but it is dependent on fuel meat thermal conductivity which is influenced by fuel meat morphology and material composition. Particularly, fuel meat thermal conductivity degradation is mostly influenced by Al matrix depletion by IL growth since it is believed that IL has poor thermal conductivity.

The variation of fuel meat morphology is induced by three major phenomena : fuel swelling, IL formation, and pore formation. Details of models implemented in the code are described in the following subsection.

2.1.1. FUEL SWELLING

U-Mo fuel swelling is dependent on Mo content. An empirical correlation for U-10Mo fuel swelling was documented by Kim [1]. U-10 wt% Mo fuel swelling is given as a function of fission density (FD) as follows :

$$\begin{aligned} \left(\frac{\Delta V}{V_0}\right)_f &= 5.0 f_d & f_d \leq 3 \times 10^{21} \text{ fission/cm}^3 \\ \left(\frac{\Delta V}{V_0}\right)_f &= 15 + 6.3(f_d - 3) + 0.33(f_d - 3)^2 & f_d \geq 3 \times 10^{21} \text{ fission/cm}^3 \end{aligned} \quad (1)$$

where f_d is in 10^{21} fission/cm³.

The correlation for U-7 wt% Mo fuel swelling is also expressed as a function of FD as follows [2]:

$$\begin{aligned} \left(\frac{\Delta V}{V_0}\right)_f &= 5.0 f_d & f_d \leq 2 \times 10^{21} \text{ fission/cm}^3 \\ \left(\frac{\Delta V}{V_0}\right)_f &= 10 + 6.7(f_d - 2) + 0.58(f_d - 2)^2 & f_d \geq 2 \times 10^{21} \text{ fission/cm}^3 \end{aligned} \quad (2)$$

where f_d is in 10^{21} fission/cm³.

Compared to the U-10Mo fuel, the fuel swelling model for U-7Mo gives higher swelling rate since grain subdivision is assumed to occur at lower FD due to lower Mo content.

2.1.2. INTERACTION LAYER

IL growth is believed to cause an increase in meat volume. A time-dependent volume fraction of IL in meat needs to be modeled to evaluate volume expansion by IL growth.

IL growth models by using in-pile test data have been reported [3],[4]. The available IL growth model for in-pile tests is given as a modified Arrhenius equation, in which the fission rate is multiplied to account for fission-enhanced diffusion:

$$Y_0^2 = 2.6 \times 10^{-8} \sqrt{\dot{f}} \exp\left(-\frac{3850}{T}\right)t \quad (3)$$

where Y_0 is IL thickness for pure Al matrix in μm , \dot{f} the fission rate in fission/ $\text{cm}^3\text{-sec}$, T the temperature in K, and t the irradiation time in second.

The addition of Si in the Al matrix reduced IL thickness growth. It is also known that IL growth is dependent on the Mo content in the fuel. Additional factors to consider Si and Mo effects on IL growth are multiplied to Eq.(3) as follows:

$$Y^2 = Y_0^2 f_{Si} f_{Mo} \quad (4)$$

where Y is IL thickness for Si-added Al matrix in μm f_{Si} is the reduction factor by Si addition into the matrix and f_{Mo} the Mo content factor on IL growth. Detailed explanation on these additional factors can be found in [4].

2.1.3. PORE FORMATION

Pores are formed in dispersion fuel; 1) pores within fuel particles, 2) pores in interaction layers (ILs), 3) pores at the interfaces (Fuel-IL, IL-Al). The pores contain fission gases. Pores in the ILs, specifically at IL-Al interfaces, tend to be larger than those in the fuel particles. Pore formation degrades fuel performance and integrity and has a potential to cause fuel failure.

Mechanism of pore formation, particularly at the interface between IL and Al matrix has been studied by different authors **Error! Reference source not found.**,[7]. It is assumed that the large pore formation is initiated with as-fabricated pores in the meat and fission gases released to those pores is a driving force of pore growth.

The advanced code is desired to have capability to predict fuel failure caused by pore formation and growth. To fulfil this, pore formation mechanism needs to be investigated further.

2.1.4. MASS RELOCATION

The mass transport of the meat in the dispersion fuel plate observed at the meat end region where fission density is highest along the width of the plates, has been studied [5],[6]. It is believed that the stresses caused by fission induced fuel swelling, and chemical volume expansion by interaction layer growth were mitigated by the creep deformation of a continuous phase which surrounds fuel particles.

The following equation was employed for the creep rate of the U-Mo fuel particles as:

$$\dot{\epsilon}_c = A_c \sigma \dot{f} \quad (5)$$

where $\dot{\epsilon}_c$ is the equivalent creep rate in s^{-1} , A_c the creep rate constant in cm^3/MPa , and \dot{f} the fission rate in fission/ cm^3 -sec.

Recently updated modelling for mechanical deformation of fuel particles and meat swelling caused by fission-induced creep is considered in the developed code.

2.2. CODE STRUCTURE

Finite element analysis will be employed to calculate the temperature distribution in the fuel meat and cladding region. A fuel plate sectioned in length direction is shown in Fig. 1. Typical plate length is longer than any other dimension, so that it is assumed that heat conduction in the length direction is negligible. It also allows strain out of plane to be constant or zero, which is plane strain condition.

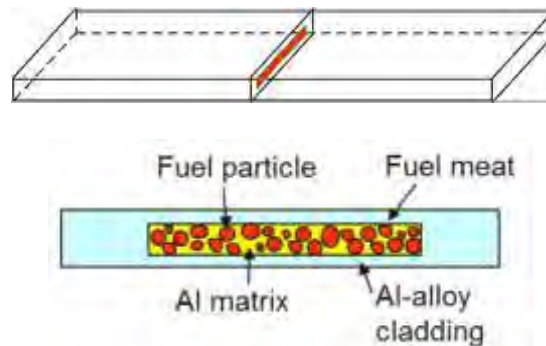


Fig. 1 A schematic of dispersion fuel plate and cross section at axial mid-plane.

The temperature distribution throughout the fuel meat and cladding in 3-dimension is calculated at each node. The models used in the temperature calculations assume a transversally symmetrical fuel plate surrounded by coolant.

User supplied conditions such as coolant information including coolant inlet temperature, coolant flow velocity, and coolant mass will be used to determine boundary conditions. User supplied fission rate will be used to calculate temperature distribution from the coolant to the meat centerline. A film temperature rise from the bulk coolant to cladding surface is calculated by finding film heat transfer coefficient for a given coolant and geometry. The temperature at the interface between clad and meat is calculated by using Fourier's law. The temperature rise to the meat centerline is determined by solving heat conduction equation for fuel particle, Al matrix, and IL with heterogeneously.

The modeled governing equations for temperature distribution calculation is given as follows:

$$\begin{aligned}
 -\nabla \cdot (k_{fuel}(T)\nabla T) &= q''' \\
 q''_{meat} &= -k_{clad}\nabla T \\
 q''_{clad} &= h_c(T_{c,o} - T_{coolant})
 \end{aligned}
 \tag{6}$$

Where q''' is the power density in the meat, k the thermal conductivities, q''_{meat} the total heat flux from the meat, q''_{clad} the heat flux from the cladding surface, $T_{c,o}$ the cladding outer surface, and $T_{coolant}$ the bulk coolant temperature.

With assumption on strain condition as mentioned, meat and cladding deformation calculation will be performed after obtaining temperature distribution. An accurate calculation of stresses in the meat and the cladding is needed to accurately calculate the strain and evaluate a potential of large pore formation and fuel failure.

Strain caused by irradiation can be obtained by solving the mechanical equilibrium equation as follows:

$$\sigma + \rho(T)f''' = 0
 \tag{7}$$

where ρ is the density, f''' is volumetric forces induced by fission, and σ the stress tensor.

Fig. 2 shows the overall structure of the new code system. Each performance model will be classified in several modules. Mechanical response prediction for each plate component will be performed with prescribed condition from previous thermal analysis.

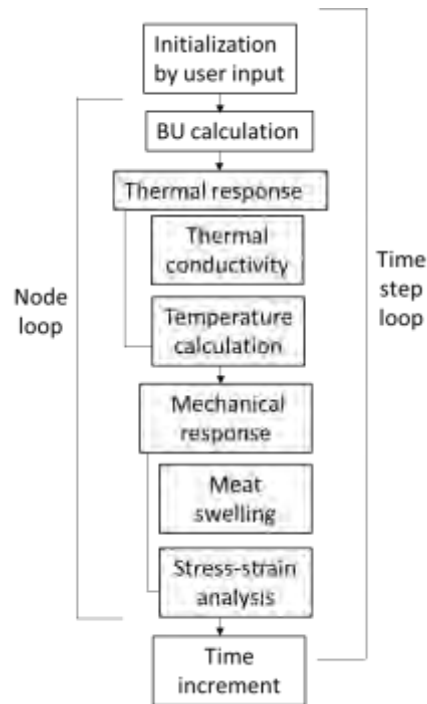


Fig. 2 Overall structure of research reactor fuel performance code.

3. CONCLUSION

Thermo-mechanical code dedicated to the modeling of U-Mo dispersion fuel plates is being under development in Korea to satisfy a demand for advanced performance analysis and safe assessment of the plates. The major physical phenomena during irradiation are considered in the code such that interaction layer formation by fuel-matrix interdiffusion, fission induced swelling of fuel particle, mass relocation by fission induced stress, and pore formation at the interface between the reaction product and Al matrix.

The framework of performance analysis code for U-Mo dispersion fuel has been established with newly updated models with studies on advanced fuel performance modeling.

ACKNOWLEDGMENTS

We would like to acknowledge helpful discussion and kind consultation by Yeon Soo Kim. UNIST was supported by the National Research Foundation of Korea (NRF) grant funded by the Korean government (Ministry of Education, Science and Technology) (No. 2011-0031771), and in part by National Nuclear R&D Program sponsored by Ministry of Science, ICT and Future Planning. (NRF-2013M2A8A1041241) for the KAERI contribution.

REFERENCES

- [1] Yeon Soo Kim, G.L. Hofman, J. Nucl. Mater., 419 (2011) 291.
- [2] Yeon Soo Kim, G.Y. Jeong, G.L. Hofman, J. Nucl. Mater., submitted (2015).
- [3] D.M. Wachs, D.E. Burkes, S.L. Hayes, W. Skerjanc, G.L. Hofman, Yeon Soo Kim, H.J. Ryu, Proc. Int. Meeting on Reduced Enrichment for Research and Test Reactors (RERTR), Cape Town, South Africa, Oct.29 - Nov. 2, 2006.
- [4] Yeon Soo Kim, G.L. Hofman, H.J. Ryu, J.M. Park, A.B. Robinson, D.M. Wachs, Nucl. Eng. Technol., 45 (2013) 827.
- [5] Yeon Soo Kim, G.L. Hofman, J.S. Cheon, J. Nucl. Mater., 436 (2013) 14.
- [6] G.Y. Jeong, Yeon Soo Kim, D-S. Sohn, J. Nucl. Mater., submitted (2015).
- [7] A. M. Tentner, A. Bergeron, Y. S. Kim, G. L. Hofman, J. G. Stevens, S. Van den Berghe, V. Kuzminov, Proc. Int. Meeting on Reduced Enrichment for Research and Test Reactors (RERTR), Vienna, Austria, Oct.12 - 15, 2014.
- [8] A. Leenaers, S. Van den Berghe, E. Koonen, V. Kuzminov, C. Detavernier, J. Nucl. Mater. 458 (2015) 380.

EVALUATION OF PERFORMED EXPERIMENTS ON FAST MULTIPLYING SYSTEMS WITH HEU FUEL FOR RECEIVING BENCHMARK DATA ON CRITICALITY

S.N.SIKORIN, S.G.MANDZIK, S.A. POLAZAU, A.V. KUZMIN,
Y.V.DAMARAD, I.S. SOLTAN

*The Joint Institute for Power and Nuclear Research – Sosny,
99 Academic Krasin Street, 220109 Minsk - Republic of Belarus*

ABSTRACT

Benchmark criticality experiments of fast heterogeneous configurations with HEU fuel were performed using “Giacint” critical facility of the Joint Institute for Power and Nuclear Research – Sosny of the National Academy of Sciences of Belarus. The critical assemblies’ cores have consisted from fuel assemblies of without a jacket. Fuel assemblies contain 19 fuel rods of two types. The first one is metallic U (90% U-235); the second one is UO₂ (36% U-235). The active area length is 500 mm. The clad material is stainless steel. Three types of fuel assemblies with different content fuel rods were used. Side radial reflector: an inner layer – Be, an outer layer – stainless steel. The top and bottom axial reflectors – stainless steel. The analysis of the experimental results obtained from these benchmark experiments by developing detailed calculation models and performing simulations for the different experiments is presented. The sensitivity of the obtained results for the material specifications and the modeling details were examined. The analyses used the MCNP and MCU computer programs. This paper presents and compares the analytical model details, the obtained experimental and analytical results.

1. Introduction

This paper presents the experimental and analytical parameters of criticality of the uranium-containing fast neutron multiplication systems with a core based on fuel assemblies with 36% and 90% U-235 fuel rods. The experiments were performed using the “Giacint” critical facility of the Joint Institute for Power and Nuclear Research – Sosny (JIPNR-Sosny) of the National Academy of Sciences of Belarus [1]. The experimental results were analyzed in order to estimate whether they can be used as benchmark criticality data.

2. Fast critical assemblies

The fast critical assemblies represent a lattice (35.7 mm pitch) of fuel assemblies with fuel rods based on metal uranium and uranium dioxide, 90% and 36% enrichment by U-235, respectively, with a beryllium-steel reflector (Fig 1). The critical assemblies included the core, the side reflector, the top and bottom axial reflectors and the control and protection system (CPS) rods. The cores of critical assemblies, comprising fuel assemblies, are surrounded by several rows of beryllium and steel reflector units. These elements of the critical assemblies are placed on the stainless-steel support grid. The neutron detectors are attached on special poles around the critical assemblies.

The support grid of the critical assemblies is placed on the frame and represents a stainless-steel cylinder, 950 mm in diameter and 40 mm in thickness. The support grid has 18.2 mm diameter holes drilled in the hexagonal lattice with the 35.7 pitch; the holes receive the shanks of the fuel assemblies and the side reflector units.



Fig 1. The fast critical assembly

The fuel assemblies (Fig 2) represent assemblies without a casing and comprises 19 fuel rods. There are three types the fuel assemblies: type 1 — 16 fuel rods type 2 and 3 fuel rods type 1; type 2 — 19 fuel rods type 2; type 3 — 19 fuel rods type 1 (Fig 3). The fuel rods are arranged around the hexagonal grid with the 8 mm pitch and are fixed by means of the end parts. The fuel assemblies have dimensions for the 34.8 mm wrench, with the total length 1047 mm (the active part in 500 mm long, the top shank of the fuel rod is 60 mm, the top end parts of the assembly are 216 mm, and the bottom end parts of the cassette are 211 mm). All top and bottom end parts of the fuel assemblies are made from stainless steel.

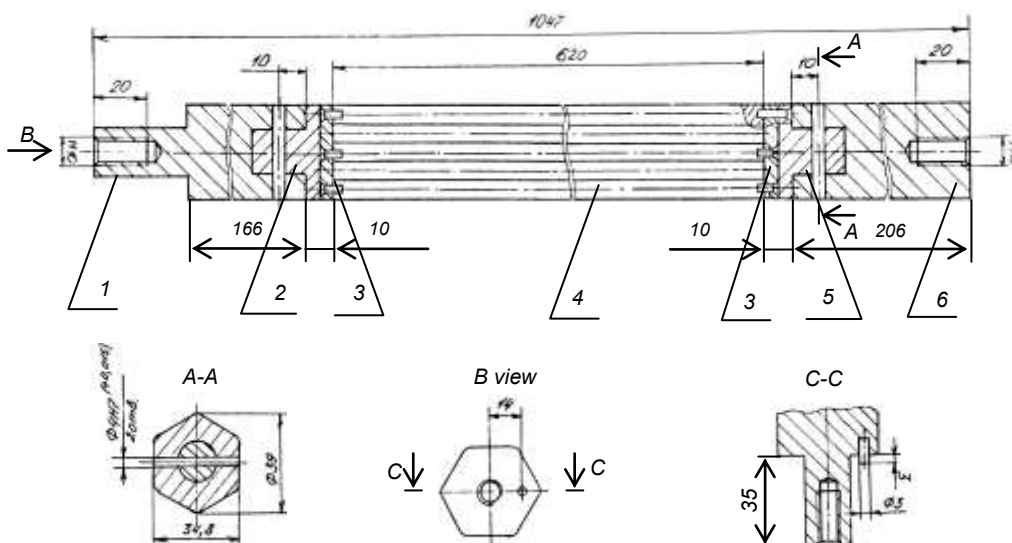


Fig 2. Fuel assembly:
1, 2 – bottom end parts, 3 – tube plate, 4 – fuel rods, 5, 6 – top end parts

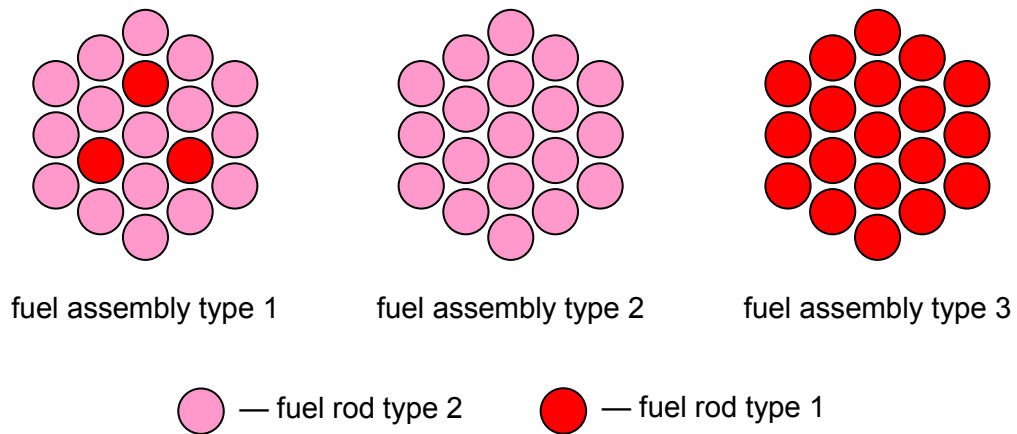


Fig 3. Layout of fuel rods in the fuel assemblies

The type 1 fuel rod (Fig 4) comprises a fuel core, a clad and end parts. The fuel rod cladding is from stainless steel with the outer diameter 7 mm and the wall 0.2 mm thick. The fuel core comprises tablets, 6.4 mm in diameter and 5 mm in height, made from metal uranium 18.9 g/cm³. The U-235 enrichment is 90%. The total core height is 500 mm. The U-235 weight in the fuel rod is 259.8 g. The top shank of the fuel rod is made from stainless steel with the 60 mm length and 6.6 mm diameter. The bottom end part of the fuel rod comprises the bottom shank 10 mm long and 6.6 mm in diameter and the bushing 50 mm long with the 6.6 mm diameter. The fuel rod is sealed, with the total length 620 mm.

The type 2 fuel rod (Fig 4) has the same structure as type 1 fuel rod, but with a different fuel core, comprising tablets with the 6.4 mm diameter and the 4-7 mm height, made from uranium dioxide 9.8 g/cm³. The enrichment by U-235 is 36%. The total fuel core height is 500 mm. The 90% U-235 weight in the fuel rods is 49.1 g.

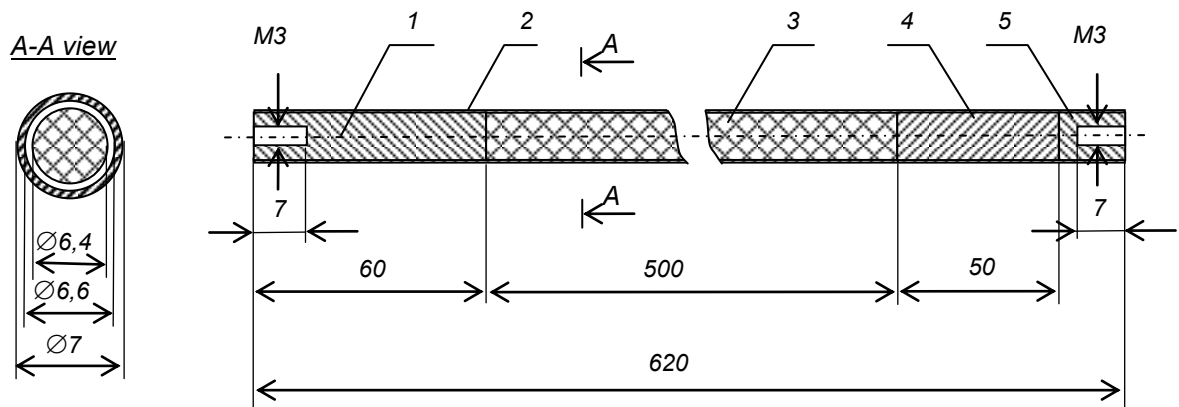


Fig 4. Fuel rod type 1 (type 2):
1 – upper end part; 2 – cladding; 3 – fuel core; 4, 5 – lower end part

The side reflector of the critical assemblies is several rows of the beryllium and stainless steel reflector units. The bottom axial reflector of the critical assemblies comprises bottom plugs of the fuel rods, bottom end parts of the fuel assemblies and the support plate. The top axial reflector of the critical assembly comprises top ends parts of the fuel rods and top end parts of the fuel assemblies.

The beryllium reflector unit (Fig 5) represents a hexagonal prism beryllium prism for the 34.8 mm wrench, 972 mm long. The bottom part of the unit bears a stainless steel shank, representing a seating surface when loaded into the critical assembly. The top part of the unit bears a stainless steel head for the 34.8 mm wrench, 40 mm long. The total length of the beryllium reflector unit is 1047 mm.

The steel reflector unit (Fig 6) is made from stainless steel, representing a hexagonal prism for the 34.8 mm wrench, 1047 mm long. The bottom part of the unit bears a shank, representing a seating surface when the critical assembly is installed on the support plate.

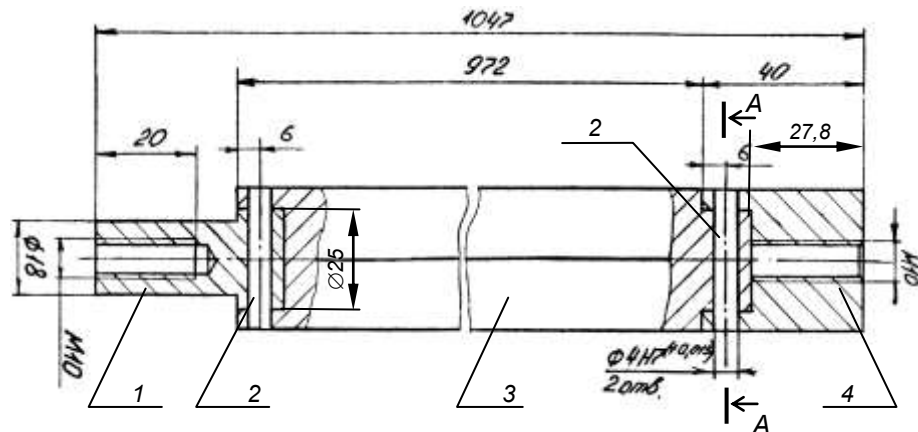


Fig 5. Beryllium reflector unit:
1 – bottom end part; 2 – pin; 3 – beryllium prism; 4 – top end part

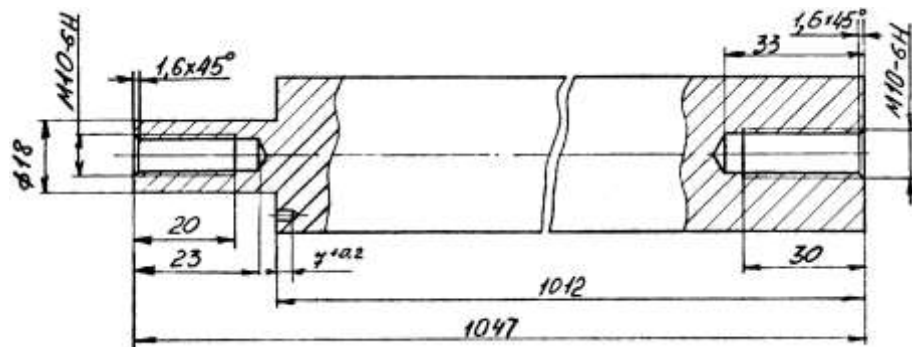
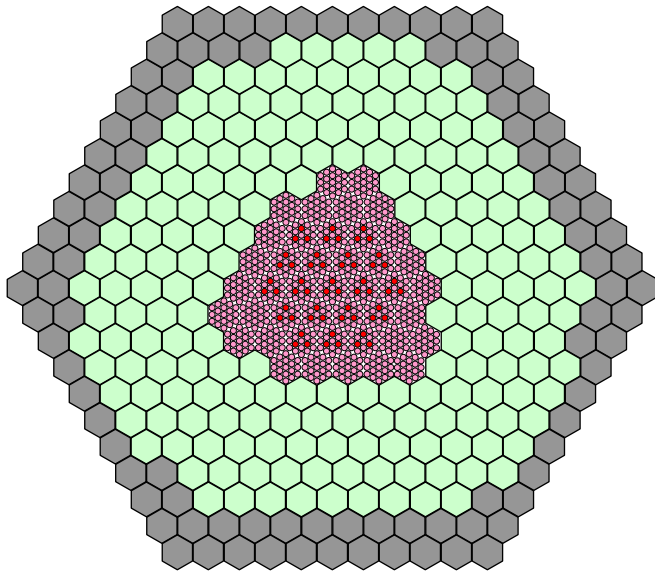


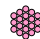



Fig 6. Steel reflector unit

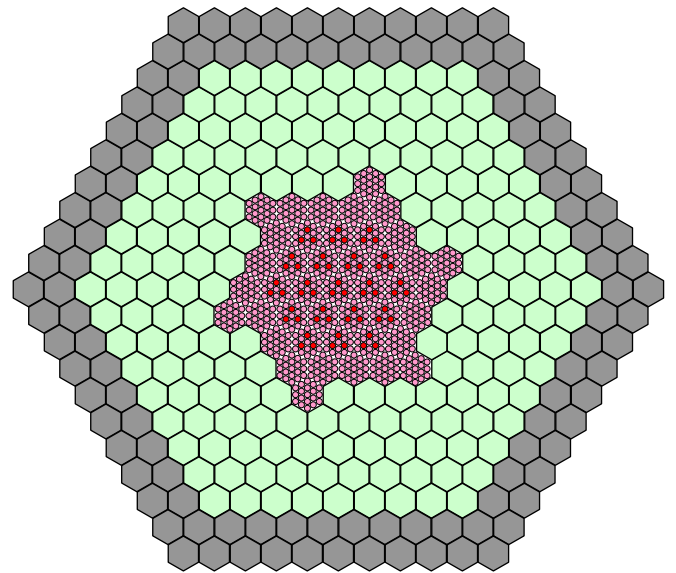
The control and protection system of this critical assembly included three rods for emergency protection (EP), three rods for manual regulation (MR) and three rods of compensating reactivity (CR).

3. Neutron physical parameters of the critical assemblies

Figures 7 – 10 represent loading charts of the fast critical assemblies. The core and reflector compositions of the fast critical assemblies are presented in Tab 1.



-  — fuel assembly type 2
-  — fuel assembly type 1
-  — beryllium reflector unit
-  — steel reflector unit







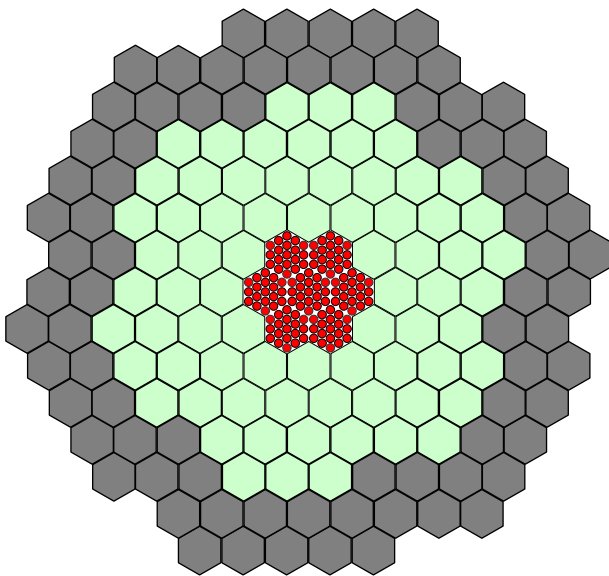

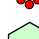

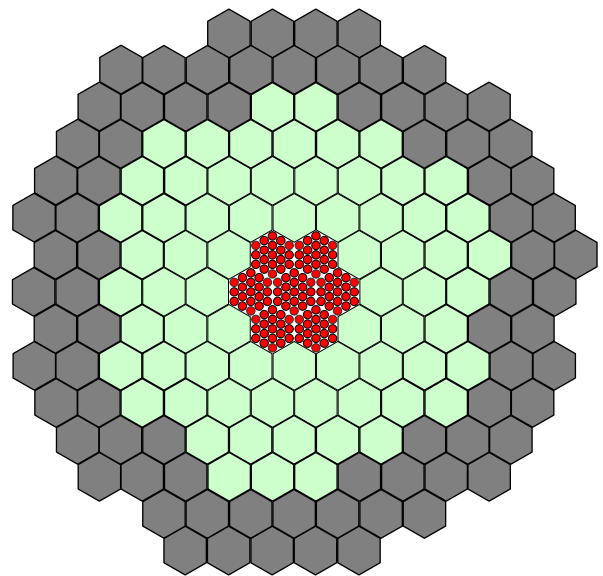
-  — fuel assembly type 2
-  — fuel assembly type 1
-  — beryllium reflector unit
-  — steel reflector unit

Fig 7. Loading chart of the critical assembly type 1

Fig 8. Loading chart of the critical assembly type 2



-  — fuel assembly type 3
-  — beryllium reflector unit
-  — steel reflector unit






-  — fuel assembly type 3
-  — beryllium reflector unit
-  — steel reflector unit

Fig 9. Loading chart of the critical assembly type 3

Fig 10. Loading chart of the critical assembly type 4

The critical assembly	The fuel assembly, pcs			Beryllium reflector unit, pcs	Steel reflector unit, pcs
	type 1	type 2	type 3		
Type 1	19	24	—	189	99
Type 2	19	24	—	174	114
Type 3	—	—	7	72	78
Type 4	—	—	7	69	78

Tab 1: The core and reflector compositions of the fast critical assemblies

The neutron physical characteristics of the critical assemblies are measured by the experimental unit "Reactivity Meter", using the inverted solution of reactor kinetic equation [2, 3]. In order to exclude spatial effects of reactivity, the measurements were made using three ionization chambers, arranged at every 120° behind the side reflector of the critical assembly.

For estimating the results of the critical experiments we calculated the effective neutron multiplication coefficient K_{eff} of the fast critical assemblies. The calculations were made by the Monte Carlo method using the MCNP-4C [4] and MCU-PD [5] computation codes. The experimental data and the calculation results are presented in Tab. 2.

The critical assembly	Reactivity measurement result *, β_{eff}	K_{eff} calculation result		β_{eff} calculation result
		MCNP-4C	MCU-PD	MCU-PD
Type 1	0,43 ± 0,02	1,00447 ± 0,00012	1,00349 ± 0,00037	0,007454 ± 0,000003
Type 2	-0,09 ± 0,01	1,00176 ± 0,00017	1,00059 ± 0,00043	0,007467 ± 0,000003
Type 3	0,60 ± 0,02	1,00310 ± 0,00022	1,00130 ± 0,00050	0,007227 ± 0,000003
Type 4	0,03 ± 0,01	0,99860 ± 0,00022	0,99764 ± 0,00036	0,007227 ± 0,000003

* – total error of experimental results for the given confidence probability 0,68.

Tab 2: The experimental data and the calculation results of the fast critical assemblies

4. Conclusions

Analysis of the experimental data (including data on the composition and sizes of the critical assembly components) and of the calculated K_{eff} allows a conclusion that the results of criticality experiments obtained on this assembly can be used as benchmark data.

5. References

- [1] Sikorin S., Hryharovich T. Research Nuclear Installations in Republic of Belarus / Enhancing Use and Safety of Research Reactors through Networking, Coalitions and Shared Best Practices, IAEA, Vienna, Austria, 10-14 February 2014. — CD.
- [2] S.A. Polazau, S.N. Sikorin, "Digital reactimeter on the basis of the microcomputer and apparatus «CAMAC»", Proceedings of the Academy of Sciences of Belarus, Power engineering physical series, № 4, pp. 87-92, 1987.
- [3] G.I. Buznitsky, A.I. Golovach, F.A. Grinevich, V.V. Luk'yanets, N.M. Sidoruk, S.N. Sikorin "An analogous meter for measuring nuclear reactor reactivity", Proceedings of the Academy of Sciences of Belarus, Power engineering physical series, № 1, pp.22-27, 1992.
- [4] "MCNP – A General Monte Carlo N-Particle Transport Code, Version 4C," Ed. J. F. Briesmeister, Report LNL, LA-13709-M, 2000.
- [5] Application Description and User's Manual for MCU-PD program: report №36-10/30-11 / NRC "KURCHATOV INSTITUTE" . — Moscow, 2011. — 569 p.

JRTR INITIAL CRITICALITY CALCULATIONS AND NUCLEAR COMMISSIONING TESTS

MUSTAFA K. JARADAT, S. ALKHAFAJI, K. ABU SALEEM
*Research Reactor Project, Jordan Atomic Energy Commission
P. O. Box 70, Amman 11934, Jordan*

CHANG JE PARK
*Sejong University, 209 Neungdong-ro, Gwangjin-gu, Seoul, Republic of Korea
And Reactor Core Design Division, Korea Atomic Energy Research Institute
1045 Daeduk-Daero, Yuseong-Gu, Daejeon, 305-353, Korea*

ABSTRACT

The Jordan Research and Training Reactor (JRTR) is a multi-purpose open-tank in pool type reactor under construction with nominal power of 5 MW. The core consists of 18 fuel assemblies with low enriched uranium (LEU) of ^{235}U enrichment of 19.75%. During the commissioning of JRTR many tests will be performed. In this work the initial criticality and fuel loading pattern are simulated using Monte Carlo code McCARD. One fuel loading scheme had been chosen based on lowest amount of fuel loaded into the core and the smallest number of fuel assemblies loaded. Also the control rods worth calculation using swap method have been modeled for a fully loaded core. These calculations should be compared with measured results during commissioning tests of JRTR.

1. Introduction

Jordan Research and Training Reactor (JRTR) is a multi-purpose open-tank-in-pool type reactor under construction with nominal power of 5 MW. The JRTR core consists of standard and special MTR fuel assemblies. A standard fuel assembly is a plate-type, a total of 21 fuel plates with aluminum-clad constitute. The fuel for the core is low enriched uranium (LEU) with a ^{235}U enrichment of 19.75 weight %. Each fuel plate is composed of a fuel meat with surrounding aluminum cladding. The fuel meat is made of fine and homogeneous dispersion of U_3Si_2 particles in a continuous aluminum matrix with a uranium density of 4.8 g U/cm^3 . The JRTR core configuration contains 18 fuel assemblies with four control absorber rods and two second shutdown rods. The control absorber rod is a square tube with the neutron absorbing material made of Hafnium, while for the second shutdown rods B4C powder is used as the neutron absorbing material. The core has a central flux trap, four beam ports, and several irradiation holes. The reactor is light water moderated and cooled and reflected with beryllium and heavy water. ^[1]

2. Initial Core Description

The initial core configuration is determined based on the following strategies: the initial core should be similar to the equilibrium core; the excess reactivity should be enough for a good

fuel economy, the reactor controllability should be maintained, the power peaking factor should be as low as possible, the transition from the initial core to the equilibrium core should be easy, and the number of fuel types should be minimized.

The initial core is configured using fuel assemblies of different densities. Fuel assemblies are fully loaded at the appropriate locations in view of the controllability of reactivity worth in the core and the safety margin. Figures 1 and 2 depict the core configuration and the initial fuel loading with 4 different densities of 4.176, 4.784, 5.878, and 6.543 g/cm³. Table 1 lists the major parameters of the fuel and core. ^[1]

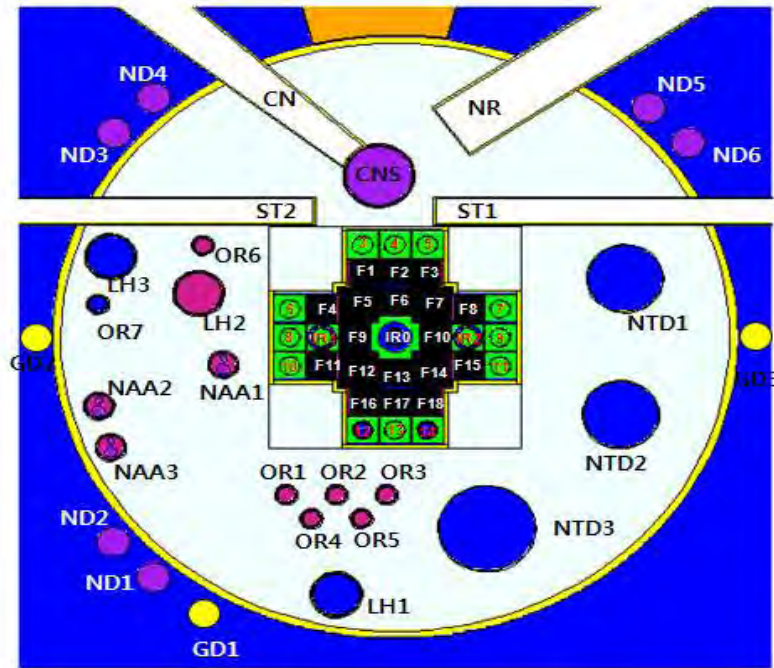


Fig.1 Plan View of the JRTR Core

	F01 4.0 5.878	F02 4.8 6.543	F03 4.0 5.878	
F04 2.6 4.784	F05 2.6 4.784	F06 1.9 4.176	F07 2.6 4.784	F08 2.6 4.784
	F09 1.9 4.176		F10 1.9 4.176	
F11 2.6 4.784	F12 2.6 4.784	F13 1.9 4.176	F14 2.6 4.784	F15 2.6 4.784
ID gU/cc Density (g/cm ³)	F16 4.0 5.878	F17 4.8 6.543	F18 4.0 5.878	

Fig.2 Initial Fuel Loading of JRTR

Table (1) Major Parameters of the Core, Fuel Assembly and Fuel Plate

Reactor Core	Data
Number of fuel assembly sites	18
Number of irradiation sites in the Be reflector	12
Number of control absorber rods	4 (Hf)
Number of second shutdown rods	2 (enriched B ₄ C)
Number of beam tubes	4
Reactor power	5 MW
Fuel Meat, Plate and Assembly	Data
Fuel meat thickness	0.51 mm
Cladding thickness	0.38 mm
Fuel plate thickness	1.27 mm
Fuel plate width	70.7 mm
Fuel plate length	680 mm
Coolant channel thickness	2.35 mm
Number of fuel plate/Fuel assembly	21
Fuel assembly width	76.2 mm
Fuel assembly height	1015 mm
Material Property	Data
Fuel meat	U ₃ Si ₂ -Al
Uranium density in fuel meat	4.8 gU/cm ³
Fuel meat density	6.543 g/cm ³
Cladding	AG3NE (aluminum alloy)
Cladding density	2.7 g/cm ³

3. JRTR Commissioning Tests

The commissioning of JRTR is required to demonstrate that the requirements and intents of the design as stated in the safety analysis report can be met. The commissioning activities should include adequate testing and inspection of structures, systems and components based on the importance of reactor safety. A graded approach for testing should be properly established in advance from the planning stage. The tests have to be arranged in functional groups and in a logical sequence and to be conducted with written procedures. The commissioning tests and stages are divided into few different sequences as follows;

- a) Stage A for pre-fuel loading tests.
- b) Stage B for fuel loading tests, initial criticality tests and low power tests.
- c) Stage C for power ascension and power tests. ^[2]

In stage B neutronics tests must be carried out following the test procedures, so simulation results of these tests must be provided in advance. Some of these tests are:

- a) Fuel loading and approach to the first criticality of JRTR
- b) Configuration of operation core
- c) Tests and experiments at zero-power
- d) Test and experiments at each power level.

In this work the initial criticality of the JRTR core and control absorber rods worth were investigated using McCARD code. McCARD is a Monte Carlo Code for Advanced Reactor Design & Analysis. It was developed in the Department of Nuclear Engineering of Seoul National University since 1998. McCARD is a Monte Carlo (MC) neutron-photon transport simulation code designed exclusively for neutronics analyses of various nuclear reactors and fuel systems. McCARD estimates of neutronic design parameters of a nuclear reactor or fuel

system such as effective multiplication factor (k_{eff}), neutron flux and current fission power, etc. by using continuous-energy cross section libraries and detailed geometrical data of the system. [3]

4. Results of JRTR Fuel Loading and Initial Criticality:

Fuel loading, removal of the absorber or addition of the moderator during the approach to criticality necessitates calculations or estimates to predict changes in core reactivity, and periodic measurements of subcritical multiplication to determine subsequent safe increments of reactivity.

For fuel loading to reach first criticality of the core the fuel assemblies are loaded into the core one by one until the core approach criticality. After adding each fuel assembly the multiplication factor must be checked before adding the next one. When the core reaches critical state the control rods should be inserted into the core before adding fuel assembly until the core is fully loaded and the control rods are at the critical position. So the fuel loading pattern should be defined in advance before starting real fuel loading into the core to avoid approaching any super critical state.

Criticality calculations using McCARD were performed to determine fuel loading scheme to approach to criticality. For fuel loading 20 core configurations were simulated for the first criticality but four configurations were suggested for fuel loading of JRTR core as shown in figure (3) because they can make the reactor critical without control rods.



Fig.3 JRTR core fuel loading configurations

Since the fuel assemblies for the initial core have different densities and hence they have different uranium content, one of the four configurations will be chosen for JRTR first criticality based on the following criteria:

1. The minimum number of fuel assemblies loaded into the core.
2. The lowest mass of uranium loaded into the core.
3. The uniformity of the fuel assemblies' distribution into the core.

The differences between the suggested configurations are shown in table (2) based on number of FA, Uranium mass and Uniformity of FA distribution. Configuration 1 has the lowest number of fuel assemblies to reach criticality which is 11 but the fuel assemblies' distribution is non-uniform while Configurations 3 and 4 have higher uranium content and higher number of fuel assemblies but they have uniform fuel assemblies. Configuration 3 is chosen to be followed for JRTR initial criticality because it has smaller uranium content than configuration 4 although they have the same number of fuel assemblies.

Table (2) Differences between suggested JRTR core configurations for initial loading

Core Configuration	Number of FA	k-eff	Total Uranium Mass (kg)	Total U-235 Mass (kg)	FA Distribution
1	11	0.99962	16.09	3.18	Non-Uniform
2	12	0.99319	17.24	3.41	Non-Uniform
3	14	0.99687	19.86	3.92	Uniform
4	14	1.00863	21.50	4.25	Uniform

The core pattern and fuel assemblies order in the core is shown in figure (4) for critical and fully loaded core. During approach to criticality dummy fuel assemblies are used to fill empty fuel assembly spaces in the core to maintain uniform flow distribution.

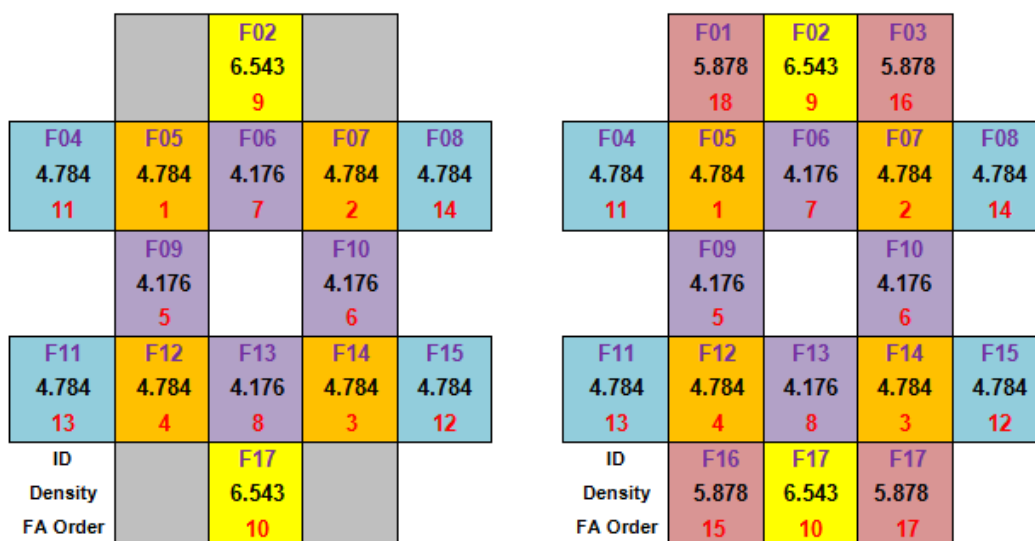


Fig.4 Fuel loading pattern for initial criticality

During fuel loading neutron count rates must be recorded and inverse of multiplication must be calculated to determine the critical mass of the core. The inverse of multiplication method ($1/M$) method $n = S\Lambda/\rho$ is used to determine the critical mass using the following formula:

$$M = n_m/n_o = 1/(1 - k_{eff})$$

Where M is the subcritical multiplication factor; the reciprocal of the multiplication is plotted against the mass of the fuel in figure (5).

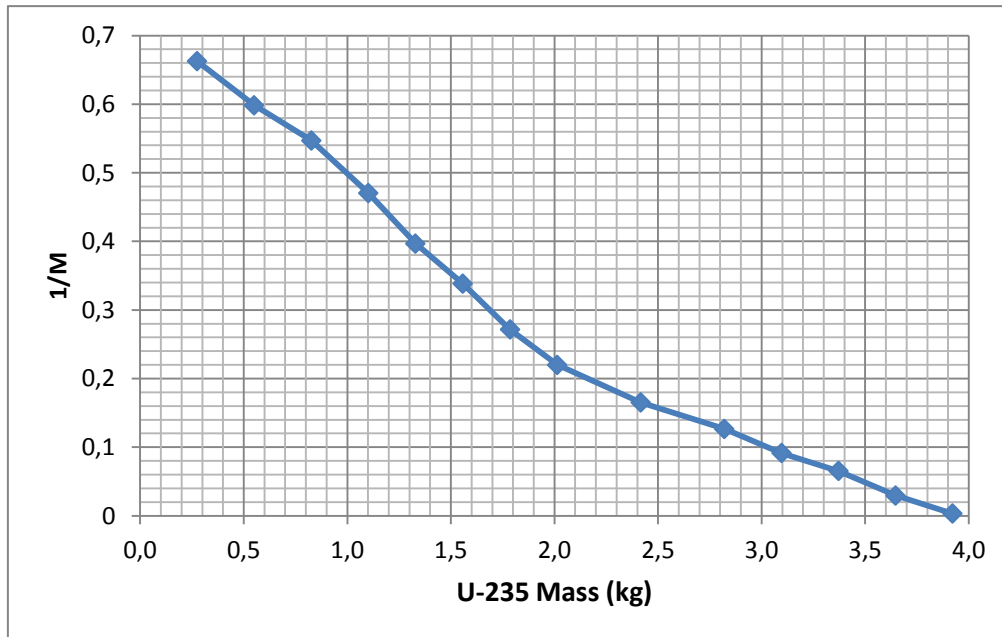


Fig.5 Fuel mass with inverse of multiplications

It can be found by interpolation that the critical mass of the core is about 4 kg of U-235 for this configuration with 14 fuel assembly loaded into the core. Table (3) shows the results of the inverse of multiplications with control rod positions for critical state. As shown in the table the control rods needed to be inserted to avoid super criticality as the core approaching criticality.

Table (3) Inverse of multiplications with control rod positions

Number of FAs Loaded	Assembly ID	Mass of U-235 in The Core	k_{eff}	1/M	Control Rod Position (cm)
1	FA05	0.275	0.33747	0.66253	ARO
2	FA07	0.551	0.40159	0.59841	ARO
3	FA14	0.826	0.44285	0.54715	ARO
4	FA12	1.102	0.48944	0.47056	ARO
5	FA09	1.330	0.60317	0.39683	ARO
6	FA10	1.558	0.66157	0.33843	ARO
7	FA06	1.786	0.72840	0.2716	ARO
8	FA13	2.014	0.78001	0.21999	ARO
9	FA02	2.417	0.83496	0.16504	ARO
10	FA17	2.821	0.87331	0.12669	ARO

11	FA04	3.096	0.90861	0.09139	ARO
12	FA15	3.372	0.93477	0.06523	ARO
13	FA11	3.647	0.97042	0.02958	ARO
14	FA08	3.922	0.99687	0.00313	ARO
15	FA16	4.279	1.00198	—	53 (22.1% In)
16	FA03	4.635	0.99976	—	45 (33.8% In)
17	FA18	4.992	0.99977	—	39 (42.6% In)
18	FA01	5.348	0.99949	—	36 (47.1% In)

5. Results of JRTR Control Rods Worth:

The other test is calculating the CARs worth using rod swap method to determine the worth of each control rod separately when all fuel assemblies are loaded into the core. In this test one control rod is fully withdrawn and one control rod is fully inserted and the other two control rods are at critical position. Then to calculate the CAR worth the test starts by inserting the pre-calibrated CAR which is already out of the core and recording the reactivity while the fully inserted rod is withdrawn until the reactor become critical and recording the reactivity. This procedure continues until the fully inserted rod becomes fully withdrawn. Finally the worth of this rod can be calculated. By exchange of positive and negative reactivity the nuclear reactor is kept at a relatively constant power. Figure (6) shows the positions of the CAR and the rod swap technique.

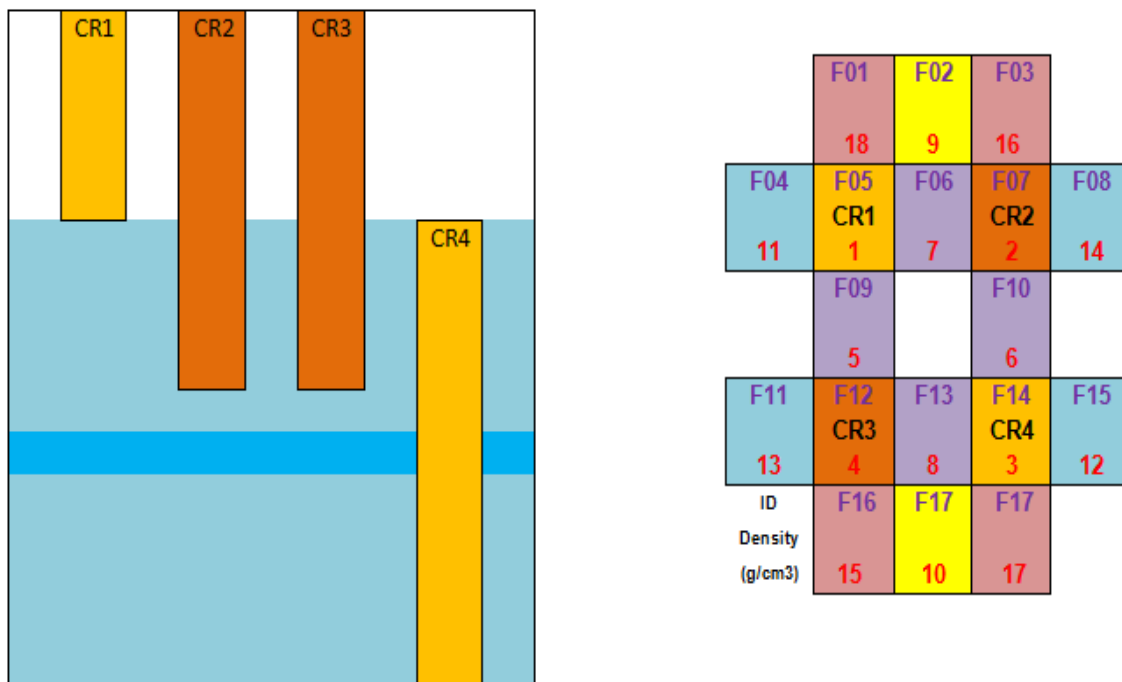


Fig.6 Control rod swapping method to calculate the control rods worth

McCARD simulation for CAR4 worth calculations using rod swapping method is shown in figure (7) for CAR4 integral worth and figure (8) CAR4 deferential worth.

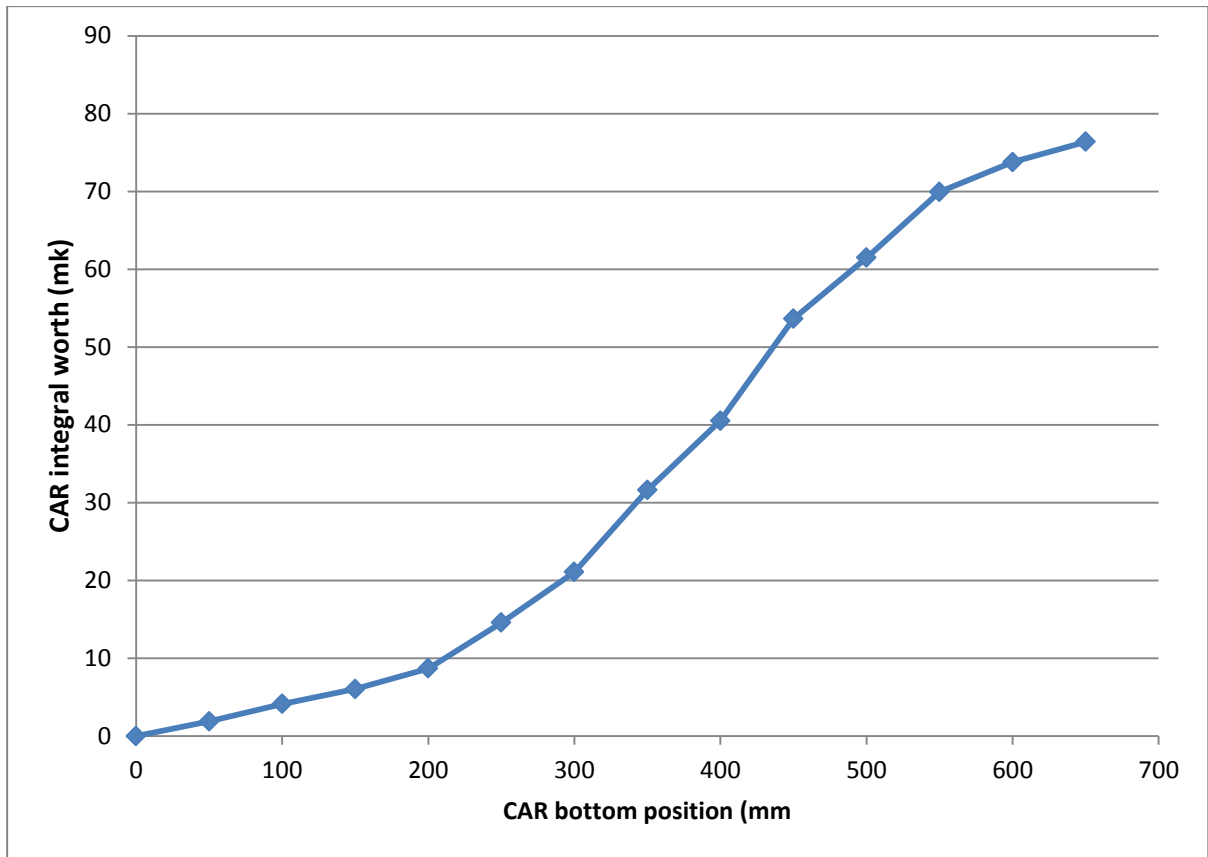


Fig. 7 Integral worth of CAR4 by rod swapping method

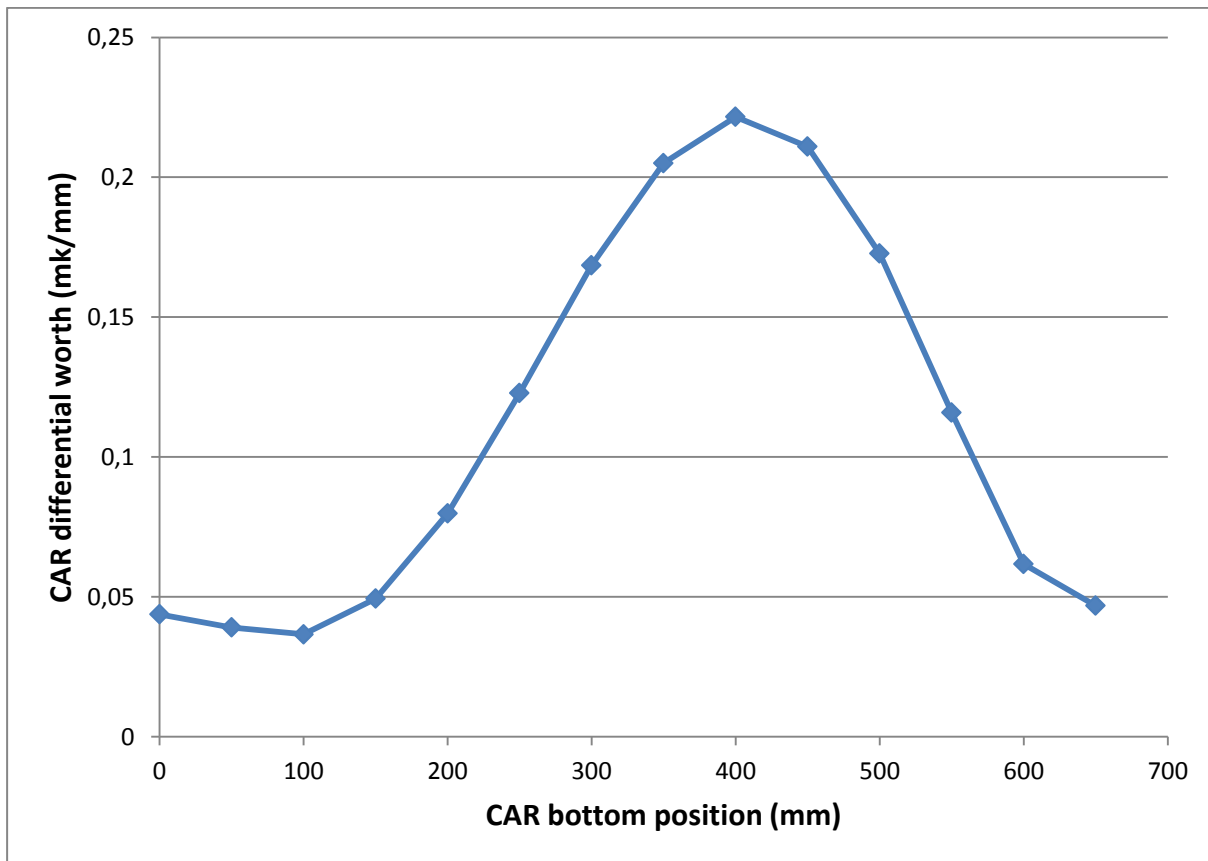


Fig. 8 Differential worth of CAR4 by rod swapping method

The total CARs worth is calculated for core with 15, 16, 17, and 18 fuel assemblies to show the change of the control rods worth with adding fuel assemblies to the core as shown in figure (9) for the integral worth and figure (10) for the differential worth.

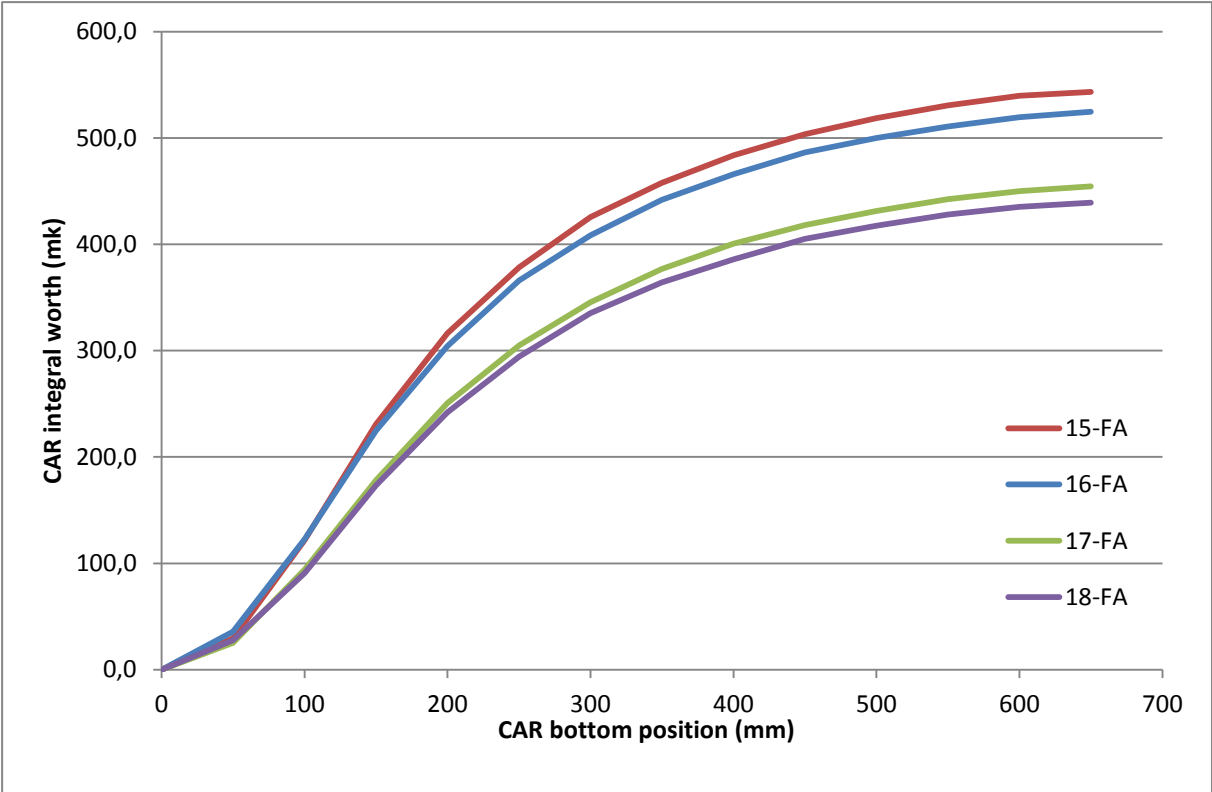


Fig. 9 Integral CARs worth for different number for FA loaded into the core

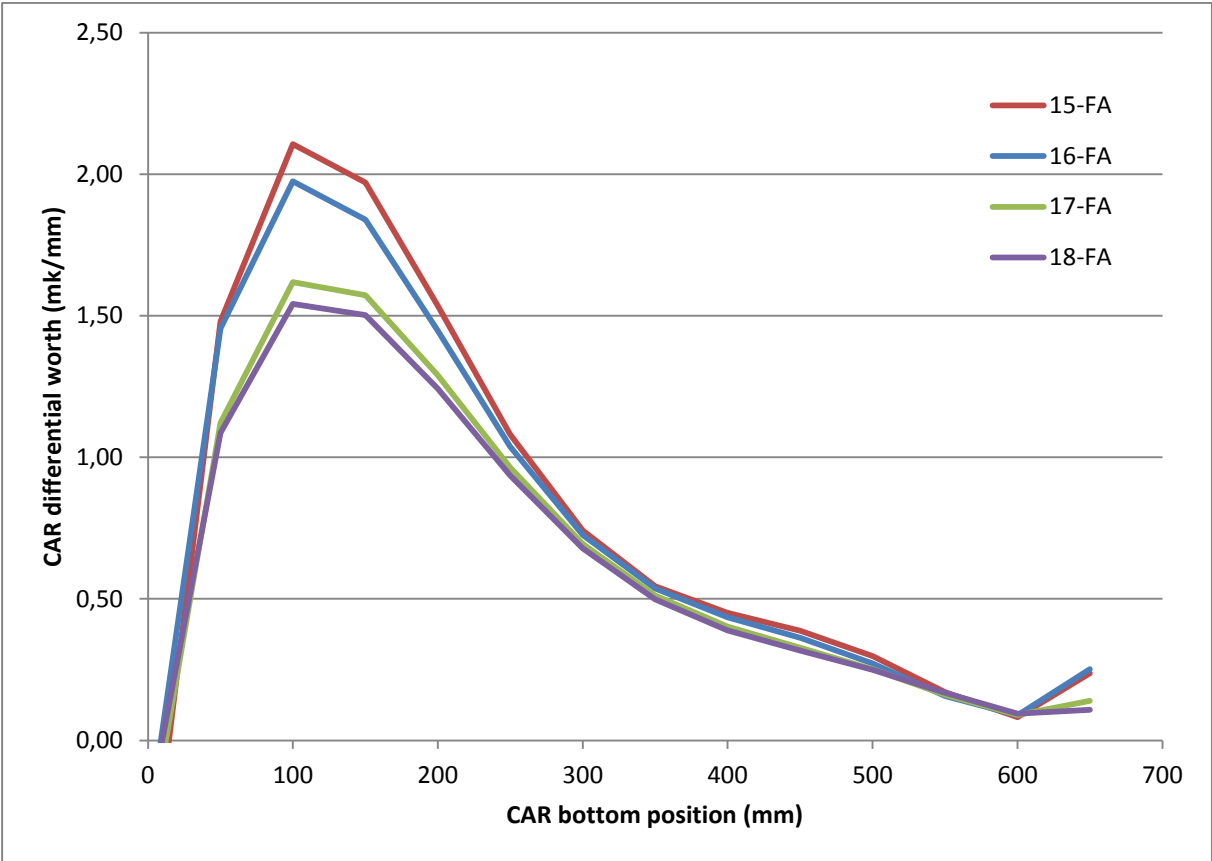


Fig. 10 Differential CARs worth for different number for FA loaded into the core

6. Conclusions

In this work the JRTR initial criticality and control rod worth calculations by rod swap method were simulated using McCARD code. Fuel loading to reach initial criticality is very important during commissioning stage of the reactor, so if the core subcriticality conditions measured during the approach to criticality deviate significantly from calculations made before the operations, further loading of the core should be stopped until the deviations are analyzed and appropriate corrective action must be taken.

For JRTR core, one fuel loading pattern was chosen based on specific criteria, and the criticality reached with 14 fuel assemblies and all control rods are fully withdrawn from the core. Also the control rods worth calculation using swap method have been modeled for a fully loaded core.

Many other tests should be simulated and the final procedures must be finished before starting the test measurement process during commissioning stage, like measuring the reactor characteristics at zero power: void coefficient, shutdown margin, delayed neutrons yield, thermal and fast neutron flux distribution at fuel and irradiation sites, neutron energy spectrum, and power distribution. Also to measure the reactor characteristics at each power level such as temperature coefficients, power defect, and xenon behavior.

References

1. JAEC, 2014, "Jordan Research & Training Reactor Final Safety Analysis Report", Revision 0, prepared by KAERI, DAEWOO E&C.
2. IAEA, 2006, "Commissioning Of Research Reactors", IAEA Safety Standards Series No. NS-G-4, Vienna, Austria.
3. H. Shim, B. Han, J. Jung, H. Park, C. Kim, 2012, "MCCARD: Monte Carlo Code for Advanced Reactor Design and Analysis", Nuclear Engineering and Technology, Vol.44 No.2.

A COMPREHENSIVE ANALYSIS OF THE TECHNICAL FEASIBILITY OF THE MIR RESEARCH REACTOR CONVERSION TO LOW-ENRICHED URANIUM FUEL

A.L. IZHUTOV, V.A. STARKOV, V.V. PIMENOV, V.A. UZIKOV, V.E. FEDOSEEV
*Research Reactor Complex, SSC "Research Institute of Atomic Reactors"
Dimitrovgrad-10, 433510 – Russian Federation*

S.V. MAYNSKOV, T.A. OSIPOVA
*National Nuclear University MEPhI (Moscow Engineering Physics Institute)
Dimitrovgrad, 433511 – Russian Federation*

ABSTRACT

Presented are the results of a calculation analysis of the technical feasibility of the MIR reactor conversion to low-enriched uranium fuel. Two fuel types with 19.7% enrichment were considered: uranium dioxide UO_2 and alloy $U9\%Mo$. The neutronic and thermal-hydraulic calculations of the reactor core parameters were performed. The analysis has shown that the reactor experimental capabilities will be preserved at conversion.

To justify safety of using LEU fuel the comprehensive calculation simulation of the accidents with the most conservative initial events was performed. Two types of the accidents were considered: LOCA and RIA with the worst possible consequences. This work was fulfilled with the financial support of Argonne National Laboratory (USA).

1. Introduction

Research reactor conversion to low-enriched uranium (LEU) fuel is one of the objectives of the Reactor Conversion Program (RERTR) under the Global Threat Reduction Initiative (GTRI). At present, an agreement has been reached between the National Nuclear Security Administration (U.S. Department of Energy) and ROSATOM State Corporation to study the technical feasibility of converting six Russian research reactors to LEU fuel including the MIR reactor [1].

The conducted analysis covered two stages. At the first stage the key objective was to obtain comparative parameters of the reactor cores with HEU and LEU fuels, i.e. to determine whether such conversion is possible. The next stage included the feasibility of safety to use a new fuel type (LEU) based on the analysis of accident consequences.

2. Brief description of the MIR reactor

The MIR reactor is located at the site of JSC "State Scientific Center – Research Institute of Atomic Reactors", Dimitrovgrad. Its main purpose is testing of materials, items and experimental FAs, operating modes, and refinement of the next generation advanced nuclear reactor coolant technology.

The reactor core (Fig. 1) is made of hexagonal beryllium blocks. Along the axis of the blocks there are direct-flow zirconium channels to accommodate standard and experimental FAs. Such core arrangement was selected in view of the minimal mutual impact of the neighboring tested

items. For this purpose, each channel with a tested item is surrounded by six channels with standard FAs.

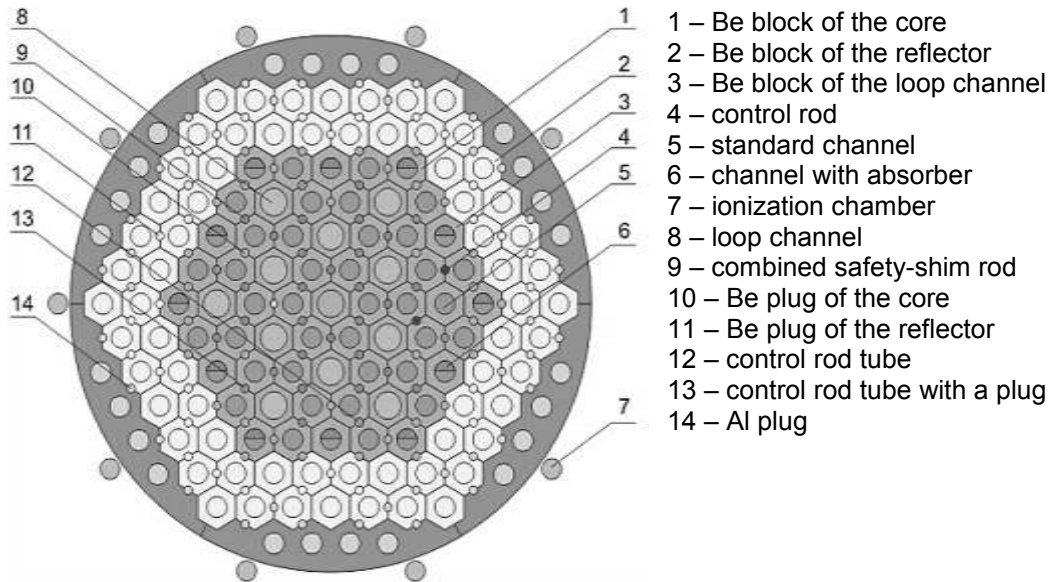


Fig 1. MIR core arrangement

A beryllium stacking of the core and reflector is arranged along a triangular grid. It is made of 127 hexagonal blocks spaced at 150 mm with width across flats of 148.5 mm. Four central rows of Be blocks serve as a moderator, and two external rows are a reflector.

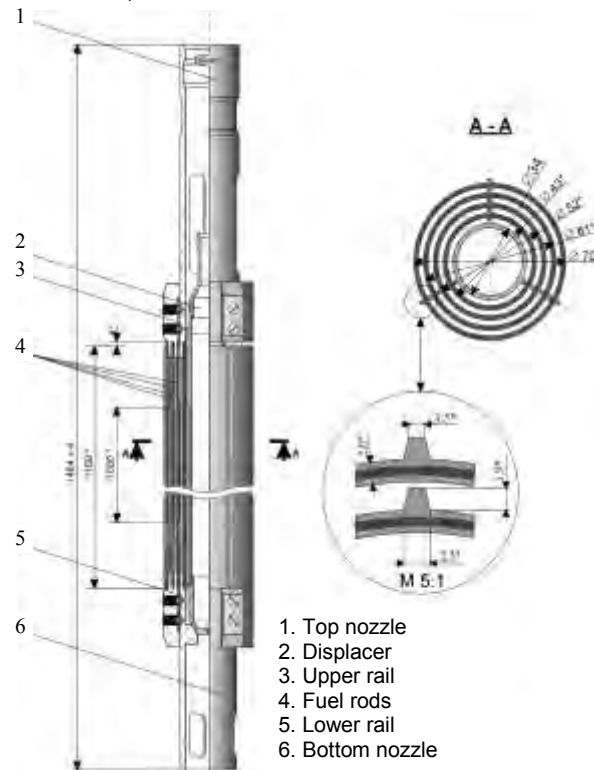


Fig 2. Standard FA

A standard FA of the MIR reactor (Fig. 2) is made of four annular coaxially positioned fuel rods. Each fuel rod is a three-layer tube. Fuel layer is enclosed on both sides in aluminum alloy

cladding. Fuel is uranium dioxide dispersed in the aluminum matrix. Enrichment in ^{235}U makes up 90%.

MIR heat removal is a two-circuit process with five circulation paths in the primary circuit, two paths in a pool cooling circuit and four paths in the secondary circuit. A cooling tower is the end user of heat.

The primary circuit is designed for heat removal from the core and its transfer to the secondary circuit (water recirculation circuit) as well as for maintaining the active medium.

The primary cooling circuit includes five circulation paths of the same type joined by inlet and pressure headers (Fig. 3). Each path consists of pipelines, stop and control valves, a heat exchanger, and the main circulation pump (MCP). From the MCP pressure header the coolant flows via two pipelines in the system consisting of circular and supply collectors connected to each other by eleven U-shape sleeves. From the supply header the coolant flows downwards to cool standard FAs. The outlet pipelines are joined in two hot collectors from which the coolant flows in an oxygen activity attenuator connected to the MCP inlet header by two pipelines. A pressurizer and a gas separator are connected to the inlet header. From the inlet header the coolant enters heat exchangers where heat is transferred to a water recirculation circuit.

Heat received from the primary circuit and pool cooling circuit by the water recirculation circuit coolant is transferred to the surrounding medium in a cooling tower.

In case of MIR primary circuit failure there is a double emergency cooling system (ECS): ECS #1 is connected to the inlet header and the core, ECS #2 supplies water from the reactor pool to the standard channels.

3. Input data

In a calculation analysis two LEU fuels were considered: UO_2 oxide and U9%Mo alloy. According to preliminary assessments, ^{235}U loading in LEU FAs shall make up approximately 460 g to preserve the reactivity margin. It is suggested to provide such ^{235}U content by taking the following measures:

- increasing fuel content in the fuel meat (for both fuels);
- increasing fuel meat thickness (for both fuels);
- increasing the amount of fuel rods (only for UO_2).

The main comparative geometry and process parameters of HEU and LEU FAs are shown in Table 1.

Parameter	HEU	LEU-1	LEU-2
Fuel	UO_2	UO_2	U9%Mo
Enrichment in ^{235}U , %	90	19.7	19.7
FA diameter, mm	70		
Fuel meat height, mm	1000		
Fuel rod thickness, mm	2		
Width of a gap between the fuel rods, mm	2.5		
The number of fuel rods in a FA	4	6	4
The total heat removal surface, m^2	1.37	1.72	1.37
^{235}U mass in a FA, g	350	460	460
Fuel meat density, g/cm^3			
- ^{235}U	0.91	0.57	1.02
- U	1.01	2.90	5.16
Fuel volume fraction in the fuel meat, rel. units	0.11	0.317	0.33

Table 2: Comparative analysis of HEU and LEU FAs

In case of using oxide LEU fuel it is not possible to provide ^{235}U loading of 460 g only by increasing fuel meat density and thickness. This is limited by the maximum admissible UO_2 density in the meat that can be implemented in fuel rod fabrication. Therefore, the number of fuel rods in a FA with such fuel is increased up to 6 with a corresponding change in inner displacer geometry. As for U9%Mo alloy, ^{235}U loading may be provided without any changes in the amount of fuel rods in a FA.

4. Neutronic parameters

To solve the problems related to obtaining HEU and LEU fuel core parameters, a detailed neutronic calculation model was developed using the MCU-RR code (Monte Carlo Universal – Research Reactor) [2]. MCU-RR is intended to compute neutron and photon flux functionals in research reactors using the Monte Carlo method based on the assessed nuclear data without introducing any additional approximations in the description of geometry of the considered system and physics of particles-substance interaction. Changes in the fuel nuclide content were taken into account using a burnup module (BURNUP) [3].

The HEU and LEU fuel core parameters obtained in the calculations are presented in Table 2.

Parameter	Value		
	HEU UO_2	LEU UO_2	LEU U9%Mo
Average fuel burnup in the core, %			
✓ reactor run beginning	29.5	34.5	33.8
✓ reactor run end	33.3	37.3	36.6
Reactivity loss rate, $10^{-3} \% \Delta k/k/\text{MWd}$	4.26	3.22	2.91
Control rod performance, $\% \Delta k/k$	28.7	28.3	27.4
Reactivity margin in an unpoisoned state, $\% \Delta k/k$	13.0	12.8	12.6
EFA power to surrounding FAs power ratio in an unpoisoned state, rel. units	0.70	0.69	0.68

Table 2: Comparative analysis of HEU and LEU fuel neutronic parameters

The analysis of the computation results shows that in conversion to LEU fuel there is an increase in the fuel cycle duration, and as a result, an increased burnup depth in discharged FAs. A lower reactivity loss rate is explained mainly by an increased ^{235}U mass in the core. Control rod performance and reactivity margin change within the range of 3-4%. The latter parameter in the Table describing the ability to provide the necessary power in a loop channel due to power of the surrounding FAs changes insignificantly, therefore the target EFA power is provided at almost similar power of surrounding standard FAs. The annual average MIR operating parameters are specified in Table 3.

Parameter	Value		
	HEU UO_2	LEU UO_2	LEU U9%Mo
The average amount of discharged FAs at the end of the cycle, pcs	3.9	2.6	2.7
The average burnup of ^{235}U in a discharged FA, %	50.5	54.4	53.1
The annual demand in FAs	62.4	41.6	43.2
Annual consumption, kg			
✓ ^{235}U	21.8	19.1	19.9
✓ U	24.2	97.0	100.9
Annual fast neutron fluence ($E>0.1$ MeV) on the VVER fuel	3.65	3.50	3.42

cladding in the core mid plain, 10^{21} cm^{-2}			
---	--	--	--

Table 3: MIR annual average operating parameters

It should be particularly mentioned that MIR conversion to LEU fuel will lead to a considerable reduction in annual FA consumption (by 30-33%) and annual consumption of ^{235}U (by 8-12%). At that, the total uranium consumption will increase by approximately 4 times. The annual fast neutron fluence (one of the reference parameters) will decrease by 4-6%.

5. Thermal and hydraulic parameters

The thermal and hydraulic calculations were performed to show the feasibility of thermal and physical parameters of reactor safe operation. The following parameters have been calculated:

- Heat flux distribution along the fuel rod surface;
- Distribution of washed fuel rod surface temperatures, fuel-to-cladding interaction temperatures and peak fuel temperatures along the core height;
- Onset-of-surface boiling ratio and departure from nucleate boiling ratio.

To obtain the temperature of the onset of surface boiling, Bergles-Rohsenow [4] and Forster-Greif [5] correlations were used. The critical heat flux density was obtained by a Mirshak correlation [6].

Since power of a standard FA in a maneuvering mode can achieve the peak value of 3.2 MW according to the operational procedure, all thermal and hydraulic parameters were calculated taking into account this value. The coolant temperature at the FA inlet was taken equal to 40°C , and the coolant flow rate was taken equal to $70 \text{ m}^3/\text{h}$.

The peak temperatures of the cladding and fuel meat for each fuel type are presented in Table 4, and thermal and physical ratios – in Table 5.

Parameter	Value		
	HEU UO_2	LEU UO_2	LEU U9%Mo
Peak cladding temperature, $^\circ\text{C}$	141	140	142
Peak fuel meat temperature, $^\circ\text{C}$	158	156	162

Table 4: Peak temperatures of an outer fuel rod in the FA with power of 3.2 MW

Parameter	Value		
	HEU UO_2	LEU UO_2	LEU U9%Mo
Heat flux, kW/m^2	4002	3449	4042
Coolant velocity in a gap between fuel rods, m/s	9.1	7.2	9.1
Onset-of-surface boiling ratio			
• Bergles-Rohsenow correlation	1.45	1.50	1.44
• Forster-Greif correlation	1.58	1.60	1.57
Departure from nucleate boiling ratio	4.5	4.8	4.4

Table 5: Thermal and physical criteria of MIR safe operation

The data given in Table 5 were obtained for a coordinate on a fuel rod with the peak outer cladding surface temperature. The analysis of the results shows no worsening of thermal and physical parameters in MIR reactor conversion to LEU fuel.

6. Accident analysis

To show the feasibility of safe conversion to LEU fuel accident (LOCA, RIA) consequences were analyzed using the RELAP5/MOD3.2 thermal and hydraulic code [7]. As part of this work a computational model of the MIR primary circuit was developed (Fig. 3) that includes the main components of cooling and safety systems. A simulated process of the accident development is divided into two stages. At the first stage the reactor systems are brought into a stationary operating mode. The calculation of the accident mode is done at the second stage after the initiating event occurs.

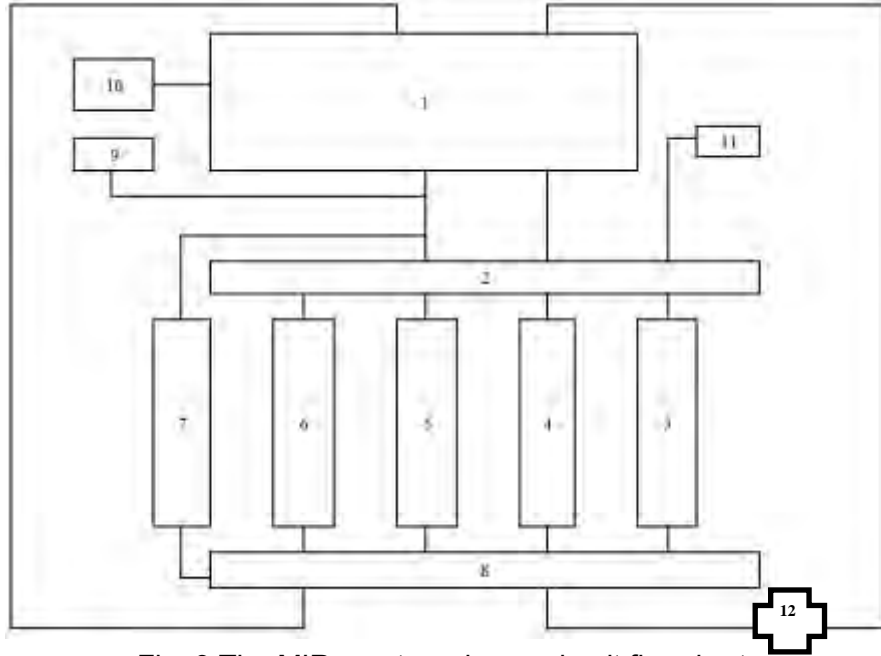


Fig. 3 The MIR reactor primary circuit flowchart

1 – reactor; 2 – inlet header; 3, 4, 5, 6, 7 – pipelines and equipment of the first, second, third, fourth and fifth legs; 8 – pressure header; 9 – pressurizer and degassing system; 10 – emergency cooling system #2 (ECS #2); 11 – emergency cooling system #1 (ECS #1); 12 – pipeline break point

6.1 MIR reactor primary circuit loss-of-coolant accident analysis

A double-ended instantaneous full cross-section pressure pipeline break is taken as a postulated initiating event of the primary circuit loss-of-coolant accident. It is assumed that the break occurs in the region between the header ring and valve P-1 at a lower height point (Fig. 3, position 12).

In accordance with [8], the overlapping on the initiating event of an undetected uncontrolled system element failure is considered (an ECS #2 pump failure) as well as one failure of any safety system element – a failure of an ECS #1 valve connecting the supply line and channels. In addition, the regulatory documents [9] postulate jamming of one of the most efficient scram rod. Thus, five control rods of six possible are inserted in the core.

The initiating event occurs in the calculation at the 1600th second.

The pipeline break leads to deterioration of the core cooling conditions caused by loss of pressure and coolant flow rate. The core is protected from dewatering by the following systems and equipment:

- ECS #1;
- ECS #2;
- MCP.

In this case a mode of coolant blowdown into the break mainly impacts these processes determining the time history of a change in pressure and coolant flow rate through the channels in the core.

There are three main phases of the accident. The first phase is reduction of the coolant flow rate through a FA and multiple circulation overturn in the FA with the highest power density. This phase is described by the high power density at a sharp loss of heat removal which can lead to departure from nucleate boiling in the maximum stressed FAs.

The second phase is described by MCP shutoff, coolant backflow through the core at rather high rates in the FA (1÷2 m/s) and ECS actuation.

The third phase is described by a significant reduction of power density in the FA and cooling quasi-steady mode with the flow rates via the channels equal to the feed flow rates.

Early after the initiating event the total coolant flow rate from the primary circuit into the break sharply increases, and there is coolant backflow from the direction of the core. An expansion wave runs along the circuit and the pressure in the core drops sharply leading to an alarm signal at the 0.2 s when a set point is achieved to reduce pressure in the hot collector up to 0.45 MPa (Fig. 4). After initial strong fluctuations the pressure in the circuit is partially restored, and then it decreases gradually.

With a 0.05 s delay the safety rods of 2.8 β_{eff} efficiency will start inserting in the core. This leads to an abrupt reactor power decrease.

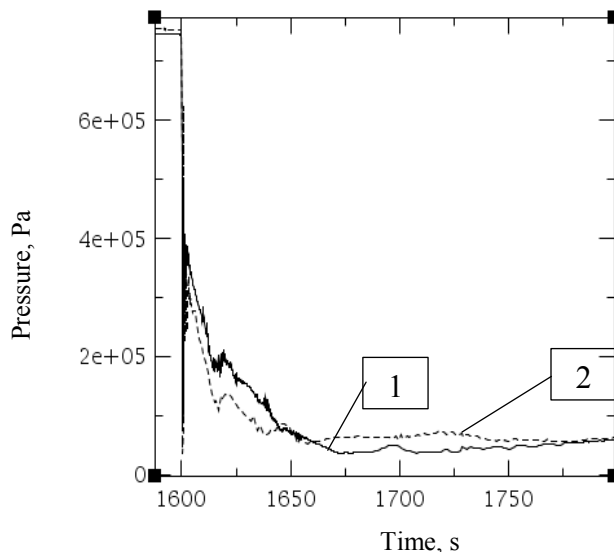


Fig. 4 Change in pressure in hot collectors
(1 – U9%Mo, 2 – UO₂)

In case of using U9%Mo+Al fuel ECS #2 is actuated at the 54th second, and in case of using UO₂+Al fuel – at the 47th second when an alarm set point is achieved to reduce the level up to 1500 mm in the pressurizer. When the emergency signal starts ECS #1 is also actuated with a 25 s delay, however, the main coolant flow from this system runs into the break, and there is the overlapping of a failure on valve KG-5 in the hot collector supply line resulting in no coolant flowing into the core. As per the same set point a signal comes to close the valve, and the pressurizer is cut off from the circuit during 33 seconds.

As a result of an abrupt drop of pressure and coolant flow rate via the maximum stressed FA, in some regions in the gaps between the fuel rods a low heat transfer factor flow mode is implemented (~100-300 W/m²·K). During the 6th second of the process the melting temperature of aluminum matrix and cladding is achieved (660 °C (933 K)) for both FA types due to residual power density in fuel in the separate maximum stressed regions of the fuel rods. These FAs are not considered in further thermal-hydraulic calculations.

For a realistic analysis it is necessary to take into account the blistering effect of fuel rods. After achieving the temperature $\sim (460-550) \text{ }^\circ\text{C}$ due to the blistering effect the outer fuel cladding contacts the channel body wall [10].

This effect increases radial thermal conductivity, and residual power density is removed to the reactor pool water. Thus, the maximal temperature that can be achieved on the fuel rods is determined by the blistering temperature ($460-550 \text{ }^\circ\text{C}$). The effect is possible due to the unique design feature of the MIR reactor (the channel-type reactor immersed in a water pool and tube-type fuel).

Out-of-pile tests of the MIR irradiated fuel showed that at the temperature of $(450\pm 480) \text{ }^\circ\text{C}$ a process of gaseous swelling and blistering starts (Fig. 5).

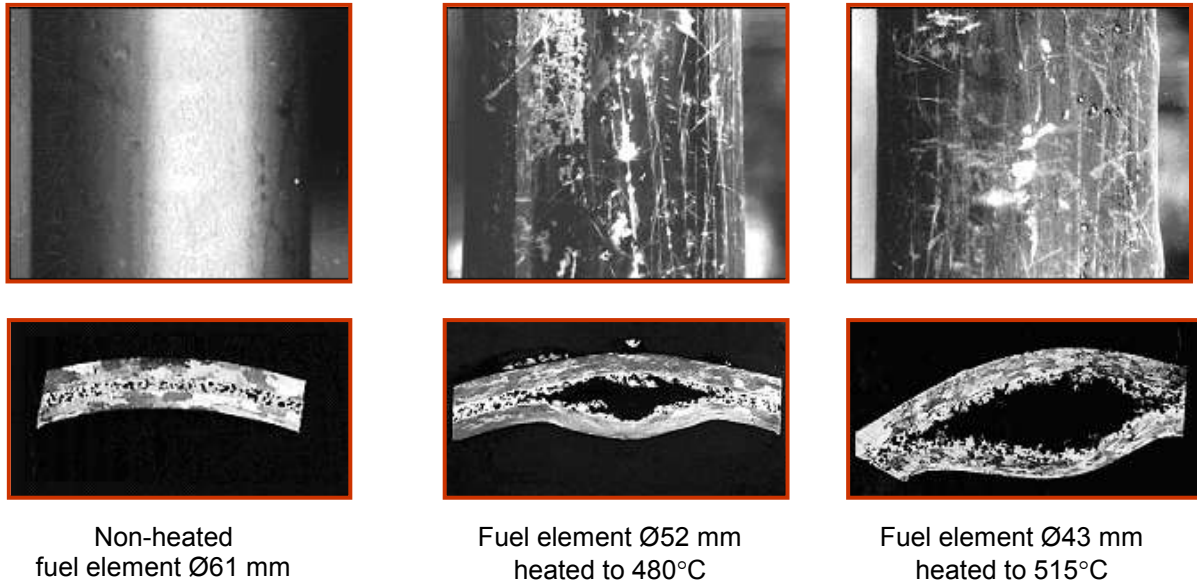


Fig. 5 Gaseous swelling and blistering of the MIR irradiated fuel

During the first seconds after the initiating event the averaged groups of FAs with UO_2+Al fuel show a slight increase in the temperature of the fuel rod claddings (Fig. 6) not exceeding 430K ($157 \text{ }^\circ\text{C}$) due to changes in the flow mode caused by fluctuations of pressure and coolant flow rate. From the 130th second fluctuation modes of coolant flow in the channels are set leading in their turn to fuel cladding temperature fluctuations. At that, the second and third less-stressed groups of FAs show the maximal coolant heating (up to the saturation temperature) as well as coolant boiling along the entire length of the fuel rods.

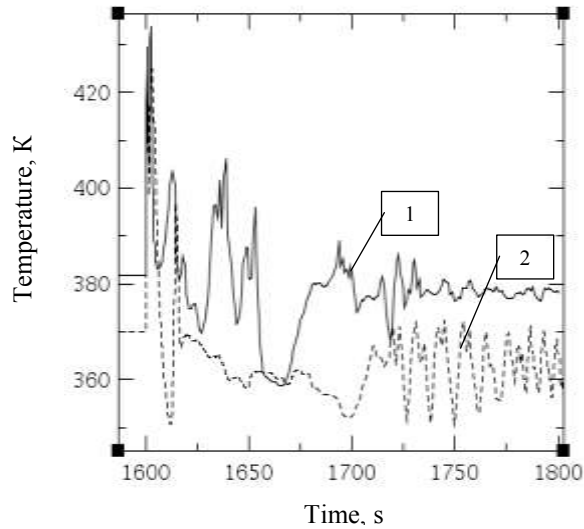


Fig. 6 Peak cladding temperature of the averaged FA groups (1 – U9%Mo, 2 – UO₂)

In the averaged FA groups with U9%Mo+Al fuel the cladding temperature does not exceed 440K (167 °C). At the 150th second there is a relatively stable distribution of the coolant flow rate in the channels under calculations that results in some stabilization in the temperature mode of the fuel rods. The second less-stressed FA group shows the maximal coolant heating (up to the saturation temperature) as well as coolant boiling at the fuel rod top. ECS #2 compensates sufficiently the coolant loss in the reactor channels, which provides safe heat removal from 5 FA groups after the 200th second under a significant decrease of power density (except for the maximum stressed FA).

Thus, as a result of the calculation analysis of the MIR reactor primary circuit pipeline break accident with actuating the emergency cooling system of the pool cooling circuit it is shown that ECS coolant supply from below into the FA operating channels ensures distillate entering the core. That is why after residual power density reduction the core will be filled with water, which provides safe heat removal from the FAs (except for the maximum stressed FA).

6.2 The results of the calculations of the accident with a non-authorized extraction of the maximum efficiency shim rod

The accident initiating event (shim rod non-authorized extraction) occurs at the 100th second. According to the calculation results the accident temporal development with moving a shim rod is practically the same for both fuels (Tab. 6).

Duration of the process for fuel U9%Mo+Al, s	Duration of the process for fuel UO ₂ +Al, s	Description of the event
0	0	All the reactor systems are in the stationary state.
0+	0+	Positive reactivity insertion – a shim rod is extracted.
2.2	2.28	Pre-alarm set point is achieved to actuate scram rods as reactor power increases.
3.5	3.5	Emergency set point is achieved to actuate scram rods.

Duration of the process for fuel U9%Mo+Al, s	Duration of the process for fuel UO ₂ +Al, s	Description of the event
3.55	3.55	Scram rods drop into the core, driving FAs with absorber start inserting into the core (taking into account the delay time).
3.6	3.8	Reactor power achieves the peak value of 97.1 MW; fuel and coolant temperature increases.
4.0+	4.0+	Power decreases. The reactor is in the subcritical state.
100+	100+	New core cooling mode is stabilized.

Tab 6: Consequence of the key event during the accident development

Figure 7 presents the time history of the peak temperature of fuel and the maximum stressed fuel rod cladding as well as washing coolant temperature at the elevation with the maximal temperature of fuel and cladding for both fuels.

The temperature values for UO₂+Al at the peak load at the 3.8th second are 181 °C (454 K) for the fuel meat and 172 °C (445 K) for the fuel rod cladding. The temperature of the coolant washing the stressed fuel rod at that point makes up 89 °C (362 K) not exceeding the saturation temperature at the set pressure. The minimal departure from nucleate boiling ratio (Bernat's correlation) is achieved at the maximal fuel rod heating making up K ~1.7.

The temperature values for U9%Mo+Al at the peak load at the 3.6th second make up 185 °C (458 K) for the fuel meat and 176 °C (449 K) for the fuel cladding. The maximal temperature of the coolant washing the stressed fuel rod at the same point is 88 °C (361 K) that does not exceed the saturation temperature at the set pressure. The minimal departure from nucleate boiling ratio (Bernat's correlation) is achieved at the maximal fuel rod heating making up K ~1.5.

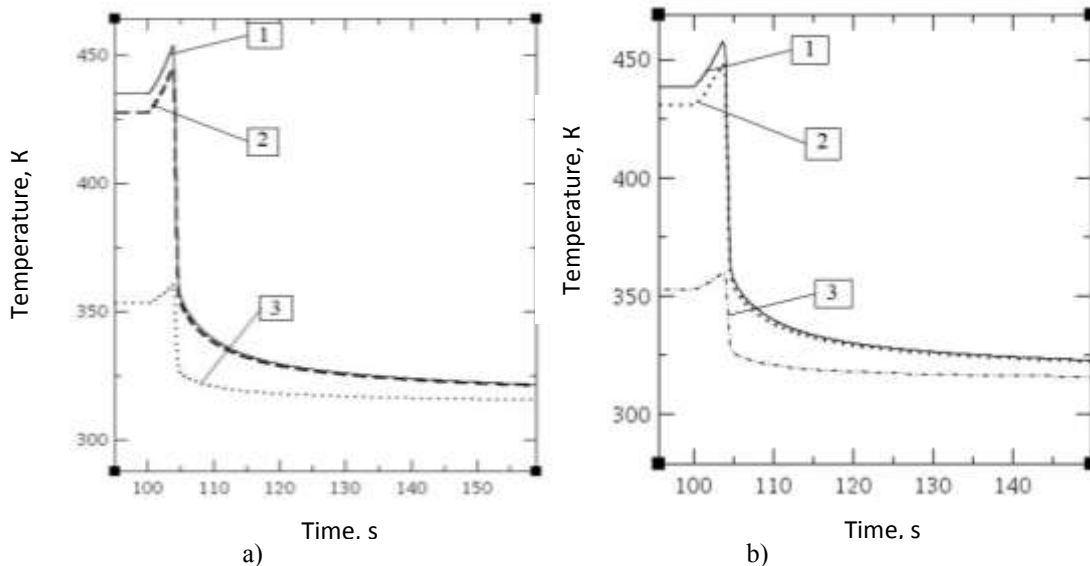


Fig. 7 Change in the maximal temperature of fuel (1), fuel rod cladding (2) and coolant (3): a - UO₂; b - U9%Mo

7. Conclusion

The calculation analysis revealed that conversion of the MIR research reactor to LEU fuel will result in the following changes of its parameters:

1. Fast neutron flux density on the test fuel rod claddings in the loop channels will decrease by 4-6%.
2. Reactivity loss rate as fuel burns up will decrease by 24-32%.
3. Uranium consumption will increase by approximately 4 times with a simultaneous decrease in ^{235}U consumption by 8-12%.
4. Annual FA consumption will decrease by approximately 30%.

In addition, the performed analysis related to accident consequences showed that the existing emergency systems are able to provide reactor cooling and its maintenance in a safe subcritical state.

Thus, the results of the calculation analysis show the possibility in principal of MIR conversion to LEU fuel with no worsening of its safety operating parameters and no significant changes in its experimental capabilities.

References

1. *Izhutov A.L., Mainskov S.V., Pimenov V.V., Starkov V.A., Svyatkin M.N.* State of Work on Calculation Studies of the MIR Reactor Conversion. 33rd International Meeting on Reduced Enrichment for Research and Test Reactors. Chile. Santiago. 23-27 October. 2011.
2. *Gomin E.A.* MCU-4 Status. VANT, Nuclear Reactor Physics Series, 2006. Issue 1. P.6-32.
3. *Yudkevich M.S.* BURNUP Software for Calculation of Reactor Isotopic Composition during the Reactor Run. Preprint IAE-6048/5-M., 1997.
4. *Bergles A.E., Rohsenow W.M.* The determination of forced convection surface boiling heat transfer. Transactions ASME 86//Journal of Heat Transfer. Series C. – 1964. – P. 365-371.
5. *Fabrega S.* Le calcul thermique des reacteurs de recherche refroidis par eau/Rapport CEA-R-4114, 1971.
6. *Mirshak S., Durant W.D., Towell R.H.* Heat Flux at Burnout. DuPont, DP-335, February, 1959.
7. RELAP5/MOD3, Volume 1-7. Code manual. NUREG/CR-5535 INEL-95/0174, 1995.
8. Nuclear Research Facility Safety Report Content Requirements, NP-049-03, Gosatomnadzor, Moscow, 2003.
9. Research Reactor Nuclear Safety Rules, NP-009-04, Gosatomnadzor, Moscow, 2004.
10. *A.L. Izhutov, V.V. Aleksandrov, A.Ye. Novoselov et. al.* "Results of out-of-pile tests of the MIR reactor irradiated fuel at high temperatures". Transactions of 9th International Topical Meeting on Research Reactor Fuel Management, Budapest, Hungary, April 10-13, 2005, pp.137-143.

NEUTRONIC COMPARISON OF HIGH DENSITY FUELS (U-MO-AL AND U₃Si₂-AL) FOR RESEARCH REACTORS

R. O. R. MUNIZ, A. T. SILVA, D. B. DOMINGOS, A. SANTOS, M. YAMAGUCHI
*Instituto de Pesquisas Energéticas e Nucleares - Comissão Nacional de Energia Nuclear
(IPEN/CNEN-SP)*

Av. Professor Lineu Prestes, 2242, Cidade Universitária, 05508-000 São Paulo, SP - Brazil

ABSTRACT

The aim of this paper is to compare the infinite multiplication factor (K_{∞}), obtained through neutronic calculation with the code Scale 6.0, for fuel elements reflected in all directions containing U₃Si₂-Al and U-Mo-Al dispersion fuels. The U₃Si₂-Al dispersion fuels used in the calculation have a uranium density between 3.0 and 5.5 gU/cm³ and the U-Mo-Al dispersion fuels have densities ranging from 4.0 to 7.52 gU/cm³ and 7 and 10% Mo addition. The results show that the K_{∞} calculated for U-Mo-Al fuels are smaller than that for U₃Si₂-Al fuels and increases between the uranium densities of 4 and 5 gU/cm³ and decreases for higher uranium densities.

1. Introduction

Nuclear fuels composed by uranium metal alloys in monolithic and dispersed forms have been considered for research and power reactors due to their density properties and fast heat transfer. Among several candidates, U-Mo alloys are one of the most promising systems for plate type fuel elements owing to its broad gamma-phase stable field. This fact allows extensive fabrication capability since cubic gamma-phase shows good plasticity, higher strength and elongation [1]. Because of the high uranium density and good irradiation stability of U-Mo alloys, this fuel in the form of a dispersion in an Al matrix is the choice for the conversion of research and material test reactors currently using highly enriched uranium (HEU) to low-enriched uranium (LEU). The formation of an interaction layer between U-Mo particles and the Al matrix as a result of inter-diffusion has become a major issue for the performance of this fuel [2]. The formation of an interaction product in this dispersion fuel is unfavorable because of its low thermal conductivity and volume expansion as it consumes the Al matrix. Depending on the irradiation conditions (high burnup or high heat flux), large pores are formed at the interface of the interactions products and the Al matrix, which could eventually lead to a fuel plate failure. Many post irradiation tests have been conducted for uranium alloys with a molybdenum content between 6 to 10% by weight allowing the characterization of U-Mo-Al interaction [3], and this fuel qualification is a on-going process.

U₃Si₂-Al dispersion fuel with a uranium density of 3.5 gU/cm³ is being considered as the fuel for the first core of the new Brazilian Multipurpose Reactor (RMB) [4]. The aim of this paper is to compare the calculated infinite multiplication factor (K_{∞}), obtained through neutronic calculation with the code Scale 6.0 [5], for fuel elements reflected in all directions using U₃Si₂-Al and U-Mo-Al dispersion fuels. These results will be utilized in the future to verify the core performance improvements that can be obtained for an already designed research reactor using a different fuel assembly with higher densities.

The U₃Si₂-Al dispersion fuel used in the calculation has a uranium density between 3.0 and 5.5 gU/cm³ and the U-Mo-Al dispersion fuels have densities ranging from 4.0 to 7.52 gU/cm³ and 7 to 10% Mo addition. The percentage by weight of molybdenum (Mo) in the dispersion changes the neutronic behavior of the fuel since the neutron absorption by Mo is considerable higher than that by Silicon (Si). Fig 1 shows a comparison between the neutron absorption cross section of Mo and Si [6].

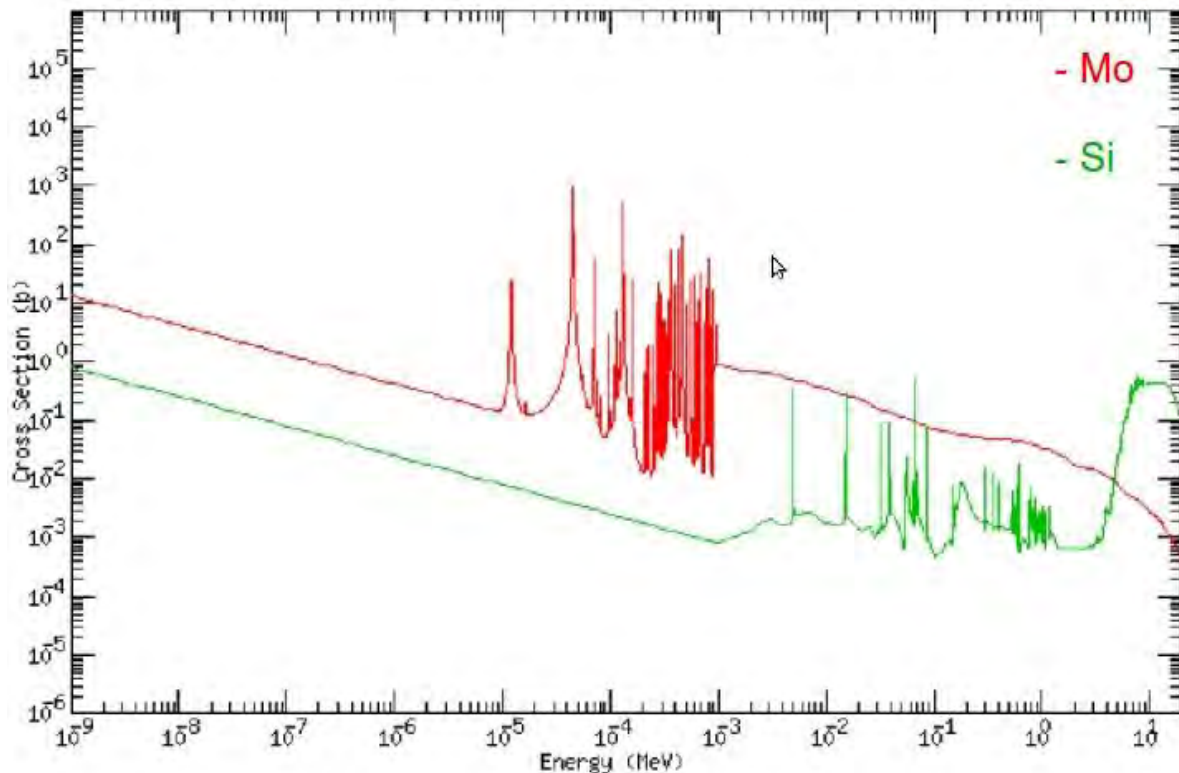


Fig 1: Neutron absorption cross section for Mo and Si.

2. Infinite multiplication factor (k_{∞}) calculation

2.1 Computer simulation

The computer code Scale 6.0 was used to calculate the infinite multiplication factor. The cross sections were processed with the modules Triton and Bonami that uses the Bondarenko method for calculating the self-shielding in the energy ranges of the unresolved resonance regions. The neutron transport was calculated with KENO V.a using the Monte Carlo method for the neutron fluxes determination.

The fuel elements proposed and analyzed in this work (Fig 2) consisted of 21 rectangular aluminum coated plates and its structure is an aluminum frame where the fuel plates are fitted. The internal plates in the fuel element measure 7.049 cm x 61 cm, 0.135 mm thick, and the two external fuel plates are 0.150 mm thick. Both the U_3Si_2 -Al meat and the U-Mo-Al meat are 6.5 cm x 61 cm, 0.061 cm thick. The space between the plates forms the cooling channel that is 0.245 cm thick. In the simulation this area was filled with water as well as the region around the fuel element which was modeled as a layer of 0.05 cm of water.

The concentrations used in this study are the same used in the reference [7] to simulate one U-Mo-Al plate and where only one U_3Si_2 -Al uranium density was considered.

3. Results and conclusions

The calculated infinite multiplication factors (K_{∞}) obtained from the simulations with the code scale 6.0 are shown in Tables 1, 2 and 3. Fig 3 presents the infinite multiplication factors plotted against U_3Si_2 -Al uranium density ranging from 3.0 to 5.5 gU/cm³. Fig 4 presents the infinite multiplication factors plotted against U-Mo-Al with uranium densities from 4.0 to 7.52 gU/cm³ and 7 and 10% Mo addition.

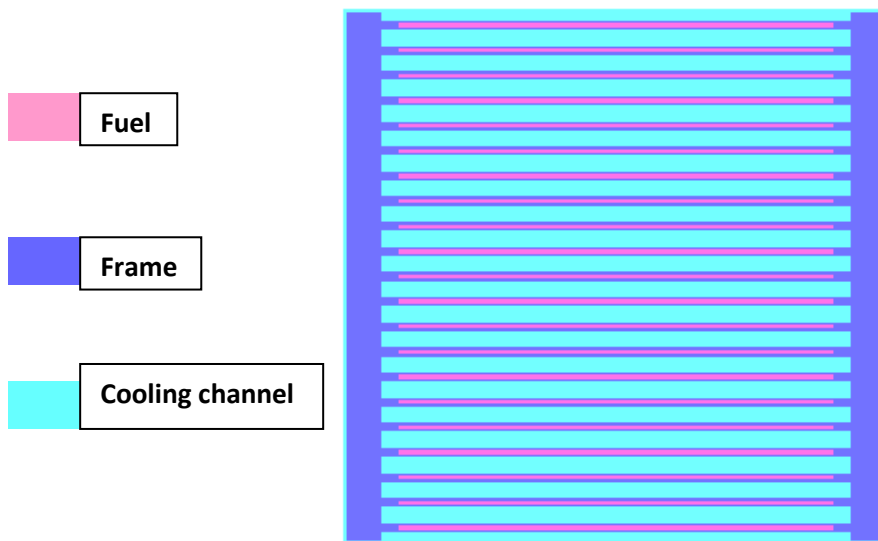


Fig 2: Fuel element cross section.

Tab 1: Infinite multiplication factors for U_3Si_2/Al fuels ranging from 3.0 to 5.5 gU/cm³.

Uranium density (gU/cm ³)	K_{∞}	* σK_{∞}
3.00	1.60245	0.00011
3.30	1.61618	0.00011
3.50	1.62388	0.00010
3.80	1.63320	0.00010
4.00	1.63843	0.00011
4.30	1.64479	0.00010
4.50	1.64847	0.00011
4.80	1.65258	0.00010
5.00	1.65558	0.00010
5.30	1.65779	0.00010
5.50	1.65925	0.00011

* Uncertainty

Tab 2: Infinite multiplication factors for U-7wt%Mo-Al fuels ranging from 4.0 to 7.52 gU/cm³.

Uranium density (gU/cm ³)	K _∞	σK _∞
4.01	1.62851	0.00011
4.55	1.63652	0.00010
5.02	1.64365	0.00011
5.55	1.64402	0.00011
6.02	1.64499	0.00011
6.55	1.64497	0.00011
7.02	1.64440	0.00011
7.52	1.64285	0.00011

Tab 3: Infinite multiplication factors for U-10wt%Mo/Al fuels ranging from 4.0 to 7.11 gU/cm³.

Uranium density (gU/cm ³)	K _∞	σK _∞
4.01	1.62273	0.00011
4.52	1.63037	0.00011
5.02	1.63485	0.00010
5.56	1.63746	0.00011
6.00	1.63801	0.00011
6.54	1.63793	0.00011
7.01	1.63678	0.00011
7.11	1.63657	0.00011

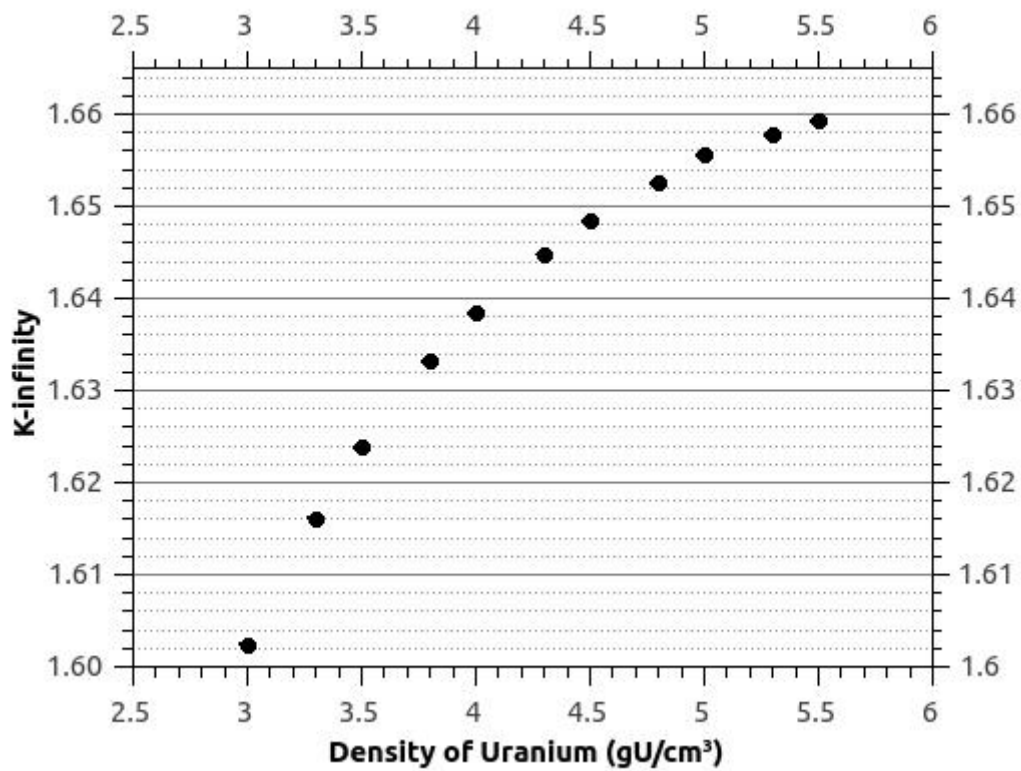


Fig 3: K_{∞} for U_3Si_2-Al fuels with uranium densities ranging from 3.0 to 5.5 gU/cm^3 .

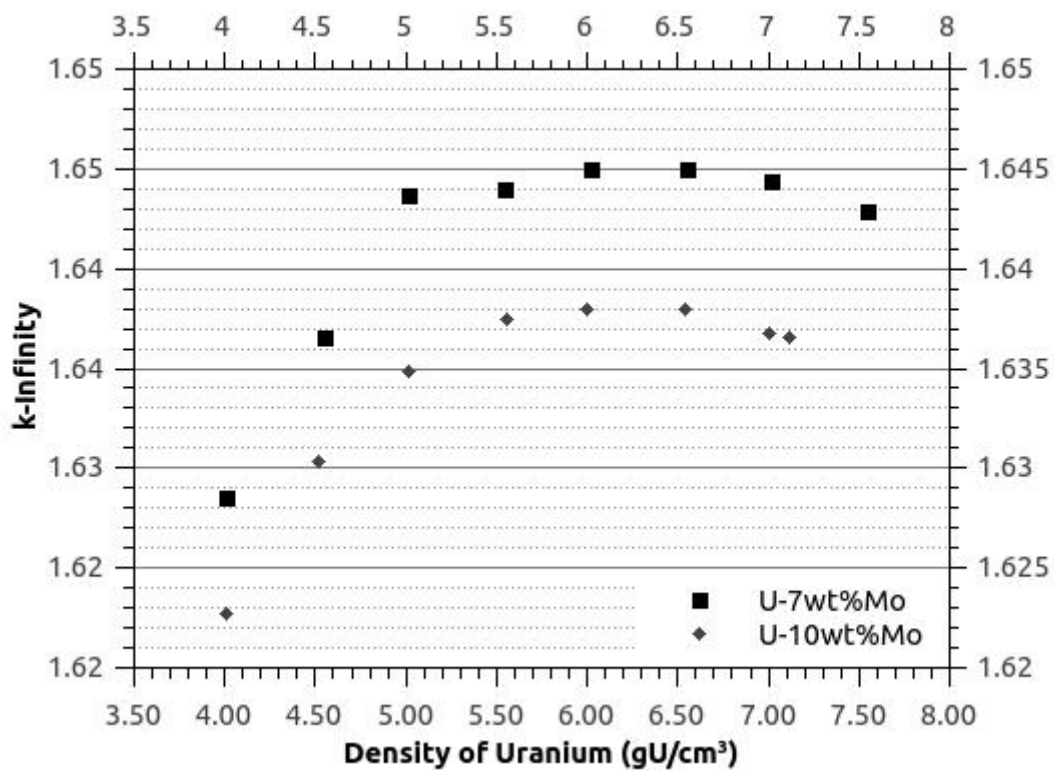


Fig 4: K_{∞} for U-7wt%Mo-Al and U-10wt%Mo-Al with uranium densities ranging from 4.01 to 7.52 gU/cm^3 .

It can be seen from Fig 3 that the K_{∞} values obtained for different uranium densities with U-10wt%Mo/Al fuels are below those obtained with U-7wt%Mo/Al fuels. This behavior was expected due to the different absorption cross section of the two materials.

The potential benefits of the high density fuel will depend on the research reactor to be upgraded. A priori, it is difficult for potential users to clearly understand what kind of economic or improvement benefits can be expected. Further works are being conducted in order to identify improvements in core performance (higher neutron fluxes) and on the impact of fuel density on the cost of the research reactor fuel cycles (to reduce the number of fuel assemblies needed for operation) [8].

The results of this work confirm those obtained in reference 7, where was examined only a generic fuel plate. In a next step It will be analysed the performance of the U_3Si_2 -Al and U-Mo-Al fuels with burnup.

Acknowledgements

The authors are grateful for financial support from CAPES.

4. References

- [1] D. A. Lopes, T. A. G. Restivo, R. G. Gomide, A. F. Padilha, "Processing Window Design for U Alloys", *Transactions RRFM 2012*, Prague, 18-22 March, pp. 46-51 (2012).
- [2] H. J. Ryu, J. M. Park, J. H. Yang, C. K. Kim, Y. H. Jung and Y. S. Kim, "Interdiffusion in the Si-Rich Layer of U-Mo/Al-Si Fuel", *Transactions RERTR 2010*, Lisbon-Portugal, October 10-14, 2010.
- [3] M. K. Meyer, D. M. Wachs, J. -F. Jue, D. D. Keiser, J. Gan, F. Rice, A. Robison, N. E. Wooltenhulme, P. Medvedev, G. L. Hofman, Y.-S. Kim, "U.S. Progress in the Development of Very High Density Low Enrichment Research Reactor Fuels", *Transactions RRFM 2012*, Prague, 18-22 March, pp. 10-13, 2012.
- [4] J. A. Perrotta, A. J. Soares, "RMB: The New Brazilian Multipurpose Research Reactor", *International Journal for Nuclear Power, atw vol. 60 (2015), Issue 1, January*.
- [5] "Scale: A Modular Code System for Performing Standardized Computer Analyses for Licensing Evaluation", ORNL/TM-2005/39, Version 5.1, Vols. I-III, November 2006. This code is available from Radiation Safety Information Computational Center at Oak Ridge National Laboratory as CCC-732.
- [6] Cross Section Plotter. "<http://atom.kaeri.re.kr>" (2013).
- [7] R. O. R. Muniz, D. B. Domingos, A. Santos, A. T. Silva, T. G. João, V. O. Aredes, "Neutronic Comparison of the Nuclear Fuels U_3Si_2 /Al and U-Mo/Al", *Transactions of 2013 International Nuclear Atlantic conference – INAC 2013*, Recife, PE, Brazil, 24-29, 2013.
- [8] E. A. Vilarino, "Core Performance Improvements Using High Density Fuel in Research Reactors", *Transactions RRFM 2013*, St. Petersburg-Russia, 21-25 April, pp. 68-75, 2013.

COMPARISON OF LOW ENRICHED URANIUM (UAl_x-Al AND U-Ni) TARGETS WITH DIFFERENT GEOMETRIES FOR THE PRODUCTION OF MOLYBDENUM-99

D. B. DOMINGOS, A. T. SILVA, T. G. JOÃO, R. O. R. MUNIZ

*Instituto de Pesquisas Energéticas e Nucleares - Comissão Nacional de Energia Nuclear
(IPEN/CNEN-SP)*

Av. Professor Lineu Prestes, 2242, Cidade Universitária, 05508-000 São Paulo, SP - Brazil

ABSTRACT

The IEA-R1 reactor of IPEN-CNEN/SP in Brazil is a pool type research reactor cooled and moderated by demineralized water and having Beryllium and Graphite as reflectors. In 1997 the reactor received the operating licensing for 5 MW. A new research reactor is being planning in Brazil to replace the IEA-R1 reactor. This new reactor, the Brazilian Multipurpose Reactor (RMB), planned for 30 MW, is now in the detailed design phase. Low enriched uranium (<20% ²³⁵U) targets (UAl_x dispersed in Al and metallic U foils with different geometries) are being considered for the production of Molybdenum-99 (⁹⁹Mo) by fission in Brazil. Neutronic and thermal-hydraulics calculations were performed to determine the production of ⁹⁹Mo for the UAl_x-Al targets irradiated in the IEA-R1 reactor core and for three different types of targets (UAl_x-Al, U-Ni cylindrical and U-Ni plate) irradiated in a reactor conception with the same power of the RMB. The neutronic analyses showed that the total activity obtained for ⁹⁹Mo for 10 UAl_x-Al miniplates with a mass of 20,1 g of ²³⁵U irradiated in the IEA-R1 reactor core was 1406.63 Ci. Considering that the time needed for the chemical processing and recovering of the ⁹⁹Mo will be seven days after the irradiation, the total ⁹⁹Mo activity available for distribution will be 240.48 Ci. No thermal-hydraulics design limit was overtaken. The same calculations were performed for three targets (UAl_x-Al, U-Ni cylindrical and U-Ni plate) irradiated in a reactor conception of 30 MW with a ²³⁵U mass of 20.1 g. The ⁹⁹Mo activities produced were, respectively, 2,980.62 Ci, 3,166.6 Ci and 3495.23 Ci for the three targets. At the end of 7 days of irradiation, the total activity obtained for the targets were, respectively, 509.57 Ci, 541.36 Ci and 597.5 Ci. The thermal hydraulics analyses show that a minimum coolant speed of 7 m/s for the UAl_x-Al target, 8 m/s for the U-Ni cylindrical target and 9 m/s for the U-Ni plate target will be necessary through the irradiation device to cool the targets and not exceeding the thermal-hydraulics design limits.

1. Introduction

^{99m}Tc, product son of ⁹⁹Mo, is one of the most utilized radioisotopes in nuclear medicine in the world. Annually it is used in approximately 20 to 25 million procedures of medical diagnosis, representing about 80% of all the nuclear medicine procedures [1]. Since 2004, given the worldwide interest in ⁹⁹Mo production, the International Atomic Energy Agency (IAEA) has developed and implemented a Coordinated Research Project (CRP) [2] to help interested countries start a small-scale domestic ⁹⁹Mo production in order to meet the requirements of the local nuclear medicine. The purpose of this CRP is to provide interested countries with access to non-proprietary technologies and methods for production of ⁹⁹Mo using targets of thin foils of metallic low enriched uranium (LEU), UAl_x-Al miniplates of LEU type or by neutron activation reaction (n, gamma), for example, using gel generators. Brazil, through IPEN-CNEN/SP, began its CRP participation in late 2009. IPEN-CNEN/SP provides radiopharmaceuticals to more than 300 hospitals and clinics in the country, reaching more than 3.5 million medical procedures per year. The use of radiopharmaceuticals in the country over the last decade has grown at a rate of 10% per year and IPEN/CNEN-SP is primarily responsible for this distribution. ^{99m}Tc generators are the most used ones and are responsible for more than 80% of the radiopharmaceuticals applications in Brazil.

IPEN/CNEN/SP imports all the ^{99}Mo used in the country (450 Ci of ^{99}Mo per week or 24,000 Ci per year approximately). In the past, IPEN/CNEN-SP developed the ^{99}Mo production route from neutron activation of ^{98}Mo targets in the IEA-R1. However, the quantity produced does not meet the Brazilian needs of this isotope. Due to the growing need for nuclear medicine in the country and because of the short ^{99}Mo supply observed since 2008 on the world stage, IPEN/CNEN-SP has decided to develop its own project to produce ^{99}Mo through ^{235}U fission. This project has three main goals: 1) research and development of ^{99}Mo production from fission of LEU targets, 2) discussion and decision on the best production route technique, and 3) feasibility study of IPEN/CNEN-SP in reaching a routine production of ^{99}Mo . The main goal of IPEN/CNEN-SP is to accommodate the Brazilian demand for radiopharmaceuticals. Nowadays, this demand is about 450 Ci of ^{99}Mo per week and the future need, after six years, is estimated at around 1,000 Ci per week. One of the analyses planned in this project is to study the characteristics and specifications of $\text{UAl}_x\text{-Al}$ and metallic uranium thin foils targets. The first aim of the present work was to perform neutronic calculations to evaluate the ^{99m}Mo production through fission at the IEA-R1 reactor and at a reactor conception with the same power of the RMB [3], designate in this paper as RC. The second aim of this work is to perform thermal-hydraulics calculations to determine the maximal temperatures achieved in the targets during irradiation and compared them with the design temperature limits established for $\text{UAl}_x\text{-Al}$ e uranium thin foils targets.

2. $\text{UAl}_x\text{-Al}$ and uranium thin foil targets used in the neutronic and thermal-hydraulics analysis

The $\text{UAl}_x\text{-Al}$ targets of LEU type proposed and analyzed in this work are aluminum coated miniplates (Fig 1). Each miniplate measures 4.7 cm x 17 cm, 0.152 cm thick, corresponding to a total volume of 12.2 cm³. The $\text{UAl}_x\text{-Al}$ meat is 4.0 cm x 11.8 cm, 0.076 cm thick, leading to a total volume of 3.59 cm³. Considering this volume and a ^{235}U mass in the target equals to 2.01 g, the ^{235}U density ($\rho_{\text{U-235}}$) in the target meat is 0.58 g $^{235}\text{U}/\text{cm}^3$. For a 19.9% ^{235}U enrichment, the uranium density in the target is $\rho_{\text{U}} = 2.91 \text{ gU}/\text{cm}^3$. This corresponds to a UAl_x volume fraction of 45% and an aluminum volume fraction of 55% in the dispersion.

A special Miniplate Irradiation Device (MID) was designed for the irradiation of the $\text{UAl}_x\text{-Al}$ targets in the IEA-R1 and in the reflector part of the RC (Fig 2), whose external dimensions are 76.2 mm x 76.2 mm x 88.74 cm. The miniplates will be allocated in a box with indented bars placed inside the external part of the MID. Fig 3 shows the MID cross section. As seen from Fig 3, up to ten $\text{UAl}_x\text{-Al}$ targets can be placed in the box with indented bars inside of the MID.

The targets of metallic Uranium foils with cylinder geometry analyzed at IPEN/CNEN-SP were based on targets that were examined in the Tajoura reactor in Libya to produce ^{99}Mo [4]. The targets were mounted in cylindrical geometry, in a tubular arrangement. The metallic U foil was covered with a Ni sheet before being placed concentrically inside the aluminum tubes. The dimensions of the target are (see Fig 4):

1. One foil of uranium (LEU) of 46.05 cm x 87.7 mm x 135 μm ;
2. Coating nickel foil of 20 μm thickness;
3. Two aluminum cylinder having 46.05 cm length, outside diameters of 27.88 and 30.00 mm, and inside diameters of 26.44 and 28.22 mm, respectively;
4. ^{235}U mass of 20.1 g, with 19.9% enrichment of ^{235}U .

Fig 5 shows the set of concentric cylinders (Fig 6) positioned in a device with the same dimensions of the MID.

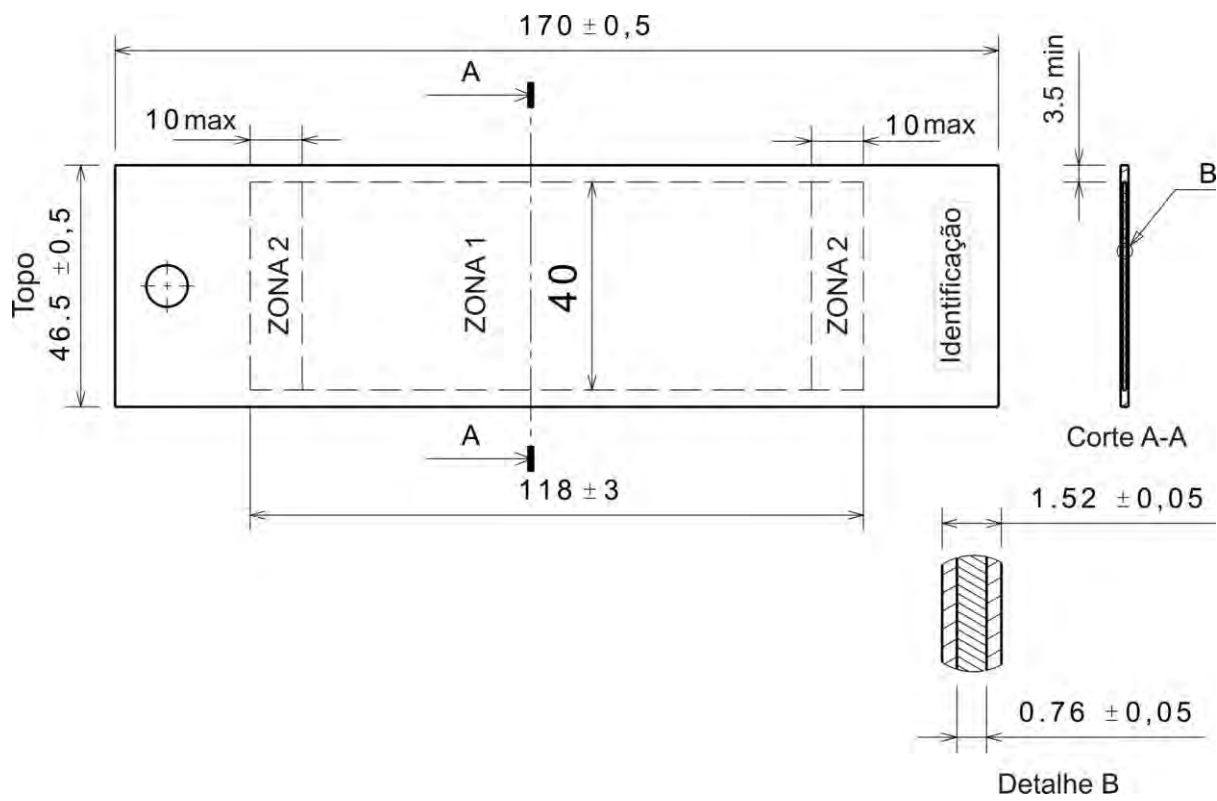


Fig 1: UAlx-Al miniplate dimensions.

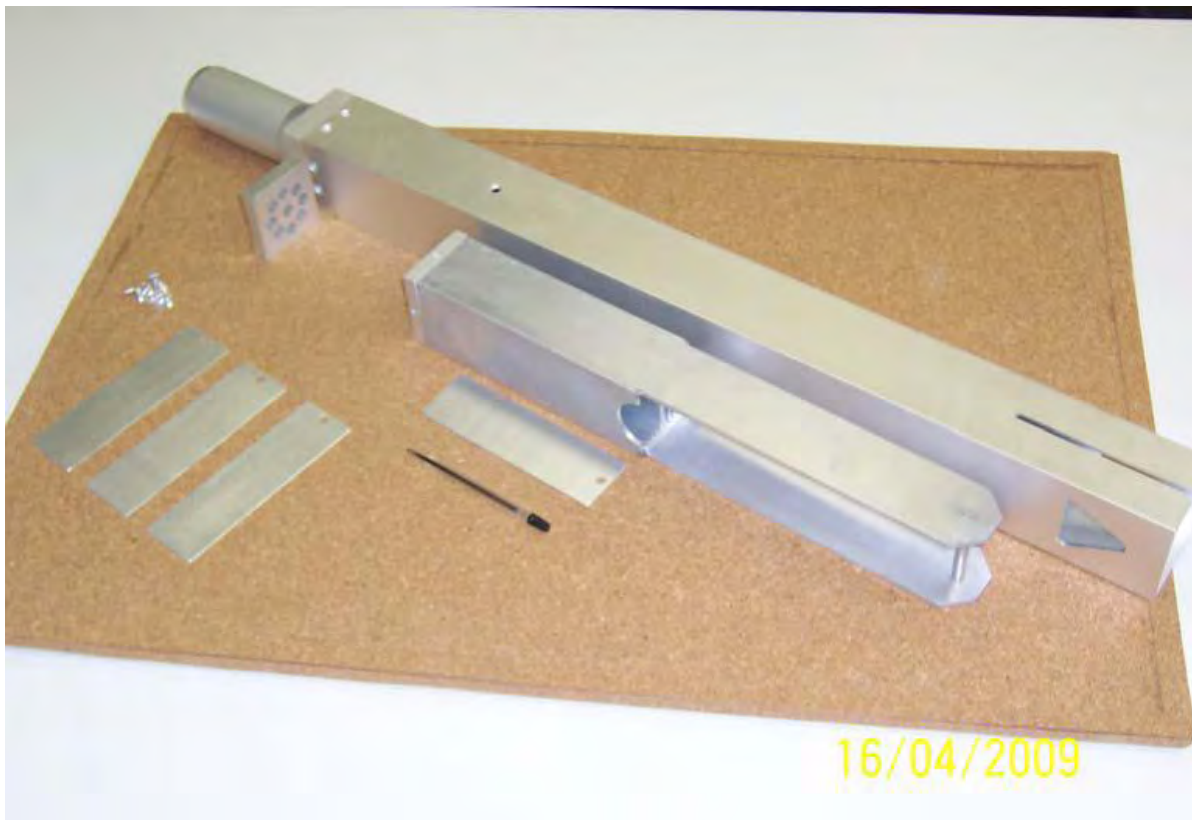


Fig 2: Miniplate irradiation device – MID.

Radius	Length (cm)
AB	1.00
AC	1.322
AD	1.394
AE	1.396
AF	1.4095
AG	1.411
AH	1.5
AI	1.75
AJ	1.9
AK	2.2
AL	3.81

Fig 4: Irradiation device horizontal cross section for the U-Ni target with cylinder geometry.



Fig 5: Set of concentric cylinders positioned in the MID.

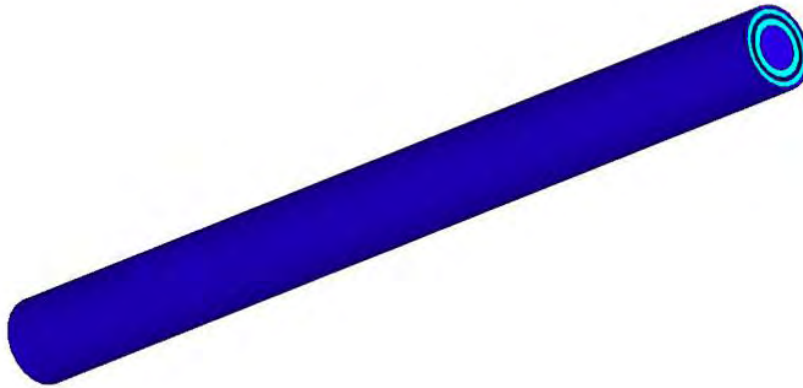


Fig 6: Set of concentric cylinders of U-Ni foil target.

The targets of metallic uranium foils with plate geometry were based on targets that were examined in the Paskitan research reactor [5] and consists of a uranium foil (19.99% ^{235}U) with a thickness of 135 μm enveloped in 20 μm thick nickel foil and placed between two aluminum plates that are welded from all sides. Each U-Ni plate has a uranium density of 2.01 g. The geometry of the foil plate target is shown in Figures 7 and 8.

For the performed calculations, the U-Ni targets (cylindrical and plate geometries) were modeled in the same irradiation device utilized for the calculations of the UAix-Al targets.

The targets were modeled and simulated in peripheral core position of the RC, in the heavy water reflector. The target irradiation time was defined according to their current and planned operating cycle.

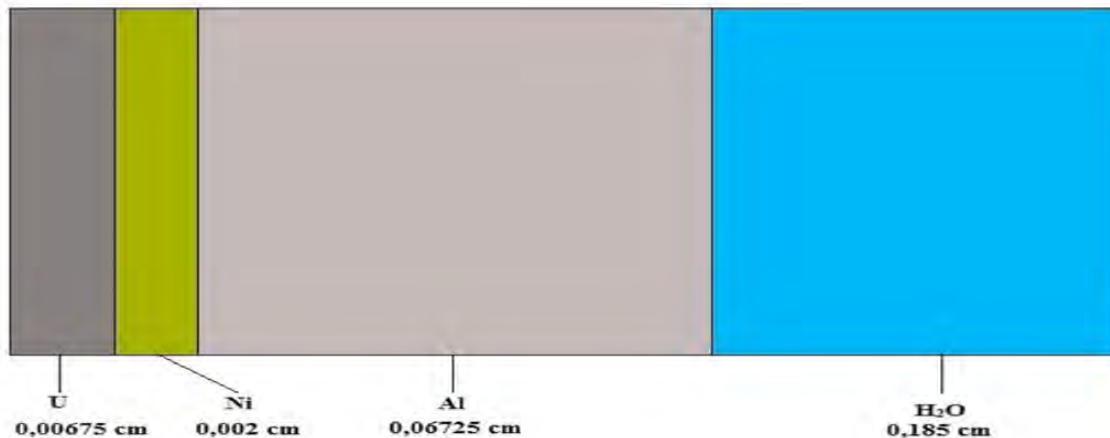


Fig 7: Half the thickness of U-Ni LEU target with plate geometry (67.5 μm), nickel foil, aluminum plate and cooling channel.

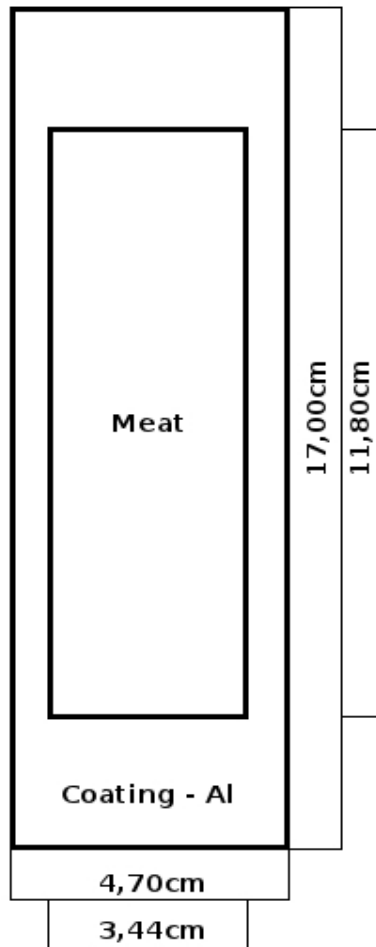


Fig 8: Width and height of the U-Ni plates.

3. Neutronic calculation for UAl_x-Al and U-Ni targets

The cores of the IEA-R1 and RC reactors as well as the UAl_x-Al and the U-Ni targets used for the ⁹⁹Mo production were modeled with the HAMMER-TECHNION [6] and CITATION [7] numerical codes.

To simulate the targets in the IEA-R1 reactor, it was created a fictitious core, reflected with Beryllium, composed of 24 fuel elements of U₃Si₂-Al, 4 control elements, with density of 1.2 gU/cm³. All fuel and control elements were taken as new and the adopted power operation was 5 MW. The cross sections of all elements were generated with HAMMER-TECHNION. The code CITATION was used to create the 3D model of the core and to determine parameters such as K-effective, neutron flux and power density. The SCALE 6.0 code system [8] was used to perform burnup calculations for each target and also to determine the ⁹⁹Mo activity at the end of irradiation. The target irradiation times for each reactor were defined according to their current and planned operating cycle. The UAl_x-Al targets were modeled and simulated in the IEA-R1 core central position. The target irradiation time was three (3) days. At the end of irradiation, the total activity obtained for the 10 UAl_x-Al was 1,406.63 Ci. Considering that the time needed for the chemical processing and recovering of the ⁹⁹Mo will be seven days after the irradiation, the total ⁹⁹Mo activity available for distribution will be 240.48 Ci [9].

The RC conceptual design used was an open pool type, 30 MW thermal power reactor. The RC core has a 5x6 configuration with MTR-type U_3Si_2 -Al fuel elements with 19.75 wt% uranium-235 enrichment. The reactor core is light water cooled and moderated, using heavy water as reflector. The UAl_x -Al and U-Ni targets were modeled and simulated in a peripheral core position at the heavy water reflector using 30 U_3Si_2 -Al fuel elements whose density was 1.9 gU/cm^3 . The total activity obtained for the 10 UAl_x -Al miniplates and for the U-Ni cylindrical and plate type targets were, respectively, 2,980.62 Ci, 3,166.6 Ci and 3,495.23 Ci. Considering that the time needed for the chemical processing and recovering of the ^{99}Mo will be seven (7) days after the irradiation, the total activity obtained for the 10 UAl_x -Al miniplates and for the U-Ni cylindrical and plate types targets were, respectively, 509.57 Ci, 541.36 Ci and 597.5 Ci.

4. Thermal Hydraulics Calculation for the Irradiation Device

A thermal-hydraulics model MTCR-IEA-R1 [10] was developed in 2000 at IPEN/CNEN-SP using a commercial program Engineering Equation Solver (EES). The use of this computer model enables the steady-state thermal and hydraulics core analyses of research reactors with MTR fuel elements. The following parameters are calculated along the fuel element channels: fuel meat central temperature (T_c), cladding temperature (T_r), coolant temperature (T_f), Onset of Nucleate Boiling (ONB) temperature (T_{onb}), critical heat flux (Departure of Nucleate Boiling-DNB), flow instability and thermal-hydraulics safety margins MDNBR and FIR. The thermal-hydraulics safety margins MDNBR and FIR are calculated as the ratio between, respectively, the critical heat flux and the heat flux for flow instability and the local heat flux in the fuel plate. Furthermore, the MTCR-IEA-R1 model also utilizes in its calculation the involved uncertainties in the thermal-hydraulics calculation such as: fuel fabrication uncertainties, errors in the power density distribution calculation, in the coolant flow distribution in the core, reactor power control deviation, in the coolant flow measures, and in the safety margins for the heat transfer coefficients. The calculated thermal-hydraulics core parameters are compared with the design limits established for MTR fuels: a) cladding temperature $< 95^\circ\text{C}$; 2) safety margin for ONB > 1.3 , or the ONB temperature higher than coolant temperature; 3) safety margin for flow instability > 2.0 ; and 4) safety margin for critical heat flux > 2.0 . For the targets, it was considered the following design limits: 1) no material may experience a temperature greater than $\frac{1}{2}$ any target material melting temperature. The lowest melting temperature for any of the proposed target materials is that of the aluminum cladding, whose melting temperature is 660°C . Therefore 330°C is the maximum allowable temperature for the LEU target; 2) the pool coolant must be kept below its saturation temperature. In this work it was adopted as target design limit the cladding temperature that initiated the coolant nucleate boiling (T_{ONB}) for a given coolant pressure and superficial heat flux given by Bergles and Rosenow correlation [11].

In order to evaluate the temperatures achieved in the targets different coolant velocities were tested through the MID. For the temperature calculations of the UAl_x -Al targets the thermal-hydraulics model MTCR-IEA-R1 was used and the results were obtained for the analysis of the IEA-R1 and RC cores. The same procedure was used to calculate the temperatures achieved in the U-Ni target with plate geometry. For the calculation of the temperatures of the U-Ni targets with cylindrical geometry was utilized the software ANSYS CFX [12]. The power density (25 KW/cm^3) calculated in the ID position in the RC reflector with the code MTCR-IEAR1 was utilized as input data to determine the temperatures in the U-Ni target with cylindrical geometry.

The placement of the MID in the core central position of IEA-R1 reactor will deviate part of the reactor flow rate to cool the UAl_x -Al targets. The flow rate in the core of the IEA-R1 reactor is 3,400 gpm which provides a flow rate of approximately $23 \text{ m}^3/\text{h}$ per fuel element, and sufficient to cool a standard fuel element. The insertion of the MID in the IEA-R1 reactor core will divert part of the reactor core coolant to cool the UAl_x -Al miniplates. Thus, a MID

thermo-hydraulic analysis was developed to determine the required coolant velocity to cool the miniplates, but without damaging the fuel elements in the reactor core. Coolant velocities from 5 to 15 m/s were tested through the MID. Table 1 provide the calculated UA_{Ix-AI} target temperatures for different coolant velocities through the MID in the IEA-R1 reactor core. The simulations considered the MID with ten identical UA_{Ix-AI} miniplates. Table 1 show that coolant velocities equal or higher than 5 m/s through the MID are sufficient to cool the targets without achieving ONB temperatures. The calculated cladding temperatures are below the value of 128.5 °C, indicating one-phase flow through the targets. As calculated in the reference 13, even coolant velocities of 1.78 m/s will be sufficient to cool the targets and a coolant flow restrictor (see Fig 1) was fabricated in order to maintain a MID flow rate of 12 m³/hr in the reactor core during target irradiation.

Tab 1: Target temperatures versus DIM coolant velocities in the IEA-R1 reactor.

Coolant velocity (m/s)	UA _{Ix-AI} meat central temperature (°C)	UA _{Lx-AI} aluminum cladding temperature (°C)	ONB Temperature (T _{ONB}) (°C)	Coolant Temperature (°C)
5	111.2	99.06	128.5	45.00
6	103.2	91.07	128.5	44.48
7	97.38	85.21	128.5	44.11
8	92.89	80.71	128.5	43.84
9	89.32	77.14	128.5	43.63
10	86.42	74.24	128.5	43.46
11	85.15	72.98	128.5	43.39
12	82.93	70.75	128.5	43.27
13	81.04	68.86	128.5	43.16
14	79.40	67.23	128.5	43.08
15	77.98	65.80	128.5	43.00

Table 2 provides the calculated UA_{Ix-AI} target temperature results for different coolant velocities through the MID placed in the peripheral RC core position in the heavy water reflector. The simulations considered the MID with ten identical UA_{Ix-AI} miniplates. Table 2 shows that a velocity of 7 m/s is necessary to cool the targets. For this velocity no design limit was achieved for the analyzed irradiation device. The calculated cladding temperatures are below the value of 134.7 °C, indicating one-phase flow through the targets.

Tab 2: UA_{Ix-AI} target temperatures versus different MID coolant velocities in the peripheral core position of the RC.

Coolant velocity (m/s)	UA _{Ix-AI} meat central temperature (°C)	Aluminum cladding temperature (°C)	T _{onb} (°C)	Coolant temperature (°C)
5	189.0	162.6	134.7	48.51
6	172.5	146.1	134.7	47.38
7	160.3	134.0	134.7	46.58
8	151.0	124.6	134.7	45.99
9	143.5	117.1	134.7	45.53
10	137.4	111.0	134.7	45.17
11	132.3	105.9	134.7	44.87
12	130.0	103.6	134.7	44.75
13	126.0	99.6	134.7	44.52
14	122.5	96.2	134.7	44.33
15	119.5	93.1	134.7	44.17

Tables 3 and 4 provide the calculated U-Ni target temperatures for different coolant velocities through the ID in the RC core peripheral position, respectively, for plate and cylindrical geometries. Tab 4 presents for the U-Ni target with cylindrical geometry the temperature of the aluminum tube.

Tab 3: Calculated temperatures for the U-Ni target with plate geometry versus different coolant velocities through the ID.

Coolant velocity (m/s)	Aluminum cladding temperature (°C)	T _{onb} (°C)
5	191.4	132
6	171.1	132
7	156.1	132
8	144.5	132
9	135.2	132
10	127.7	132
11	121.4	132
12	118.8	132
13	113.6	132
14	109.3	132
15	105.6	132

Tab 4: Aluminum tube temperatures for the U-Ni target with cylindrical geometry versus different coolant velocities through the ID.

Coolant velocity (m/s)	Aluminum tube temperature (°C)	T _{onb} (°C)
5	166	137
6	149	137
7	137	137
8	127	137
9	119	137
10	113	137
11	107	137
12	103	137
13	99	137
14	95	137
15	92	137
16	90	137

Tab 3 provides the calculated target temperature results for different coolant velocities through the MID placed in the peripheral core position in the heavy water reflector. A velocity of 8 m/s is necessary to cool the targets. For this velocity no design limit was achieved for the analyzed irradiation device. The calculated aluminum cladding temperatures are below the value of 132°C, indicating one-phase flow through the U-Ni targets with plate geometry.

Table 4 provides the calculated U-Ni aluminum tube temperatures for different coolant velocities through the MID placed in the peripheral core position in the heavy water reflector. A velocity of 9 m/s is necessary to cool the target. For this velocity no design limit was achieved for the analyzed irradiation device. The calculated aluminum tube temperatures are below the value of 137°C, indicating one-phase flow through the U-Ni target with cylinder geometry.

5. Conclusion

From the neutronic calculations presented here, for a uranium amount of 20.1 g in the analyzed targets a ^{99}Mo activity of 1406.63 Ci was obtained for 7 days irradiation time in the IEA-R1 core. For the UAlx-Al target and for the U-Ni targets with plate and cylindrical geometries the calculated total ^{99}Mo activity was, respectively, 2,980.62 Ci, 3,166.6 Ci and 3,495.23 Ci. Initially, $^{99\text{m}}\text{Tc}$ generators will be distributed seven (7) days after the end of the irradiation. Consequently, the total ^{99}Mo activity is expected to reach a value of 240.48 Ci for UAl_x-Al targets irradiated in the IEA-R1 core. For the UAl_x-Al target and U-Ni targets with plate and cylinder geometries irradiated in the peripheral core position of the RC the total ^{99}Mo activity is expected to reach values of 509.57 Ci, 541.36 Ci and 597.5 Ci, respectively. From these values, it is noted that the Brazilian current demand of 450 Ci of ^{99}Mo per week may be addressed irradiating the targets in a peripheral core position of the RC.

Through the thermal-hydraulics calculations it was determined the minimum flow necessary to cool the targets. No design limit was achieved for the analyzed targets. The calculated cladding temperatures are below the value of 95°C, and the coolant temperatures are below the ONB temperature, indicating one-phase flow through the irradiation devices.

Acknowledgments

The authors are grateful for financial support from CAPES and FAPESP.

6. References

- [1] G. F. Wienciek, A. B. Vandegriff, A. A. Levya, and A. S. Hebden, "Status and Progress of Foil and Target Fabrication Activities for the Production of ^{99}Mo from LEU", *RERTR 2008 – 30th International Meeting on Reduced Enrichment for Research and Test*, Washington, October 5-9, 2008.
- [2] I. N. Goldman, N. Ramamoorthy, and P. Adelfang, "Progress and Status of the IAEA Coordinated Research Project: Production of Mo-99 using LEU Fission or Neutronic Activation", *RERTR 2007, September 23-27, 2007, Prague, Czech Republic*.
- [3] J. A. Perrotta, A. J. Soares, "RMB: The New Brazilian Multipurpose Research Reactor", *International Journal for Nuclear Power*, atw vol. 60 (2015), Issue 1, January.
- [4] F. M. Bsebsu, F. Abotweirat and S. Elwaer, "Feasibility Study Part-I Thermal Hydraulic Analysis of LEU Target for ^{99}Mo Production in Tajoura Reactor", *RERTR 2007, September 23-27, 2007, Prague, Czech Republic*.
- [5] A. Mushtaq, Massod Iqbal, Ishtiaq Hussain Bokhari and Tayab Mahmood, "Low Enriched Uranium Foil Plate Target for the Production of Fission Molybdenum-99 in Pakistan Research Reactor-I", *Nuclear Instruments and Methods in Physics Research B* 267(2009) 1109-1114.
- [6] J. Barhein, W. Rhotenstein, and E. Taviv, "The HAMMER Code System TECHNION", Israel Institute of Technology, Haifa, Israel, NP-565, 1978.
- [7] T. B. Fowler, D. R. Vondy, and G. W. Cunningham, "Nuclear Reactor Core Analysis Code: CITATION", *Oak Ridge National Laboratory, ORNL-TM-2496, Rev. 2, Suppl. 3, July 1972*.

[8] "SCALE: A Modular Code System for Performing Standardized Computer Analyses for Licensing Evaluation", *ORNL/TM-2005/39*, Version 6.1, Vols. I–III, November 2006. The code is available from Radiation Safety Information Computational Center at Oak Ridge National Laboratory as CCC-732.

[9] D. B. Domingos, *Análises Neutrônica e Termo-hidráulica de Dispositivos para Irradiação de Alvos Tipo LEU de UAlx-Al e U-Ni para Produção de Mo-99 nos Reatores IEA-R1 e RMB*, 2014, *Dissertação (Doutorado)* - Instituto de Pesquisas Energéticas e Nucleares, São Paulo.

[10] P. E. Umbehaun, "Metodologia para Análise Termo-hidráulica de Reatores de Pesquisa Tipo Piscina com Combustível Tipo Placa", 2000, *Dissertação (Mestrado)* – Instituto de Pesquisas Energéticas e Nucleares, São Paulo.

[11] A. E. Bergles, W. M. Rosenow, "The Determination of Forced-Convection Surface Boiling Heat Transfers", *Trans. of the ASME 86 (Series C-J. of Heat Transfer)*, 365-375, Aug. 1964.

[12] ANSYS CFX Reference Guide, release 12.0, April 2009.

[13] A. T. Silva, D. B. Domingos, T. G. João, P. J. B. O. Nishiyama, C. Giovedi, "Neutronic and Thermal-Hydraulics Calculations for the Production of Molybdenum-99 by Fission in Low Enriched Uranium UAlx-Al Targets", *RRFM 2015*, April 19-23, 2015, Bucharest, Romania.

NEUTRONIC AND THERMAL-HYDRAULICS CALCULATIONS FOR THE PRODUCTION OF MOLYBDENUM-99 BY FISSION IN LOW ENRICHED URANIUM UAL_x-AL TARGETS

A. T. SILVA, D. B. DOMINGOS, T. G. JOÃO

*Instituto de Pesquisas Energéticas e Nucleares - Comissão Nacional de Energia Nuclear
(IPEN/CNEN-SP)*

Av. Professor Lineu Prestes, 2242, Cidade Universitária, 05508-000 São Paulo, SP - Brazil

P. J. B. O. NISHIYAMA, C. GIOVEDI

Centro Tecnológico da Marinha em São Paulo (CTMSP)

Av. Professor Lineu Prestes, 2468, Cidade Universitária, 05508-000 São Paulo, SP - Brazil

ABSTRACT

The IEA-R1 reactor of IPEN-CNEN/SP in Brazil is a pool type research reactor cooled and moderated by demineralized water and having Beryllium and Graphite as reflectors. In 1997 the reactor received the operating licensing for 5 MW. Low enriched uranium (LEU) (<20% ²³⁵U) UAl_x dispersed in Al targets are being considered for production of Molybdenum-99 (⁹⁹Mo) by fission. Neutronic and thermal-hydraulics calculations were performed, respectively, to evaluate the production of ⁹⁹Mo for these targets in the IEA-R1 reactor and to determine the temperatures achieved in the UAl_x-Al targets during irradiation. For the neutronic calculations were utilized the computer codes HAMMER-TECHNION and CITATION, and for the thermal-hydraulics calculations was utilized the computer code MTRCR-IEAR1. The analysis demonstrated that the irradiation will occur without adverse consequences to the operation of the reactor. The total amount of ⁹⁹Mo produced was calculated with the program SCALE. Considering that the time needed for the chemical processing and recovering of the ⁹⁹Mo will be five days after the irradiation, the total ⁹⁹Mo activity available for distribution will be 176 Ci for 3 days of irradiation, 236 Ci for 5 days of irradiation, and 272 Ci for 7 days of targets irradiation.

1. Introduction

^{99m}Tc, product son of ⁹⁹Mo, is one of the most utilized radioisotopes in nuclear medicine in the world. Annually it is used in approximately 20 to 25 million procedures of medical diagnosis, representing about 80% of all the nuclear medicine procedures [1]. Since 2004, given the worldwide interest in ⁹⁹Mo production, the International Atomic Energy Agency (IAEA) has developed and implemented a Coordinated Research Project (CRP) [2] to help interested countries start a small-scale domestic ⁹⁹Mo production in order to meet the requirements of the local nuclear medicine. The purpose of CRP is to provide interested countries with access to non-proprietary technologies and methods for production of ⁹⁹Mo using targets of thin foils of metallic low enriched uranium (LEU), UAl_x-Al miniplates of LEU type or by neutron activation reaction (n, gamma), for example, using gel generators. Brazil, through IPEN-CNEN/SP, began its CRP participation in late 2009. IPEN/CNEN-SP provides radiopharmaceuticals to more than 300 hospitals and clinics in the country, reaching more than 3.5 million medical procedures per year. The use of radiopharmaceuticals in the country over the last decade has grown at a rate of 10% per year and IPEN/CNEN-SP is primarily responsible for this distribution. ^{99m}Tc generators are the most used ones and are responsible for more than 80% of the radiopharmaceuticals applications in Brazil. IPEN/CNEN-SP imports all the ⁹⁹Mo used in the country (450 Ci of ⁹⁹Mo per week or 24,000 Ci per year approximately). In the past, IPEN/CNEN-SP developed the ⁹⁹Mo production route from neutron activation of ⁹⁸Mo targets in the IEA-R1. However, the quantity produced does not meet the Brazilian needs of this isotope. Due to the growing need for nuclear medicine in the country and because of the short ⁹⁹Mo supply observed since 2008 on the world stage,

IPEN/CNEN-SP has decided to develop its own project to produce ^{99}Mo through ^{235}U fission. This project has three main goals: 1) the research and development of ^{99}Mo production from fission of LEU targets, 2) the discussion and decision on the best production route technique, and 3) the feasibility study of IPEN/CNEN-SP in reaching a routine production of ^{99}Mo . The main goal of IPEN/CNEN-SP is to accommodate the Brazilian demand for radiopharmaceuticals. Nowadays, this demand is about 450 Ci of ^{99}Mo per week and the future need, after six years, is estimated at around 1,000 Ci per week. One of the analyses planned in this project is to study the characteristics and specifications of $\text{UAl}_x\text{-Al}$ targets. The first aim of the present work was to perform neutronic calculations to evaluate the $^{99\text{m}}\text{Mo}$ production through fission at the IPEN/CNEN-SP IEA-R1 nuclear reactor. The second aim of this work is to perform thermal-hydraulics calculations to determine the maximal temperatures achieved in the targets during irradiation and compared them with the design temperature limits established for $\text{UAl}_x\text{-Al}$ targets.

2. $\text{UAl}_x\text{-Al}$ targets used in the neutronic and thermal-hydraulic analysis

The $\text{UAl}_x\text{-Al}$ targets of LEU type proposed and analyzed in this work are aluminum coated miniplates. Each miniplate measures 52 mm x 170 mm, 1.52 mm thick, corresponding to a total volume of 13.437 mm^3 . The $\text{UAl}_x\text{-Al}$ meat is 40 mm x 118 mm, 0.76 mm thick, leading to a total volume of 3.587 mm^3 . Considering this volume and a ^{235}U mass in the target equals to 2.06 g, the ^{235}U density ($\rho_{\text{U-235}}$) in the target meat is $0.58\text{ g}^{235}\text{U}/\text{cm}^3$. For a 19.9% ^{235}U enrichment, the uranium density in the target is $\rho_{\text{U}} = 2.89\text{ gU}/\text{cm}^3$. This corresponds to a UAl_2 volume fraction of 45% and an aluminum volume fraction of 55% in the dispersion.

A special Miniplate Irradiation Device (MID) was designed for the irradiation of the $\text{UAl}_x\text{-Al}$ targets in the IEA-R1 reactor. Figure 1 shows the MID which has the external dimensions of the IEA-R1 fuel element. The miniplates will be allocated in a box with indented bars placed inside the external part of the MID. Figure 2 shows the MID cross section. As seen from Figure 2, up to ten $\text{UAl}_x\text{-Al}$ targets can be placed in the box with indented bars inside of the MID.

The $\text{UAl}_x\text{-Al}$ targets were modeled and simulated, respectively, in the core central position in the IEA-R1 reactor. The target irradiation time was defined according to their current and planned operating cycle.

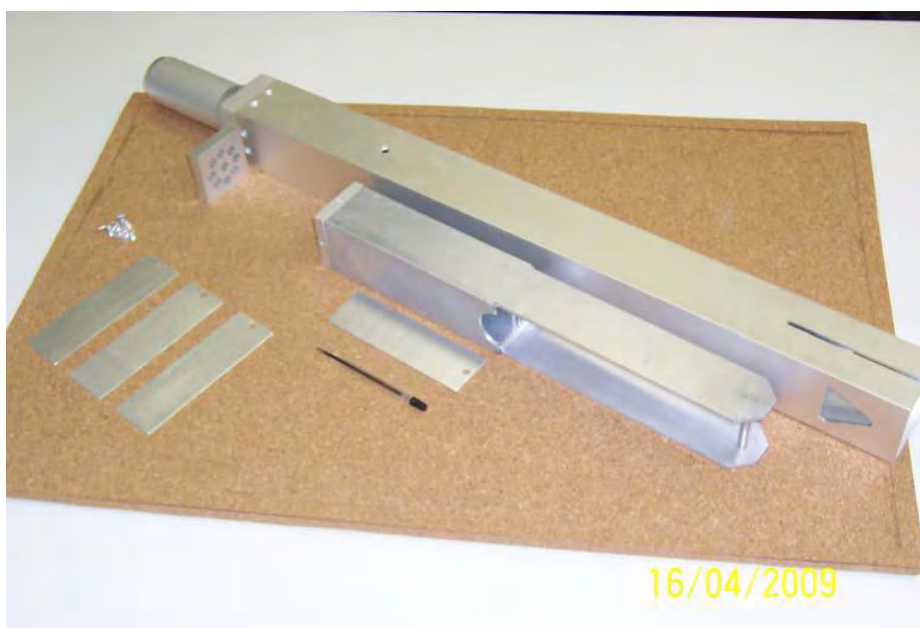


Fig 1: Miniplate irradiation device – MID.

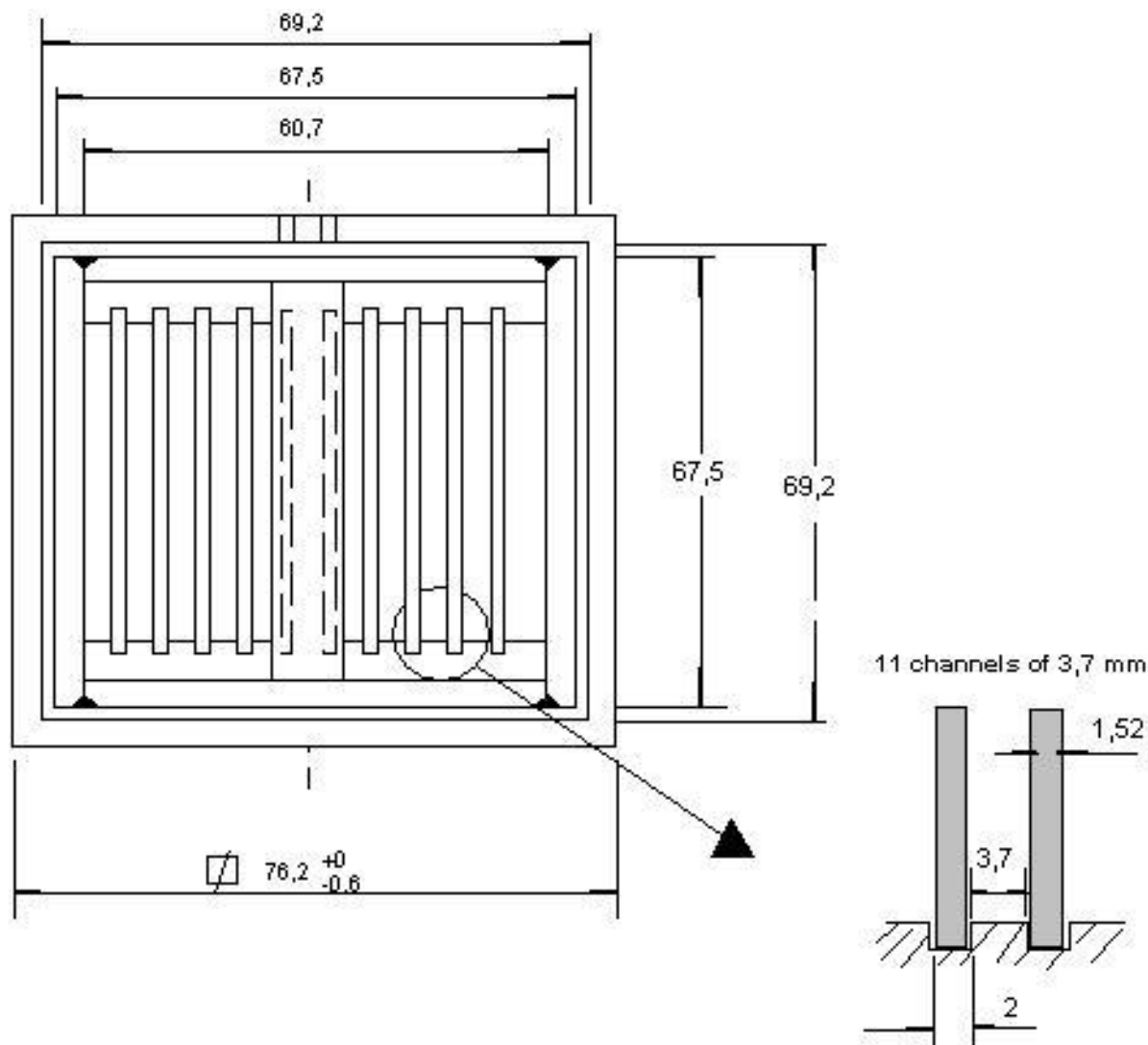


Fig 2: Cross section of the MID (dimensions in mm).

3. Neutronic calculation for the irradiation device

The IEA-R1 reactor core, as well as the $\text{UAl}_x\text{-Al}$ targets used for the ^{99}Mo production, were modeled with the HAMMER-TECHNION [3] and CITATION [4] numerical codes. The 1D cross section for each component of the two reactors and the power distribution for any position r of the reactor cores were obtained. The SCALE 6.0 [5] code system was used to perform burnup calculations for each target and also to determine the ^{99}Mo activity at the end of irradiation.

The IEA-R1 reactor has a 5x5 configuration, 5 MW, containing 24 MTR-type fuel elements with a beryllium irradiation device at its central position. The $\text{UAl}_x\text{-Al}$ targets were modeled and simulated in the core central position using 24 $\text{U}_3\text{Si}_2\text{-Al}$ fuel elements whose density was 1.2 gU/cm^3 . The calculations were developed for three irradiation periods: 3, 5 and 7 days. At the end of 3 irradiation days, the total ^{99}Mo activity obtained for the 10 $\text{UAl}_x\text{-Al}$ miniplates was 620 Ci. After 5 irradiation days, the total ^{99}Mo activity obtained was 832 Ci, and after 7 irradiation days the total ^{99}Mo activity obtained was 958 Ci. Considering that the time needed for the chemical processing and recovering of the ^{99}Mo will be five days after the irradiation, the total ^{99}Mo activity available for distribution will be 176 Ci for 3 irradiation days, 236 Ci for 5 irradiation days, and 272 Ci for 7 irradiation days of the targets [6].

4. Thermal-Hydraulics calculation for the irradiation device

A thermal-hydraulics model MTCR-IEA-R1 [7] was developed in 2000 at IPEN-CNEN/SP using a commercial program Engineering Equation Solver (EES). The use of this computer model enables the steady-state thermal and hydraulics core analyses of research reactors with MTR fuel elements. The following parameters are calculated along the fuel element channels: fuel meat central temperature (T_c), cladding temperature (T_r), coolant temperature (T_f), Onset of Nucleate Boiling (ONB) temperature (T_{onb}), critical heat flux (Departure of Nucleate Boiling-DNB), flow instability and thermal-hydraulics safety margins FIR and MDNBR. The thermal-hydraulics safety margins MDNBR and FIR are calculated as the ratio between, respectively, the critical heat flux and the heat flux for flow instability and the local heat flux in the fuel plate. Furthermore, the MTCR-IEA-R1 model also utilizes in its calculation the involved uncertainties in the thermal-hydraulics calculation such as: fuel fabrication uncertainties, errors in the power density distribution calculation, in the coolant flow distribution in the core, in reactor power control deviation, in the coolant flow rate measures, and in the safety margins for the heat transfer coefficients. The calculated thermal-hydraulics core parameters are compared with the design limits established for MTR fuels: a) cladding temperature $< 95^\circ\text{C}$; 2) safety margin for ONB > 1.3 , or the ONB temperature (T_{onb}) higher than coolant temperature; 3) safety margin for flow instability > 2.0 ; and 4) safety margin for critical heat flux > 2.0 .

For the targets, it was considered the following design limits: 1) no material may experience a temperature greater than $\frac{1}{2}$ any target material melting temperature. The lowest melting temperature for any of the proposed target materials is that of the aluminum cladding, whose melting temperature is 660°C . Therefore 330°C is the maximum allowable temperature for the LEU target; 2) the reactor core coolant temperature must be kept below its saturation temperature. In this work it was adopted as target design limit the cladding temperature that initiated the coolant nucleate boiling (T_{ONB}) for a given coolant pressure and superficial heat flux given by Bergles and Rosenow correlation [8].

The placement of the MID in the core central position of IEA-R1 reactor will deviate part of the reactor flow rate to cool the UAlx-Al targets. The flow rate in the core of the IEA-R1 reactor is 3,400 gpm which provides a flow rate of approximately $23 \text{ m}^3/\text{h}$ per fuel element, and sufficient to cool a standard fuel element. The insertion of the MID in the IEA-R1 reactor core will divert part of the reactor core coolant to cool the UAlx-Al miniplates. Thus, a MID thermo-hydraulic analysis was developed to determine the required flow rate to cool the miniplates, but without damaging the fuel elements in the reactor core. Flow rates from 1 to $20 \text{ m}^3/\text{hr}$ were tested through the MID. Table 1 provide the calculated UAlx-Al target temperatures for different flow rates through the MID in the IEA-R1 reactor core. The simulations considered the MID with ten identical UAlx-Al miniplates. Table 1 show that flow rates higher than $10 \text{ m}^3/\text{h}$ through the MID are sufficient to cool the targets without achieving ONB temperatures. The calculated cladding temperatures are below the value of 123.1°C , indicating one-phase flow through the targets. A coolant flow restrictor was fabricated in order to maintain a MID flow rate of $12 \text{ m}^3/\text{hr}$ in the reactor core during target irradiation (see Figure 1).

Tab 1: Target temperatures versus DIM flow rates and coolant velocities.

Flow rate (m^3/h)	Coolant velocity (m/s)	UAlx-Al meat central temperature ($^\circ\text{C}$)	UALx-Al aluminum cladding temperature ($^\circ\text{C}$)	ONB Temperature (T_{ONB}) ($^\circ\text{C}$)	Coolant Temperature ($^\circ\text{C}$)
1	0.18	478.4	470.4	123.1	92.3
2	0.36	301.6	293.6	123.1	67.0

3	0.53	239	231	123.1	58.6
4	0.71	203.2	195.2	123.1	54.5
5	0.89	179.8	171.8	123.1	52.0
6	1.07	163.1	155.1	123.1	50.3
7	1.24	150.5	142.5	123.1	49.1
8	1.42	140.7	132.7	123.1	48.2
9	1.60	132.8	124.8	123.1	47.6
10	1.78	126.3	118.3	123.1	47.0
11	1.95	120.8	112.8	123.1	46.6
12	2.13	116.2	108.2	123.1	46.2
13	2.31	112.1	104.1	123.1	45.9
14	2.49	108.6	100.6	123.1	45.6
15	2.66	105.5	97.5	123.1	45.3
16	2.84	102.8	94.8	123.1	45.1
17	3.02	100.3	92.3	123.1	45.0
18	3.20	98.1	90.1	123.1	44.8
19	3.37	96.1	88.1	123.1	44.6
20	3.55	94.2	86.2	123.1	44.5

5. Conclusion

From the neutronic calculations presented for ten targets of UAl_x-Al dispersion fuel with low enriched uranium (LEU) and density of 2.889 gU/cm³, ⁹⁹Mo activities of 620 Ci, 832 Ci and 958 Ci were obtained, respectively for three (3), five(5) and seven (7) irradiation days in IEA-R1 reactor core at a reactor power of 5 MW. Initially, ^{99m}Tc generators will be distributed five (5) days after the end of the irradiation. Consequently, the total ⁹⁹Mo activity is expected to reach, respectively, values of 176 Ci, 236 Ci and 272 Ci for UAl_x-Al targets irradiated during three (3), five (5) and seven (7) irradiation days in the core central position of the IEA-R1 reactor. From these values, it is noted that the Brazilian current demand of 450 Ci of ⁹⁹Mo per week and the future projected demand of 1,000 Ci will not be achieved with the proposed UAL_x-Al targets in the core central position of IEA-R1 reactor.

Acknowledgments

The authors are grateful for financial support from the CAPES, CNEN and FAPESP.

6. References

[1] G. F. Wienciek, A. B. Vandegriff, A. A. Levya, and A. S. Hebden, "Status and Progress of Foil and Target Fabrication Activities for the Production of ⁹⁹Mo from LEU", *RERTR 2008 – 30th International Meeting on Reduced Enrichment for Research and Test*, Washington, October 5-9, 2008.

- [2] I. N. Goldman, N. Ramamoorthy, and P. Adelfang, "Progress and Status of the IAEA Coordinated Research Project: Production of Mo-99 using LEU Fission or Neutronic Activation", *RERTR 2007*, September 23-27, 2007, Prague, Czech Republic.
- [3] J. Barhein, W. Rhotenstein, and E. Taviv, "The HAMMER Code System TECHNION", *Israel Institute of Technology*, Haifa, Israel, NP-565, 1978.
- [4] T. B. Fowler, D. R. Vondy, and G. W. Cunningham, "Nuclear Reactor Core Analysis Code: CITATION", *Oak Ridge National Laboratory*, ORNL-TM-2496, Rev. 2, Suppl. 3, July 1972.
- [5] SCALE: A Modular Code System for Performing Standardized Computer Analyses for Licensing Evaluation, *ORNL/TM-2005/39*, Version 6.1, Vols. I-III, November 2006. The code is available from Radiation Safety Information Computational Center at Oak Ridge National Laboratory as CCC-732.
- [6] P. J. B. O. Nishiyama, "Análises Neutrônica e Termo-hidráulica de um Dispositivo para Irradiação de Alvos Tipo LEU de UAlx-Al para Produção de ⁹⁹Mo no Reator IEA-R1". 2012. *Dissertação (Mestrado)* – Instituto de Pesquisas Energéticas e Nucleares, São Paulo.
- [7] P. E. Umbehaun, "Metodologia para Análise Termo-hidráulica de Reatores de Pesquisa Tipo Piscina com Combustível Tipo Placa". 2000. *Dissertação (Mestrado)* – Instituto de Pesquisas Energéticas e Nucleares, São Paulo.
- [8] A. E. BERGLES, W. M. ROSENOW, "The Determination of Forced-convection Surface Boiling Heat Transfers. *Trans. of the ASME 86 (Series C-J. of Heat Transfer)*, 365-375, Aug. 1964.

LOW ENRICHED URANIUM FOIL TARGETS WITH DIFFERENT GEOMETRIES FOR THE PRODUCTION OF MOLYBDENUM-99

D. B. DOMINGOS, A. T. SILVA, T. G. JOÃO

*Instituto de Pesquisas Energéticas e Nucleares - Comissão Nacional de Energia Nuclear
(IPEN/CNEN-SP)*

Av. Professor Lineu Prestes 2242, Cidade Universitária, 05508-000 São Paulo, SP - Brazil

ABSTRACT

A new research reactor is being planned in Brazil to take care of the demand of radiopharmaceuticals in the country and conduct research in various areas. This new reactor, the Brazilian Multipurpose Reactor (RMB), planned for 30 MW, is now in the detailed design phase. Two low enriched (<20% ^{235}U) metallic uranium foil targets (cylinder and plate geometries) are being considered for production of Molybdenum-99 (^{99}Mo) by fission. Neutronic and thermal-hydraulics calculations were performed to compare the production of ^{99}Mo for these targets in a reactor conception with the same power of the RMB and to determine the temperatures achieved in the targets. For the neutronic calculations were utilized the computer codes HAMMER-TECHNION, CITATION and SCALE and for the thermal-hydraulics calculations were utilized the computer codes MTRCR-IEA-R1 and ANSYS CFX.

1. Introduction

$^{99\text{m}}\text{Tc}$, decay product of ^{99}Mo , is one of the most utilized radioisotopes in nuclear medicine in the world. Annually it is used in approximately 20 to 25 million procedures of medical diagnosis, representing about 80% of all the nuclear medicine procedures [1]. Since 2004, given the worldwide interest in ^{99}Mo production, the International Atomic Energy Agency (IAEA) has developed and implemented a Coordinated Research Project (CRP) [2] to help interested countries start a small-scale domestic ^{99}Mo production in order to meet the requirements of the local nuclear medicine. The purpose of CRP is to provide interested countries with access to non-proprietary technologies and methods for production of ^{99}Mo using targets of thin foils of metallic low enriched uranium (LEU), $\text{UAl}_x\text{-Al}$ miniplates of LEU type or by neutron activation reaction (n, gamma), for example, using gel generators. Brazil, through IPEN/CNEN-SP, began its CRP participation in late 2009. IPEN/CNEN-SP provides radiopharmaceuticals to more than 300 hospitals and clinics in the country, reaching more than 3.5 million medical procedures per year. The use of radiopharmaceuticals in the country over the last decade has grown at a rate of 10% per year and IPEN/CNEN-SP is primarily responsible for this distribution. $^{99\text{m}}\text{Tc}$ generators are the most used ones and are responsible for more than 80% of the radiopharmaceuticals applications in Brazil. IPEN/CNEN-SP imports all the ^{99}Mo used in the country (450 Ci of ^{99}Mo per week or 24,000 Ci per year approximately). In the past, IPEN/CNEN-SP developed the ^{99}Mo production route from neutron activation of ^{98}Mo targets in the IEA-R1. However, the quantity produced does not meet the Brazilian needs of this isotope. Due to the growing need for nuclear medicine in the country and because of the short ^{99}Mo supply observed since 2008 on the world stage, IPEN/CNEN-SP has decided to develop its own project to produce ^{99}Mo through ^{235}U fission. This project has three main goals: 1) the research and development of ^{99}Mo production from fission of LEU targets, 2) the discussion and decision on the best production route technique, and 3) the feasibility study of IPEN/CNEN-SP in reaching a routine production of ^{99}Mo . The main goal of IPEN/CNEN-SP is to accommodate the Brazilian demand for radiopharmaceuticals. Nowadays, this demand is about 450 Ci of ^{99}Mo per week and the future need, after six years, is estimated at around 1,000 Ci per week. One of the analyses planned in this project is to study the characteristics and specifications of metallic uranium thin foils targets. The first aim of the present work is to perform neutronic calculations to

evaluate the ^{99m}Mo production through fission in a reactor conception (RC) with the same power of the RMB [3], which is in the detailed design phase. The second aim of this work is to perform thermal-hydraulics calculations to determine the maximal temperatures achieved in the targets during irradiation and compared them with the design temperature limits established for U-Ni targets.

2. U-Ni targets used in the neutronic and thermal-hydraulic analysis

The targets of metallic uranium foils with cylinder geometry analyzed at IPEN/CNEN-SP were based on targets that were examined in the Tajoura reactor in Libya to produce ^{99}Mo [4]. The targets were mounted in cylindrical geometry, in a tubular arrangement. The metallic U foil was covered with a Ni sheet before being placed concentrically inside the aluminum tubes. The dimensions of the target are (see Fig 1):

1. One foil of uranium (LEU) of 46.05 cm x 87.7 mm x 135 μm ;
2. Coating nickel foil of 20 μm thickness;
3. Two aluminum cylinder having 46.05 cm length, outside diameters of 27.88 and 30.00 mm, and inside diameters of 26.44 and 28.22 mm, respectively;
4. ^{235}U mass of 20.1 g, with 19.9% enrichment of ^{235}U .

The targets of metallic Uranium foils with plate geometry were based on targets that were examined in the Paskitan research reactor [5] and consists of a uranium foil (19.99% ^{235}U) with a thickness of 135 μm enveloped in 20 μm thick nickel foil and placed between two aluminum plates that are welded from all sides. The geometry of the foil plate target is shown in Figures 2 and 3.

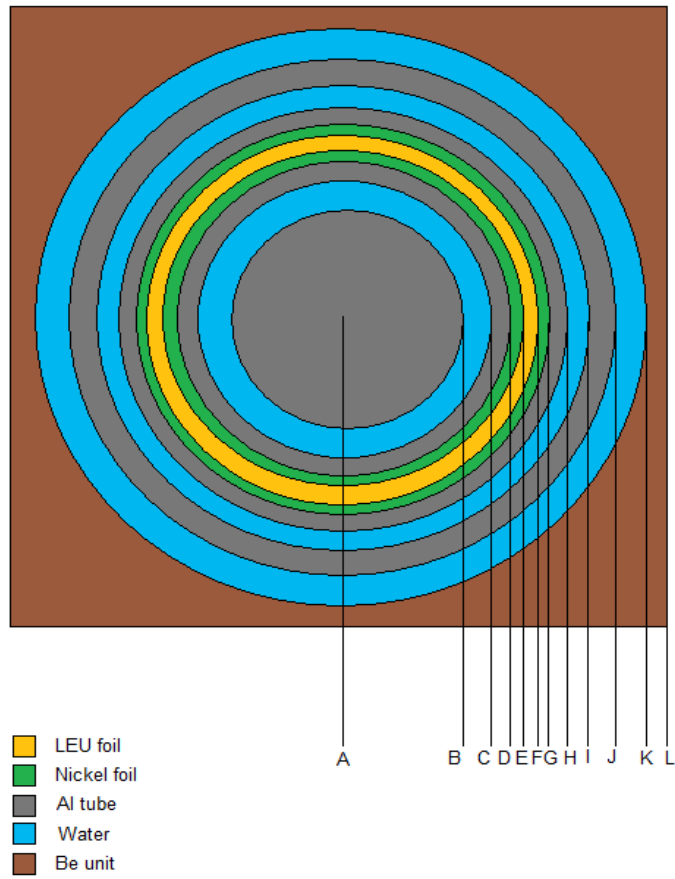
For the performed calculations, the U-Ni targets with cylindrical and plate geometries were modeled in the same irradiation device (ID), whose external dimensions are 76.2 mm x 76.2 mm x 88.74 cm (Fig 4).

For both targets a ^{235}U mass equals to 20.1 g was considered in the neutronic calculations. As seen from Fig 3, ten U-Ni targets with plate geometry were placed in the box with indented bars inside of the ID. Each U-Ni target with plate geometry has a ^{235}U mass equals to 2.01 g. The set of concentric cylinders of the metallic uranium foils with cylinder geometry was positioned in the same ID.

The targets were modeled and simulated in a peripheral core position of the RC, in the heavy water reflector. The target irradiation time was seven (7) days.

3. Neutronic calculations for the irradiation device

The RC core as well as the U-Ni LEU targets (cylinder and plate geometries) used for the ^{99}Mo production were modeled with the HAMMER-TECHNION [6] and CITATION [7] numerical codes. The 1D cross section for each component of the reactor was generated by the computer code HAMMER-TECHNION. The computer code CITATION was used for the three-dimensional core and radial and axial density curves calculations. These data were used as input data for the thermal-hydraulics irradiation device analysis. The power distribution for any position r of the reactor core matrix plate was obtained. The SCALE 6.0 code system [8] was used to perform burnup calculations for each target and also to calculate the ^{99}Mo activity at the end of irradiation. The target irradiation time for the reactor was defined according to their current and planned operating cycle.



Radius	Length (cm)
AB	1.0000
AC	1.322
AD	1.3940
AE	1.3960
AF	1.4095
AG	1.4110
AH	1.5000
AI	1.7500
AJ	1.9000
AK	2.2000
AL	3.8100

Fig 1: Irradiation device horizontal cross section for the U-Ni target with cylinder geometry.

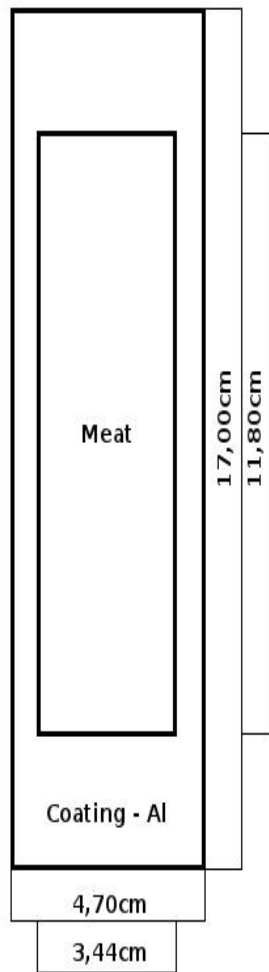


Fig 2: Width and height of the U-Ni plates.

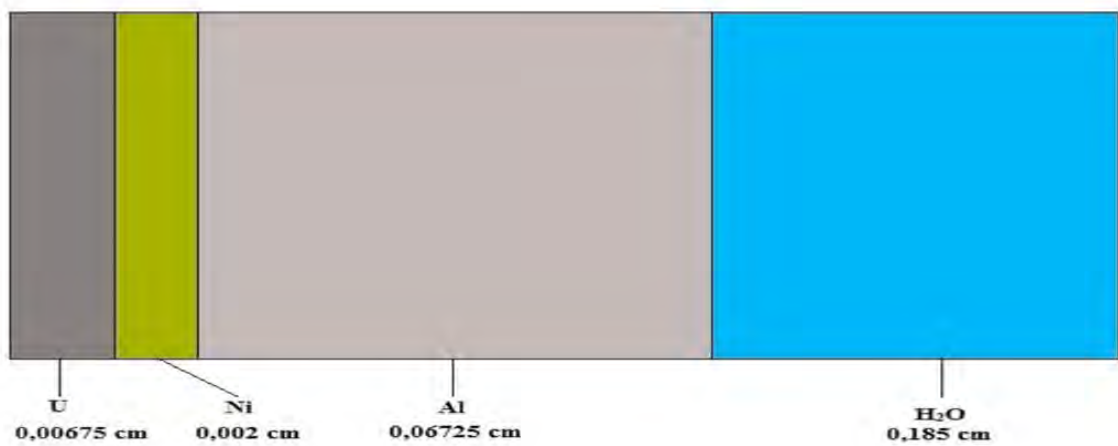


Fig 3: Half the thickness of U-Ni LEU target with plate geometry (67.5 μm), nickel foil, aluminum plate and cooling channel.

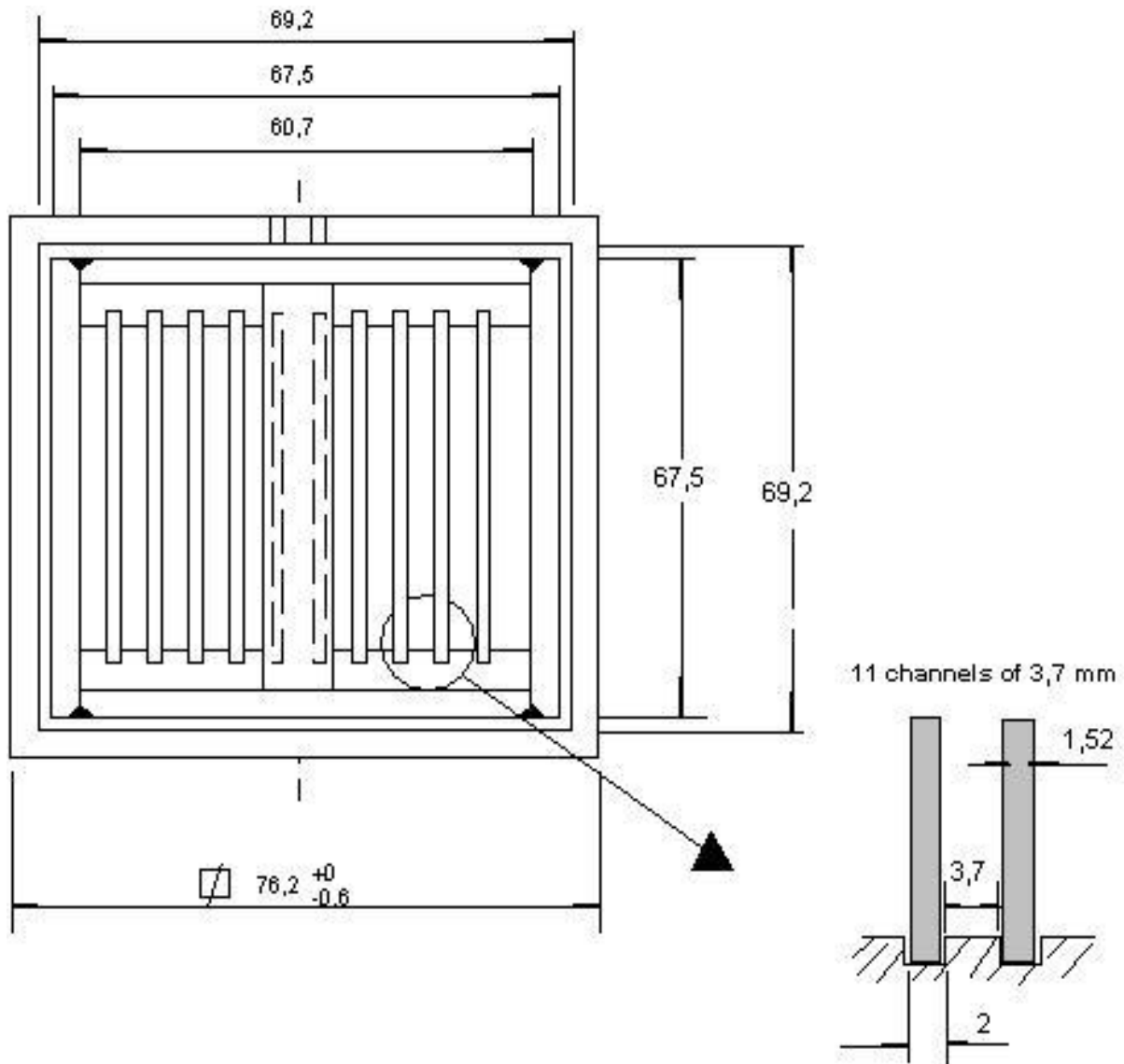


Fig 4: Irradiation device horizontal cross section for the U-Ni targets with plate geometry.

According to its conceptual design, RC is an open pool type, 30 MW thermal power reactor. The core has a 5x6 configuration with MTR-type U_3Si_2-Al fuel elements with 19.75 wt% ^{235}U enrichment. The reactor core, containing 30 U_3Si_2-Al fuel elements with a uranium density of 1.9 gU/cm^3 , is light water cooled and moderated, using heavy water as reflector. The U-Ni LEU targets were modeled and simulated in a peripheral core position in the heavy water reflector. At the end of 7 days of irradiation, the total activities obtained for the U-Ni plate and cylinder geometries were, respectively, 3,495.23 Ci and 3,166.6 Ci. Considering that the time needed for the chemical processing and recovering of the ^{99}Mo will be seven days after the irradiation, the total activity obtained for the U-Ni plate and cylinder geometries were, respectively, 597.5 Ci and 541.36 Ci.

4. Thermal-Hydraulics calculation

A thermal-hydraulics model MTCR-IEA-R1 [9] was developed in 2000 at IPEN/CNEN-SP using a commercial program Engineering Equation Solver (EES). The use of this computer model enables the steady-state thermal and hydraulics core analyses of research reactors with MTR fuel elements. The following parameters are calculated along the fuel element

channels: fuel meat central temperature (T_c), cladding temperature (T_r), coolant temperature (T_f), Onset of Nucleate Boiling (ONB) temperature (T_{onb}), critical heat flux (Departure of Nucleate Boiling-DNB), flow instability and thermal-hydraulics safety margins MDNBR and FIR. The thermal-hydraulics safety margins MDNBR and FIR are calculated as the ratio between, respectively, the critical heat flux and the heat flux for flow instability and the local heat flux in the fuel plate. Furthermore, the MTCR-IEA-R1 model also utilizes in its calculation the involved uncertainties in the thermal-hydraulics calculation such as: fuel fabrication uncertainties, errors in the power density distribution calculation, in the coolant flow distribution in the core, reactor power control deviation, in the coolant flow measures, and in the safety margins for the heat transfer coefficients. The calculated thermal-hydraulics core parameters are compared with the design limits established for MTR fuels: a) cladding temperature $< 95^\circ\text{C}$; 2) safety margin for ONB > 1.3 , or the ONB temperature higher than coolant temperature; 3) safety margin for flow instability > 2.0 ; and 4) safety margin for critical heat flux > 2.0 .

Thermal-hydraulics calculations were developed to determine the maximal temperatures achieved in the U-Ni targets during irradiation and to compare the temperature results with the design temperature limits established for the U-Ni targets. For the targets, it was considered the following design limits: 1) no material may experience a temperature greater than $\frac{1}{2}$ any target material melting temperature. The lowest melting temperature for any of the proposed target materials is that of the aluminum cladding, whose melting temperature is 660°C . Therefore 330°C is the maximum allowable temperature for the LEU target; 2) the pool coolant must be kept below its saturation temperature. In this work it was adopted as target design limit the cladding temperature that initiated the coolant nucleate boiling (T_{ONB}) for a given coolant pressure and superficial heat flux given by Bergles and Rosenow correlation [10].

In order to evaluate the temperatures achieved in the U-Ni targets different coolant velocities were tested through the irradiation device (ID). For the temperature calculations of the U-Ni targets with plate geometry the thermal-hydraulics model MTCR-IEA-R1 was used and the results were obtained simultaneously with the RC core analysis. For the calculation of the temperatures of the U-Ni targets with cylindrical geometry was utilized the software ANSYS CFX [11]. The power density ($25 \text{ KW}/\text{cm}^3$) calculated in the ID position in the RC reflector was utilized as input data to determine the temperatures in the U-Ni target with cylindrical geometry.

Tables 1 and 2 provide the calculated U-Ni target temperatures for different coolant velocities through the ID in the RC peripheral position respectively for plate and cylindrical geometries.

Tab 1: Calculated temperatures for the U-Ni target with plate geometry versus different coolant velocities through the ID.

Coolant velocity (m/s)	Aluminum cladding temperature ($^\circ\text{C}$)	T_{onb} ($^\circ\text{C}$)
5	191.4	137
6	171.1	137
7	156.1	137
8	144.5	137
9	135.2	137
10	127.7	137
11	121.4	137
12	118.6	137
13	113.6	137
14	109.3	137
15	105.6	137

Tab 2: Aluminum tube temperatures for the U-Ni target with cylindrical geometry versus different coolant velocities through the ID.

Coolant Velocity (m/s)	Aluminum cladding temperature (°C)	T _{onb} (°C)
5	166	132
6	149	132
7	137	132
8	127	132
9	119	132
10	113	132
11	107	132
12	103	132
13	99	132
14	95	132
15	92	132

Table 1 provides the calculated target temperature results for different coolant velocities through the ID placed in the peripheral core position in the heavy water reflector. A velocity of 9 m/s is necessary to cool the targets. For this velocity no design limit was achieved for the analyzed irradiation device. The calculated aluminum cladding temperatures are below the value of 137°C, indicating one-phase flow through the U-Ni targets with plate geometry.

Table 2 provides the calculated U-Ni aluminum tube temperatures for different coolant velocities through the ID placed in the peripheral core position in the heavy water reflector. A velocity of 8 m/s is necessary to cool the target. For this velocity no design limit was achieved for the analyzed irradiation device. The calculated aluminum tube temperatures are below the value of 132°C, indicating one-phase flow through the U-Ni target with cylinder geometry.

5. Conclusion

From the neutronic calculations presented here, for the uranium amount of 20.1 g in the analyzed U-Ni targets with plate and cylindrical geometries, a ⁹⁹Mo activity of, respectively, 3,495.23 Ci and 3,166.6 Ci was obtained at the end of 7 days irradiation time. Initially, ^{99m}Tc generators will be distributed seven (7) days after the end of the irradiation. Consequently, the total ⁹⁹Mo activity is expected to reach values of 597.5 Ci and 541.36, respectively, for U-Ni targets with plate and cylinder geometries. From these values, it is noted that the Brazilian current demand of 450 Ci of ⁹⁹Mo per week may be addressed for the RC conception addressed in this paper.

Acknowledgments

The authors are grateful for financial support from CAPES and FAPESP.

6. References

[1] G. F. Wienciek, A. B. Vandegriff, A. A. Levya, and A. S. Hebden, "Status and Progress of Foil and Target Fabrication Activities for the Production of ⁹⁹Mo from LEU", *RERTR 2008* –

30th International Meeting on Reduced Enrichment for Research and Test, Washington, October 5-9, 2008.

[2] I. N. Goldman, N. Ramamoorthy, and P. Adelfang, "Progress and Status of the IAEA Coordinated Research Project: Production of Mo-99 using LEU Fission or Neutronic Activation", *RERTR 2007*, September 23-27, 2007, Prague, Czech Republic.

[3] J. A. Perrotta, A. J. Soares, "RMB: The New Brazilian Multipurpose Research Reactor", *International Journal for Nuclear Power*, atw vol. 60 (2015), Issue 1, January.

[4] F. M. Bsebsu, F. Abotweirat and S. Elwaer, "Feasibility Study Part-I Thermal Hydraulic Analysis of LEU Target for ⁹⁹Mo Production in Tajoura Reactor, *RERTR 2007, September 23-27, 2007, Prague, Czech Republic*.

[5] A. Mushtaq, Massod Iqbal, Ishtiaq Hussain Bokhari and Tayyab Mahmood, "Low Enriched Uranium Foil Plate Target for the Production of Fission Molybdenum-99 in Pakistan Research Reactor-I, *Nuclear Instruments and Methods in Physics Research B* 267 (2009) 1109-1114.

[6] J. Barhein, W. Rhotenstein, and E. Taviv, "The HAMMER Code System TECHNION", *Israel Institute of Technology, Haifa, Israel, NP-565*, 1978.

[7] T. B. Fowler, D. R. Vondy, and G. W. Cunningham, "Nuclear Reactor Core Analysis Code: CITATION", *Oak Ridge National Laboratory, ORNL-TM-2496, Rev. 2, Suppl. 3*, July 1972.

[8] SCALE: A Modular Code System for Performing Standardized Computer Analyses for Licensing Evaluation, *ORNL/TM-2005/39, Version 6.1, Vols. I-III*, November 2006. It is available as CCC-732 from Radiation Safety Information Computational Center at Oak Ridge National Laboratory.

[9] P. E. Umbehaun, "Metodologia para Análise Termo-hidráulica de Reatores de Pesquisa Tipo Piscina com Combustível Tipo Placa". 2000. *Dissertação (Mestrado)* – Instituto de Pesquisas Energéticas e Nucleares, São Paulo.

[10] A. E. BERGLES, W. M. ROSENOW, "The Determination of Forced-Convection Surface Boiling Heat Transfers. *Trans. of the ASME* 86 (Series C-J. of Heat Transfer), 365-375, Aug. 1964.

[11] ANSYS CFX Reference Guide, release 12.0, April 2009.

HORUS3D/N NEUTRONICS CALCULATION TOOL DEDICATED TO JHR DESIGN AND SAFETY STUDIES - DEVELOPMENT, VALIDATION, BIASES AND UNCERTAINTIES QUANTIFICATION

C. VAGLIO-GAUDARD, F. JEURY*, C. D'ALETTO, J.F. VIDAL,
J.M. VIDAL, L. GAUBERT, J. POLITELLO
CEA¹, DEN², Cadarache research center, Reactor Studies Department,
13108 Saint-Paul-Lez-Durance, France

*Corresponding author: florence.jeury@cea.fr

ABSTRACT

The international Jules Horowitz Material Testing Reactor (JHR) is under construction at CEA Cadarache research center, in southern France. Its first criticality is foreseen by the end of the decade.

In order to perform JHR design and safety studies, a specific neutronics calculation tool, HORUS3D/N, based on deterministic codes and the European nuclear data library JEFF3.1.1, was developed. The purpose of this neutronics calculation tool is to predict JHR neutronics parameters: reactivity, power distribution, control rod reactivity worth,...

The calculation scheme relies on a two-level approach, with in the first level, a 2D flux calculation on restricted geometries with a fine energy meshing, and a cross section collapsing into a reduced energy meshing with the APOLLO2 lattice code. These collapsed cross sections are introduced into a full 3D core calculation with the CRONOS2 diffusion code in the second level.

The HORUS3D/N development followed the Verification & Validation – Uncertainty Quantification (V&V-UQ) process. This validation step aims at quantifying all the biases and uncertainties associated with HORUS3D/N calculations. These biases and uncertainties originate from both the nuclear data and the deterministic calculation scheme, for JHR calculations at beginning of life or during depletion (in particular for the JHR core at equilibrium).

The biases and uncertainties due to nuclear data are quantified by comparing the Monte Carlo reference TRIPOLI-4[®] calculations using the JEFF3.1.1 nuclear data library, with experimental data.

The biases and uncertainties due to the HORUS3D/N calculation scheme are assessed by comparing HORUS3D/N deterministic calculations with reference route calculations:

- 2D and 3D continuous-energy Monte Carlo TRIPOLI-4[®] calculations, for the JHR beginning of life core calculations,
- 2D APOLLO2-MOC deterministic calculations, using the Method Of Characteristics flux solver for the JHR core calculations during depletion.

Both reference routes are described with a heterogeneous geometry. They use the same JEFF3.1.1 nuclear data library as that of HORUS3D/N.

This paper describes the very latest developments implemented in the HORUS3D/N neutronics calculation tool and on the reference route considering depletion. These new developments take into account the APOLLO2.8/REL2005/CEA2005 package recommendations already applied for light water reactor studies. Moreover, the spatial meshing of the HORUS3D/N reference route was refined and optimized.

This paper also provides a synthesis of the biases and uncertainties associated with the different neutronics parameters calculated with this new version of the HORUS3D/N calculation scheme, for JHR safety studies.

¹ CEA: Commissariat à l'Energie Atomique et aux Energies Alternatives.

² DEN: Direction de l'Energie Nucléaire.

1 Introduction

The Jules Horowitz Reactor (JHR) [1] is the future Material Testing Reactor under construction in France. It will be a major research infrastructure in Europe designed to support existing power plant operations and lifetime extension, as well as future reactor design. Its objectives are to test the new structural material and fuel behavior under irradiation for the development of the GEN-III and GEN-IV reactors and also to demonstrate the satisfactory stainless steel behavior for current French Pressurized Water Reactor (PWR) lifetime extension. The JHR will also supply 25% to 50% of the European demand for radio-isotopes, mainly ⁹⁹Mo, for medical applications [2], and n-doped silicon for high power electronics.

The JHR first criticality is planned for the end of the decade.

The design and safety studies have been carried out using the neutronics calculation tool, HORUS3D/N, developed since the 2000s to meet the specific needs of JHR [3].

In this paper, after a brief description of the JHR, the HORUS3D/N calculation package will be presented. It will then focus on the very latest developments implemented in HORUS3D/N. These developments followed the Verification & Validation – Uncertainty Quantification (V&V-UQ) process, which aims at quantifying the biases and uncertainties associated with neutron calculations. At the end, the paper will provide a synthesis of the biases and uncertainties associated with the different neutronics parameters calculated using the new version of HORUS3D/N for JHR safety studies.

2 The Jules Horowitz Reactor

The JHR is a tank-in-pool type reactor using light water as its coolant and moderator. The maximum thermal power is 100 MW.

The core (600 mm. fuel active height) can contain 34 to 37 fuel elements, inserted in an aluminum alloy rack. When one of the 37 cells of the rack is free of a fuel element, an experimental device can be inserted. Up to 20 experimental devices can be loaded in the core or in the reflector and irradiated at the same time.

In order to obtain a high power density and thus reach a high fast neutron flux level ($\sim 5 \times 10^{14}$ n/cm²/s, $E \geq 0.907$ MeV), the fuel elements (see Fig.1) consist of 3 sets of curved plates assembled with aluminum stiffeners. The plates are clad with Al-Fe-Ni. A hafnium control rod, connected to an aluminum follower (the follower is an aluminum tube replacing the absorber part of the control rod when it is withdrawn), or an experimental device can be loaded in the central hole. A boron insert is positioned 1 cm above the active height in each plate to prevent departure from nucleate boiling at the top of the core water channels.

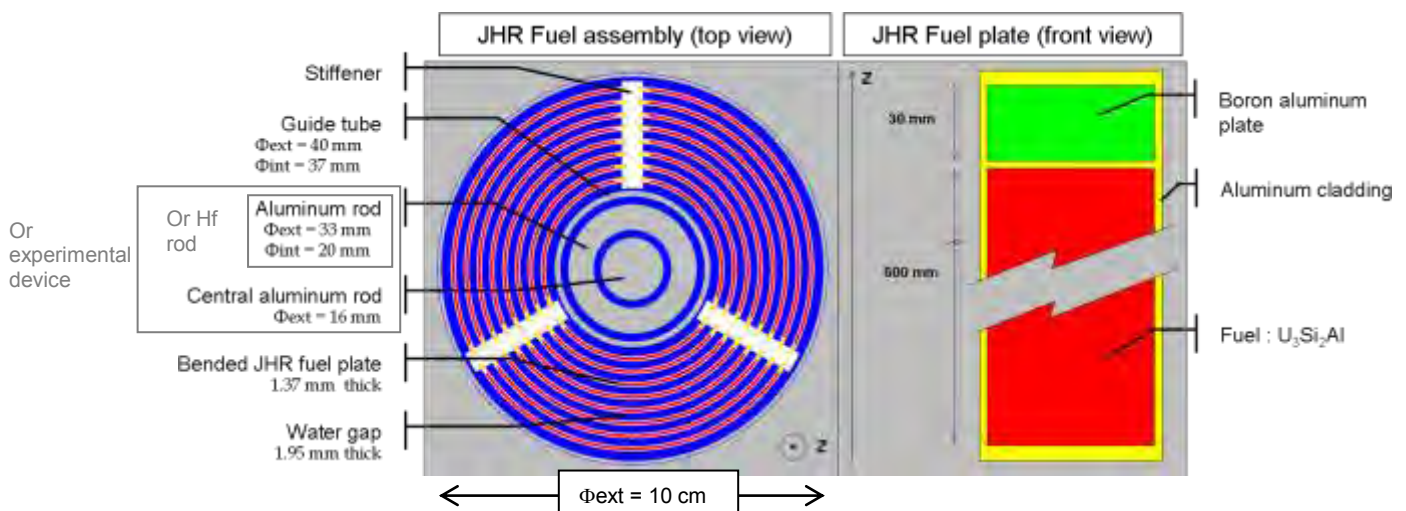


Fig.1: JHR fuel element and JHR fuel plate description

The JHR will start with a standard density low enriched U_3Si_2 fuel ($e\% \text{ }^{235}U = 19.75\%$, density 4.8 g.cm^{-3}), and with a maximum thermal power of 100MW.

The core will operate with a cold fuel (fuel temperature $\sim 100^\circ\text{C}$) and a slightly pressurized light water (pressure = 8 bars; temperature = 35°C).

The core area is surrounded by a reflector which optimizes the core cycle length and provides intense thermal fluxes in this area ($\sim 5 \times 10^{14} \text{ n/cm}^2/\text{s}$, $E \leq 0.625 \text{ eV}$). The reflector area is made of beryllium blocks. Experiments can be performed either in the core itself, as seen above, or in reflector static locations (Fig.2) but also on displacement systems as an effective way to investigate transient regimes occurring in incidental or accidental situations.

This provides a flexible experimental capability that can create up to 16 dpa/year - in comparison to the 2-3 dpa/year produced in industrial Light Water Reactors (LWR) - for in-core material experiments (with 275 full power operation days per year) and 600 W.cm^{-1} for in reflector simple 1% ^{235}U enriched fuel experiments.

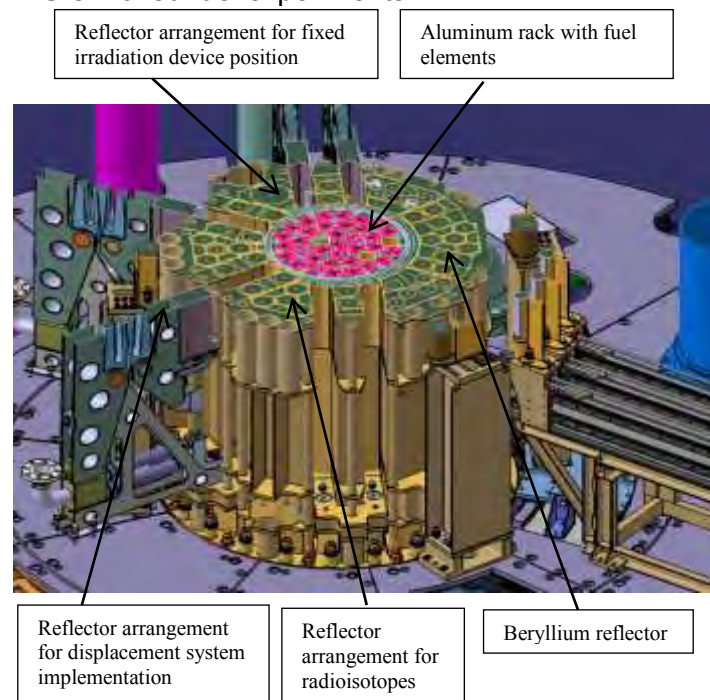


Fig.2: JHR description

3 The HORUS3D/N neutronics calculation package

The JHR innovative design led to the development of a specific neutronics tool, HORUS3D/N. The industrial route of this neutronics calculation tool is based on an APOLLO2 [4]/CRONOS2 [5] deterministic calculation scheme and the JEFF3.1.1 [6] European nuclear data library. It is a two-step calculation route (see Fig.4) with:

- **for the first calculation step:** several APOLLO2 two-dimensional (2D) fuel assembly calculations (one per component loaded in the center of the assembly) with fine energy-meshing to obtain self-shielded and depleted cross sections collapsed into 6 energy groups. The $1/6^{\text{th}}$ assembly symmetry is used for the calculation. This first step provides libraries, tabulated versus burnup, for each kind of component present in the JHR,
- **for the second calculation step:** a 3D full core diffusion calculation on a hexagonal spatial meshing [3]. Despite the apparently irregular arrangement of the fuel element in the core, the assembly pattern has a hexagonal macro-symmetry (Fig.3). With the iso-parametric finite element method in the CRONOS2 code, each hexagonal mesh cell can be considered as a "Super Finite Element" (SFE). These SFEs need a conform mesh of arbitrary triangles, which form the basic finite elements. The fuel elements are meshed as dodecagons. The reflector region is modelled with a series of particular SFEs, allowing for an accurate modeling of radial and azimuthal heterogeneities.

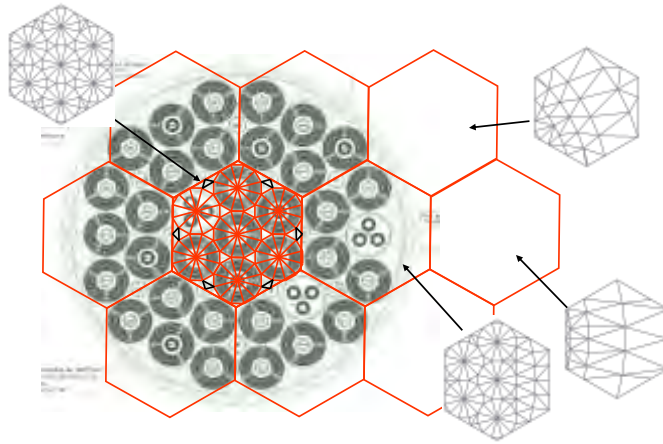


Fig.3: Division of the core by the hexagonal macro-symmetry and attribution of SFEs for the CRONOS calculation

The HORUS3D/N development follows the Verification & Validation – Uncertainty Quantification (V&V-UQ) process [9]. This validation step aims at quantifying all the biases and associated uncertainties of HORUS3D/N calculations. These biases and uncertainties originate from both the nuclear data and the deterministic calculation scheme, for JHR calculations at beginning of life or during depletion (in particular for the JHR core at equilibrium).

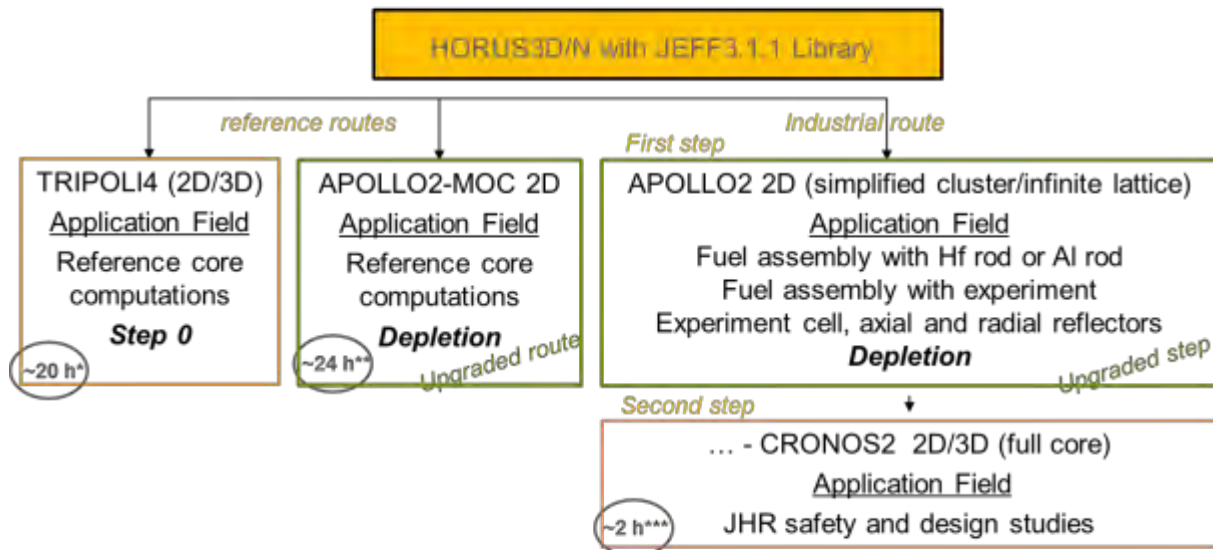
The biases and uncertainties due to nuclear data are quantified by comparing Monte Carlo reference TRIPOLI-4[®] [13] calculations using the JEFF3.1.1 nuclear data library, with experimental data.

The biases and uncertainties due to the HORUS3D/N calculation scheme are assessed by comparing HORUS3D/N deterministic calculations with reference route calculations (Fig.4):

- 2D and 3D continuous-energy Monte Carlo TRIPOLI-4[®] calculations, for the JHR beginning of life core calculations,
- 2D APOLLO2-MOC deterministic calculations [7], [8], for the JHR depleted core calculations.

Both reference routes are described with a heterogeneous geometry and use transport solver. They use the same JEFF3.1.1 nuclear data library as HORUS3D/N.

The very latest developments concern the APOLLO2 first step of the HORUS3D/N industrial route, and the reference route for depletion (see Fig.4).



Calculations performed on an AMD Opteron Linux DELL 2.3 Ghz computer
 * For 3D TRIPOLI4 core computations, at step 0, in parallel mode using 32 processors
 ** For 2D APOLLO2 core computations, depleted up to 82 GWj/t (mean burn-up of the JHR core), on one processor
 *** For 3D CRONOS2 core computations, depleted up to 82 GWj/t (mean burn-up of the JHR core), on one processor

Fig.4: HORUS3D/N package calculation routes and upgraded routes

The following chapter will focus on these very latest developments.

4 HORUS3D/N package developments

Different developments were performed in HORUS3D/N last year: the reflector geometry is now updated in consistency with the JHR design evolution, the material balance with the main impurities is now considered, and, in the industrial route, new features are now available. The main developments are presented hereafter. They take into account the APOLLO2.8/REL2005/CEA2005 package recommendations developed by CEA for light water reactor studies [10]. Moreover, the spatial meshing of the HORUS3D/N APOLLO2 core reference route was refined and optimized.

4.1 Industrial route developments

4.1.1 Self-shielding and flux computations

As mentioned above, these developments concern the first step of the industrial route, i.e. the APOLLO2 libraries³ calculations for CRONOS2 (see Fig.4). The 2D calculation scheme for the different clusters (fuel assembly with Al rod, fuel assembly with Hf rod, fuel with experiments - Fig.1, and experiments in cell) and the radial reflector modelling, was improved by taking into account the APOLLO2.8/REL2005/CEA2005 package recommendations. The main developments for the fuel clusters are the following:

- concerning the self-shielding computations:
 - the use of the SHEM-281 group energy mesh on 1 D cylindrical simplified geometry,
 - for the U_3Si_2 -Al fuel: the resonant mixture self-shielding treatment for ^{235}U , ^{238}U , ^{239}Pu and ^{240}Pu , is used in the 33-200 eV intermediate range, in order to rigorously account for resonance mutual shielding of these major actinides above 23 eV. Below 23 eV, the 281-group energy mesh (SHEM) is fine enough to avoid resonance self-shielding approximations,
 - for the Hafnium absorber: the resonant mixture self-shielding treatment for ^{177}Hf , ^{179}Hf , ^{176}Hf , ^{178}Hf , ^{180}Hf , is used up to 1keV in order to rigorously account for resonance mutual shielding of these isotopes in this energy range.

³ Multi-group self-shielded cross sections for different fuel temperatures, moderator densities and fuel burn-ups, collapsed into 6 energy groups in the case of the JHR.

- concerning the flux computations:
 - the spatial meshing of the fuel assembly is performed with 24 angular sectors, i.e. 4 angular sectors on $1/6^{\text{th}}$ of the assembly and 205 calculation regions (see Fig.5), allowing for a better assessment of the azimuthal thermal flux gradient near the stiffeners,
 - the computations are performed using the APOLLO2 Method Of Characteristics (MOC) flux solver with the SHEM-281 group energy mesh (no collapsing), at time-step zero and in depletion,
 - the calculations are based on fine tracking values: Tracking step: $\Delta R=0.04\text{cm}$, radial direction number in $[0, \pi]$: $N\Phi=24$, polar direction number in $[0, \pi/2]$: $N\Psi=3$ (Bickley quadrature), associated with a P3 anisotropy scattering order,
 - neutron leakage: homogeneous B1 model with research of critical buckling.

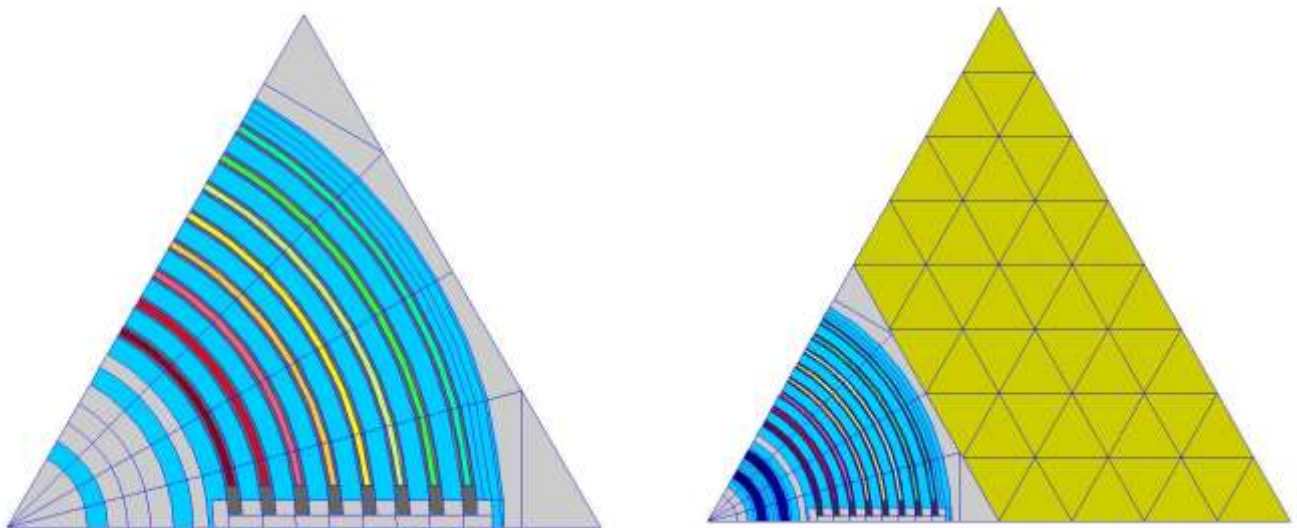


Fig.5: Flux computation geometry with APOLLO2 TDT-MOC flux solver:
 $1/6^{\text{th}}$ of the fuel assembly with Al rod follower at the center of the assembly (205 calculation regions)
 (left hand side)
 and $1/6^{\text{th}}$ of the fuel assembly with hafnium rod with its homogenized environment in green
 (right hand side)

Table 1 summarizes the main developments performed on the HORUS3D/N v4.2 industrial route, in comparison with the previous versions (HORUS3D/N v4.1/v4.0). These new developments induced the adaptation of about 70 APOLLO2 procedures developed in the GIBIANE language.

Table 1: industrial route - APOLLO2 computation options - fuel clusters and reflector modellings

		HORUS3D/N v4.2 (new version)	HORUS3D/N v4.1/v4.0 (previous versions)
APOLLO2	version	APOLLO2.8-4	APOLLO2.8-3
Library	version	JEFF3.1.1 (CEAV5.1.2, processed for APOLLO2)	JEFF3.1.1 (CEA2005V4.1.2, processed for APOLLO2)
Self-shielding	energy mesh	SHEM - 281 groups	XMAS - 172 groups
	method	Livolant-Jeanpierre resonant mixture +	Livolant-Jeanpierre resonant mixture +
	geometry	1D Cylindrical for most of the cases	
Flux calculation	energy mesh (collapsed cross sections)	No collapsing (281 g) <i>Except for:</i> - axial reflector: 6 g - radial reflector: 22 g (t0 only)*	6 g (collapsed from Pij 1D calculation) <i>Except for:</i> - fuel assembly+Hf rod: 172g - radial reflector: 20 g (t0 only)
	geometry	1/6 th of the fuel assembly with or without environment, "RZ" assembly for the axial reflector	
	spatial mesh	24 angular sectors	6 angular sectors
	solver	MOC (2D) <i>Except for:</i> - axial reflector: SN	Pij (2D) <i>Except for:</i> - axial reflector: SN
	Anisotropic scattering	P3	P0-corrected
	tracking	cyclic	cyclic
	Fine tracking values	- Tracking step: $\Delta R = 0.04$ cm - radial direction number in $[0, \pi]$: $N\Phi = 24$ - polar direction number in $[0, \pi/2]$: $N\Psi = 3$ - polar quadrature: "Bickley"	- Tracking step: $\Delta R = 0.05$ cm - radial direction number in $[0, \pi]$: $N\Phi = 24$ - polar direction number in $[0, \pi/2]$: $N\Psi = 2$ - polar quadrature: "Bickley"
	neutron leakage: homogeneous B1 model	critical buckling	geometrical buckling
Results		<i>self-shielded and depleted cross sections collapsed into 6 energy groups (input data for CRONOS2)</i>	

(*): obtained from the 2D core computations (see § 4.2), with homogenized fuel assemblies.

The number of flux calculation regions (205 for 1/6th of the assembly), and the order of anisotropic neutron scattering (P3) were optimized, i.e. a validation step (comparison of the computations with Monte Carlo TRIPOLI-4[®] calculations at step 0) performed on the 2 main fuel clusters (fuel assembly with Al rod, fuel assembly with Hf rod) showed that they correspond to the most computation time accuracy compromise:

- the computation region number of 205 is sufficient; finer meshing doesn't yield significant accuracy gains,
- the P3 scattering is necessary, in particular to evaluate the Hf absorption rate better; the computation time remains acceptable (~40 s with P3 to be compared to ~20 s with P0-corrected order).

4.1.1 Validation of the first step of the HORUS3D/N industrial route

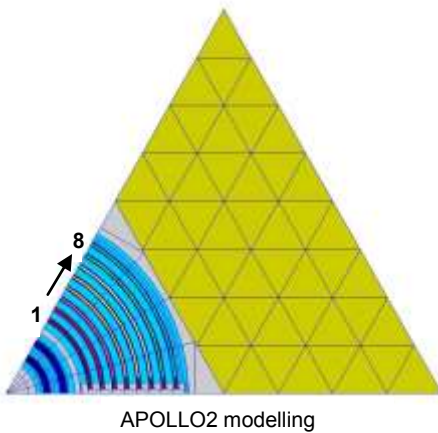
An important validation step was performed on the APOLLO2 assembly scheme with the calculation options presented in Table 1. This validation step was carried out on the 2 main fuel clusters: the fuel assembly with Al rod and the fuel assembly with Hf rod.

It consisted in comparing the APOLLO2 results with the Monte Carlo TRIPOLI-4[®] computations at step 0 with the same JEFF3.1.1 library.

Different computations were compared: reactivity, fission rate per fuel plate, hafnium rod efficiency. The results are the following:

- the reactivity is overestimated by $\sim +30$ pcm for the fuel assembly with Al rod,
- the hafnium rod efficiency is overestimated by +1.1%,
- the discrepancy of the fission rate per fuel plate is less than 0.4% (see Table 2).

Table 2: Fuel assembly with Hf rod – biases on the fission rate per fuel plate



Fuel plate	TRIPOLI-4 [®]	std (%) MC unc.	(A2-T4)/T4 (%)	
			P0c	P3
1	0.503	0.008	-0.6%	0.1%
2	0.628	0.007	-0.5%	-0.1%
3	0.759	0.007	0.0%	0.3%
4	0.896	0.006	0.1%	0.3%
5	1.040	0.006	0.2%	0.2%
6	1.196	0.005	-0.1%	-0.1%
7	1.375	0.005	0.1%	0.1%
8	1.604	0.005	0.1%	-0.4%

These very good results validate the new APOLLO2 assembly scheme.

4.2 Reference route in depletion developments

4.2.1 Self-shielding and flux computations

The developments of the APOLLO2-MOC reference route (see Fig.3), follow, as APOLLO2 in the industrial route (see 4.1) the same APOLLO2.8/REL2005/CEA2005 package recommendations.

Table 3 summarizes the main developments performed on this route.

Table 3: reference route - APOLLO2-MOC computation options – 2D core

		HORUS3D/N v4.2 (new version)	HORUS3D/N v4.1/v4.0 (previous versions)
APOLLO2	version	APOLLO2.8-4	APOLLO2.8-3
Library	version	JEFF3.1.1 (CEAV5.1.2)	JEFF3.1.1 (CEA2005V4.1.2)
Self-shielding	energy mesh	SHEM - 281 groups	XMAS - 172 groups
	method	Livolant-Jeanpierre resonant mixture +	Livolant-Jeanpierre resonant mixture +
	geometry	1D Cylindrical for most of the cases	
Flux calculation	energy mesh (collapsed cross sections)	22 g (collapsed from Pij 1D calculation)	20 g (collapsed from Pij 1D calculation)
	geometry	2D core	
	spatial mesh	Assembly: 12 angular sectors Reflector: new optimized spatial mesh	Assembly: 6 angular sectors
	solver	MOC	MOC
	Anisotropic scattering	P3	P0 corrected
	tracking	Non cycling	cyclic
	Fine tracking values	- Tracking step: $\Delta R = 0.04$ cm - radial direction number in $[0, \pi]$: $N\Phi = 24$ - polar direction number in $[0, \pi/2]$: $N\Psi = 3$ - polar quadrature: "Bickley"	- Tracking step: $\Delta R = 0.05$ cm - radial direction number in $[0, \pi]$: $N\Phi = 24$ - polar direction number in $[0, \pi/2]$: $N\Psi = 2$ - polar quadrature: "Bickley"

.../...

Table 3: reference route - APOLLO2-MOC computation options – 2D core (continued)

		HORUS3D/N v4.2 (new version)	HORUS3D/N v4.1/v4.0 (previous versions)
Flux calculation	Leakage	Axial buckling No axial leakage when compared with TRIPOLI4 or CRONOS2	
Results		Reactivity, power distribution, ... in depletion	

The spatial meshing of the reflector (16506 calculation regions), the assembly spatial meshing (12 angular sectors) and the anisotropic scattering order (P3) were optimized, i.e. a validation step (comparison of the computations with Monte Carlo TRIPOLI-4[®] calculations⁴ at step 0) showed that they correspond to the most computation time accuracy compromise:

- the assembly spatial meshing with 12 angular sectors is sufficient to evaluate the azimuthal thermal flux,
- P3 anisotropic scattering enables us to reduce the reactivity discrepancy ($\Delta\rho = -11$ pcm with P3, $\Delta\rho = -92$ pcm with P0-corrected); the computation time remains acceptable (22 min. to be compared to 11 min. with P0-corrected order) (see Table 4).

Table 4: APOLLO2-MOC/TRIPOLI4 discrepancies - loaded core (37 fuel assemblies), no experiments in the core nor in the reflector, no Hafnium control rods, at JHR begin of life

	HORUS3D/N v4.2	
	P0-c	P3
Reactivity		
$\Delta\rho$ (pcm)	-92	-11
Plate power distribution		
mean deviation (%)	+1.1	+1.1
min. deviation (%)	-2.6	-2.9
max. deviation (%)	+2.9	+3.0
Computation time (Step 0)	11min.	22min.

The following paragraph focuses on the work performed to optimize the spatial meshing of the reflector, considering the REL2005 recommendation.

4.2.2 Reflector spatial meshing optimization

Before HORUS3D/Nv4.1, for APOLLO2-MOC calculations, the spatial meshing of the core and of the reflector was performed with the pre-processing user interface SILENE. The spatial meshing generation was a time-intensive task (duration of several weeks), with a serious risk of error.

Therefore, the decision was made to introduce a more modern and high performance pre-processing user interface into HORUS3D/N: the SALOME platform [14], in order to:

- generate a spatial meshing in a few minutes, and thus follow the evolution of JHR design easily,
- have the same geometric model between Monte Carlo and deterministic schemes, and thereby limit the risk of error and the computation biases,
- have a greater flexibility and thus refine areas of interest.

Up to now, only the reflector zone has been concerned with these new developments. HORUS3D/Nv4.1 was an intermediate version used to test the feasibility of the SALOME integration.

⁴ Monte Carlo TRIPOLI-4[®] Computations are performed with 4.10^8 particles (corresponding to a standard deviation on k_{eff} of 5 pcm).

In HORUS3D/Nv4.2, thanks to SALOME, the spatial meshing of the reflector was upgraded in order to:

- follow the APOLLO2.8/REL2005/CEA2005 package recommendations (see Fig.6), i.e. refine the radial mesh near the core in order to respect the thermal neutron flux gradient:

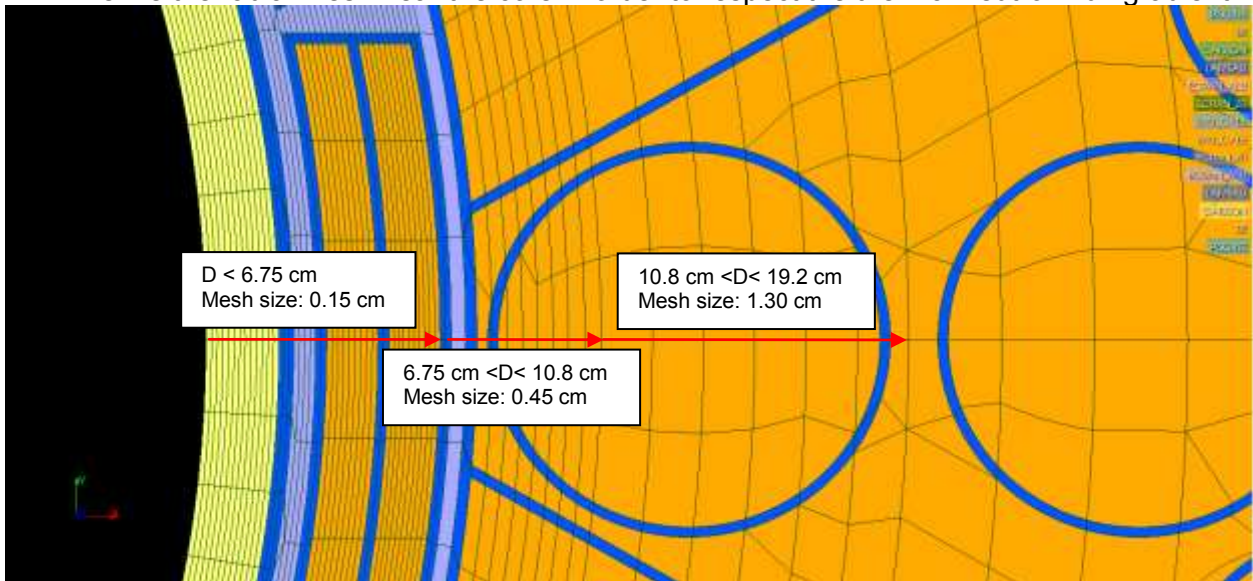


Fig.6: reflector meshing with SALOME in compliance with APOLLO2.8/REL2005/CEA2005 package recommendations

- define a specific meshing for each experiment (see Fig.7) without changing the meshing of the rest of the reflector:

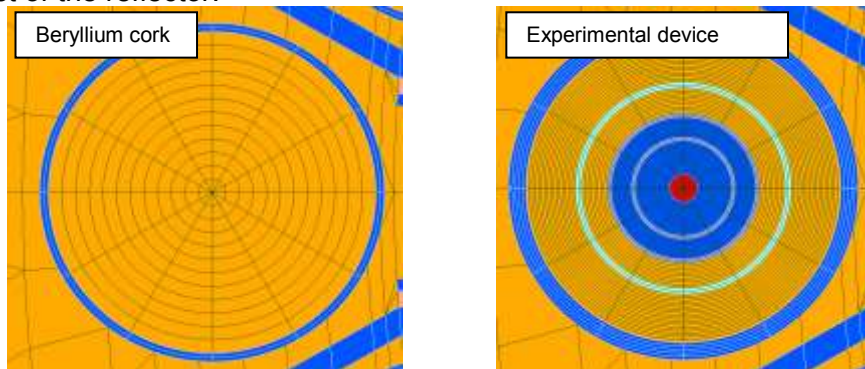


Fig.7: specific meshing with SALOME – Beryllium cork (left hand side) – experimental device (right hand side)

- optimize the mesh number (i.e. define the meshing which corresponds to the most computation time accuracy compromise).

Table 5 presents the mesh number of the two last versions of HORUS3D/N (see Fig.8). One can notice that the mesh number of the reflector is equivalent between the 2 versions. Thus, this new meshing doesn't increase the computation time, but it is optimized (refine meshing in the areas of interest) and generated much more quickly: a few minutes with SALOME, in comparison to 3 to 4 weeks with SILENE.

Table 5: mesh number of HORUS3D/N v4.2 and v4.0 versions - loaded core (37 fuel assemblies), no experiments in the core nor in the reflector

	HORUS3D/N v4.2 (reflector meshing with SALOME)	HORUS3D/N v4.0 (meshing with SILENE)
Core	25686*	16140*
Reflector	16506	13349
Total	42192	29489

(*): HORUS3D/N v4.2: 12 angular sectors for each assembly; HORUS3D/N v4.0: 6 angular sectors for each assembly.

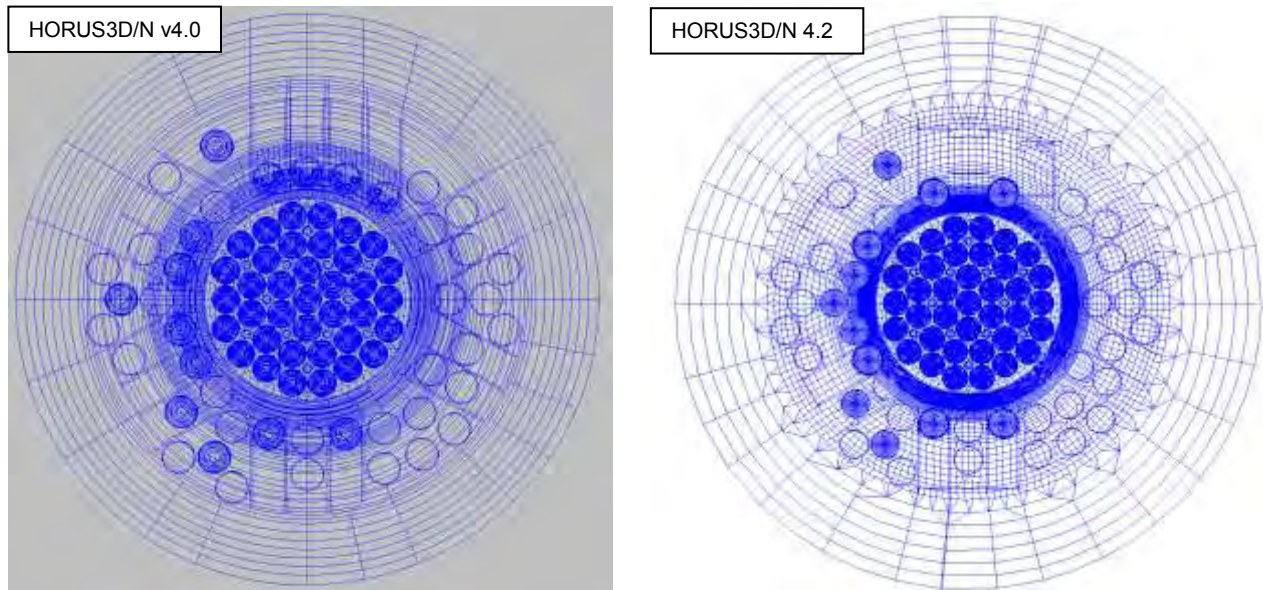


Fig.8: core and reflector meshing for v4.0 and v4.2 HORUS3D/N versions

4.2.3 Validation of the reference route in depletion

An important validation step was performed on the 2D APOLLO2-MOC core scheme of HORUS3D/N v4.2 (with the optimized meshing – see § 4.2.2, and the calculation options as presented in Table 3).

It consisted in comparing the 2D APOLLO2-MOC results versus the 2D Monte Carlo TRIPOLI-4^{®5} at step 0 with the same JEFF3.1.1 library.

Different configurations were studied increasing successively the core perturbation:

- 37 Fuel Elements, without experiments, without Hafnium rod (“37FE” configuration),
- 34 Fuel Elements, maximal core experimental loading (7 Fuel elements with experiments +3 cells loaded with experiments), without Hafnium rod (“34FE” configuration),
- 34 Fuel Elements, maximal core experimental loading, with 10 Hafnium rods (“34FE_10Hf” configuration),

the reflector being loaded or not with the 12 experiments.

The results were compared to those of the previous version, the 2D APOLLO2-MOC core scheme of HORUS3D/N v4.0.

Table 6 and Table 7 summarize the discrepancy between the 2 versions when compared to the Monte-Carlo TRIPOLI-4[®] code, for the plate power distribution and the reactivity, respectively. Fig.9 gives an example for the plate power distribution computation.

Table 6: Plate power distribution at JHR beginning of life - APOLLO2-MOC v4.2 and v4.0/TRIPOLI-4[®] discrepancies

REFLECTOR	CONFIG	HORUS3D/N v4.2			HORUS3D/N v4.0		
		mean deviation (%)	max. deviation (%)	min. deviation (%)	mean deviation (%)	max. deviation (%)	min. deviation (%)
Without experiments	37FE	1.1%	3.0%	-2.9%	1.9%	4.2%	-3.5%
	34FE	1.2%	2.7%	-4.4%	1.9%	4.6%	-6.0%
	34FE_10Hf	1.5%	3.3%	-5.4%	2.2%	4.8%	-6.6%
With experiments	37FE	1.1%	3.1%	-2.3%	2.1%	4.8%	-3.6%
	34FE	1.2%	2.3%	-4.6%	2.1%	4.7%	-6.2%
	34FE_10Hf	1.6%	3.3%	-5.4%	2.5%	5.4%	-6.8%

⁵ Monte Carlo TRIPOLI-4[®] Computations are performed with a total number of $4 \cdot 10^8$ neutron histories (corresponding to a standard deviation on k_{effectif} of 5 pcm).

Table 7: Reactivity at JHR beginning of life - APOLLO2-MOC v4.2 and v4.0/ TRIPOLI-4[®] discrepancies

REFLECTOR	CONFIG	HORUS3D/N v4.2	HORUS3D/N v4.0
		$\Delta\rho$ (pcm)	$\Delta\rho$ (pcm)
Without experiments	37FE	-11	-33
	34FE	61	67
	34FE_10Hf	-209	-72
With experiments	37FE	-8	-46
	34FE	66	62
	34FE_10Hf	-207	-85
Computation time (Step 0)		~20 min.	~10 min.

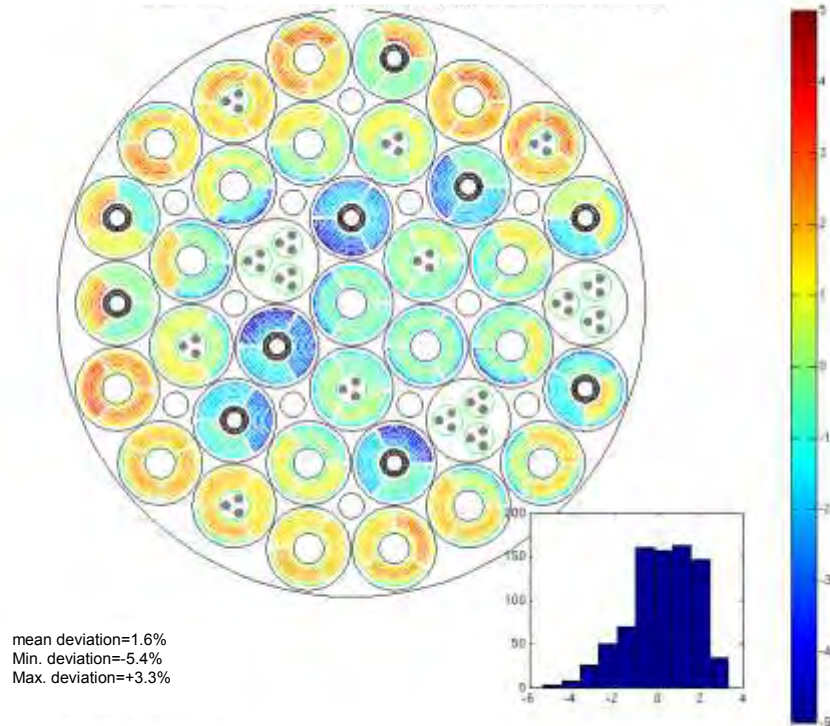


Fig.9: Plate power distribution at JHR beginning of life - APOLLO2-MOC v4.2/ TRIPOLI-4[®] discrepancies (in %) - 34 Fuel Elements, maximal core experimental load, 10 Hafnium rods ("34FE_10Hf" configuration), maximal reflector experimental load

Regarding the plate power distribution, APOLLO2-MOC v4.2 was improved significantly in comparison to the previous version. The mean deviation is strongly reduced: dropping from 2.5% in the v4.0 version to 1.6% in the v4.2 version in the most disturbed configuration (see Table 6).

Regarding the reactivity, APOLLO2-MOC v4.2 computations, when compared to TRIPOLI-4[®], slightly underestimate the reactivity in the less disturbed configurations (-11 pcm) (see Table 7). The 10 Hafnium rods reactivity worth is overestimated by 4%.

The computation time remains acceptable (20 min. at step 0, in comparison to 10 min. for the previous version) (see Table 7).

These very good results validate the 2D APOLLO2-MOC reference core scheme of HORUS3D/N v4.2.

The development of the HORUS3D/N industrial route (see Fig.4) followed the Verification & Validation – Uncertainty Quantification (V&V-UQ) process. First, it was submitted to a Verification step including non-regression tests, and then to a Validation process in order to Quantify the biases and Uncertainties to be applied to each parameter computed with the calculation route.

The following chapter briefly presents this validation process and focuses on the main results of this step: the biases and uncertainties quantification.

5 HORUS3D/N industrial route global validation

The HORUS3D/N simulations are used to predict neutronics parameters with quantifiable confidence and across the JHR application domain. The V&V-UQ process aims at determining to what degree a calculation tool is an accurate representation of the “real world”, i.e. it aims at quantifying the biases and uncertainties associated with the HORUS3D/N computations. These biases and uncertainties have two origins:

- the nuclear data which are physical parameters input and which describe all the interactions between neutrons with matter,
- the models, and more generally, all the approximations used in the APOLLO2/CRONOS2 calculation scheme (approximation of the real geometry, energy cutting, resonance self-shielding, depletion, flux solver, etc.).

5.1 Nuclear data validation

The biases and uncertainties due to nuclear data are quantified by the comparison between Monte Carlo reference TRIPOLI-4[®] calculations and an integral experiment.

In order to provide JHR representative measurement data the AMMON program was launched between late 2010 and early 2013 in the EOLE zero-power critical mock-up (see [9] for details). The AMMON experiment consists of an experimental zone dedicated to the analysis of the JHR neutron and photon physics surrounded by a driver zone. The experimental zone, for the reference configuration, contains 7 JHR fresh fuel standard assemblies-like (see § 2) inserted in an aluminum alloy hexagonal rack (30 cm side length). The driver zone for the reference configuration consists of 622 standard Pressurized Water Reactor (PWR) fuel pins (3.7% ²³⁵U enriched UO₂), with Zircaloy-4 cladding and stainless steel overcladding. The hexagonal lattice pitch of the driver pins was optimized in order to reproduce, as well as possible, the same neutron spectrum as the one of the experimental zone. 5 configurations were studied (see Fig.10):

- a reference configuration with 7 JHR fresh fuel assemblies,
- a configuration with a hafnium control rod totally or half inserted in the middle assembly,
- a configuration with a beryllium block replacing the middle assembly,
- a configuration with water in the middle of the middle assembly (withdrawn Hf rod follower),
- a configuration with water replacing the middle assemblies.

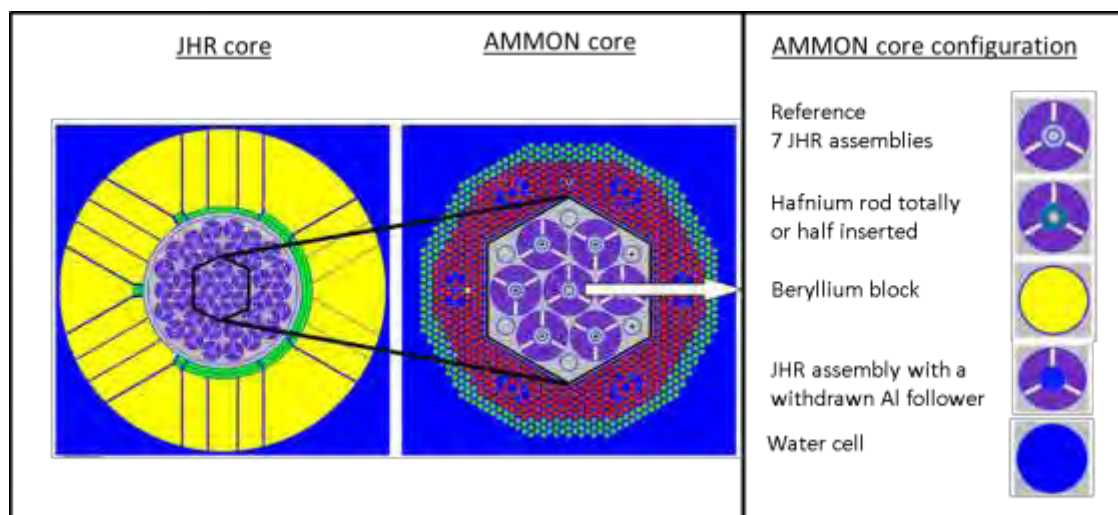


Fig.10: configurations of the AMMON experiment

The interpretation of the AMMON experiments with reference TRIPOLI-4[®] calculations using the JEFF3.1.1 nuclear data library, allowed us to quantify the biases and uncertainties originating from the nuclear data⁶. These results were transposed from the AMMON experiment to the real

⁶ Few physical assumptions are made in TRIPOLI-4[®] that is why the biases are supposed to come only from nuclear data.

JHR core with the representativity methodology [11], [12], for the JHR-Beginning Of Life but also for the JHR in equilibrium. Indeed, a specific study showed that the ^{239}Pu (produced in the $\text{U}_3\text{Si}_2\text{-Al}$ fuel thanks to ^{238}U radiative capture) contribution in assembly fission rates remains limited (<10%) compared to the ^{235}U contribution during the JHR life (the JHR neutron spectrum can be considered as constant). Thus, even if the AMMON experiments were performed on fresh JHR fuel, the results can also be transposed to the JHR in equilibrium.

The biases and uncertainties on the different neutronics parameters computed with HORUS3D/N originating from the nuclear data are summarized in [9]. They are not recalled here. Only the results of the global validation step are presented in chapter 6.

The biases and uncertainties on the different neutronics parameters computed with HORUS3D/N, due to nuclear data and to the calculation scheme (see § 5.2) are summarized in chapter 6.

5.2 HORUS3D/N scheme validation

An important HORUS3D/N scheme validation step was carried out during late 2014. It consisted in assessing the biases and uncertainties due to the scheme itself (geometry approximation, energy cutting, flux solver,...) by comparing HORUS3D/N industrial route computations with reference routes calculations (see chapter 3, especially Fig.4):

- 2D and 3D continuous-energy Monte Carlo TRIPOLI-4[®] calculations, for the JHR beginning of life core calculations,
- 2D APOLLO2-MOC deterministic calculations, using the Method Of Characteristics flux solver, for the JHR core calculations during depletion.

The validation studies will be completed in 2015 with the use of TRIPOLI-4[®] in its new depletion mode, for the comparison with the HORUS3D/N calculations.

The scheme application domain matches the JHR operation domain, i.e.:

. Concerning the reactor configuration:

- fuel assembly: 34 to 37 fuel assemblies with or without Hafnium rods,
- maximal core experimental load: 7 fuel elements with experiments + 3 cells loaded with experiments
- maximal reflector experimental load: 12 experiments

. Concerning the time step:

- beginning of cycle (no xenon, samarium at saturation)
- Xenon equilibrium
- Mid cycle
- End of cycle.

Over 100 validation cases were performed to cover the JHR operation domain and to ensure statistical representativeness.

The detail of this study is not presented in this paper. Only the results of the global validation step are presented hereafter.

The biases and uncertainties on the different neutronics parameters computed with HORUS3D/N, due to the calculation scheme and to nuclear data (see § 5.1) are summarized in chapter 6.

6 HORUS3D/N performances: biases and uncertainties quantification

The results of the validation steps presented in chapter 5 were combined as follows for each JHR relevant parameter computed with the HORUS3D/N industrial route:

- Biases:
$$\text{Biases}_{\text{Global}} = \text{Biases}_{\text{Scheme}} + \text{Biases}_{\text{ND}} \quad (1)$$

- Uncertainties:
$$\sigma_{\text{Global}} = \sqrt{(\sigma_{\text{Scheme}})^2 + (\sigma_{\text{ND}})^2} \quad (2)$$

With:

Biases_{scheme}: Biases of HORUS3D/N due to the calculation scheme, see § 5.2,

Biases_{ND}: Biases of HORUS3D/N due to Nuclear data see § 5.1,

σ_{scheme} : uncertainties of HORUS3D/N due to the calculation scheme, see § 5.2,

σ_{ND} : uncertainties of HORUS3D/N due to Nuclear data, see § 5.1.

Table 8 summarizes the results of the global validation of HORUS3D/N v4.2.

Table 8: HORUS3D/N v4.2 biases and uncertainties assessment

		Biases and uncertainties (2σ)	
		Step 0	Depletion
Reactivity of the critical core at nominal and cold conditions	Without control rod	-71 pcm \pm 650 pcm	-233 pcm \pm 827 pcm
	With control rods	-366 pcm \pm 811 pcm	-663 pcm \pm 911 pcm
Initial core reactivity (with 8 IA)		-862 pcm \pm 640 pcm	-
Xenon equilibrium antireactivity		-	+0% \pm 3.2%
Xenon antireactivity at the peak		-	+0% \pm 16.9%
Samarium antireactivity		-	+0% \pm 2.5%
Integral rod worth		+5.9% \pm 4.7%	+6.4% \pm 3.6%
Differential rod worth		+4.3% \pm 3.2%	+8.9% \pm 3.2%
In core experiment reactivity worth		-1.5% \pm 6.0%	-3.4% \pm 6.1%
In reflector experiment reactivity worth		-72 pcm \pm 39 pcm	-92 pcm \pm 31 pcm
Hot assembly power		+0% \pm 5.4%	+0% \pm 5.4%
Hot plate power		-2.6% \pm 4.6%	-2.6% \pm 4.6%
Burnup distribution – Assembly level		-	+0% \pm 4.1%

7 Conclusion

The HORUS3D/N neutronics calculation tool, dedicated to JHR design and safety studies was upgraded in 2014 in order to take into account the APOLLO2.8/REL2005/CEA2005 package recommendations already applied for light reactor studies: HORUS3D/N v4.2 was thus released by the end of 2014. An important validation step was carried out to quantify the biases and uncertainties to be associated with each neutronics parameter computed with the new scheme. Thanks to the AMMON experiments, and to the improvement of the scheme, the performances were improved, allowing a better assessment of the JHR safety margins. Consequently, a complete validation file of the JHR neutronics calculation tool is obtained.

The development of a new neutronics deterministic calculation tool dedicated to JHR operation and loading studies will begin by the end of 2015. The objective of the tool is to deal with time constraint (a JHR loading will have to be fully calculated in a few days) and user experience (the studies will be performed routinely by JHR operators). The new HORUS3D/N v4.2 tool will serve as a starting point for these new developments.

8 REFERENCES

- [1] D. Iracane, "The Jules Horowitz Reactor, a new Material Testing reactor in Europe," *Nucl. Eng. Tech.*, 38, 5, 437-442, 2006
- [2] OECD/NEA, "The supply of medical radioisotopes – Implementation of the HLG-MR policy approach: results from a self-assessment by the global $^{99}\text{Mo}/^{99\text{m}}\text{Tc}$ supply chain," NEA/SEN/HLGMR(2013)4, 2013
- [3] C. Döderlein, T. Bonaccorsi, C. D'Aletto, J. Di Salvo, O. Gueton, L. Lamoine, F. Moreau, G. Naudan, P. Siréta, "The 3D neutronics scheme for the development of the Jules-Horowitz-Reactor," Proc. Int. Conf. PHYSOR2008, Interlaken, Switzerland, September, 2008
- [4] R. Sanchez, I. Zmijarevic, M. Coste-Delclaux, E. Masiello, S. Santandrea, E. Martinolli, L. Villatte, N. Schwartz, N. Guler, "APOLLO2 Year 2010," *Nucl. Eng. Tech.*, 42, 5, 474-499, 2010
- [5] J.J. Lautard, S. Loubière, C. Magnaud, "CRONOS, a modular computational system for neutronic core calculations," *Proc. IAEA Topical Meeting*, Cadarache, France, 1990
- [6] A. Santamarina et al., "The JEFF-3.1.1 nuclear data library", NEA, JEFF Report 22, 2009
- [7] S. Santandrea, R. Sanchez, "Analysis and improvements of the DPN acceleration

- technique for the method of characteristics in unstructured meshes,” *Annals of Nuclear Energy*, 32, 163-193, 2005
- [8] N. Huot, A. Aggery, D. Blanchet, C. d’Aletto, J. Di Salvo, C. Doderlein, P. Sireta, G. Willermoz, “The JHR neutronics calculation scheme based on the method of characteristics,” *Proc. Int. Conf. M&C2005*, Avignon, France, 2005
 - [9] C. Vaglio-Gaudard, A.C. Colombier, J.P. Hudelot, O. Leray, M. Lemaire, V. Sergeyeva, J. Di Salvo, A. Gruel, P. Siréta, “Analysis of the AMMON experimental program in the EOLE facility supporting the qualification of the JHR neutron and photon tools”, *IEEE TNS*, **61**, 4, 2014
 - [10] A. Santamarina, D. Bernard, P. Blaise, L. Erradi, P. Leconte, R. LeTellier, C. Vaglio, J.F. Vidal, “APOLLO2.8: a validated code package for PWR neutronics calculations,” *Proc. Int. Conf. ANFM2009*, Hilton Head Island, South Carolina, USA, April, 2009
 - [11] O. Leray, C. Vaglio-Gaudard, J.P. Hudelot, A. Santamarina, G. Noguere, “Sensitivity and uncertainty analysis applied to the JHR reactivity prediction,” *Proc. Int. Conf. PHYSOR2012*, Knoxville, Tennessee, USA, 2012
 - [12] V.V. Orlov, A.A. Van’kov, A.I. Voropaev, Y.A. Kazanskij, V.I. Matveev, V.M. Mugarov, E.A. Khodarev, “Problem of fast reactor physics related to breeding,” *Atomic Energy Review*, 18. 4, 989-1077, 1980
 - [13] E. Brun, F. Damian, C.M. Diop, E. Dumonteil, F.X. Hugot, C. Jouanne, Y.K. Lee, F. Malvagi, A. Mazzolo, O. Petit, J.C. Trama, T. Visonneau and A. Zoia, “TRIPOLI-4, CEA, EDF and AREVA Reference Monte Carlo Code”, *Proc. Int. Conf. SNA+MC 2013*, Paris, France, 2013
 - [14] www.salome-platform.org

UNCERTAINTY ASSESSMENT FOR REACTIVITY INDUCED ACCIDENT OF 5-MW POOL-TYPE RESEARCH REACTOR

SOO-BEEN YUM, SU-KI PARK

*Safety Analysis Group, Korea Atomic Energy Research Institute,
989-111 Daedeokdaero, Yuseong, Daejeon, 305-353, Republic of Korea*

ABSTRACT

Best estimate plus uncertainty (BEPU) is a promising approach to a safety analysis for nuclear reactors, and the uncertainty calculation is the most important concern for it. BEPU ensures realistic safety margins and secures a higher reactor effectiveness by taking the global uncertainty assessment for the parameters, whereas the previous uncertainty analysis considers each parameter separately. The reactivity induced accident (RIA) of a 5MW open-pool type research reactor was selected as a sample problem for a BEPU uncertainty assessment. We selected an insertion of cold water event, which causes a reactivity insertion by temperature feedbacks. The significant contributors to the reactor safety are identified and then input sets are sampled. 124 calculations were performed for the uncertainty evaluation, which is the number of code runs required for a 95%/95% tolerance level of the 3rd order Wilk's formula. MOSAIQUE software developed by KAERI was used for automated sampling of the uncertainty parameters, a global uncertainty calculation, and post processing of the results. We calculated the fuel centerline temperature (FCT) and the critical heat flux ratio (CHFR) with 95%/95% tolerance level and compared them with those from conservative analyses. In addition, the impact of each design parameters on the safety parameters was estimated by sensitivity analyses.

1. Introduction

1.1 Objective

US NRC revised its regulations in 1989, such that BEPU is able to replace the previous conservative approach to reactor safety analyses. Following the new regulation, ATUCHA unit 2 in Argentina recently obtained an operating license with the final safety analysis report using the BEPU approach. These two examples show the global trends of a safety analysis, which are shifting from a conservative analysis to BEPU. Figure 1 shows a comparison of the safety parameters calculated by different methodologies. BEPU estimates safety parameters more realistically compared to those by conservative analyses, reducing the excessive conservatism in a safety analysis and increasing the margin in the reactor operation.

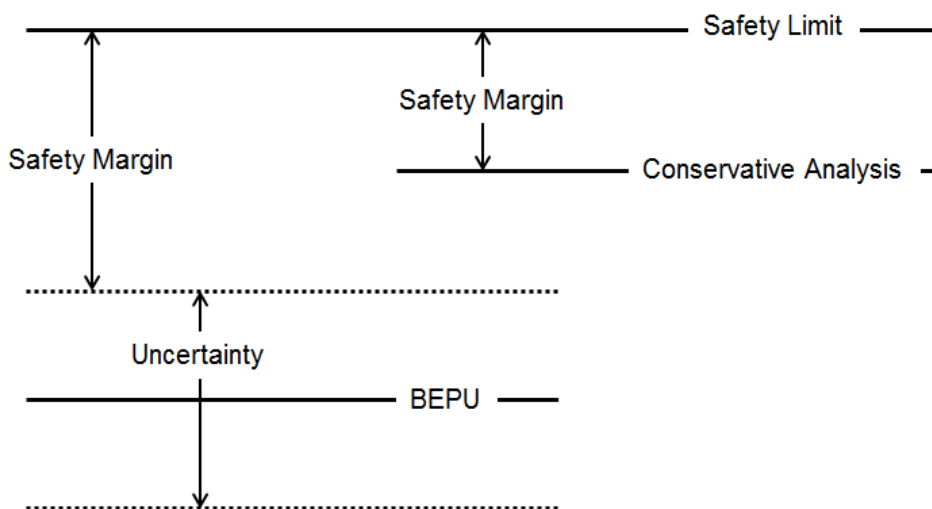


Fig 1. Comparison of different analysis methodologies

Following these international trends, we introduced the BEPU safety analysis for a reactivity induced accident of a 5-MW pool-type research reactor. The core safety parameters and input parameters affecting the parameters are selected first, and the overall uncertainties of the safety parameter are then calculated using a non-parametric uncertainty analysis. The safety parameters including uncertainties are presented and the importance of each parameter is ranked based on sensitivity analyses.

1.2 MOSAIQUE

MOSAIQUE (Module for SAmpling Input and Quantifying Estimator) software was developed in KAERI to conduct a probabilistic uncertainty analysis of computerized simulation models [1]. The software provides automated sampling, calculation and post processing, therefore reduces a lot of time and effort required to perform a BEPU analysis.

MOSAIQUE has three main functions: (1) sampling of input parameters, (2) calculating global uncertainties of the safety parameters, and (3) post processing of uncertainty bands of safety parameters and sensitivity of the input parameters.

1.3 Reactivity induced accident

For a BEPU uncertainty assessment, the RIA of a 5-MW open pool-type research reactor is selected as a sample problem. The scenario selected for the analysis is an insertion of cold water which is a RIA caused by reactivity feedbacks of coolant and fuel temperature when the primary cooling pump starts suddenly during the natural convection mode. Figure 2 shows the schematics of two cooling modes at the reactor; the natural convection mode and the forced convection mode by primary cooling pumps. During the natural convection mode, the temperature at the upper guide structure is higher than that of reactor pool since the core is cooled by the natural circulation of coolant via flap valves. When a primary cooling pump starts to operate suddenly, the hot water at the upper guide structure enters the core first, but the relatively cold pool water enters soon after few second. Then the reactor power increases by the reactivity feedbacks of coolant and fuel temperature. The insertion of cold water is the most complicated event among RIAs because the thermal hydraulic variables and the reactor kinetic variables are cross-linked and change together during the event. The safety parameters investigated for the event are the maximum fuel centerline temperature (MFCT) and minimum critical heat flux ratio (MCHFR).

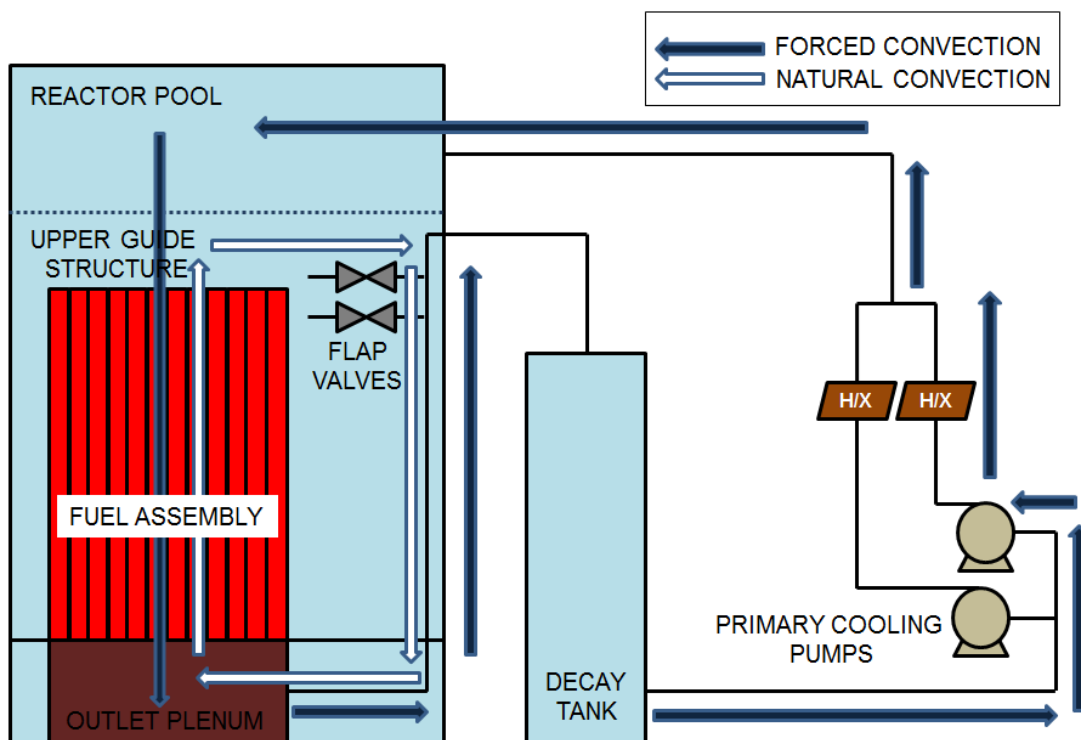


Fig 2. Schematic diagram during forced convection and natural convection mode

2. Uncertainty assessment

2.1 Frozen code selection

The behaviors of the reactor core and the systems are analyzed by the MARS-KS. MARS-KS is a consolidated and restructured version of the RELAP5/MOD3.2 and COBRA-TF codes and this code has been improved for the regulatory and best estimative purposes [2]. MARS-KS 1.3, the latest version, is used for the safety analyses of the event, since it has the best performance and accuracy at the moment.

2.2 Input parameter selection

#	Events
1	The reactor is in training operation, cooled by natural convection.
2	One PCS pump starts a sudden operation.
3	A positive reactivity is inserted by the of cold water insertion.
4	The power increases up to the power level trip set point.
5	The reactor trip signal is generated after the signal delay time.
6	The control absorber rods begin to drop into the core.

Tab 1: Sequence of event

Phenomenon	Relevant variables
Natural circulation	Initial core power, Pool inlet temperature
Forced convection	Mass flow rate, Pool level, Heat transfer coefficient,
Fuel behavior	Fuel corrosion layer, Heat flux hot channel factor
Reactivity insertion	Coolant temperature coefficient, Fuel temperature coefficient

Tab 2: Main phenomena and their relevant physical parameters

Table 1 summarizes the sequence of event during the insertion of cold water event. The important physical phenomena of the event and the relevant key design parameters expected to influence the reactor safety are summarized in Table 2.

The range of each key parameter for BEPU and conservative analysis are listed in Table 3. All parameters are assumed to have a uniform distribution. The characteristics of each input parameter are described below.

1) Initial core power: The initial core power affects the mass flow rate during natural convection mode. It determines the temperature difference through the core channel, which is related to the reactivity insertion at the event initiation. It also affects the trip time since the trip parameter of the event is the power level. In this event, the initial core power is 0.92%FP to 5.4%FP, including the operation range and sensor uncertainty.

2) Pool inlet temperature: The difference between the pool water temperature and the initial core inlet temperature determines the reactivity insertion at the event initiation. The pool inlet temperature influences the critical heat flux and the maximum fuel temperature. The possible range of pool inlet temperature is 12°C to 48°C. This range includes the operation range and sensor uncertainty.

3) Mass flow rate: The mass flow rate determines the cooling capability of the reactor core, and therefore, the temperature feedback effect is affected by this parameter. In the analyses, the mass flow rate is controlled by adjusting the primary coolant pump head. The possible range of the mass flow rate by a pump is 82.5kg/s to 101.5kg/s. This range includes the operation range and sensor uncertainty.

4) Pool level: The pool level determines the core pressure, which is related to the saturation temperature of the core coolant. The saturation temperature affects the inlet subcooling, which influences the critical heat flux in the fuel channel. The possible range of the pool level is 9.65m to 10.12m. This range also includes the operation range and sensor uncertainty.

5) Fuel corrosion layer: The corrosion layer on the fuel cladding has a low conductivity of less

than 2W/m·K. The fuel corrosion layer is a thermal insulator between the coolant and the fuel cladding, which affects the fuel temperature. The range of the fuel corrosion layer thickness is assumed to be 33µm to 100 µm.

6) Heat flux hot channel factor: The heat flux hot channel factor (HCF) is multiplied to the core heat flux when calculating the MFCT and MCHFR to compensate for the fuel meat fabrication tolerances. The HCF is originated from the U235 homogeneity and U235 loading per plate. The combined uncertainty of HCF is 19% including the factors and the additional core calculation uncertainty.

7) Heat transfer coefficient: The Dittus-Boelter correlation [3] in MARS-KS is used to calculate the heat transfer coefficient in the channel since the coolant is a single phase during RIA. The uncertainty of the correlation for a liquid is ±12.75%. The heat transfer coefficient is controlled by changing the heated equivalent diameter. The range of the heated equivalent diameter, which corresponds to the range of heat transfer coefficient, is 2.89x10⁻³m to 1.04x10⁻²m.

8) Fuel temperature coefficient: The fuel temperature coefficient is the reactivity insertion per unit temperature change of the fuel. The possible range of the coefficient is -2.7x10⁻²mk/K to -6.3x10⁻³mk/K.

9) Coolant temperature coefficient: The coolant temperature coefficient is the reactivity insertion per unit temperature change of the coolant. The coolant temperature range is converted into the density range adopted in MARS-KS. The coolant temperature coefficient has a range of -2.1x10⁻¹mk/K to -4.9x10⁻²mk/K.

Number	Models/Parameters	Operating range	Distribution
1	Initial core power	0.92%FP~5.4%FP (5.4%FP)*	Uniform
2	Pool inlet temperature	12°C~48°C (48°C)*	Uniform
3	Mass flow rate	82.5kg/s~101.5kg/s (82.5kg/s)*	Uniform
4	Pool level	9.65m~10.12m (9.65m)*	Uniform
5	Fuel corrosion layer	33µm~100µm (100µm)*	Uniform
6	Heat flux hot channel factor	0%~19% (19%)*	Uniform
7	Heat transfer coefficient	87.25%~112.75% (87.25%)*	Uniform
8	Fuel temperature coefficient	-2.7x10 ⁻² mk/K~-6.3x10 ⁻³ mk/K (-2.7x10 ⁻² mk/K)*	Uniform
9	Coolant temperature coefficient	-2.1x10 ⁻¹ mk/K~-4.9x10 ⁻² mk/K (-2.1x10 ⁻¹ mk/K)*	Uniform

()*: Input parameters for conservative analysis

Tab 3: Uncertainty parameters for insertion of cold water

2.3 Non-parametric uncertainty calculation

Non-parametric uncertainty calculation is a statistical technique and the required number of code runs is independent from the number of input parameters. Equation (1) shows Wilk's formula [4], which determines the number of code runs required for a certain percentile value with a certain confidence level. Table 4 shows the number of code runs to estimate a 95% probability value with a 95% confidence level, which is a 95%/95% tolerance level. The table also shows the analytical confidence level calculated from the formula.

$$\beta \leq 1 - \sum_{j=n-p+1}^n \binom{N}{j} \gamma^j (1-\gamma)^{N-j} \quad (1)$$

(γ : probability, β : confidence level, N: number of sample, p: order of Wilk's formula)

Order	Number of code runs	Analytical confidence (%)
1	59	95.1505
2	93	95.0024
3	124	95.0470
4	153	95.0555
5	181	95.0837

Tab 4: Wilk's formula

124 sets of input parameters were sampled, and the same number of code runs were conducted by the 3rd order Wilk's formula. The input sets were automatically generated by MOSAIQUE using a Simple Random Sampling (SRS) method. The safety parameters, MFCT and MCHFR, were then calculated using MARS-KS with the inputs.

2.4 Calculating the overall uncertainties

To calculate the final MFCT and MCHFR, the bias that stems from the scale effect and separate/integral effect test should be considered. However, this bias is assumed to be 0 in this analysis, and therefore, MFCT_{95/95} and MCHFR_{95/95} are the results of the BEPU analyses. MFCT_{95/95} and MCHFR_{95/95} mean the 95%/95% values of MFCT and MCHFR estimated from the analyses, by selecting the 3rd largest MFCT and the 3rd smallest MCHFR among the calculated results. Table 5 shows the comparison of the MFCT and MCHFR estimated by BEPU and conservative analyses for the event. The conservative analysis results were evaluated by MARS-KS calculation with the most conservative combinations of input parameters as shown in Table 3.

The differences of MFCT and MCHFR from two different approaches are 2.95°C and 1.09, respectively. The conservative analysis seems to show excessive conservatism in MFCT and MCHFR than those from the BEPU analyses although the bounding values of the design parameters are the same for both methods.

Output uncertainty parameter		BEPU analysis value	Conservative analysis value
MFCT	°C	68.37	71.32
MCHFR	-	7.81	6.72

Tab 5: MFCT and MCHFR from BEPU and conservative analyses

2.5 Sensitivity analysis

The impact of each design parameter on the safety parameters are estimated through sensitivity analyses. The importance of the input parameters on the safety parameters is represented quantitatively by Pearson's correlation coefficient [5]. Pearson's correlation coefficient shows the relationship between the two quantities, as shown in Equation (2).

$$Pearson = corr(X, Y) = \frac{cov(X, Y)}{\sigma_X \sigma_Y} = \frac{E[(X - \mu_X)(Y - \mu_Y)]}{\sigma_X \sigma_Y} \quad (2)$$

(X, Y: parameter, μ_X , μ_Y : expected value, σ_X , σ_Y : standard deviation, cov(X, Y): covariance of X and Y)

The Pearson correlation is a measure of linear dependence between the parameters, which is +1/-1 when the variables are in a perfect linear/inverse linear relationship. The larger absolute value of the Pearson's correlation coefficient means a stronger dependency between the parameters. Figures 2 through 7 show the Pearson's correlation coefficients between the input parameters and trip time, maximum heat flux, critical heat flux (CHF),

MFCT, and MCHFR, respectively. The key design parameters relevant to MFCT and MCHFR are the initial power, the pool inlet temperature, the hot channel factor and the mass flow rate. The other design parameters, whose coefficients are between -0.2 and +0.2 [6], shows a relatively smaller relationship to MFCT and MCHFR because they are physically irrelevant, or the influence is shadowed by major parameters owing to their small uncertainty. The following are the main findings from the figures.

1) As the initial core power increases, as it can be seen in Figure 3, the reactor power reaches the trip set-point faster and the reactor trips earlier. Figure 4 shows that the maximum heat flux of the event increases as the initial core power increases because the reactivity insertion by the temperature feedback effect decreases with time. Therefore, as the initial power increases, the MFCT increases and the MCHFR decreases, as shown in Figures 6 and 7, respectively.

2) The pool inlet temperature determines the fuel temperature directly, and therefore shows a strong positive correlation with MFCT, as shown in Figure 6. The CHF is proportional to the inlet subcooling, resulting in the negative correlation shown in Figure 5. On the other hand, the maximum heat flux at the trip decreases as the pool inlet temperature increases, as shown in Figure 4. The higher inlet temperature reduces the temperature difference along the core by a higher density change per unit of temperature, and therefore the initial reactivity insertion rate decreases. However, the MCHFR shows a negative correlation with the pool inlet temperature (Figure 7), since the change in the maximum heat flux is smaller than the critical heat flux change.

3) Since the critical heat flux is divided by HCF to include the uncertainty of the fuel characteristics as shown in Equation (3), MCHFR shows a strong negative correlation with HCF (Figure 7). However, the HCF shows a negligible correlation with the MFCT (Figure 6) because the factor is multiplied with the temperature difference between the fuel surface and the fuel centerline, which is very small compared with the uncertainty of T_{clad} . T_{clad} is a function of the coolant temperature as well as the fuel temperature, and therefore, only a 2 to 4°C difference between the fuel centerline and the fuel surface can be shaded by the T_{clad} uncertainty.

$$CHF = \frac{q_{CHF}}{q_{actual} \times HCF}$$

(q_{CHF} : critical heat flux, q_{actual} : calculated actual heat flux from the fuel) (3)

$$FCT = T_{clad} + HCF(T_f - T_w)$$

(T_{clad} : fuel cladding temperature, T_f : fuel centerline temperature, T_w : fuel surface temperature)

4) As the CHF is proportional to the mass flow rate (Figure 5), the MCHFR is also proportional to the mass flow rate (Figure 7). The high mass flow rate enhances the core cooling and decreases the fuel temperature; however, it increases the maximum heat flux at the same time by increasing the fuel temperature feedback. The two factors compete each other, and therefore the influence of mass flow rate on MFCT is small, as shown in Figure 6.

5) When the feedback coefficient of the coolant temperature is large in absolute value, the reactivity insertion and power increase at the event initiation becomes greater. Since the feedback coefficients are negative, the coolant temperature coefficient shows a negative correlation with maximum heat flux. However, since the change in maximum heat flux caused by a coolant temperature feedback is much smaller than the critical heat flux change, the coolant temperature coefficient shows negligible correlations with MCHFR. In the same manner, as shown in Figure 6, the coolant temperature coefficient shows a negligible correlation with MFCT. In addition, the fuel temperature coefficient does not show a clear negative correlation with the maximum heat flux, because the fuel temperature increase by higher core power is canceled with an enhanced core cooling by a cold coolant and high mass flow rate.

6) Since the corrosion layer acts as a thermal insulator between the coolant and fuel cladding, MFCT is proportional to the thickness of the corrosion layer. However, the effect of the corrosion layer on the MFCT is small because it is shaded by other strong parameters (Figure 6).

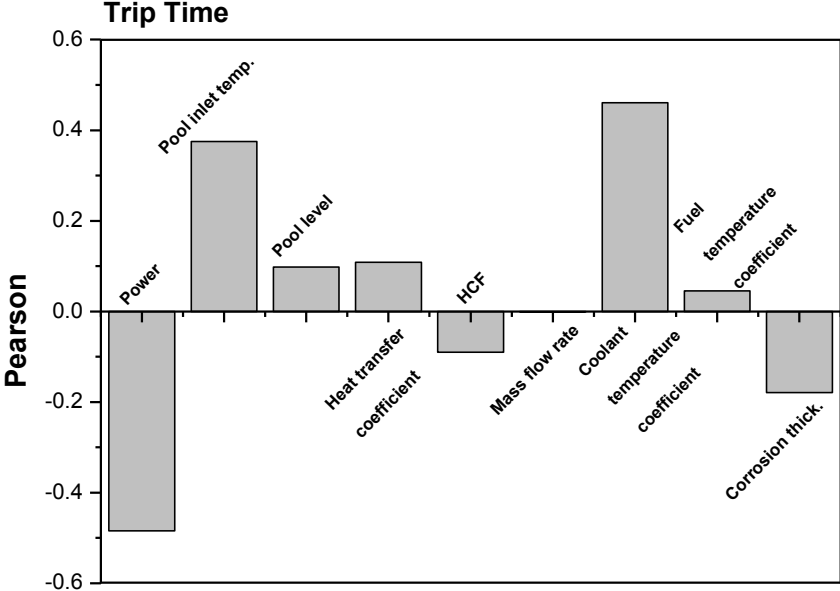


Fig 3. Pearson correlation coefficient for trip time

Fig 4. Pearson correlation coefficient for maximum heat flux

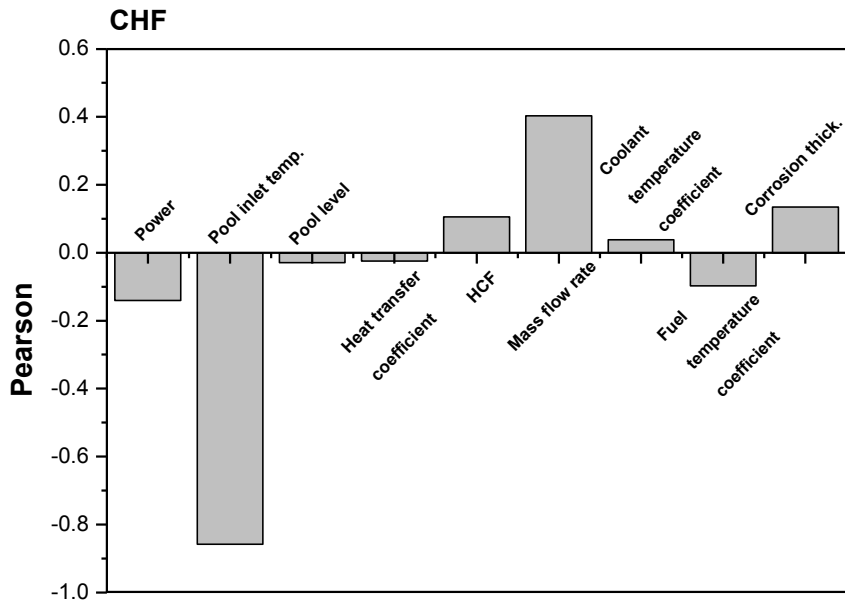


Fig 5. Pearson correlation coefficient for CHF

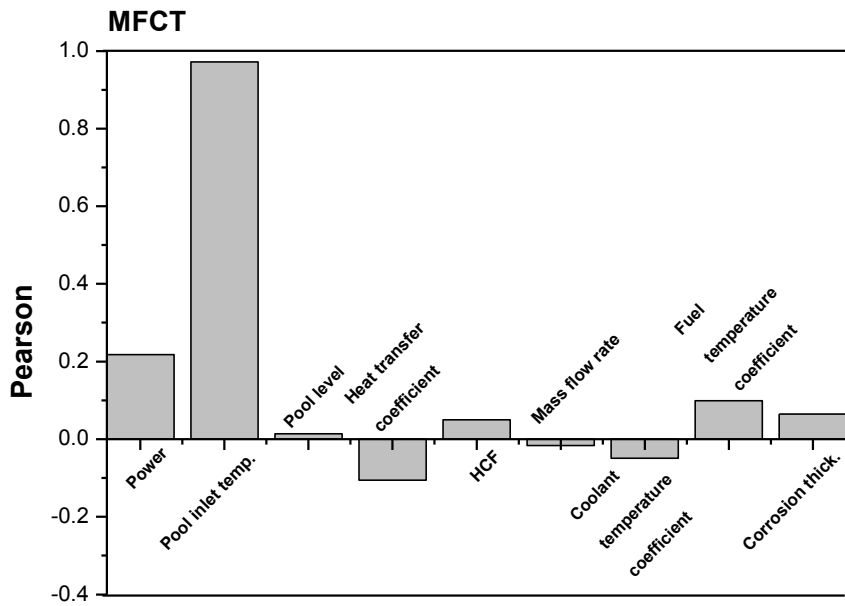


Fig 6. Pearson correlation coefficient for MFCT

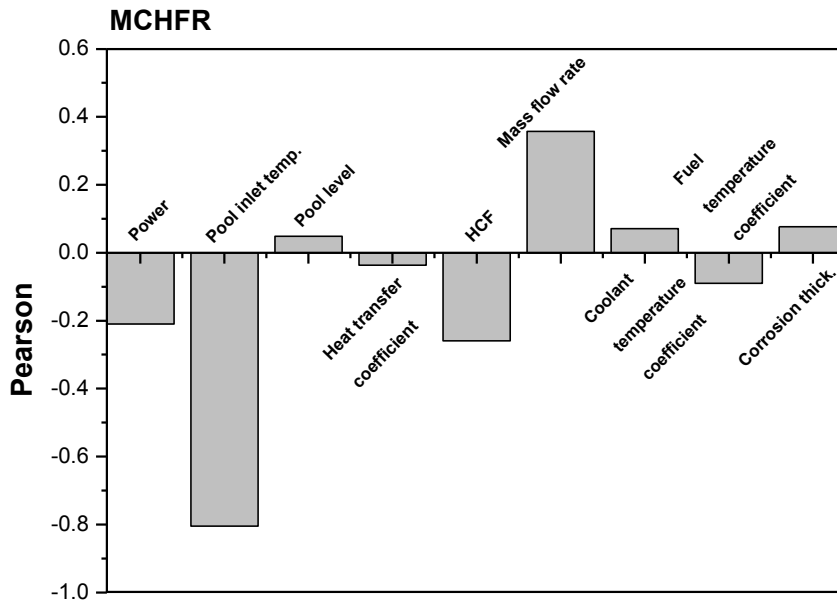


Fig 7. Pearson correlation coefficient for MCHFR

3. Conclusions

A BEPU methodology was applied to an insertion of cold water event of a 5-MW pool-type research reactor. The key input parameters for the event were identified based on the important phenomena during the event. 124 sets of input parameters were sampled, and the same numbers of code runs were used to evaluate the uncertainty of the key safety parameters, MFCT and MCHFR. The MFCT and MCHFR from the BEPU analyses were presented with a 95%/95% tolerance level. Comparing the results from BEPU and those from conservative analysis, the safety parameters show more margins from the safety limits with the BEPU approach, which means the possibility of a higher operability and enhanced efficiency. The importance of each input parameter on the safety parameters was then analyzed through sensitivity analyses. The most important parameters on MFCT and MCHFR are the pool inlet temperature, mass flow rate, HCF and initial core power. The procedures and results in this paper show the applicability and advantages of a BEPU safety analysis over conservative analysis on a research reactor.

References

- [1] H.G.Lim, et al., 2011. MOSAIQUE-A network based software for probabilistic uncertainty analysis of computerized simulation models, Nuclear Engineering and Design 241, 1776-1784.
- [2] Hwang, M.K. and Chung, B.D., 2011, Improvement of MARS code reflood model. In:19th International Conference on Nuclear Engineering (ICONE-19), Chiba, Japan, May 16-19.
- [3] F. W. Dittus, et al., 1985. Heat Transfer in Automobile Radiators of the Tabular Type, Heat and Mass Transfer 12, 3-22.
- [4] Nutt, W.T. and Wallis, G.B., 2004, Evaluation of nuclear safety from the output of computer codes in the presence of uncertainties, Rel. Eng. Sys. Saf. 83:57-77.
- [5] Lehmann, E.L., 1975, Nonparametrics, Statistical Methods Based on Ranks, Holden-Day, Inc, California, USA.
- [6] S.J.Son, et al., 2003, Medical statistics, Chonnam National University Medical School, Republic of Korea.

CONTRIBUTIONS TO PROBABILISTIC SAFETY ASSESSMENT STUDIES FOR TRIGA RESEARCH REACTORS

DANIELA MLADIN, MIREA MLADIN

Reactor Phys., Nucl. Safety & Fuel Performance Dept., Institute for Nuclear Research
Campului, 1, 115400 Mioveni, Romania
daniela.mladin@nuclear.ro

ABSTRACT

Probabilistic safety assessment (PSA) is used since the eighties for evaluations of the nuclear safety. It provides a method to calculate the risk to public and personnel in a complex facility such as: nuclear reactor, chemical plant, waste storage, etc. Suitable use of the PSA techniques proved to be a very strong tool to increase safety and efficiency of the design, construction, operation, modification and management of such industrial installations. During the last decades, a large volume of information and experience has accumulated from application of PSA to nuclear power plants. This information and the general PSA methodology can be very useful for the analysts working with PSA for research reactors. The trust of public in the nuclear energy does not necessarily accompany the development of scientific studies and technical methods for radioactive release prevention. The accident at Fukushima-Daichii produced significant psychological effects, even inside the nuclear community. Whatever the prevailing attitudes at a certain period of time towards the nuclear and whatever the regulation requirements, PSA stands as the main way to quantify risk and to analyze the safety of a project and of the operational configuration. Obviously, resources are directed especially where risk – defined as probability times consequences – is high, namely at nuclear power plants. However, the later years have shown an increasing presence of PSA methods inside the research reactors community. Some developed countries have already imposed PSA analyses as mandatory for the licensing of research reactors.

In Romania, approaching a PSA project for a research reactor is a scientific endeavour that was not undertaken before these studies, which aim to comply with the nowadays growing extent of safety evaluations for nuclear installations. The paper describes a wide range of PSA level 1 and level 2 aspects, applied to the Romania TRIGA 14 MW reactor. Deterministic analyses were also done for determining the radioactive inventory and release of fission product in cases where accident sequences are leading to fuel damage.

1. Introduction

Probabilistic Safety Assessment (PSA) is a method of evaluating risk to public and to personnel in a nuclear installation, such as a nuclear power plant (NPP), chemical plant, research reactor, waste disposal facility, etc. A large volume of information has accumulated in the last decades through application of PSA at power reactors. This information, in general, and PSA methodology in particular, may be useful for improving knowledge and skill of analysts working in PSA for research reactors. Anyway, due to differences between power reactors and research reactors, PSA techniques used for power reactors need to be analyzed attentively as to their applicability to research reactors. Many of research reactors have a long operating period (as well as NPPs), but also have a variety of associated experimental installations. These installations suffer ageing and obsolescence, and generally require separate consideration of their renewal at a reasonable cost. The research reactors (RRs) are more simple facilities than NPPs, having not so many systems, and are accordingly easier to analyze than a power plant. Actually, it is important to mention that the RRs are more flexible, the access to the reactor core is easier and core configuration can be changed due to

experimental requirements. The experimental aspects for RRs add a new dimension to the PSA's application.

Now a date, there are more than 300 research reactors in the world. These include a variety of constructive types and thermal power ranges, from few tens of watts up to 100 MW. Modern projects ([1], [2]) have included PSA evaluation of postulated accident sequences, while national regulatory requirements referring to design and operation of research reactors have continuously enlarged and improved as a result of international practices and recommendations.

While the methodological basis approach about PSA for RRs is known, the availability of data remains unsolved yet, due to diversity of research reactors. For this reason, IAEA, has organized a few dedicated CRPs, in order to collect failure data for PSA use for RRs ([3], [4], [5]). There is an information system called DARES (DAtabase for REsearch Reactor Safety), installed at JRC centre in Petten, Holland, for collecting information/data referring to PSA for RRs ([6]) Thirty research reactors from Europe, Argentina, Australia, Canada, South Africa and United States contributed with information to this system DARES.

2. Probabilistic Safety Assessment (PSA) for TRIGA Steady State 14 MW reactor

The purposes of the PSA analysis for TRIGA SSR are:

- Treatment of internal and external IEs;
- Evaluation and calculation of sequences that are leading to fuel failure and fission product release.

Premises of the analysis:

- Only reactor was considered as possible source of radioactive releases. Although, the fuel failure in the irradiation devices, designed for this event may represent a radiological risk for the operating personnel if particular safety barriers are inefficient, this failure is not considered as a final state in the event trees.
- Operation at maximum power (14 MW) is considered as being the bounding case in risk assessment, and PSA evaluations have been made for this situation.
- Reactor fuel was considered damaged when the fuel temperature limit is exceeded, according to the TRIGA Final Safety Report ([8]).
- Quantification analysis was performed using specific reliability data of TRIGA SSR reactor, fruit of the collection and processing of raw data for obtaining reliability data ([10]), but also generic data taken from IAEA available sources for research reactors ([3], [9]).
- For quantification of human errors it was used OAT (Operator Action Tree) ([11]) or THERP ([12]).
- The analysis of source term, inventory and transport of fission product in the primary circuit and in the reactor hall, as support of Level 2 PSA was performed.

2.1 Evaluation of initiating events for TRIGA SSR 14 MW

This subchapter presents the possible initiating events (IEs) for TRIGA SSR 14 MW reactor based on Safety Analysis Report ([8]) subsequent deterministic analysis, and initiating event list considered by IAEA ([13]) for research reactors. Initiating events frequencies together with their corresponding calculation method used are included in Table 1.

2.2 Description of the final core damage states for TRIGA reactor

According to [15], based on thermohydraulic analysis, only three final core damage states D1, D2, D3 were considered. Table 2 includes the percent of damaged core, mean frequencies and statistical confidence intervals limits (5%, 95%). The highest contribution (about 100 %) is due to D1 state, failure of 725 fuel elements in water.

Initiating Event	Method of calculation	Frequency (occ./year)
Loss of power supply LOFPS IE	Fault Tree Analysis	7.88E-03
Criticality during handling (fuel insertion error) CDHAL IE	Human Error Analysis (TESEO method) + Operating experience	2.10E-02
Loss of flow (failure of Primary Pumps Lines) LOFA IE	Fault Tree Analysis	1.74E-01
Fuel Channel Blockage FCB IE	TESEO + Maintenance Requirements	7.50E-03
Spuriously close of pool isolation valves (pneumatic valve DN 800) SP-CLOS IE	Fault Tree Analysis	1.67E-03
Loss of coolant accident (Primary Pipe Rupture) LOCA1 IE	Formula for Steel Pipes Rupture (Thomas)	1.00E-02
Loss of coolant accident through transfer gate failure followed by beam tube rupture LOCA2 IE	Fault Tree Analysis	1.67E-09
Earthquake	Safety Analysis of the Romanian TRIGA facility designer	1.00E-04

Table 1. Postulated initiating events, method of calculation, frequencies

Final core damage state	Percent of damaged core	Mean frequency / year	Confidence interval 5% / year	Confidence interval 95% / year
D1	100%, in water	7.28E-06	6.73E-06	1.07E-05
D2	80%, in air	3.98E-15	2.84E-16	2.37E-14
D3	100%, in air	2.09E-15	1.40E-16	1.33E-14

Table 2. Final core damage states for TRIGA reactor

The main contribution leading to D1 state is due to combination of initiating event, LOFA, common cause failure of control rod mechanisms (46.5%) or common cause failure of control rods (24%).

2.3 Radioactive release categories for TRIGA reactor

The radioactive release categories (Table 3) depend on the release quantities in the reactor hall, on hall isolation and on the state of radioactive products removal system (emergency ventilation system). Three reactor hall states are considered (Table 4.), depending on the successful reactor hall isolation and availability of the emergency ventilation and its associated air filters. These states combined with the three core damages states for TRIGA reactor produce nine categories of radioactive releases.

The radioactive releases states and their associated corresponding frequencies and confidence interval limits are given in the Table 5. One can note that the radioactive release state, R1 is dominant, followed by R2 state.

Contribution to R1 state is given by the LOFA IE and combination of common cause failures (CCF) of control rod (23.8%) and control rod mechanisms (46.1%). Combination of LOFPS IE and common cause failure of control rod mechanisms contributes with 12.9% to R1. Contribution to R2 fission products state is given by combinations of LOFA IE, common cause failures of control rod mechanisms, failure of dosimetry alarm unit (32.5%) or combinations of LOFA IE, common cause failures of control rod, failure of dosimetry alarm unit (16.8%). Combination of LOFPS IE, common cause failure of control rod mechanisms and failure of tri-phase inverter contributes with 12.9% to R2.

Release category	Core damage state	Containment state (reactor hall)
R1	D1	C1
R2	D1	C2
R3	D1	C3
R5	D2	C1
R6	D2	C2
R7	D2	C3
R8	D3	C1
R9	D3	C2
R10	D3	C3

Table 3. Radioactive release categories ([16])

State index	Reactor hall isolation available	Emergency ventilation available
C1	Yes	Yes
C2	Yes	No
C3	No	-

Table 4. Containment states (reactor hall) ([16])

Radioactive release category	Mean frequency / year	Confidence interval 5% / year	Confidence interval 95% / year
R1	7.28E-06	6.73E-06	9.67E-06
R2	4.40E-08	4.14E-08	7.61E-08
R3	2.54E-10	3.31E-11	7.98E-10
R5	3.98E-15	2.74E-16	2.36E-14
R6	1.81E-17	1.22E-18	9.97E-17
R7	1.69E-19	5.05E-21	9.29E-19
R8	2.09E-15	1.70E-16	1.27E-14
R9	9.45E-18	7.33E-19	5.85E-17
R10	8.90E-20	3.32E-21	5.49E-19

Table 5. Frequencies and confidence interval limits for radioactive release states

2.4 Short description of TRIGA Event Trees

Some assumptions were made for the evaluation of the event trees. These are:

- The unavailability of the emergency cooling does not lead to fuel damage. Actually, the inertia of the main pumps and the natural convection loop formed after flow reversal are able to remove the residual heat after a reactor shutdown from 14 MW power level, as the reactor commissioning tests, done in 1979, demonstrate. Moreover, safety analysis results indicate that the emergency loop is able to remove heat for a coast-down time of the main pumps larger than 2 seconds, in a scenario in which the scram is initiated at 0.2 sec. after the scram signal on flow-rate decrease ([17]).
- Natural convection is passively initiated through the emergency pump system without any dedicated components such as natural convection valves as for other research reactors.
- Secondary cooling system is not influencing upon the accident sequences because the time scale of a transient that can lead to fuel damage is quite small, making insignificant the global heat transfer to the secondary circuit. Also, if the rapid shutdown of the reactor is successful, the residual heat can be absorbed by the large volume of water in the pool and primary circuit.

LOFPS event tree

When external power supply to the reactor fails (S1 and S2 6 kV buses), the reactor should normally be scrammed by the interruption of electrical power to the control rods electromagnets. Success of the control rods insertion into the active core leads to a stable state. Next heading is the power supply in emergency mode of the TCA bus from the tri-phase inverter by the TCC1 and TCC2 buses. These two buses are connected to the batteries B1 and B2 that feed the reactor console, the emergency lighting, the emergency pump and the emergency ventilation. Reactor hall isolation was not considered because the

loss of external power supply will automatically shutdown the normal ventilation. The difference between the final release states, R1 and R2, produced by the failure of control rods gravitational movement, is the availability of the emergency ventilation. The later can fail either because of emergency power supply or by internal causes residing in the emergency ventilation system.

CDHAL event tree

The CDHAL IE considered in the analysis refers to the manipulation and accidental reinsertion of fuel bundles into the reactor core. Actually, such an event happened during early nineties when fuel bundle handling tool uplifted 2 bundles instead of one. To avoid dropping upon the core, the operator inserted the bundles into an inappropriate double location and the reactor became critical with all rods down and no power supply at console. Fuel moving action sheet was not properly set and allowed for intermediate configuration with insufficient reactivity compensation. The frequency of this IE was calculated using the TESEO (Technique to Estimate Operator's Errors) method and the estimated number of operations on the TRIGA SSR core. In spite of the large value for this IE frequency, ($2.10E-02$), the event was further excluded from the IE list, based on deterministic calculation that indicates that for fuel damage to occur, a very large value for reactivity insertion would be needed because TRIGA reactor has a large negative temperature prompt coefficient of reactivity.

LOFA event tree

The LOFA IE refers to the main circulating pump lines unavailability when reactor power level is 14 MW. For the IE to happen, it is necessary that two out of two main circulating pumps in operation fail. According to deterministic analyses ([15]), the loss of forced flow is considered by failure of both main pumps in operation at 14 MW reactor power level. If the primary cooling is lost, the reactor can be cooled by the emergency pump only, after the reactor shutdown. Deterministic analyses were necessary for calculating the evolution of the reactor fuel temperature when the scram initiation does not follow the decrease of the coolant flow-rate, in other words when the automatic shutdown system fails. Thus, in the accident sequences, testing of the manual shutdown appears, too. Fission product release states are marked only on the branch with no flow-rate scram, no inlet-outlet temperature difference scram, no fuel temperature scram, and also with failure of the manual scram. Should the regulations of the reactor are to be formally fulfilled, one will be compelled to postulate that failure of the emergency pump after operation at 14 MW leads to fuel damage even after a successful scram of the reactor. Actually, as already discussed, commissioning tests demonstrated that failure of the emergency pump does not produce fuel damage. Further on, if automatic scram fails, manual scram is tested. Success of the manual scram in a reasonably short time leads to a no consequence final state, too. The release states R1, R2, imply fission product release, resulting from failure of manual scram, and are different in what concerns ventilation filters and reactor hall isolation.

Fuel channel blockage (FCB) event tree

This IE can appear due to handling during maintenance, through dropping of an object in the reactor pool. This object could block flow inside the fuel bundles or could affect locally the space between fuel elements (a subchannel). The event, with a rather large calculated appearance frequency ($7.50E-03$ / year) was excluded due to project of TRIGA bundle and based on deterministic analysis in SAR. Special for this type of event, the reactor design provides the existence of cooling lateral holes in the bundle walls, in case that the its surface would be blocked by an object dropped in the reactor pool. Subchannel blocking was also excluded based on SAR, which contains analysis of flow reduction effects about temperatures fuel, concluding with, that the reduction in this way of the local flow does not lead to fuel damage.

Spuriously close of pool isolation valves (SP-CLOS) event tree

The initiating event frequency was calculated as being $1.67E-03/\text{year}$. The spuriously close of pool isolation valves event tree is leading to loss of flow event tree.

Loss of coolant accident – Primary pipe rupture (LOCA1) event tree

Such a transient is worth to be analyzed considering all designed protections against it (pool isolation valves, antisiphon valves). The IE supposes the rupture of primary circuit main pipe in the region of the pipe line at the lowest elevation (-18 meters), where there is enough room for water to drain from the pool. The rupture of the primary circuit pipe may lead to diminishing of the reactor pool water level down to fuel uncovering. The first heading in the event tree is “automatic shutdown (scram) due to pool level decrease”. As a result of water level decrease, automatic isolation of the pool is triggered by means of pneumatic valves at outlet and inlet of the 800 mm diameter primary pipe. These pneumatic valves are fed by two redundant compressed air systems 6 bars and 10 bars, respectively. If automatic pool isolation is not successful, manual isolation can be done using the same two valves and manual valves on the same line. Continuing on the event tree, the antisiphon system is tested. This consists in opening some floating valves letting air penetrate inside the primary line, thus interrupting the siphon and preventing the pool water decrease below the level of these valves. If the antisiphon system fails, core damage will result and reactor hall isolation is tested, which implies closing the normal ventilation air paths. As a result of fission product detection inside the reactor hall, emergency ventilation is triggered, which is the last heading in the LOCA event tree. If no automatic scram results from pool water level decrease, the operator can scram the reactor manually. This branch of the event tree further tests the same headings as above, starting with the manual pool isolation. If manual shutdown of the reactor fails and the antisiphon system is successful, the three release states will depend on the reactor hall isolation systems and on the emergency ventilation, R1, R2, R3 will be 100% underwater. If the antisiphon system is unsuccessful, the final states R8, R9, R10, will be associated with release of fission product in air.

Loss of coolant – beam tube plus transfer gate (LOCA2) event tree

There are two pneumatic fittings from the transfer gate which separate the reactor pool from the transfer pool. In case of loss of air, the pneumatic fittings will deflate and the pool water floods in the transfer pool through the transfer gate. However, this event alone will not be enough to produce core uncovering since the transfer channel is only a few meters below the pool surface. Each of two TRIGA reactors (ACPR and CCR) has two kinds of beam tubes: radial and tangential. In case of rupture of the beam tube, a water quantity floods in beam room. Against this event, protection measures were taken by design, the volume of beam room being such that about 1 m water level still remains in the pool. In these conditions the quantity of water remaining in the reactor pool is 84 m^3 . The IE evaluated takes into account simultaneous possibility of loss of water from pool through transfer gate and ruptures of beam tubes. The calculation of frequency for this initiating event supposes the unavailability of the pneumatic fitting from transfer gate combined with failure of beam tubes. The frequency for this IE ($1.67E-9/\text{year}$) is very small and, applying a cut-off criterion, the initiating event LOCA2 was not further taken into account.

External event – earthquake

Due to Vrancea seismic zone, the site is exposed at earthquakes. Analysis was performed by the Romanian designer of the facility for a maximum earthquake intensity $I = VI \frac{1}{2}$ MSK. In case of TRIGA reactor, the earthquake may initiate scenarios that can be combined in four groups, treated as scenarios for internal initiating events, as follows:

- ✓ If the earthquake causes a damage of reactor building, the event tree would be reduced at flow blockage case.
 - ✓ If the reactor building falls down, two event trees would be developed, once for flow blockage and another for core damage.
 - ✓ If in case of an earthquake pipe ruptures can appear, event tree will be treated as in case of LOCA IE, both small and large pipes ruptures.
 - ✓ The earthquake may produce a loss of electrical power supply, the event tree will be treated as in case of LOFPS IE.
- The seismic analysis for TRIGA SSR in progress.

3. TRIGA modelling with CATHARE2

The nodalization of the problem is depicted in Figure 1, and it was realized using GUIHARE v1.5.1 graphic interface of CATHARE 2 code. The reactor hall has two boundary conditions for inlet and outlet of air, simulating the air circulation done by the ventilation system (13600 m³/h in emergency mode). The water volume is preserved but some components have been collapsed: two pumps at nominal power are represented by a single pump with mass flow rate of 500 l/s, the two heat exchangers are represented by only one composed of inlet volume (weight=2), individual thin tubes (weight=2x1262), outlet volume (weight=2). Since reactor core is not modeled, no heat transfer was considered and consequently there was no need for secondary system. The purpose of the model is to calculate the fission products transport in the primary system and containment, and the evolution of the activity in different zones. The core damage is simulated by means of a radio-chemical components source (SOURCE operator) at the axial level of the core inside the volume representing the pool. The source for the four radio-elements included in CATHARE2 (Kr-87, Xe-133, I-131 and Cs-137) had to be calculated by other means and included in the defined flow of the SOURCE operator as an activity concentration per kg of gas.

3.1 Calculation of fission product source

An average TRIGA LEU bundle was modeled (figure 2) using SAS2H module from SCALE 4.4 ([18]). Work described in ([7]) produced by General Atomic Company, gives the correlation used to calculate the release of fission products from TRIGA fuel, both gaseous and volatile metals:

$$\psi = 1.5 \cdot 10^{-5} + 3.6 \cdot 10^3 \cdot e^{-1.34 \cdot 10^4 / T} \quad (1)$$

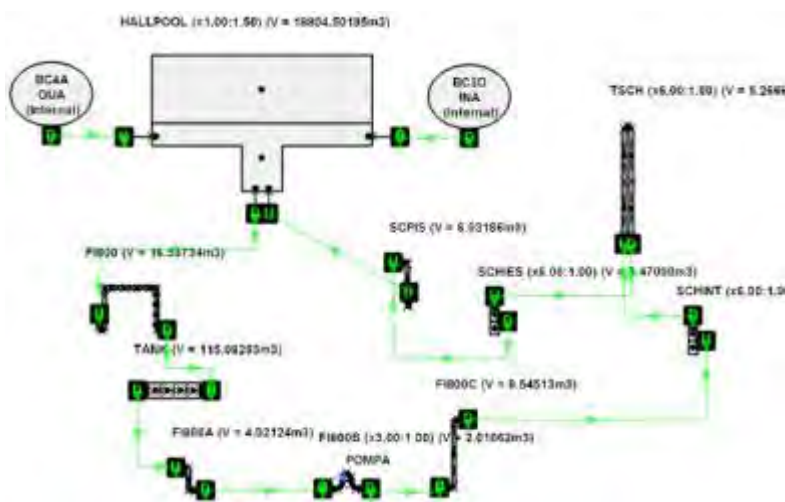


Figure 1. Nodalization of TRIGA model for fission products transport (GUIHARE v1.5.1 [14])

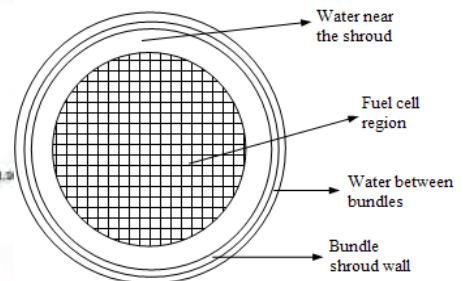


Figure 2. Regions of the TRIGA bundle model for SAS2H

, where T is the fuel temperature (K). Release fractions given by (1) assume failed or ruptured cladding. The Final Safety Analysis Report indicates 940 °C as the fuel limit temperature when cladding temperature may be at the same value as the fuel.

The calculations were done in the following assumptions:

- one hundred percent of the noble gases in the fuel-clad gap are released;
- twenty five percent of the Iodine and Cesium are released from the fuel elements, the remainder being considered deposited on the relatively cool cladding. For an underwater accident only 10.9% of the release is considered gas (10% assumed to form organic compounds that escape pool water and 1% of the balance not dissolved in the pool water). Thus, only 2.725% from the I and Cs content of the fuel-clad gap forms the CATHARE gas source for these elements, the rest (22.275% of the gap content) being introduced as liquid source;
- for fuel damage while in air, the release for noble gases (Xe and Kr) is 100% of the fuel-clad gap inventory, and for the I and Cs the release fraction is considered as 25%.

Fission product	Mass / bundle (kg)	Release / core with 29 bundles (kg)	Source in liquid phase (kg)	Source in gas phase (kg)
Kr(Kr-87)	4.45E-04	7.36E-04	0.	7.36E-04
Xe(Xe-133)	1.49E-04	2.46E-04	0.	2.46E-04
I(I-131)	1.31E-04	5.41E-05	4.82E-05	5.90E-06
Cs(Cs-137)	2.97E-02	1.23E-02	1.09E-02	1.34E-03

Table 6. Inventory per bundle and fission product sources for an underwater release. Whole core release in 100 s (100% for noble gases and 25% for I and Cs)

Fission product	Mass / bundle (kg)	Gas release from 80% of the core (kg)
Kr(Kr-87)	4.45E-04	5.89E-04
Xe(Xe-133)	1.49E-04	1.97E-04
I(I-131)	1.31E-04	4.33E-05
Cs(Cs-137)	2.97E-02	9.82E-03

Table 7. Inventory per bundle and fission product sources for release in air. Release from 80% of core in 1500 s (100% for noble gases and 25% for I and Cs)

3.2 Calculation of the radio-elements transport

Using the CATHARE2 model described above, it was investigated the capabilities of the code to calculate the concentration of each fission product in different zones of the TRIGA facility, pool, primary lines, delay tank and reactor hall. It should be mentioned that fission products are treated in CATHARE2 as pure species (i.e. no chemical interactions) and are introduced as gaseous or liquid sources at the location of reactor core in the model. The efforts were towards through support PSA calculation, in which it intended the evolution of reactor stack fission product releases, defining quantitative containment states function of CATHARE's fission product transport results and functioning of ventilation system in normal operation (unsuccessful condition) and in case of accident, emergency (successful condition). The following gives a synthesis of the results of these support analyses.

Underwater release: Maximum of the release is rapidly attained (at about 100 s) since the accident sequence with core damage involves no scram at full power. Two basic series of results are calculated, with a residual flow rate in the primary circuit: normal operation of the ventilation system with air flow rate 24360 m³/h, and ventilation system in emergency mode: air flow rate is 18500 m³/h, efficiency of the filters is 100% for Iodine and 10% for Cesium. Figure 3 presents, as an example of time evolution, the release rate of Krypton at LOFA with emergency ventilation and normal ventilation.

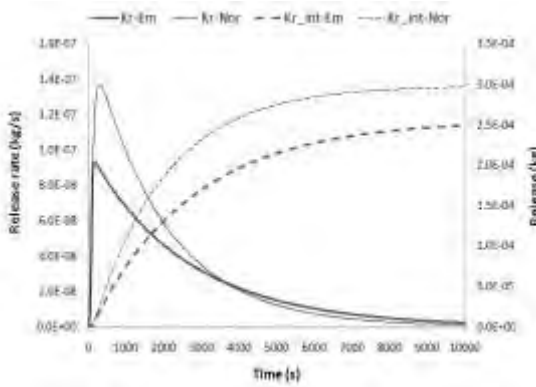


Figure 3. Instantaneous and integral stack release of Krypton at LOFA with emergency ventilation and normal ventilation

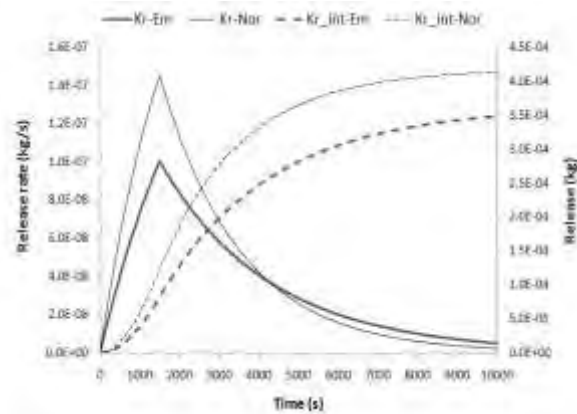


Figure 4. Instantaneous and integral Krypton stack release at LOCA with emergency ventilation and normal ventilation

Release in air: appears in case of Loss of Coolant Accident (LOCA). The maximum of instantaneous releases for all fission products is at 1500 s (end of release), the origin being the moment of fission products source opening which coincides with the damage for the maximum loaded fuel group (ppf=1.92).

The circuit here is empty (residual liquid phase), the fission products source is placed at the same elevation as before (1.5 m above the bottom of the pool) but the release is gaseous, inside the non-condensable (air). Figure 4 presents, as an example of time evolution, the release rate of Krypton with emergency ventilation and normal ventilation at LOCA.

4. Conclusions

As a result of the PSA study for the TRIGA reactor presented, several specific conclusions can be drawn regarding to the nuclear safety characteristics of the facility:

- Core Damage Frequency (CDF) is 7.28×10^{-6} /year and comes almost entirely from the frequency of the D1 core damage state, which is produced by the loss of flow with no scram, and has as significant contributors combination of loss of flow IE with the common cause failure of the control rods and control rods mechanisms;
- Total fission product release frequency is about 7.28×10^{-6} /year and is due to the release states R1 (CDF+ success of the reactor hall systems) and R2 (CDF+ success of the reactor hall systems +failure of ventilation system to switch to the emergency mode). The R1 release state is characterized by a stack release rate, on the curve's peak, of about 1×10^{-7} kg/s noble gases (Xe and Kr) and 1.5×10^{-7} kg/s Cesium. The R2 release state is characterized by a stack release rate, on the curve's peak, of about 1.9×10^{-7} kg/s noble gases (Xe and Kr), 1.1×10^{-9} kg/s Iodine and 2.5×10^{-7} kg/s Cesium.

5. References

- [1]. ***IAEA TECDOC-517, Application of Probabilistic Risk Assessment to Research Reactors, Vienna, 1989.
- [2] ***, ANSTO "Replacement Research Reactor – Probabilistic Safety Assessment (PSA)", Summary for Public Release, Australian Nuclear Science and Technology Organisation (ANSTO) document number: RRRP-7225-EBEAN-004-REV0 Revision: 0, March, 11, 2005.
- [3] ***, TECDOC-636, Manual of reliability data collection for research reactor PSAs, IAEA, Vienna, 1992.
- [4] ***, IAEA TECDOC-930 Generic component reliability data for research reactor PSAs, Vienna 1997.
- [5] ***, IAEA Draft TECDOC "Reliability Data For Research Reactor PSA", draft, July 2005.

- [6] C. Kirchsteiger, J. Kubanyi, PSA support of research reactor safety management, International Eugene Wigner Training Course on Research Reactor Safety, JRC, Petten, 2006.
- [7] N. L. Baldwin, F.C. Foushee, J.S. Greenwood, Fission Product Release from TRIGA-LEU Reactor Fuels, GA-A16287, 1980.
- [8] ***, General Atomic Company, 1974. Safety Analysis Report of the Triga Steady-State Research/Materials And Testing Reactor, GA E-117-323.
- [9] ***, IAEA TECDOC-930, Generic component reliability data for research reactor PSAs, IAEA, Vienna, 1997.
- [10] D.Mladin, M.Mladin, M. Preda, I. Prisecaru, Multiple aspects of raw data collection and processing for Romanian TRIGA SSR, Nuclear Engineering and Design 240 (2010) 1630–1643.
- [11] A. Swain, Human Reliability Analysis, Training seminar course documentation, nov. 1993.
- [12] ***, IAEA Workshop on HRA - Human Reliability Analysis in PSA, Budapest, Hungary, may, 1996.
- [13] ***, IAEA Safety Series no. 35. Initiating Events at Research Reactors.
- [14] S. Litonin, GUTHARE user dictionary: pre and post-processing guide, DTS/OCC/OC2D07043/003/VOM2 OC2D07043, 2009.
- [15] M. Mladin, Analiza accidentelor de tip LOFA și LOCA la reactorul SSR, (INR's archives, in romanian language), RI 6806, SCN-Pitești, 2003.
- [16] D. Mladin, I. Prisecaru, Aspects of Probabilistic Safety Assessment for TRIGA Research Reactor, U.P.B Sci. Bull., Seria C, Vol.75, No.1, 2014.
- [17] ***, General Atomic, 1980. Results of Romanian TRIGA 14 MW Startup and Commissioning Tests, Arhiva SII SCN Pitești.
- [18] O. W. Hermann, C. V. Parks, SAS2H: A Coupled One-Dimensional Depletion and Shielding Analysis Module, NUREG/CR-0200 Revision 6 Volume 1, Section S2 ORNL/NUREG/CSD-2/V2/R6, 1008.

INVESTIGATING THE SETUP FOR IRRADIATION OF MATERIAL SAMPLES IN TRIGA ROMANIA

M. MLADIN, S.D.DULUGEAC, G.A.BUDRIMAN

*Reactor Phys., Nucl. Safety & Fuel Performance Dept., Institute for Nuclear Research
Campului, 1, 115400 Mioveni, Romania*

M. CIOCANESCU, D. BARBOS

*Reactor Dept., Institute for Nuclear Research
Campului, 1, 115400 Mioveni, Romania*

ABSTRACT

The two TRIGA reactors, a 14 MW Steady State and a pulsed reactor sharing the same pool, represent the main nuclear installation at the Institute for Nuclear Research in Pitesti. The Steady State Reactor (SSR) was used for fuel and material testing in dedicated irradiation devices as well as for neutron physics methods. One its current utilization directions implies the irradiation of material samples with temperature level and flux integral prescribed and sometimes with temperature gradient constraints. The paper presents, as an example, the preliminary neutron physics and thermal calculations for the setup of generic detectors irradiation inside a dedicated capsule. Shielding was considered in order to reduce the thermal flux in some of the detectors which are mixed with unshielded detectors, sharing common holders. Geometrical dimensions and energy deposited by nuclear radiation in the materials investigated is calculated for coping with thermal constraints without any external heating. Also, it illustrates the approach for the neutron physics and thermal calculation of iron samples in TRIGA at a prescribed temperature and up to a defined irradiation limit.

1. Introduction

TRIGA Romania facility includes two independent cores sharing the same pool: a 14 MW steady state research and materials testing reactor (SSR) and an operationally independent pulsing reactor (ACPR) which can deliver pulses with a peak power up to about 20000 MW and with an energy release of about 100 MJ. Fig 1 shows a cross section through the pool and biological protection, giving some indications about the two reactors and their associated devices.

Inside the SSR core, a capsule for irradiation of structural materials was accommodated and is planned to be operated up to a fast fluence ($E > 1$ MeV) of $\sim 10^{21}$ cm⁻². This capsule, called C5, contains Zr-2.5%Nb CANDU pressure tube samples in a gas medium and functions at about 270 °C [1].

This paper focuses on investigating the possibilities to reach prescribed values of fast flux integral, temperature and temperature gradients in silver-ceramic detectors with and without shielding to thermal neutrons, and fast fluence and temperature in iron samples, in capsules that preserve many of the material and geometry characteristics of the present C5 capsule. Both types of irradiation experiments pertain to the fusion technology research needs.

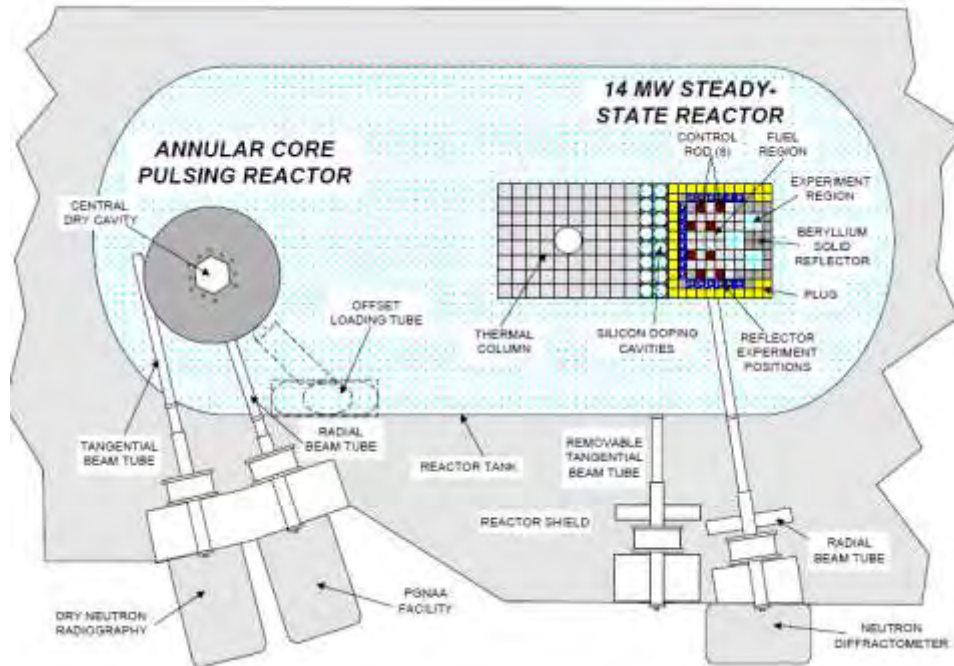


Fig 1. Schematic view of the TRIGA Romania reactors.

2. Calculation of detectors

Neutronic calculations were done with MCNPX [2] on the TRIGA SSR core model that includes a Capsule containing $3.2 \times 0.7 \times 4$ cm detectors composed of silver on a Al_2O_3 base to determine the neutron and gamma heating in the materials. The arrangement inside the capsule included both detectors covered by Ag-In-Cd and detectors without shielding, with Aluminium holders and immersed in Helium, as revealed by the detail of modeling in Fig 2. The neutronic calculation yields the group fluxes and the heating in the location chosen and at a reactor power level (10 MW) that allows fulfilling the requirements for other experiments simultaneous with the Capsule. For a requested total flux integral of $2.34\text{E}+20 \text{ cm}^{-2}$, the detectors would need roughly one month of reactor operation at 10 MW.

Thermal modeling is performed with HEATING [3], nodalization of a shielded detector inside the Capsule being shown in Fig 3. It is a R-Z cross section through a R- θ -Z model with convective boundary condition towards pool water at the outer face of the steel tube of the Capsule. Heat sources for the model resulted from a MCNP coupled neutron-photon run are given in Tab 2. Gamma heating includes prompt, capture and delayed contributions. Typical standard deviation in neutron heating tally is 1% while in gamma tallies is 0.5%. In case of Ag-In-Cd, the neutron heating tally is the major contribution to the heating source. Since there is no external heating, the temperature level and the temperature distribution across the height of the detector can be designed only using the two gap regions and the height of the lower foot of the Aluminium holder, all visible in Fig 3. The order of magnitude for these gap regions is $10^2 \mu\text{m}$.

As an example, the thermal constraints are:

- temperature more than 100 °C but not higher than 250 °C;
- existence of a 10-100 °C temperature drop on a direction orthogonal to the neutron current in the detector.

Fig 4 presents the results for two independent arrangements. The one described as “mixed” reflects the schematics in Fig 2, where shielded and unshielded detectors (called “Device Under Testing” or DUT) coexist, sharing the same Aluminium holders, while the arrangement called

“simple” can be a separate axial region with unshielded detectors. The gap regions in these two cases are different and were searched for in order to have a good match of the temperature in unshielded detectors between “mixed” and “simple” arrangements.

Tab 1. Neutron flux in shielded and unshielded detectors in TRIGA (G4 at 10 MW at axial core mid-height) vs. their lifetime conditions.

Energy domain	ITER	TRIGA (Ag-In-Cd)	TRIGA
0. - 0.5 eV	2.03E+11	4.23E+12	1.27E+13
0.5 eV - 1 MeV	1.14E+13	6.06E+13	6.37E+13
> 1 MeV	2.52E+12	1.96E+13	1.96E+13
Total flux (cm ⁻² s ⁻¹)	1.41E+13	8.45E+13	9.60E+13

Tab 2. Heat source density inside the Capsule for irradiation of detectors at 10 MW in G4 at axial core mid-height.

Material	Heating density (cal·sec ⁻¹ ·cm ⁻³)
Al	0.47
Al2O3	0.92
SS	1.73
Ag(80)-In(15)-Cd(5)	13.20

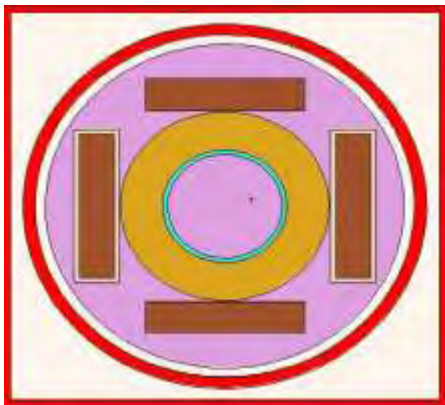


Fig 2. Detail of the neutron physics model of the Capsule accommodating the detectors.

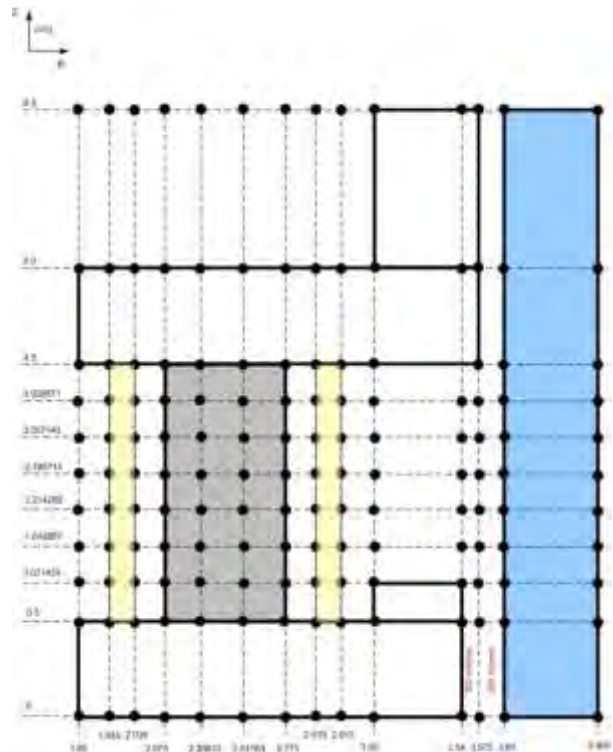


Fig 3. Example of nodalization of the heat conduction model for a covered detector inside the Capsule.

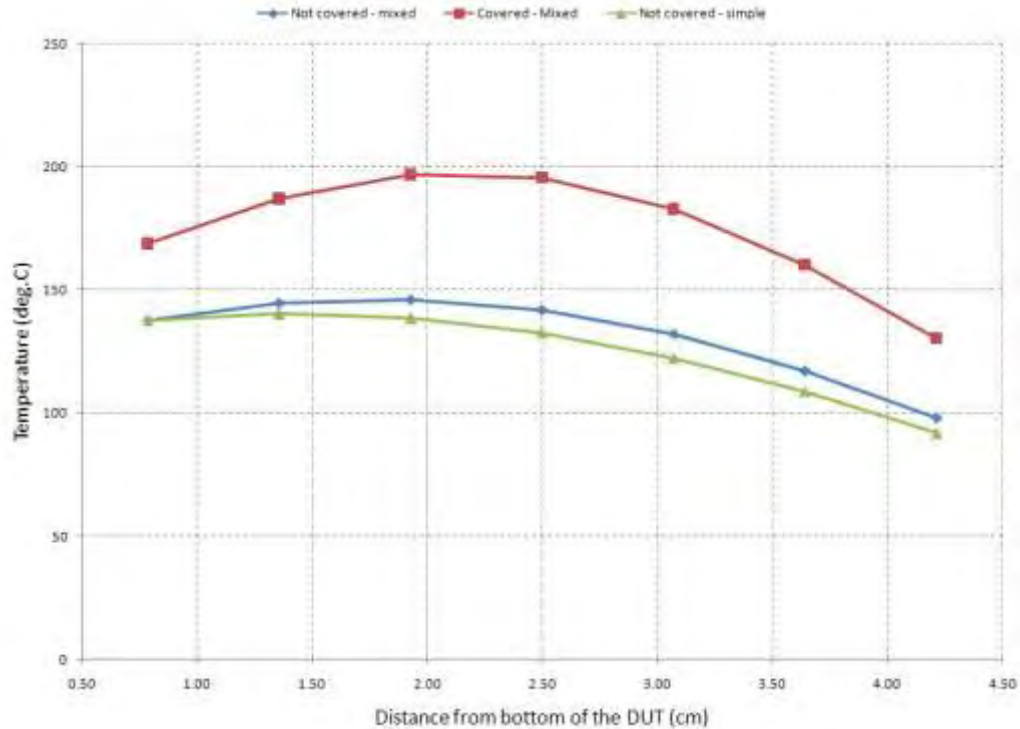


Fig 4. Temperature distribution in shielded and unshielded detectors sharing the same Aluminium holder and unshielded detectors in independent holders. Different gap sizes to match the temperature in unshielded detectors in the two arrangements.

2. Design of the iron samples irradiation

The arrangement of the Eurofer samples is quite complex, with different geometries of the samples at different floors (or axial regions inside the Capsules). A generic example for samples arrangement is provided in Fig 5. There are two different Capsules in grid positions G4 and E4, respectively (see Fig 6). The main difference between the two Capsules is the required temperature of the samples, 500 °C and 300 °C (± 50 °C), which requires holders made of different materials (i.e. Stainless Steel and Aluminium). Design of the gap thickness (between the surrounding holder and the steel tube of the Capsule) is also necessary in each case in order to obtain the targeted temperatures.

There are requirements related to extent of irradiation up to 2 DPA (or Displacement per Atom). As a first calculation, the irradiation time for the TRIGA Romania neutron spectrum (see Fig 7) inside a generic steel and gas Capsule located in G4 was obtained using the SPECTER [4] code for Stainless Steel as material. Flux input was calculated on a 96 group structure with detailed groups in the fast domain. The result is dpa 0.54 for stainless steel for one year of irradiation (200 operation days/year considered) at 10 MW reactor power level. The reactor power level is dictated by another experiment with fixed location (also visible in the core configuration presented as Fig 6). Hence, a potential project would require up to 4 years of irradiation in TRIGA Romania.

Calculations follow the same methodology: MCNPX for determining the heat source and HEATING to calculate the temperatures and design the gap thickness. Because of the complexity of the setup, homogenization of samples into rings is necessary to obtain an R-Z model of the Capsule.

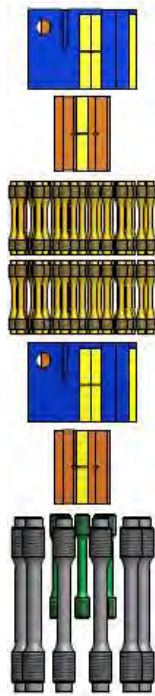


Fig 5. Example of iron samples setup inside irradiation Capsule.

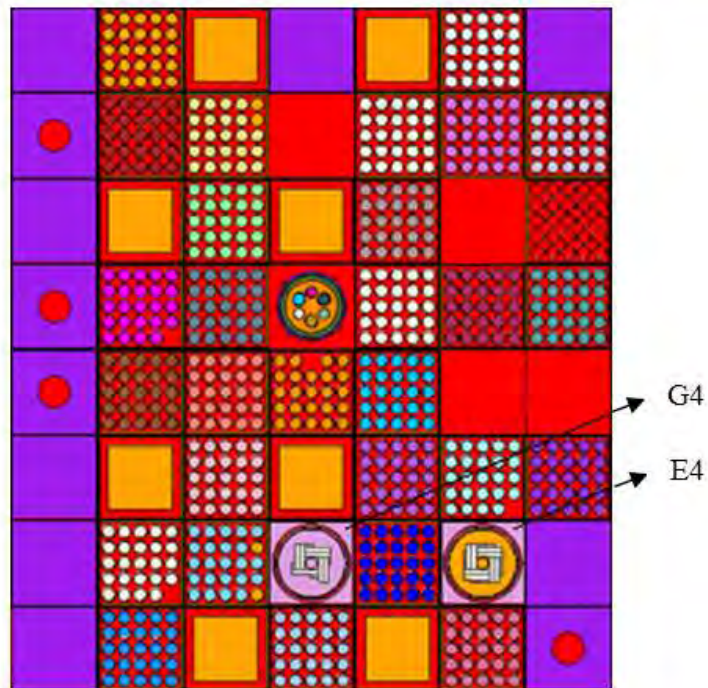


Fig 6. Core configuration with two Capsules, at 500 °C and 300 °C for iron samples irradiation (in G4 and E4, respectively).

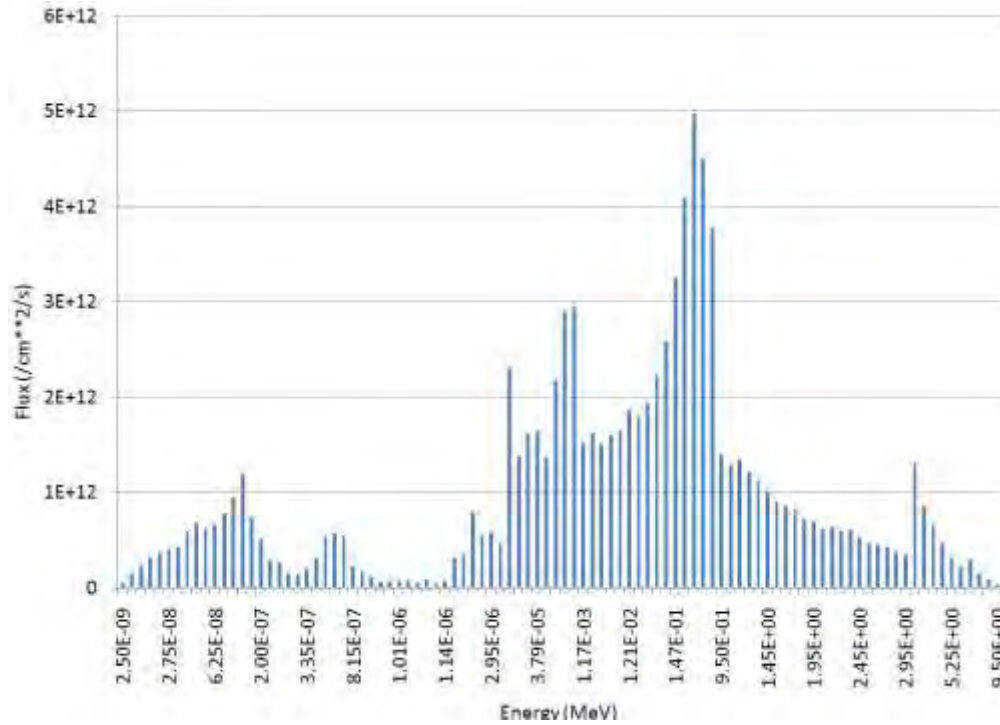


Fig 7. Neutron spectrum in steel inside a steel-gas capsule in TRIGA Romania (located in G4 grid position).

5. References

- [1] Gh. Negut, M. Ancuta et al. - The irradiation effects on zirconium alloys, Journal of Nuclear Materials, 2007.
- [2] Denise B. Pelowitz, editor - MCNPX™ USER'S MANUAL Version 2.6.0 April 2008.
- [3] K. W. Childs - HEATING 7.2 User's Manual, NUREG/CR-0200 Rev. 6
Vol. 2, Sect F10, ORNL/NUREG/CSD-2/V2/R6
- [4] L.R. Greenwood, R.K. Smither – SPECTER: Neutron Damage Calculations for Material Irradiation, ANL/FPP/TM-197.

STUDY OF MOLYBDENUM-99 PRODUCTION POSSIBILITIES IN TRIGA 14 MW REACTOR

S.D.DULUGEAC⁽¹⁾, M. MLADIN⁽¹⁾, G.A.BUDRIMAN⁽¹⁾

*Reactor Phys., Nucl. Safety & Fuel Performance Dept., Institute for Nuclear Research
Campului, 1, 115400 Mioveni, Romania
stefan.dulugeac@nuclear.ro*

ABSTRACT

Molybdenum production can be a solution for the future in the utilization of the Romanian TRIGA, taking into account the international market supply needs. Technetium-99m ($T_{1/2} = 6.02$ h) is currently the most used radio-nuclide in nuclear medicine procedures in developing countries. It labels a number of radiopharmaceuticals to assist the diagnosis of problems in different parts of the human body including heart, brain, liver, lungs, kidneys, bone, thyroid, etc. ^{99m}Tc has unique physical and nuclear properties which gives low radiation exposure to patients, high quality imaging and reliable availability in the form of $^{99}\text{Mo}/^{99m}\text{Tc}$ generators. Currently, ^{99m}Tc is exclusively produced from the decay of its 66h half-life parent Molybdenum-99.

There are two main methods to produce $^{99}\text{Mo}/^{99m}\text{Tc}$ in a nuclear reactor:

-Fission of an Uranium target. Producing the ^{99}Mo radioisotope by fission implies high neutron fluxes, expensive processing facilities for handling the fission products of Uranium, and creates important nuclear waste radioactivities. Neutron physics parameters are determined and presented, such as: thermal flux axial distribution for the critical reactor at 10 MW inside the irradiation location; reactivity introduced by three Uranium foil containers; neutron fluxes and fission rates in the Uranium foils; released and deposited power in the Uranium foils; Mo^{99} activity in the Uranium foils. The aim of the thermal-hydraulic analysis was to determine the flow rate, the outlet-inlet temperature difference through the irradiation device and the radial temperature distribution.

-Irradiation of a natural or ^{98}Mo enriched target, method called the neutron activation production method. It leads to low specific activities of ^{99}Mo and also low waste activities, and does not require expensive handling facilities. The calculations are performed with MCNP, searching the locations of the targets in setups that maximize the ^{99}Mo production in the present TRIGA core configuration. Calculations are done both with natural metallic Molybdenum pellets and with enriched pellets.

1. Introduction

Nuclear reactors are used for producing more than 40 activation products and 5 major fission product medical radioisotopes (I^{131} , Xe^{133} , Sr^{89} , Y^{90} and Mo^{99}). Concerning molybdenum, a target is typically irradiated for 5-7 days to reach optimal Mo^{99} production level (around 71-82% of saturation concentration) [1].

Technetium-99m is the primary medical radioisotope used today for performing diagnostic imaging procedures. 85% of all medical radioisotope procedures use Tc^{99m} and it is used in more than 30 radiopharmaceuticals. Technetium-99m is the radioactive daughter product of molybdenum-99. Tc^{99m} has a short half-life (6 hrs.) and emits a low-energy gamma ray (140 keV). It is readily "tagged" to a pharmaceutical that transports it to the location of interest in the body [2]. Generally two different techniques (Fig.1) are available for molybdenum-99 production for use in medical technetium-99 generation. The first one is based on neutron irradiation of molybdenum targets of natural isotopic composition (24.13% Mo^{98} abundance) or enriched in molybdenum-98. In these cases the Mo^{99} is generated via the nuclear reaction $\text{Mo}^{98}(n,\gamma)\text{Mo}^{99}$. Although this process can be carried out at low expenditure it gives a product of low specific activity and, hence, restricted applicability.

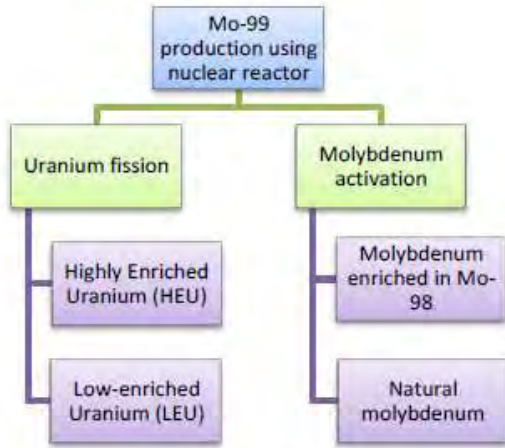


Fig.1. Summary of reactor-based Mo⁹⁹ production technologies[1]

Two types of fission targets are in use today: highly enriched uranium (HEU) typically containing more than 90 wt% of U²³⁵ and low-enriched uranium (LEU) with less than 20 wt% of U²³⁵. However, an international effort is currently underway to reduce and eventually eliminate the use of HEU targets given that they contain weapon-grade uranium [1].

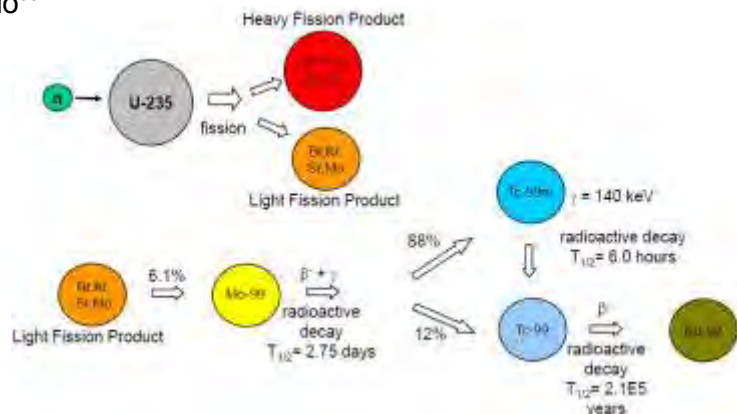


Fig.2. Diagram of Mo⁹⁹ obtained from reaction U²³⁵(n,f)Mo⁹⁹ [2]

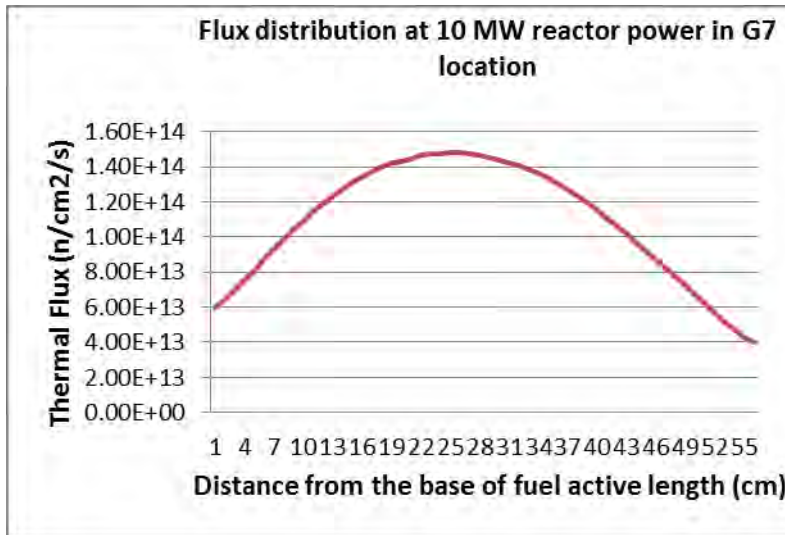


Fig.3. Axial thermal flux distribution for the critical reactor at 10 MW, Xe¹³⁵ accumulated

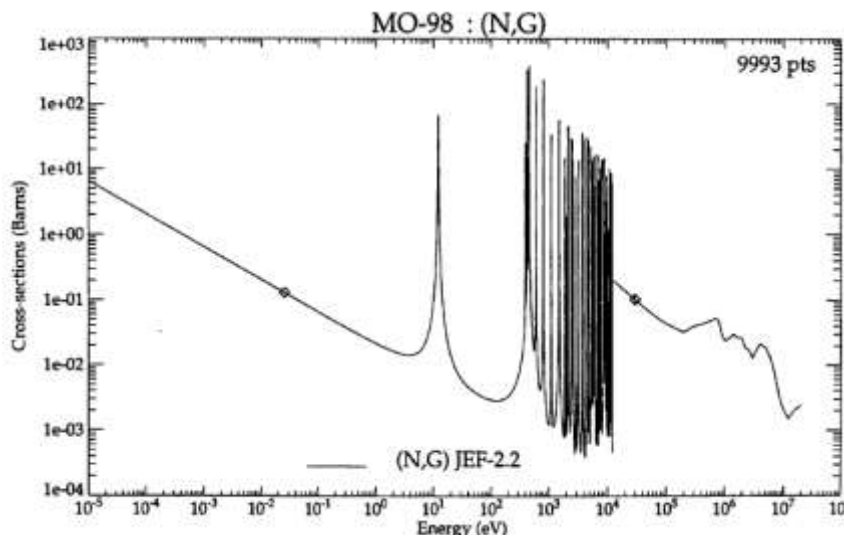
The calculations use the MCNP[4] model of the TRIGA Steady State reactor, representing the current core configuration. The reactor core is composed of 29 LEU fuel bundles, each having its specific burnup resulted from MCNPX v2.6.0 core calculations. Calculations were done at 10 MW reactor power with Xe¹³⁵ fission product poison accumulated. The average fuel and Uranium foils temperature was considered 500K and 400K, respectively.

Control rods position (in bank) at criticality was calculated at 70% extraction length; this position will determine the axial neutrons flux distribution inside irradiation location. In these conditions, calculations were launched with the irradiation device introduced in G7 (irradiation location). The resulted axial thermal flux distribution is given in Fig.3.

2. Neutron activation method

The yield of Mo^{99} from the $\text{Mo}^{98}(n,\gamma)\text{Mo}^{99}$ reaction significantly depends of the energy spectrum of the neutron flux. The aim is to produce neutrons at the right energy, or make use of the epithermal neutrons, to get a high capture probability in Mo^{98} . This works best at large capture cross section values corresponding to resonances in Mo^{98} (Fig.4).

Unfortunately, its resonance peaks in the epithermal energy region are not productively used



in water cooled reactors because fission neutrons are quickly moderated (usually by water) to thermal energies, missing the resonances, meaning a lower probability of capture.

In all cases that will be described, we used ENDFB-VII nuclear data for both Mo and isotopes entering the reactor composition zones.

Fig.4. Cross section for neutron capture in Mo^{98} showing the resonance peaks[6]

2.1 Influence of the material surrounding the target

Different materials were studied inside the experimental location: beryllium, water, graphite, silicon, nickel. Tab.1 presents a synthesis of these results. Normalization was done to the maximum Mo^{99} activity obtained for natural Mo with beryllium around the capsules containing the pellets.

Beryllium	Water	Graphite	Silicon	Nickel
1.00	0.90	0.87	0.80	0.71

Tab.1. Relative effect of different materials surrounding the target on the Mo^{99} activity

2.2 Influence of target composition and geometry

The results in Tab.1 point to beryllium and water as the best shield materials. There are two types of geometrical arrangements inside the capsule: 40 pellets placed along the z axis (Fig.5) and 181 pellets perpendicular to the z axis (Fig.6).

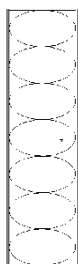


Fig.5. Setup for 40 pellets inside a capsule

Obviously, the largest total activity is in cases with 181 pellets inside one pin because of the larger mass of Mo^{98} in these cases. For beryllium around the pins, the total activity for the 98% Mo^{98} enriched pellets is lower than the corresponding activity with water, contrary to the natural Mo targets, where the maximum is reached with beryllium. This is due to the larger contribution of thermal flux, in water, for enriched pellets compared to natural Mo, coming from lack of absorbent isotopes of natural Mo other than Mo^{98} (Mo^{95} , Mo^{97}).



Fig.6. Setup for 181 pellets inside a capsule

The contribution of thermal, epithermal and fast regions of the neutron spectrum to Mo^{99} activity is illustrated by $\text{Mo}^{98}(n,\gamma)\text{Mo}^{99}$ reaction rate (Fig.8 through Fig.10). Fig.8 represents the reaction rate for natural Mo with water in location with 40 pellets inside a pin, while Fig.9 is 98% enriched in the same conditions. The absolute magnitude of the reaction rate in the natural Mo case is lower because of the lower atom density of Mo^{98} , and the contribution of

the thermal region to the total reaction rate is less important in the case with natural Mo. On the other hand, Fig.10 shows that in beryllium, the epithermal contribution is largely dominant because moderating properties of beryllium are not so good, the thermal flux being much lower than in water.

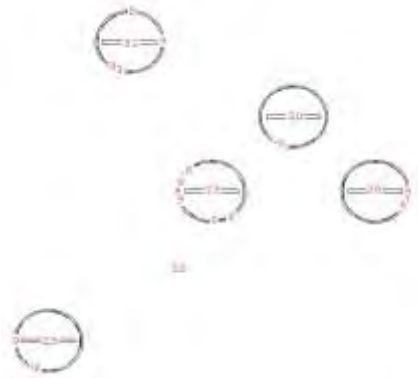


Fig.7. Placement of pins containing Mo (materials 25,28,29,30,31) in the experimental location

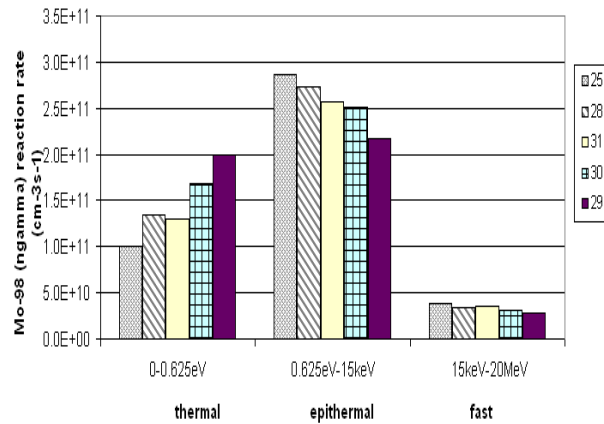


Fig.8. Mo⁹⁸(n,γ)Mo⁹⁹ avg. reaction rate in natural Mo with water in location

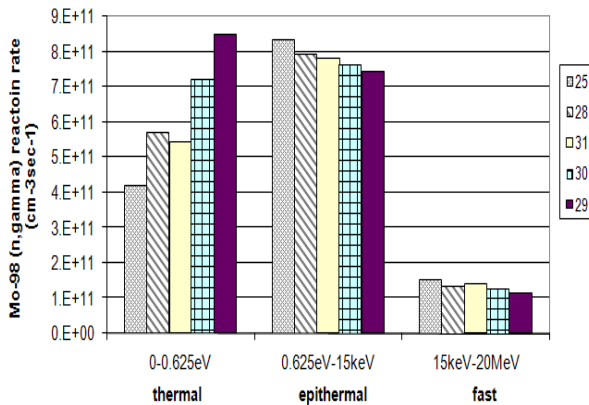


Fig.9. Mo⁹⁸(n,γ)Mo⁹⁹ avg. reaction rate in 98% enriched for individual pins with water in location

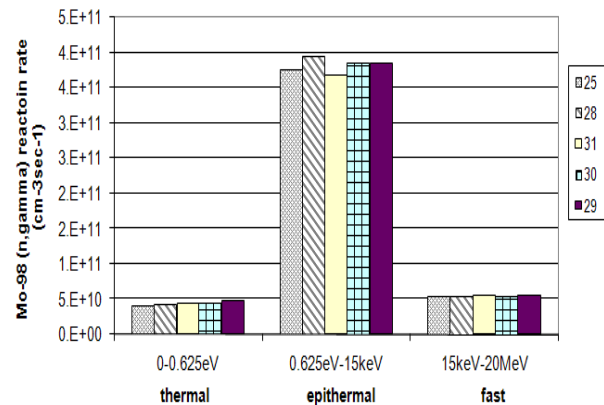


Fig.10. Mo⁹⁸(n,γ)Mo⁹⁹ avg. reaction rate in natural Mo with beryllium in location

2.3 Influence of pin placement inside the experimental location

It can be seen (Tab.2) that the maximum activity position in the 24% ⁹⁸Mo in beryllium case is the corner of a TRIGA bundle followed by the center (Fig.7). For the case with 98% Mo⁹⁸ in water, the center of the bundle is the best position followed by the corner position.

In the first calculated case (98% Mo⁹⁸ in water) we obtained a total (5 pins) Mo⁹⁹ activity of 623.1Ci, an activity per cubic centimeter of pellets equal to 30.73 Ci/cm³, and a mass activity of 3.27 Ci/g Mo⁹⁸. In the second case (natural Mo in beryllium) we obtained a total (5 pins) Mo⁹⁹ activity of 209.3Ci, an activity per cubic centimeter of pellets equal to 10.31Ci/cm³ and a mass activity of 4.46 Ci/g Mo⁹⁸.

Material		Mat25 (corner)	Mat28 (edge-center)	Mat29 (center)	Mat30 (intermediate, 2 nd row)	Mat31 (edge-corner)
H2O, 98% enrich.	Reaction rate (cm ⁻³ s ⁻¹)	1.52E+12	1.32E+12	1.62E+12	1.36E+12	1.48E+12
	Activity (Ci)	129.	113.	139.	116.	126.
Be, 24% enrich.	Reaction rate (cm ⁻³ s ⁻¹)	5.261E+11	5.13E+11	5.21E+11	4.74E+11	4.11E+11
	Activity (Ci)	45.1	43.8	44.5	40.5	35.2

Tab.2. Reaction rates and activities for 98% Mo⁹⁸ pins in water and natural Mo in beryllium

2.4 Different irradiation times; corrected Mo⁹⁸ thermal cross-section

All the results presented were calculated at 6 days irradiation time. This duration can easily be changed to obtain the activity knowing the reaction rate, using the formula[6]:

$$\Lambda = R(1 - e^{-\lambda \cdot t}) \quad (1)$$

where:

R – the total (n, γ) reaction rate in Mo⁹⁸ (cm⁻³s⁻¹)

Λ – the Mo⁹⁹ activity

λ – disintegration constant (s⁻¹)

t – irradiation time (s)

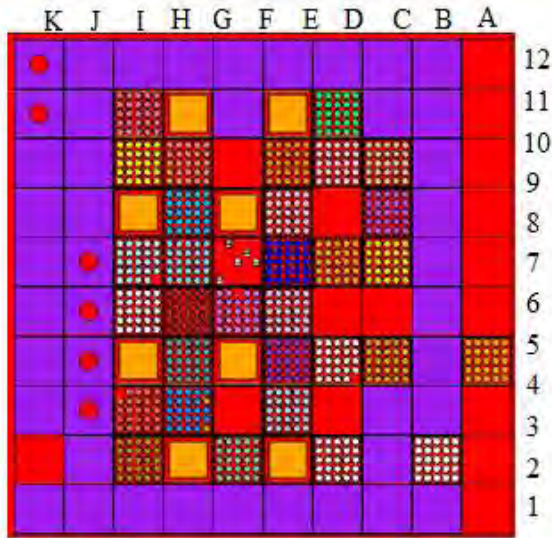


Fig.11. TRIGA core configuration

$\Phi_{th} = 1.04 \cdot 10^{14}$ cm⁻²s⁻¹; $R = 1.46 \cdot 10^{12}$ cm⁻³s⁻¹; 98% Mo-98 in H₂O $\sigma_{th}^{corr.} = 0.242$ b

$\Phi_{th} = 4.99 \cdot 10^{13}$ cm⁻²s⁻¹; $R = 4.88 \cdot 10^{11}$ cm⁻³s⁻¹; 24% Mo-98 in Be $\sigma_{th}^{corr.} = 0.687$ b

The 2200 m/s cross section for the Mo⁹⁸(n, γ)Mo⁹⁹ reaction is about 0.13 b. The larger is the corrected cross-section, the higher is the contribution to the total reaction rate of neutrons above 0.625 eV.

It is customary to express the irradiation spectrum for producing Mo⁹⁹ by means of a corrected thermal Mo⁹⁸(n, γ)Mo⁹⁹ cross-section that will characterize the location inside the reactor. Thus, knowing the thermal flux, either by measurements or by calculation with a computer code, one can determine the activity of the target using ($N \cdot \sigma \cdot \Phi_{th}$) instead of R in (1). We calculate this corrected cross-section for the XC1 (G7) location inside the TRIGA reactor, in the currently existing core configuration, for 98% enriched Mo in water, and natural Mo in beryllium as:

$$\sigma_{th}^{corr.} = \frac{R}{N \cdot \Phi_{th}} \quad (2)$$

where $N = 0.05777002$ barn⁻¹cm⁻¹ (0.014224469 for natural Mo) is the atomic density of Mo⁹⁸ in the pellets.

3. Fission method

3.1 Neutronic analysis

Molybdenum irradiation device is located in the grid position labeled G7 and its modelling appears in Fig.12 as well as in Fig.13, which gives a radial cut through the device, and in

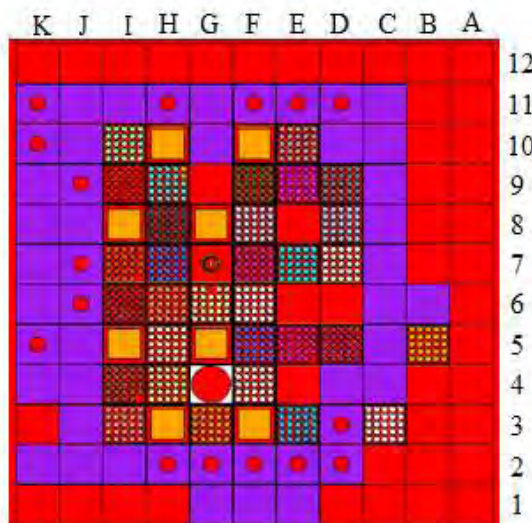


Fig.12. MCNP model of TRIGA SSR (with MCNP Visual Editor)[7]

Fig.14, showing the materials arrangement inside one of the three Uranium foil containers. The target irradiation system (Fig.13 and Fig.14) is formed by a LEU (19.75% enriched in U²³⁵) metallic uranium foil of 9 grams, 125 microns thick, wrapped in a thin (15 microns) nickel fission product-recoil barrier. The metallic uranium foil with its nickel coating surrounds an aluminum tube of 152 mm in length, 27.91 mm outer diameter and 26.44 mm inner diameter. This set, as well, is surrounded by an aluminum tube of 28.22 mm inner diameter, 30 mm outer diameter and 152 mm in length. The foil containers are vertically placed with no space between two containers, the middle one being located at the middle height of the TRIGA fuel column (active fuel length is 55.88cm).

3.1.1 Reactivity introduced by experiment

The positive reactivity introduced by the irradiation device with three foil containers was obtained by calculating the reactor with and without the irradiation device and foil containers. The resulted reactivity worth is $+0.495 \pm 0.031\%$.

3.1.2 Neutron fluxes and fission rates in the Uranium foils

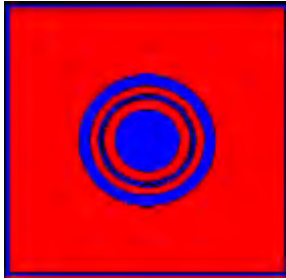


Fig.13. Radial cut through the irradiation device

Three groups neutron fluxes and fission rates were requested as tallies using the f4:n tally type in MCNP (flux averaged over a cell). Fluxes were calculated inside each of the three Uranium foils and also in exactly the same location (cell) but without the irradiation device, with water inside the experimental location. Tab.3 presents the groups boundaries and the fluxes together with their corresponding standard deviation.

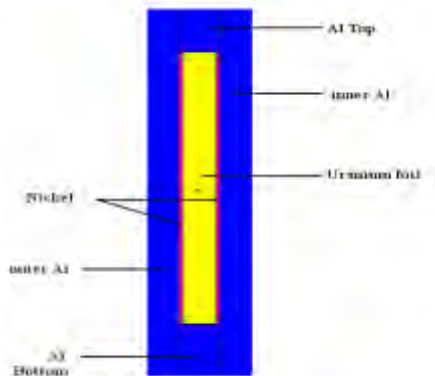


Fig.14. Axial view of one Uranium foil container

Group	Energy domain	Foil 1 (cm ⁻² s ⁻¹)	Foil 1* (cm ⁻² s ⁻¹)	Foil 2 (cm ⁻² s ⁻¹)	Foil 2* (cm ⁻² s ⁻¹)	Foil 3 (cm ⁻² s ⁻¹)	Foil 3 (cm ⁻² s ⁻¹)	Average standard deviation (%)
1	0eV-0.625eV	1.103E+14	1.811E+14	1.243E+14	2.049E+14	6.959E+13	1.134E+14	0.70
2	0.625e-0.5MeV	7.905E+13	6.031E+13	9.146E+13	7.014E+13	5.239E+13	4.010E+13	0.96
3	0.5Me-20MeV	7.882E+13	3.026E+13	9.146E+13	3.403E+13	5.070E+13	2.017E+13	1.27

Tab.3. Calculated fluxes in foils (foil1 in lowermost axial position) and water (*) normalized to 10 MW reactor power. The average standard deviation is the average over individual group values

Tab.4 presents the calculated fission reaction rates. The thermal flux is larger in water, when the irradiation device is not present. The fast flux is increased in the foils by their own fission reactions. The effect of control rods position on the foils thermal flux and fission rate is apparent in the ratio between foil1 and foil3. Power density in foil1 (the lowermost) is about 37% more than in foil3 (the uppermost). The power load is maximum for foil2.

Group	Energy domain	Foil 1 - (cm ⁻³ s ⁻¹)	Foil 2 - (cm ⁻³ s ⁻¹)	Foil 3 - (cm ⁻³ s ⁻¹)	Average standard deviation (%)
1	0eV - 0.625eV	4.636E+14	5.219E+14	2.906E+14	0.71
2	0.625eV - 0.5MeV	1.124E+13	1.285E+13	7.281E+12	1.77
3	0.5MeV - 20MeV	1.894E+12	2.205E+12	1.225E+12	1.23
	total	4.768E+14	5.370E+14	2.991E+14	0.70

Tab.4. Calculated fission rates in Uranium foils (foil1 in lowermost axial position) normalized to 10 MW reactor power. The average standard deviation is the average over individual group values

3.1.3 Released and deposited power in the Uranium foils

The released power was calculated using the fission rate and the energy recovered from fission, the latter being reported by MCNPX and considered adequate for water reactors with U^{235} ($\epsilon=201.7$ MeV). The resulted released power values generated by each foil are:

$$P_{\text{Foil1}} = 7386.63 \text{ W}; P_{\text{Foil2}} = 8320.06 \text{ W}; P_{\text{Foil3}} = 4634.57 \text{ W}$$

The deposited power inside the irradiation device is relevant for safety analysis. It was calculated in a neutron-photon transport problem, requesting energy deposition tallies for both neutrons and photons: F6:n, F6:p and F7:n. The deposited energy is a sum of different heating contributions inside each material:

Container no.	Power in Foil (W)	Fraction from released power	Power in Al (W)
1	6666.43	0.9025	522.92
2	7510.11	0.9026	591.26
3	4186.40	0.9032	366.27

Tab.5. Calculated deposited power in the Uranium foils and Aluminium for the three containers (container 1 in the lowermost axial position) normalized to 10 MW

$$H = H_{fp} + H_n + H_{\gamma_p} + H_{\gamma_d} + H_{\beta} \quad (3)$$

where: H_{fp} is due to fission products; H_n is due to neutrons; H_{γ_p} is due to prompt gammas; H_{γ_d} is due to delayed gammas; H_{β} is due to betas.

No MCNP tallies account for betas and delayed gammas, but these two contributions were scaled from conventional tallies as described in [5] for calculating deposited power in Uranium foils. The resulted deposited power in the Uranium foils and in the Aluminium for the three foil containers are given in Tab.5. The deposited power in the three Uranium foils seems to be 10% less than the released power. Standard deviation in both thermal fission rates and individual heating tallies is about 0.7%. The reason for the difference between released and deposited power lies in the very small gamma heating to total heating ratio (illustrated roughly by the f6:p/f7 ratio, equal to 0.006). There is a large escape probability of the gammas emitted inside the foil which can deposit their energy in the surrounding TRIGA fuel, while the foil offers a very small volume for interactions with the gamma flux in the reactor. Concerning the Aluminium in the irradiation device, an average of 1.34 W/g at 10 MW reactor power results from the calculation.

3.1.4 Mo^{99} activity in the Uranium foils

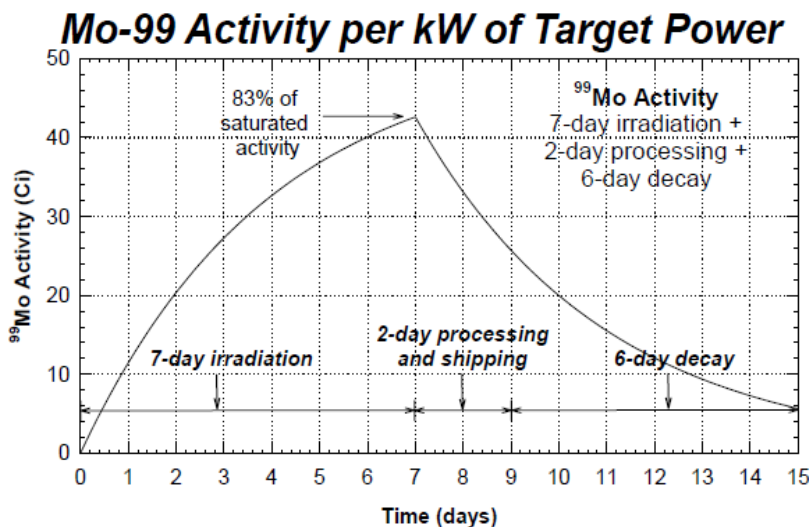


Fig.15. Mo^{99} activity per KW of target power[2]

The Mo^{99} activity as a function of the irradiation time t_i can be found from the formula:

$$\Lambda = \frac{\gamma \cdot V \cdot R_f \cdot (1 - e^{-\lambda \cdot t_i})}{3.7 \cdot 10^{10}} \quad (4)$$

where:

- Λ - Mo^{99} activity (Curie)
- γ - Mo^{99} fission yield (6.1%)
- V - Uranium foil volume (cm^3)
- R_f - fission rate ($cm^{-3}s^{-1}$)
- λ - Mo^{99} disintegration constant ($2.91729E-06 s^{-1}$)
- t_i - irradiation time (s)

Once the irradiation is over, the target is cooled for approximately 12-24 hours and then transported into the processing plant. Using data from Tab.4 for the fission rates of the foils at 10 MW reactor power, the following were obtained for each foil:

- the total Mo⁹⁹ activity of each foil (Fig.16)
- the Mo⁹⁹ activity per gram of Uranium present initially (Fig.17)
- the Mo⁹⁹ activity per gram of U²³⁵ present initially (Fig.18)

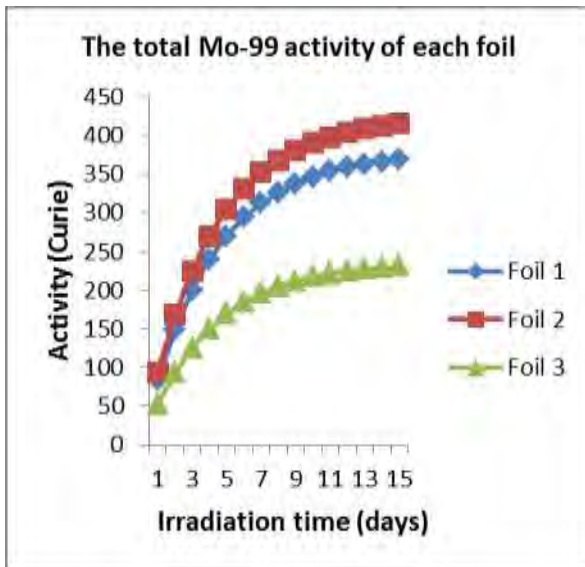


Fig.16. The total Mo⁹⁹ activity in each of the three foils (foil1 in lowermost axial position) normalized to 10 MW

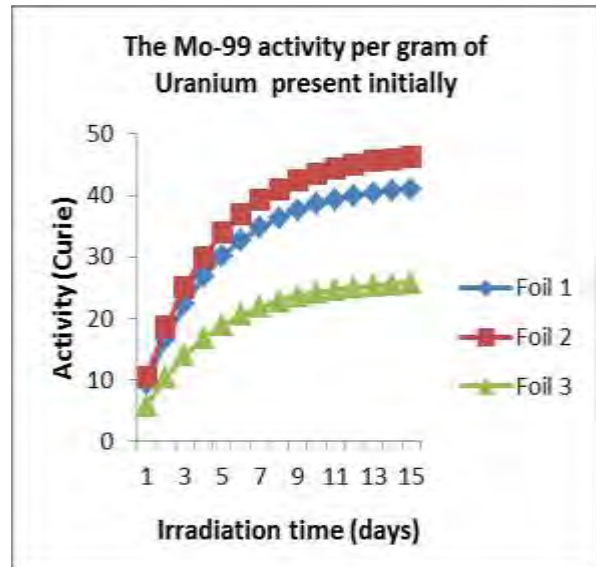


Fig.17. The Mo⁹⁹ activity per gram of U in each of the three foils (foil1 in lowermost axial position) at 10 MW

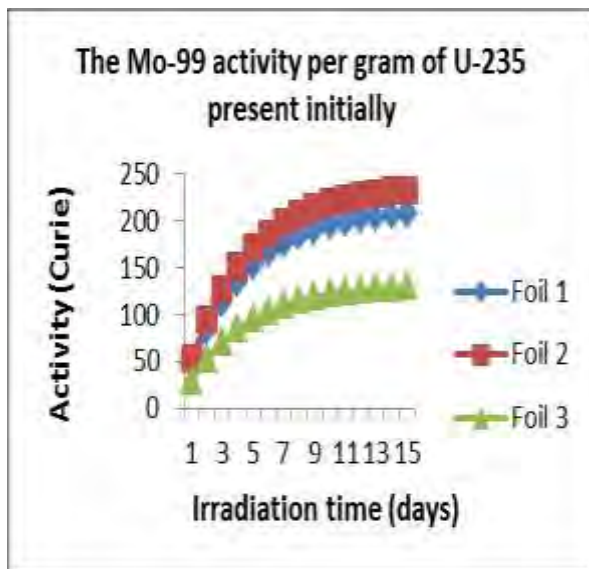


Fig.18. The Mo⁹⁹ activity per gram of U²³⁵ in each of the three foils (foil1 in lowermost axial position) at 10 MW

3.2 Thermal-hydraulic analysis

The aim of the analysis was to determine the flow rate, the outlet-inlet temperature difference through the irradiation device and the radial temperature distribution. No axial temperature distribution was searched for inside one foil; the input deposited powers calculated in the previous section was provided as 3 values, for the three foils, and the thermal-hydraulic model describes each foil container as a single wall.

3.2.1 Thermal-hydraulic model

The heat producing device with U enclosed in Ni and Al was modelled a series of cylindrical walls (thermal structures) cooled on the internal face by the inner channel and on the external face by the outer channel as in the sketch included as Fig.19. There is a gap with air between the Uranium foil (tightly coated in Nickel) and the inner and outer container Aluminum. Heat is also produced in the central Al tube (radius 1 cm) on the same length and the outer Al wall (external radius 2.1 cm). The later was considered conservatively as being cooled only by the outer channel and not by the bypass channel. The central tube is internal to the inner channel. Two primary pumps are necessary for 10 MW reactor power level. The nominal flow rate given by the two pumps is 660 kg/s (from the reactor operation records).

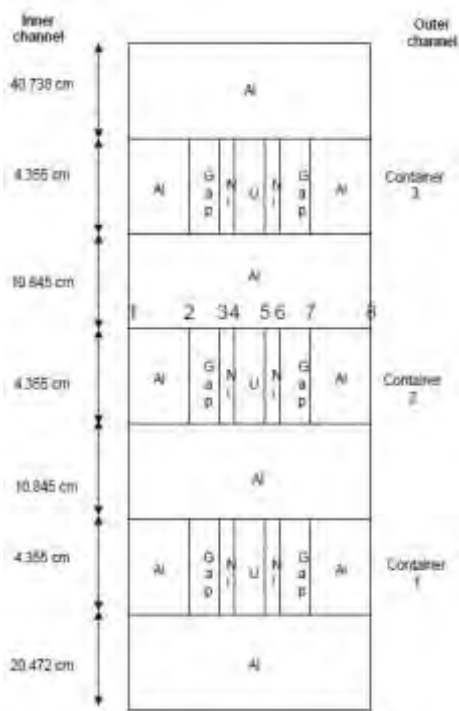


Fig.19. Arrangement of materials inside the wall. Nodes for temperature calculation are indicated

Assuming hypothetical uncertainties in calculating flow rate through the device, a sensitivity study was done also to see the effect of the flow rate on temperature distribution inside the container.

3.2.2 Results: Mass flow rate

The mass flow rates through the channels at nominal flow rate (660 kg/s) through the reactor are: inner channel $Q = 1.53$ kg/s; outer channel $Q = 1.074$ kg/s. Therefore, the heat produced by the device is removed by 2.6 kg/s of primary coolant water on a total flow area equal to 7.255 cm^2 , while through the average TRIGA channel (1.3594 cm^2) passes 0.88 kg/s.

3.2.3 Results: Water temperature

Inlet water temperature was taken 22°C . The outlet water temperature in the inner channel is 22.72°C , while in the outer channel is 24.3°C . Weighting with their respective mass flow rates, it results an outlet temperature 23.075°C ; outlet-inlet temperature difference is 1°C at nominal flow.

3.2.4 Results: Wall temperatures

The foil temperature as a function of gap width (considered as uniform though probably contact points will appear) is presented in Fig.20. There is a strong linear increase of the foil temperature with the gap width, for a 60 μm gap the temperature becomes close to the melting temperature of metallic Uranium (1132°C). The distribution of temperatures in different layers of the second fuel container (maximum power loaded) is presented in Fig.21 for an arbitrary gap width (25 μm).

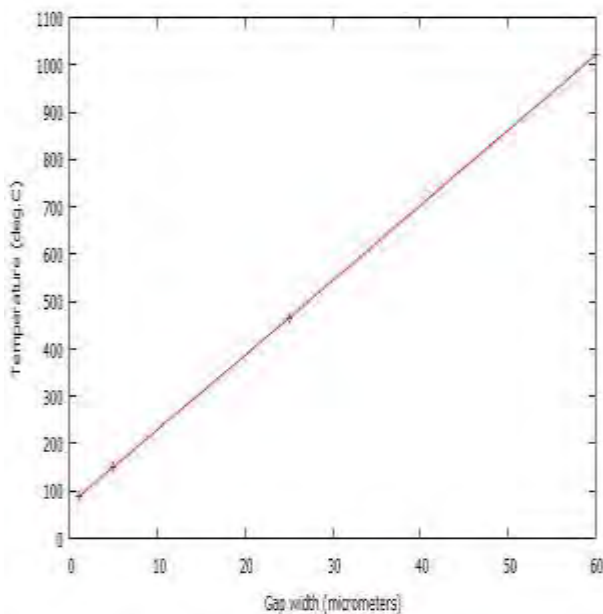


Fig.20. Uranium foil temperature (Foil2) as a function of air gap width

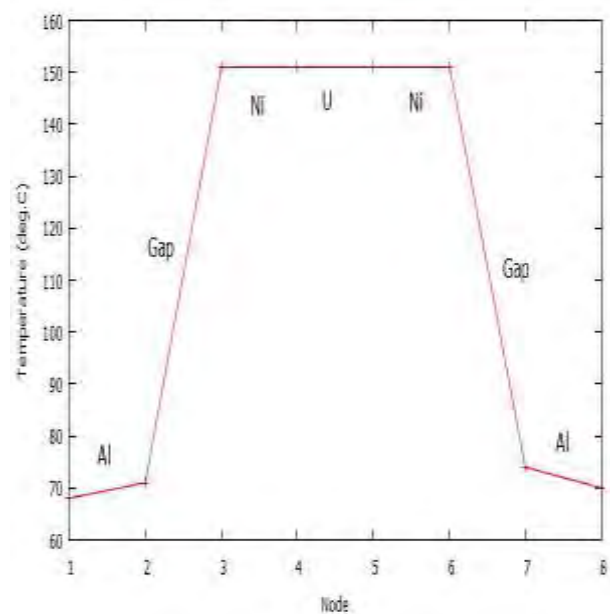


Fig.21. Temperature distribution inside container no.2; arbitrary gap width, 25 μm .

4. Conclusions

The paper focused on MCNP calculations for maximizing the ^{99}Mo activity. Two runs were done for the maximum volumetric and mass activity cases with the MCNP core model in the same arrangements of pins inside the experimental location (central, G7), at 10 MW reactor power level. We obtained, as an average over the pellets of all five pins: 30.73 Ci/cm^3 in the first case and $4.46 \text{ Ci/g } ^{98}\text{Mo}$.

All activities were calculated by MCNPX after 6 days irradiation time, but the paper offers the possibility to recalculate the activities for any irradiation time interval by providing the reaction rates for the two core calculations. Also, as a measure of the contribution of neutrons above thermal to the reaction rate, we calculated a thermal neutrons equivalent cross section of ^{98}Mo in each case. We have chosen the upper limit of the thermal energy region as 0.625 eV. Thus, knowing the thermal flux (either measured or calculated) one can easily obtain the reaction rate and consequently the activity in a location inside the core.

Reactor physics studies were done for the TRIGA core at 10 MW including the irradiation device placed in XC1 (G7 reactor core grid position) experimental location. The positive reactivity introduced by the irradiation device with three foil containers was obtained being $+0.495 \pm 0.031\%$.

Three group neutron flux at the location of the Uranium foils was calculated, both perturbed (with the device) and unperturbed (without the device, in water). The average value for the perturbed thermal flux over the three foils is $1.01 \cdot 10^{14} \text{ neutrons/cm}^2\text{-s}$ while the maximum thermal flux (foil 2) is $1.24 \cdot 10^{14} \text{ neutrons/cm}^2\text{-s}$. Fission rate inside the foils was also determined and used in the calculation of the released energy and Mo^{99} activity. The average foil Mo^{99} activity after 7 irradiation days is 286.86 Curie. Deposited power inside the three foils was calculated as a sum of contributions: fission products and betas energies deposited locally, and gammas and neutrons energy deposited as a result of interactions of the transported particles in a MCNP n,p problem. The average deposited power inside one foil is 6.12 kW and the maximum foil power is 7.51 kW. Gamma and neutron energy deposited in Aluminium such as structural material in the targets and irradiation device was also calculated, the average of the deposited power density being 1.34 W/g.

A thermal-hydraulic model was created, using power values inside the irradiation device calculated in reactor physics studies. Containers were modelled as multilayer walls with a variable air gap between the foil coated in Nickel and the aluminium inside the container. A 2.6 kg/s flow rate through the device was calculated at nominal primary circuit flow rate. The foil temperatures strongly increase with air gap width variation from 100°C , for a $1 \mu\text{m}$ gap, to over 1000°C , for a $60 \mu\text{m}$ gap. Imposing smaller flow rate values through the device does not affect dramatically the temperatures of the foil. Reducing the flow rate by a factor of three will rise the wet side temperature of the wall from 70°C to 120°C .

5. References

- [1] The supply of Medical Radioisotopes: Review of Potential Molybdenum -99/Technetium-99m Production Technologies, Nuclear Energy Agency, November 2010
- [2] The Supply of the Medical Radioisotope Tc-99m/Mo-99, Sandia National Laboratories Albuquerque, November 6, 2009
- [3] A.A. Sameh, H.J. Ache, Production Techniques of fission Mo^{99} , Institut für Radiochemie, Karlsruhe, Federal Republic of Germany, 1987
- [4] D. Pelowitz (editor). MCNPX User's Manual, version 2.6.0, April 2008
- [5] F. B. Brown, W. R. Martin, R. Mosteller, Monte Carlo - Advances and Challenges, PHYSOR-2008 Interlaken, Switzerland, 14-19 September 2008
- [6] A.I. Ryabchikov, V.S. Skuridin, E.V. Nesterov, E.V. Chibisov, V.M. Golovkov. Obtaining molybdenum-99 in the IRT-T research reactor using resonance neutrons, Nuclear Physics Institute at Tomsk Polytechnic University, 2a, Lenin Av., 634 050 Tomsk, Russia
- [7] MCNP/MCNPX Visual Editor Computer Code Manual For Vised Version 22S, Released February, 2008 A.L. Schwarz , R.A. Schwarz, and L.L. Carter

THE 14 MeV NEUTRON IRRADIATION FACILITY IN MARIA REACTOR

R. PROKOPOWICZ, K. PYTEL, M. DOROSZ, A. ZAWADKA, J. LECHNIAK,
M. LIPKA, Z. MARCINKOWSKA, M. WIERZCHNICKA, A. MAŁKIEWICZ,
I. WILCZEK, T. KROK, M. MIGDAL, A. KOZIEŁ

*Reactor Measurement and Analysis Group, Research Reactor Technology Division,
National Centre for Nuclear Research
ul. Andrzeja Sołtana 7 05-400 Otwock, Poland*

ABSTRACT

The MARIA reactor with thermal neutron flux density up to $3 \cdot 10^{14}$ cm⁻² s⁻¹ and a number of vertical channels is well suited to material testing by thermal neutron treatment. Beside of that some fast neutron irradiation facilities are operated in MARIA reactor as well. One of them is thermal to 14 MeV neutron converter launched in 2014. It is especially devoted to fusion devices material testing irradiation.

The ITER & DEMO research thermonuclear facilities are to be run using the deuterium - tritium fusion reaction. Fast neutrons (of energy approximately 14 MeV) resulting from the reaction are essential to carry away the released thermonuclear energy and to breed tritium. However, constructional materials of which thermonuclear reactors are to be built must be specially selected to survive intense fluxes of fast neutrons. Strong sources of 14 MeV neutrons are needed if research on resistance of candidate materials to such fluxes is to be carried out effectively. Nuclear reactor-based converter capable to convert thermal neutrons into 14 MeV fast neutrons may be used to that purpose.

The converter based on two stage nuclear reaction on lithium-6 and deuterium compounds leads to 14 MeV neutron production. The reaction chain is begun by thermal neutron capture by lithium-6 nucleus resulted in triton release. The neutron and triton transport calculations have been therefore carried-out to estimate the thermal to 14 MeV neutron conversion efficiency and optimize converter construction. The useable irradiation space of ca. 60 cm³ has been obtained. The released energy have been calculated. Heat transport has been asses to ensure proper device cooling. A set of thermocouples has been installed in converter to monitor its temperature distribution on-line. Influence of converter on reactor operation has been studied. Safety analyses of steady states and transients have been done. Performed calculations and analyses allow designing the converter and formulate its operation limits and conditions.

During first tested operation of the converter the 14 MeV neutron flux density was estimated to 10^9 cm⁻² s⁻¹, whereas fast fission neutrons inside converter achieved 10^{12} cm⁻² s⁻¹, and thermal neutrons were reduced down to 10^9 cm⁻² s⁻¹.

Taking into account the feasibility of almost incessant converter operation for a number of months, its arisen as one of the most powerful (in terms of fluence), currently available 14 MeV neutron source. Such a converter currently under operation in the MARIA reactor core will be presented.

1. Introduction

The MARIA reactor with thermal neutron flux density up to $3 \cdot 10^{14}$ cm⁻² s⁻¹ and a number of vertical channels is well suited to material testing by thermal neutron treatment. Beside of that some fast neutron irradiation facilities are operated in MARIA reactor as well. One of them is thermal to 14 MeV neutron converter launched in 2014. It is especially devoted to fusion devices material testing irradiation.

The ITER & DEMO research thermonuclear facilities are to be operate using the deuterium – tritium nuclear fusion reaction. Fast neutrons (of energy approximately 14 MeV) resulting from the reaction are essential to carry away the released thermonuclear energy and to breed tritium. However, constructional materials of which thermonuclear reactors are to be built must be specially selected to survive intense fluxes of fast neutrons. Strong sources of 14 MeV neutrons are needed if research on resistance of candidate materials to

such fluxes is to be carried out effectively. Nuclear reactor-based converter capable to convert thermal neutrons into 14 MeV fast neutrons may be used to that purpose.

2. The irradiation facility construction

The converter based on two stage nuclear reaction on lithium-6 and deuterium compounds leading to 14 MeV neutron production. The reaction chain is begun by thermal neutron capture by lithium-6 nucleus resulted in triton release. The nuclear reactor is used as a strong thermal neutron source.

The neutron and triton transport calculations have been therefore carried-out to estimate the thermal to 14 MeV neutron conversion efficiency and optimize converter construction. The useable irradiation space of ca. 60 cm³ has been obtained. The released energy have been calculated. Heat transport has been asses to ensure proper device cooling. A set of thermocouples has been installed in converter to monitor on-line its temperature distribution. Influence of converter on reactor operation has been studied. Safety analyses of steady states and transients have been done. Performed calculations and analyses allow designing the converter and formulate its operation limits and conditions.

The converter construction consists of a set of concentric tubes, located inside vertical channel in reactor beryllium moderator (fig. 1). The converting layer in cylindrical shape surrounds a container with irradiated samples.

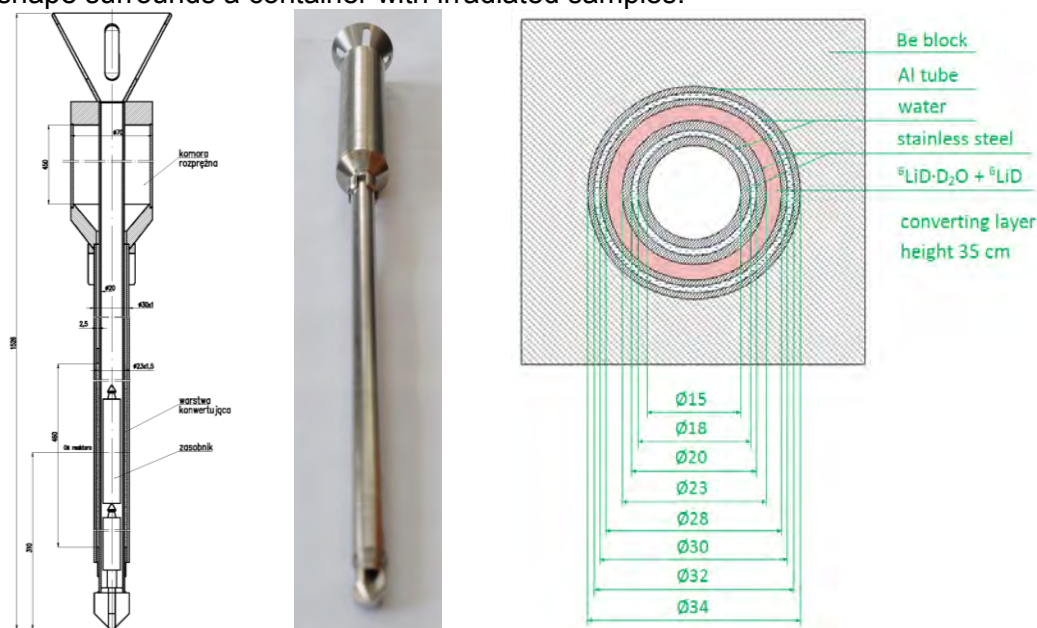


Fig. 1. Converter construction.

The neutron energy spectrum inside container depends on converter distance from nuclear fuel, and therefore on converter location in the reactor core (cf. fig. 2).

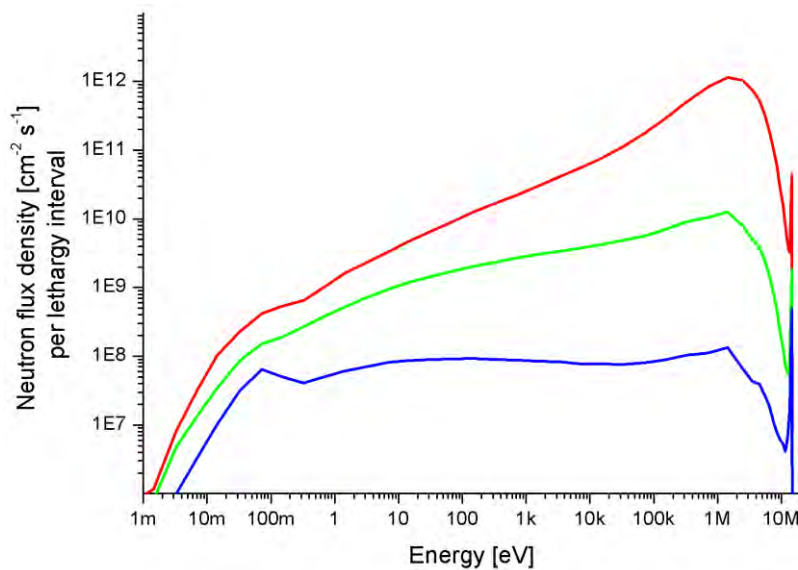


Fig. 2. Calculated neutron energy spectrum inside converter located in the middle of reactor core (red curve), in the periphery of reactor core (green curve) and in the reactor reflector (blue curve).

3. Testing Operation

During first tested operation of the converter in MARIA reactor the 14 MeV neutron flux density was estimated to over $10^9 \text{ cm}^{-2} \text{ s}^{-1}$, whereas fast fission neutrons inside converter achieved $10^{12} \text{ cm}^{-2} \text{ s}^{-1}$, and thermal neutrons were reduced down to $10^9 \text{ cm}^{-2} \text{ s}^{-1}$. The neutron flux densities have been measured by means of activation method with a set of various activation foils.

A set of ITER construction steels have been irradiated in above mentioned neutron field. Currently, they are under investigation.

4. Conclusion

Taking into account the feasibility of almost incessant converter operation for a number of months, its arisen as one of the most powerful (in terms of fluence), currently available 14 MeV neutron source.

OVERVIEW ON RRSF REPROCESSING, FROM SPENT FUEL TRANSPORTATION TO VITRIFIED RESIDUES STORAGE

J.F. VALERY, X. DOMINGO, P. LANDAU

AREVA NC

1 place Jean Millier, 92084 Paris La Défense Cedex - France

A. DUPEYRAT, P. DESCHAMPS, C. PECHARD

AREVA NC La Hague

50440 Beaumont-Hague - France

V. LALOY, M. KALIFA

AREVA TN

1 Rue des Hérons, 78180 Montigny-le-Bretonneux - France

ABSTRACT

Benefiting from its past experience, AREVA proposes to detail in pictures all the stages of a (Research Reactor Spent Fuel) RRSF reprocessing from its evacuation from reactor site to its corresponding post-reprocessing vitrified waste production and management.

1. Introduction

Reprocessing is one of the today-available options for managing back-end of Research Reactor fuel cycle.

As described in figure 1 below, this solution offers to RR:

- Non-proliferation: reducing ^{235}U enrichment of RRSF from 20-93% to below 2%,
- Final waste management optimisation: standardizing final waste package and reducing volume and radio-toxicity, removing IAEA safeguards on final waste,
- Sustainability of RRSF back-end management: long-lasting solution, re-use of valuable material for civilian purposes i.e. saving natural resources, cost-certainty, cost effective solution,...

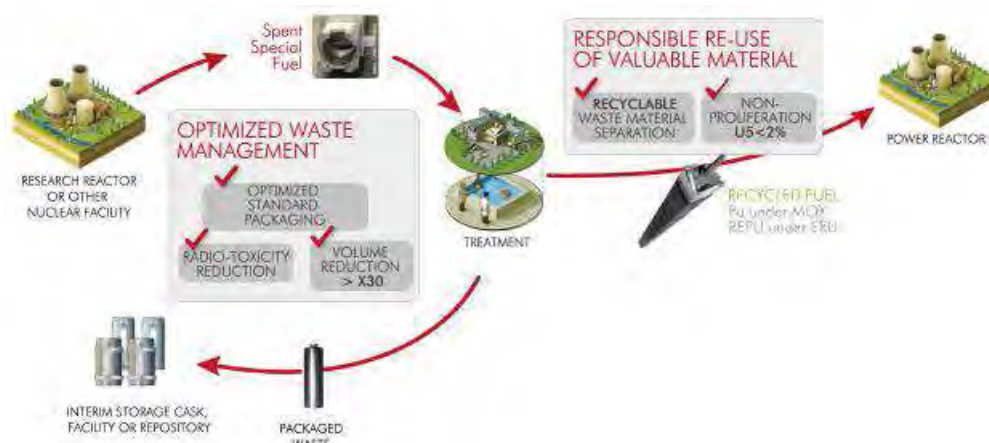


Fig. 1: RRSF reprocessing basic scheme and advantages

Over the past decades, AREVA has been transporting, unloading, storing and reprocessing RRSF in its French facilities and with its equipment.

This article encompasses pictures and figures for each step of reprocessing operations by AREVA, especially in regards to transport to and reprocessing at the AREVA La Hague site.

2. Transportation of RRSF to La Hague

Since early 1990's, around 150 MTR-type RRSF transportation casks have been transported to AREVA La Hague.

2.1. Types of transportation cask

The first high-capacity RRSF transportation cask used by AREVA (Cogema Logistics at that time) was the IU04 cask.

As of today, AREVA proposes to its customers to use the TN-MTR transportation cask for MTR-types of RRSF, especially for transportation to the La Hague site.

This cask can contain several types of basket, generic or specialized according to the RRSF. This cask offers the highest RRSF transportation capacity worldwide, with a 68-positions basket.

The TN-MTR cask can be loaded at RR site either under water or using a dry transfer system from pool to cask.



Fig.3: TN-MTR wet loading at RR site
© AREVA



Fig.4: Transfer system for loading TN-MTR at RR site © AREVA

AREVA can also propose other types of multi-purpose transportation casks, even adapted for non-MTR-type RRSF. As an example a new package, which fabrication will be completed by mid-2015, will be proposed by AREVA: the TN-LC package [1].

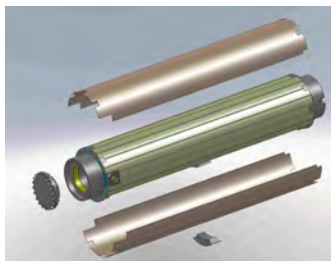


Fig.5: View of TN-LC transportation cask © AREVA



Other casks can be considered for transportation of RRSF to AREVA La Hague, after investigating the following:

- Transportation license from RR site to La Hague (i.e. French transportation license, license in the RR country, and all countries involved in this transportation),
- Receipt and unloading at La Hague (see paragraph 3.2. below).

2.2. RRSF transportation experiences

As mentioned before, **around 150 MTR-type RRSF transportation casks** have been transported to AREVA La Hague up to now.

AREVA has acquired this long-term international experience through multi-modal transportations: maritime, rail and road transportations (see Fig.6 & 7),



Fig.6: RRSF transportation on boat
© AREVA



Fig.7: TN-MTR on a truck © AREVA

AREVA has notable RRSF transportation experiences in the following countries: **Australia, Belgium, Denmark, France, Indonesia, Italy, Portugal, Sweden, Taiwan, United States of America, Uruguay** and **Venezuela**.

3. Receipt and unloading of RRSF at La Hague

The AREVA La Hague plant obtained its first authorizations for receiving and unloading RRSF in the late 1990's.

Ever since and until end-of 2014, **around 150 MTR-type RRSF transportation casks** have been received and unloaded at AREVA La Hague, corresponding to **around 5 250 MTR-type RRSF assemblies**.

As mentioned before, the transportation casks used for these receipts at La Hague were the IU04 and now the TN-MTR.

But RRSF are not only MTR-type of spent fuels. Thanks to the flexibility of its receipt-workshops, AREVA is also able to receive other types of RRSF, and other types of RRSF transportation casks.

3.1. Receipt of transportation casks at the La Hague site

At their arrival at the La Hague site (see Fig.8), and before unloading, the RRSF transportation casks are temporarily stored for a few days.

At its arrival, the transportation truck is controlled for exterior and interior contamination (see Fig.9), before control of the transportation cask itself (see Fig.10).

In preparation for unloading the cask is lifted and handled in a preparation hot-cell, next to the unloading pool (see Fig.11).

After additional controls, and notably internal shipping tests on the cask in order to detect any nuclear material leakage from RRSF assemblies, the transportation is wrapped in plastic sheet (to prevent the body of the cask from possible contamination during unloading, and consequently to facilitate the preparation of the next shipment), and moved from the preparation cell to the unloading pool (see Fig.12).



Fig.8: Truck with RRSF transportation cask arrival at La Hague © AREVA



Fig.9: Control on RRSF transportation truck at La Hague © AREVA



Fig.10: Radiological control on RRSF transportation cask, without shock absorber © AREVA



Fig.11: Cask handling to the preparation cell, before unloading © AREVA

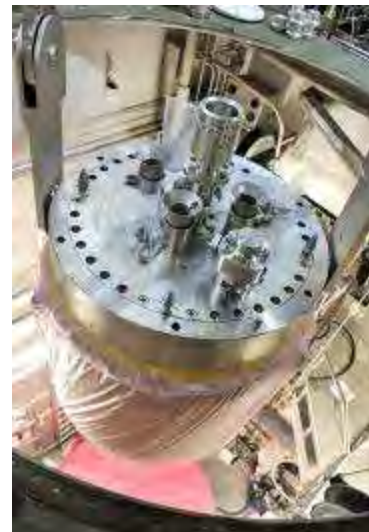


Fig.12: Cask handling from preparation cell, to unloading pool © AREVA

3.2. Wet unloading of RRSF

Until 2015, the MTR-type RRSF transportation casks are unloaded in the pool *HAO-Nord*. Starting 2016, RRSF transportation casks will be unloaded in the *NPH (Nouvelle Piscine de la Hague)* pool.

Thanks to its flexibility, the *NPH* pool workshop and related tools can be adapted to a wide range of transportation casks. For example, the TN-17/2 cask, used for Fast Reactor spent fuel transportation, is also unloaded in *NPH* pool.

Nevertheless, in case a new cask needs to be received at La Hague, feasibility studies, a safety report application to Safety Authority /authorization, design and fabrication of new equipments and possible modifications to the workshop are necessary.

After introduction of the transportation cask in the pool (see Fig.13) the top-lead of the cask is removed in order to access to RRSF. All the handling operations during unloading are performed manually, by AREVA operators (see Fig.14), but are controlled by automatism and Instrumentation & Control.

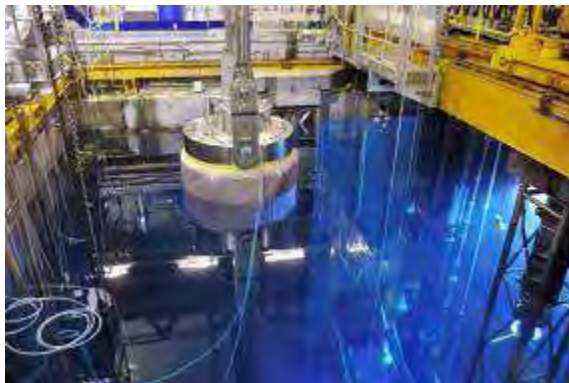


Fig. 13: RRSF transportation cask introduction in HAO pool © AREVA



Fig. 14: La Hague operator handling RRSF in HAO pool © AREVA

The RRSF are handled from the transportation cask to an intermediate unloading-basket, and then in a position into the interim-storage basket (see Fig. 15) to be transferred in the pools dedicated to wet interim storage (see Fig. 16), before reprocessing.



Fig. 15: The baskets used for RRSF transfer to wet storage © AREVA



Fig. 16: RRSF storage-basket transfer to wet storage © AREVA

4. RRSF wet interim storage at La Hague

Taking into account (i) the time needed for cooling down the RRSF, (ii) industrial reprocessing scheduling of the La Hague plant and (iii) regulatory and legal obligations related to safety authorizations and intergovernmental agreements, RRSF are stored in the La Hague storage pools for some months/years (see Fig. 17) before transfer to reprocessing facilities.



Fig. 17: La Hague wet storage “piscine C”
© AREVA

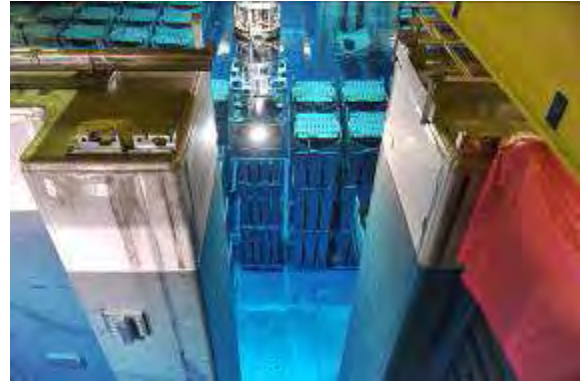


Fig. 18: RRSF storage-basket transfer to reprocessing © AREVA

RRSF storage uses La Hague-standard types of baskets with dedicated inners, adapted to each type/category of RRSF.

Several designs and fuel-types of MTR RRSF are stored in La Hague pools, but other RRSF than MTR-type can be stored, if the corresponding authorization is delivered by the French Safety Authority, after review of the receipt-storage-reprocessing-related safety file.

Depending on the RRSF type, the storage capacity of one basket varies up to more than 60 fuel elements.

After storage, RRSF are transferred to the reprocessing facilities. The first operation is to bring the storage basket (see Fig. 18) to a dedicated workshop to transfer the RRSF from the storage basket to a shuttle-basket, this operation being performed by an AREVA operator (see Fig. 19). After this transfer, RRSF in shuttle basket is ready to be sent to the dissolution facility (see Fig. 20).

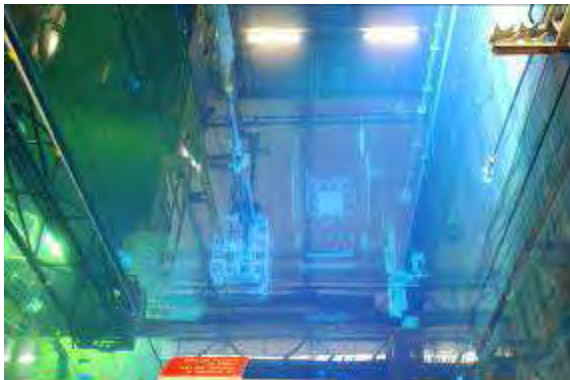


Fig. 19: RRSF transfer from storage to shuttle basket © AREVA

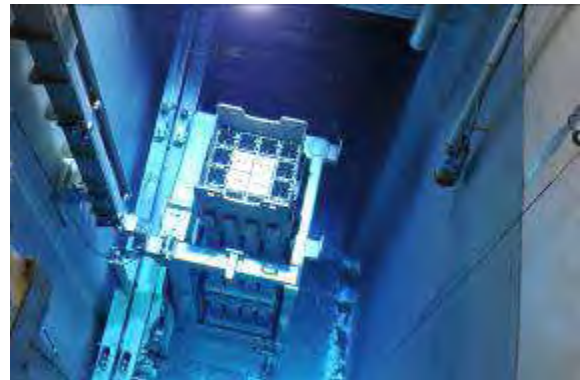


Fig. 20: RRSF shuttle basket ready to go dissolution facility © AREVA

5. RRSF reprocessing operations

From the interim wet storage pool to the dissolution facility (T1 facility in La Hague UP3 reprocessing plant), the transfer of RRSF is performed with a shuttle basket.

The RRSF is inserted one by one from the storage area to the dissolution area through the “insert-cisaille” gate¹ (see Fig.21). The RRSF is then placed into a dedicated canister,

¹ The « insert-cisaille » gate is originally designed as the entry of NPP SF from wet storage to cladding-shearing equipment, before dissolution of nuclear material.

positioned on a rack, waiting for dissolution (see Fig.22). All these operations are performed by operators with dedicated cranes and tele-manipulators (see Fig.23).



Fig.21: video of RRSF going through the "insert-cisaille" gate © AREVA

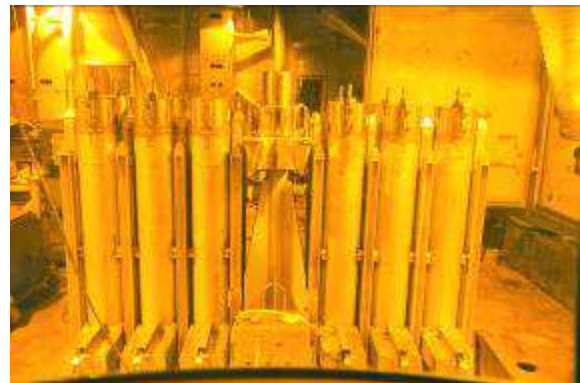


Fig.22: RRSF-canister 12-positions rack in dissolution cell © AREVA

Each canister is then positioned on the top of the dissolution pit (see Fig. 24). The RRSF are then loaded in the dissolution pit one by one by directly dropping them in the boiling nitric acid.



Fig.23: operator handling RRSF with tele-manipulator © AREVA



Fig.24: RRSF canister on top of the T1 dissolution pit © AREVA

The dissolution process is the same for UAl-type and USi-type of RRSF, and is controlled thanks to a dedicated camera placed on the top of the dissolution pit. The dissolution process is over once the RRSF totally disappeared from the pit (see Fig.25 & 26).



Fig.25: RRSF being dissolved © AREVA



Fig.26: dissolution pit empty © AREVA

However, after the dissolution step and prior to the mix with the LWR dissolution solution entering the liquid/liquid extraction for Al management, there is an additional operation performed in the case of USi-type RRSF. This additional operation consists in separating the silicon from the dissolution solution because the whole silicon quantity cannot proceed through the extraction. The concentrated silicon solution is managed through the “fines” line and vitrified with the fissions production solutions at the end of the process.

After dissolution of a RRSF batch, uranium and plutonium are separated from the fission products solutions thanks to the PUREX process. Fission product solutions are then concentrated before their vitrification.

The following Figure 27 & 28 give an overview of the whole reprocessing steps performed for UAI and USi RRSF.

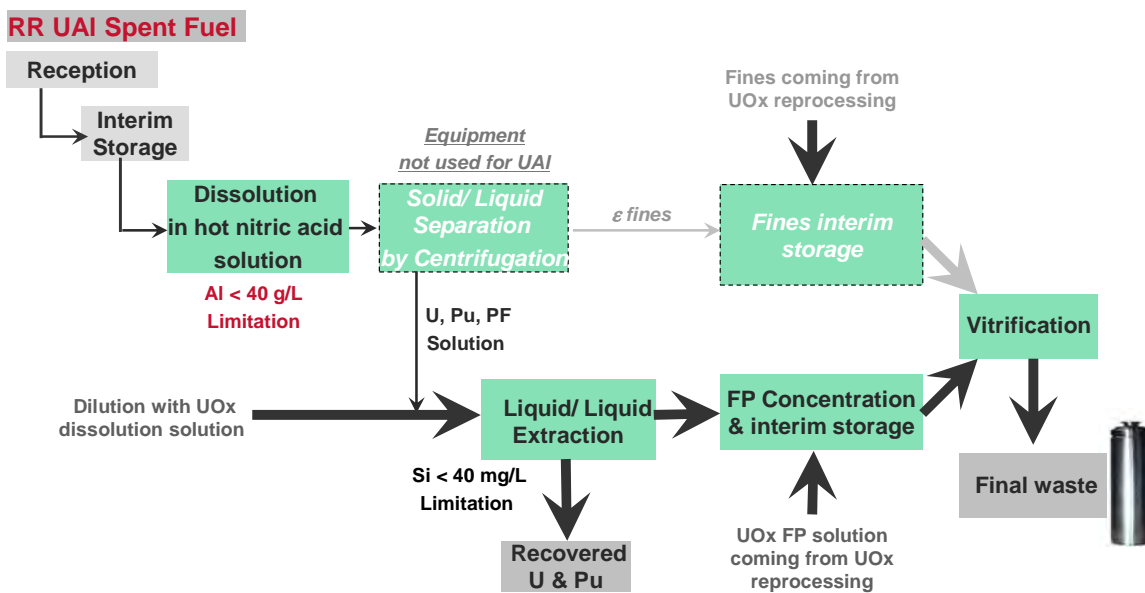


Fig. 27: Process diagram for UAI RRSF reprocessing in AREVA La Hague plant

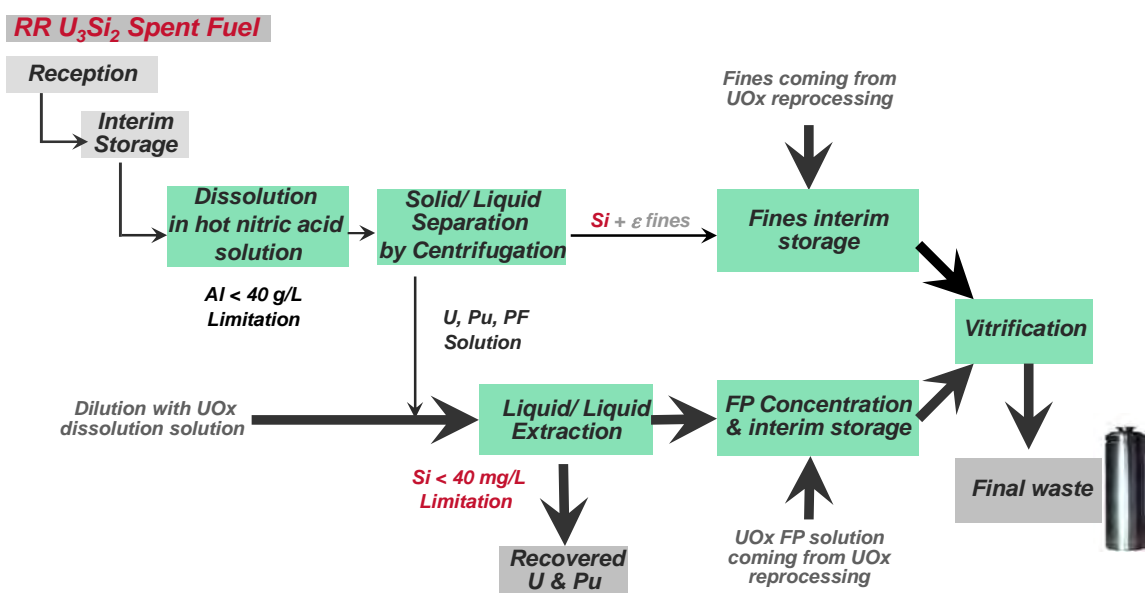


Fig. 28: Process diagram for USi RRSF reprocessing in AREVA La Hague plant

Starting at Marcoule plant and up to the 90's, **18 tons of UAl-type RRSF from 21 reactors from 11 countries** have been reprocessed with the similar reprocessing operations as the La Hague ones.

Since 2005 and as of end-of 2014, over **7.25 tons of UAl-type RRSF** fuels have already been reprocessed at industrial scale at the AREVA La Hague plant. AREVA is currently finalizing the studies in order to obtain the authorisation to reprocess USi-type RRSF from the French Safety Authority (réf. [2]).

6. Final waste production and management

6.1. Final waste attribution to customers

According to the applicable European Directive² and to French law³, the introduction on French territory of spent nuclear fuels for a reprocessing purpose has to be framed by an intergovernmental agreement (IGA) between France and the SF country of origin. This agreement settles "a forecasted schedule for reception and processing of the material and, if any, the later planned use of the material separated during reprocessing". Article L542-2 of the French Environmental Code specifies also that disposal in France of radioactive waste from abroad is forbidden, including waste resulting from RRSF reprocessing.

In regards to spent fuel reprocessing at the AREVA La Hague plants, France already signed IGAs with Italy, the Netherlands and Belgium.

Another application of French law⁴ concerns the final waste calculation method.

In order to comply with this regulation, AREVA applies a material accountancy system including a unique activity unit for waste (UAR, *Unité d'Activité de Résidu*) and a unique mass unit for waste (UMR, *Unité de Masse de Résidu*).

This system allows AREVA to calculate the amount and type of waste to be sent back to its customers. This system called EXPER (*EXPEdition des Résidus*) has been approved by decree, and has been implemented since October 2008 for all new RRSF reprocessing operations.

This system states that the UAR and UMR quantities imported in France are to be sent back from France.

In the case of silicide-type RRSF reprocessing, if all the material is dissolved, the only remaining waste corresponds to the UAR system, based on the Nd quantities imported in France in the RRSF.

The UAR system implies two possible types of vitrified residues: CSD-V (*Conteneur Standard de Déchets Vitrifiés*) and CSD-U (*Conteneur Standard de Déchets U*).

The CSD-V concentration in FP is highly superior than the CSD-U one.

The thermal power is consequently higher in CSD-V than in CSD-U.

According the regulation of each country regulation, CSD-V and CSD-U can be considered respectively as HLW and ILW.

AREVA proposes to study the conditions under which the final waste can be managed with the RR operators and their regulatory bodies.

² Council Directive 2011/70/EURATOM of 19 July 2011 establishing a Community framework for the responsible and safe management of spent fuel and radioactive waste: <http://eur-lex.europa.eu/LexUriServ/LexUriServ.do?uri=OJ:L:2011:199:0048:0056:EN:PDF>

³ French Environmental Code resulting from the law of June 28, 2006 on the sustainable management of radioactive materials and waste, and application decree no. 2008-209 of March 3, 2008 on procedures applicable to the reprocessing and recycling of foreign spent fuel and radioactive waste specifies certain conditions

Two different examples can be underlined for final waste management:

- Belgium
After reprocessing of BR2 RRSF, corresponding CSD-Vs have been jointly sent back to Belgium with residues from Belgian utilities SF reprocessing. As the LWR SF reprocessing results in much higher volumes of CSD-V than RRSF reprocessing, the residues return was almost insignificant for the BR2 operator (SCK).
- Australia
Australia does not operate any Nuclear Power Plant. Australia does not have any HLW to manage. The CSD-U was consequently the best option for Australia as it is managed as ILW and does not need large investments for long term management (in comparison with final HLW disposal).

Depending on each country regulations and specificities, AREVA can propose either CSD-V or CSD-U for a responsible and sustainable waste management.

6.2. Final waste production and interim storage

6.2.1. Final waste production

After the reprocessing operations, the concentrated fission products solutions are vitrified in the AREVA La Hague plant and the resulting glass matrix poured in universal canisters.

Currently there are two types of vitrified residues containing concentrated fission products solutions produced with two technologies:

- The **CSD-V**: these vitrified residues are produced thanks to the hot melter lines in AREVA NC's vitrification facility. They are mainly the result of the reprocessing operations for UOx and MOx spent fuels coming from Light Water Reactor and they represent the nominal glass residue production in the La Hague Plant.
- The **CSD-U**: these vitrified residues are produced thanks to the cold crucible line in AREVA NC's vitrification plant. They are the result of the reprocessing operations for spent fuels coming from past Gas Cooled Reactor and their production will be limited (number of items and time production). In comparison with CSD-Vs, these CSD-Us have a lower activity content and a lower related thermal power (~50 W versus 2000 W). Regarding French regulation, CSD-Us are High Level Activity Waste as CSD-Vs but, given their characteristics, these residues can be considered and managed as Intermediate Level Activity Waste in other countries (Australia for instance).

Both types of vitrified residues (CSD-V and CSD-U) are the result of the encapsulation of Fission Products in a stable, homogeneous, and durable glass matrix with a long-term predictable behaviour. Furthermore, their fissile material contents are very low and allow an exemption of safeguards for their interim storage and final disposal.



*Fig. 29: Universal Waste Canister (CSD) – Vitrified wastes
© AREVA*

6.2.2. Interim storage at La Hague

The interim storage of vitrified residues is performed in pits with ventilation by natural convection in the AREVA NC La Hague plant (EEVSE and EEVLH facilities).



Fig.30: Outside view of La Hague EEVSE facility © AREVA

As mentioned in paragraph 6.1, the duration of interim storage of vitrified residues coming from foreign RRSF reprocessing is agreed between France and the RR's country before starting importation in France of the RRSF, through an IGA.

De-storage of the residues and preparation for transportation, including loading in the dedicated transportation cask are performed in the *DRV* facility in AREVA La Hague. AREVA customers can witness these de-storage and preparation for transportation operations.



Fig.31: De-storage facility control room
© AREVA

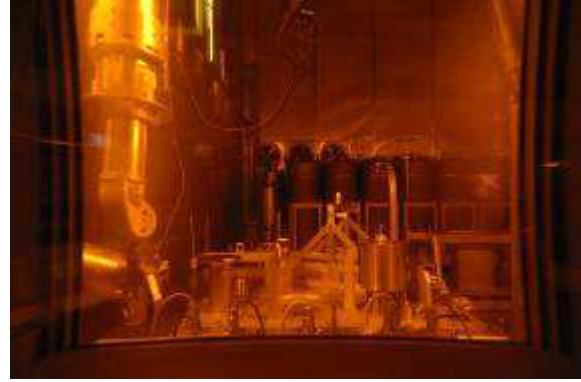


Fig.32: De-storage operations for CSD-V
© AREVA

6.3. Final waste transportation and management in the RR country

According to their UAR content (see paragraph 6.1), CSD-Vs and CSD-Us can be considered to send back final residues to foreign customers.

Transportation casks that can be used for the transport vary according to the customer's final waste interim storage policy: storage in pits/vaults, or storage in the transportation cask itself on a storage area.

6.3.1. Solutions for waste transportation

If the dedicated RR country makes the choice of interim waste management in pit/vaults, like in the AREVA La Hague plant, the TN-28 and the TN-81 residue transportation casks can be used to ship CSD-Vs or CSD-Us to the customers with a maximum of 28 universal canisters per cask. This choice has been made by Belgium for management of its final waste after RRSF reprocessing at La Hague.

In the case of an interim storage in cask, the TN-81 cask can be used as a “dual-purpose” cask ie for both residue transportation and interim storage, with a maximum of 28 universal canisters per cask. This choice has been made by Australia for management of its final waste after RRSF reprocessing at La Hague.

If needed, other types of transportation casks can be considered by AREVA for loading CSD-Vs or CSD-Us, according to customers' needs. Nevertheless, as for RRSF receipt, feasibility studies, safety report application to Safety Authority /authorization, design and fabrication of new equipments and possible modifications to the workshop are necessary.



Fig.33: AREVA TN-81 dual purpose cask
© AREVA



Fig.34: AREVA TN-28 transportation cask
© AREVA

6.3.2. Experience

AREVA has a wide experience in residues shipment to foreign customers.

In the case of residues return related to RRSF reprocessing, AREVA has already returned small quantities of CSD-V to RRSF customers, based on a joint residues management with NPP and RRSF customers (Belgian feed-back).

Indeed, in case of a nuclear power country that made the choice of reprocessing its NPP spent fuels in France, a joint return is efficient, cost effective, and reduces the number of nuclear transportations.

When there is no NPP spent fuel reprocessing in France in the RR country, and no associated return of vitrified waste, another solution can also consist in performing a CSD-U shipment CSD-U with a dedicated transport program (Australia), and benefiting from the associated advantages (see paragraph 6.2.1)

AREVA has also experience in designing, licensing and constructing the facilities dedicated to interim storage of final waste.

7. Conclusion

AREVA acquired a long-term experience on RRSF management, encompassing international and multi-modal transportation, reprocessing and waste management.

Thanks to its experience, and thanks to the high-quality of its operators, its plants and equipments, AREVA is ready to set up sustainable partnerships with its RR customers in order to robustly manage the back-end of their fuel cycle.

8. Reference

- [1] "AREVA TN Transports and Logisitcs Activities - Fleet of Transport Casks for International Shipments in Support of Research Reactor and Laboratories", N. Guibert, J. Thomas, RRFM2015, Bucharest, April 2015
- [2] "Status on silicide fuel reprocessing at AREVA La Hague", J.F. Valery, X. Domingo, P. Landau, C. Alameda-Angulo, C. Pechard, V .Laloy, RRFM2015, Bucharest, April 2015

COMPARISON BETWEEN U(Mo)/Al(Si) MINIPLATE AND U₃Si₂/Al MINIPLATE AFTER THE SAME FABRICATION PROCESS.

M. MIRANDOU ^{(1)*}, S. ARICÓ ^(1,2), S. BALART ⁽¹⁾

(1) Gerencia Materiales, Gerencia de Área Energía Nuclear.

(2) Instituto de Tecnología “Jorge Sabato”, Universidad Nacional de General San Martín.

D. PODESTÁ and J. FABRO

Departamento Elementos Combustibles para Reactores de Investigación (ECRI), Gerencia de Ciclo del Combustible Nuclear (GCCN)

Comisión Nacional de Energía Atómica (CNEA), Avda. Gral. Paz 1499, B1650KNA, San Martín, Buenos Aires, Argentina.

*corresponding author e-mail: mirandou@cnea.gov.ar

ABSTRACT

Fuel elements based in U₃Si₂ particles dispersed in an Al matrix perform satisfactorily under irradiation. This means that phases that form the interaction layer grown during fabrication process in this kind of fuels can be considered as “a proper interaction layer.”

In this work a comparison between dispersion plates made with U₃Si₂ particles/Al matrix and miniplates made with U-7wt%Mo atomized particles/Al-4wt%Si matrix, that underwent the same fabrication steps, is presented. The aim of this investigation is to determine similarities and differences between the phases formed during fabrication on both of them. Characterization was performed by OM, SEM, EDS and XRD.

On the other hand, and based in our experience that basic research on diffusion couples provides an important contribution to support studies as described above, an investigation on a new set of diffusion couples made with U-7wt%Mo and seven different Al(Si) binary alloys will be carried out during this year. Experimental details of the diffusion couples are presented in this work. The final purpose consists in determining which is the amount of Si that promotes the formation of an interaction layer as similar as possible to the one observed on the miniplate fabricated with U₃Si₂ particles.

1.Introduction

The use of low enriched uranium (LEU) in γ U(Mo) alloys is under study in dispersion or monolithic fuel elements to convert high flux research nuclear reactors [1, 2]. In this alloy, the addition from 7 to 10 wt%Mo is used to keep, in metastable condition at room temperature, γ U phase which performs well under irradiation [1, 2, 3].

U(Mo) particles dispersed in an Al-Si matrix is one of the most promising ways to fulfill the qualification of this fuel [4] as they underwent satisfactorily some of the irradiation test [5]. Post-irradiation examinations together with the analysis of the corresponding fresh plates, showed that good behavior is correlated with the formation during fabrication of a “proper interaction layer” around U(Mo) particles [6, 7]. However U(Mo) qualification is still ongoing because recent attempts to bring this fuel to high burnup at elevated power have not been totally successful [8, 9, 10]

In CNEA-Argentina a study is being carried out to determine how to obtain the better interaction layer (IL) characteristics (i. e. uniformity, composition, phases, etc) with the lesser modifications

to the fabrication process (currently used for silicide fuel elements) and the smallest amount of Si added to the matrix. Results of the characterization of the meats of miniplates made with atomized U-7wt%Mo dispersed in Al-2wt%Si and Al-4wt%Si matrices were presented at RRFM 2014 meeting [11]. In that work it was shown how the addition of 4wt%Si to Al behaves in an efficient way to ensure Si availability to form a uniform and very narrow IL surrounding U(Mo) particles on fully welded miniplates. This IL is only formed by Si-containing phases.

On the other hand, it is well known that fuel elements based in U_3Si_2 particles dispersed in an Al matrix are stable under irradiation in plate type configurations and are being used to convert to LEU a large number of research reactors without significant loss in performance. From this result it can be inferred that phases that form the IL grown during fabrication process in this kind of fuel elements also have a good performance under irradiation and can surely be considered as “a proper interaction layer.”

In this work two plates fabricated with U_3Si_2 particles dispersed in an Al matrix were analyzed to obtain information about the IL that forms during fabrication process and compare it with the one obtain for the miniplates made with U-7wt%Mo dispersed in Al-4wt%Si matrices. These plates made with U-7wt%Mo are part of the set of miniplates already presented in [11]. Only the most relevant experimental details and results will be shown here to ease comparison.

To go further in U(Mo)/Al(Si) characterization, it would be important to determine which is the Si concentration in Al(Si) alloy that promotes the formation of an IL as similar as possible to the one observed on the plates fabricated with U_3Si_2 particles. With this aim, experimental details of a set of seven diffusion couples with U-7wt%Mo and seven different Al(Si) binary alloys is presented.

2. Experimental procedure

2.1. U(Mo)/Al-4wt%Si miniplates [11] and U_3Si_2 /Pure Al plates.

Depleted U-7wt%Mo alloy (U-7Mo) as atomized particles provided by KAERI were used as fuel alloy. The powders used as matrices were prepared in two different ways: by mixing pure Al and pure Si particles (Al-4Si) or pure Al particles with eutectic Al-Si alloy particles (which Si concentration is 12 wt%) (Al-4Si_E). In both cases the final nominal concentration is Al-4wt%Si.

U-7Mo and matrix particles were mixed and cold pressed to obtain 7 gU/cm³ compacts which were positioned in an AA6061 frame and **fully welded** to AA6061 covers by TIG. Hot rolling at 500 °C up to 82 % reduction was used to obtain final size followed by a heat treatment of 1 h at 500 °C and cold rolled.

U_3Si_2 compound was fabricated in CNEA by melting low enriched uranium (20% ²³⁵U) and pure Si in an induction furnace. After melting, the material was milled and sieved to obtain the powder. Silicide particles were mixed with pure Al ones and cold pressed to obtain 4.8 gU/cm³ compacts which were positioned in an AA6061 frame and welded, **with open corners**, to AA6061 covers by TIG. Hot rolling at 500 °C up to 90 % reduction was used to obtain final size followed by a heat treatment of 1 h at 480 °C and cold rolled.

Samples were cut from each miniplate or plate and one of the Al6061 cladding was removed by a rough polishing until reaching the meat followed by a final mechanical polishing up to 1 μm diamond paste. The samples were characterized by optical microscopy (OM-Olympus BX60M), scanning electron microscopy (SEM –Philips SEM 515, and FEI QUANTA 200), energy dispersive spectroscopy (EDS-EDAX Phoenix 3.2) and X-Ray diffraction (XRD- PANalytical-Empyrean with Cu *k*_α radiation). Crystal structures identification and the estimation of lattice parameters were obtained by direct comparison between theoretical spectrum of each phase with the experimental spectra using POWDERCELL software [12].

Table 1 summarizes identification and characteristics of the miniplates and plates studied in this work.

TABLE 1. Identification and fabrication details of the sample taken from the miniplates and plates.

<i>Identification</i>	<i>In RRFM 2014 [11]</i>	<i>Fuel</i>	<i>Matrix</i>	<i>Fabrication process</i>		
				<i>Rolling Temp</i>	<i>TTF Temp. and time</i>	<i>Cooling</i>
U(Mo)/Al-4Si	4Si-FF-FW	U-7wt%Mo	Al-4Si	500 °C	500 °C – 1 h	Inside furnace
U(Mo)/Al-4Si _E	4Si _E -FF-FW	U-7wt%Mo	Al-4Si _E			
U ₃ Si ₂ /Al-IF	-	U ₃ Si ₂	Pure Al		480 °C – 1 h	Inside Furnace
U ₃ Si ₂ /Al-OF	-	U ₃ Si ₂	Pure Al			Outside Furnace

2.2. Diffusion couples

Al(Si) binary alloys were made by arc melting in a small non-consumable tungsten electrode arc-furnace with a copper crucible under highly pure argon atmosphere using high purity Al and Si. Six different alloys were fabricated: Al-0.6wt%Si (Al-0.6Si); Al-2 wt%Si (Al-2Si); Al-4wt% Si (Al-4Si); Al-5.2wt%Si (Al-5.2Si); Al-6 wt%Si (Al-6Si) y Al-7.1wt%Si (Al-7.1Si). Si concentrations corresponding to 0.6; 5.2 and 7.1 were chosen in accordance to nominal Si concentration in AA6061, AA4043 and AA356 commercial Al alloys. After melting process the Al(Si) alloys were hot rolled at 480 °C and heat treated 1 h at 550 °C. This last temperature is the same one at which diffusion couples will be studied.

Same melting procedure is used to fabricate the U-7wt%Mo alloy. Only part of the as-cast U-7Mo alloy will be heat treated at 1000°C during 2h and quenched to room temperature to promote composition homogenization. The remaining alloy will be used in the as cast condition to represent more closely U(Mo) alloy in the miniplates. Stainless-steel mechanical clamps will be used to keep in contact the alloys. Table II shows the configuration of the seven diffusion couples.

Table II. Configuration of the seven diffusion couples.

1	Al-0.6Si	U-7Mo Non homog.	Al-5.2Si
2	Al-0.6Si	U-7Mo Non homog.	Al-7.1Si
3	Al-2Si	U-7Mo Non homog.	Al-5.2Si
4	Al-2Si	U-7Mo Non homog.	Al-6Si
5	Al-4Si	U-7Mo Non homog.	Al-6Si
6	Al-4Si	U-7Mo Non homog.	Al-7.1Si
7	U-7Mo Non homog.	Al-4Si	U-7Mo Homogenized.

As it is shown in Table II, in the first six diffusion couples U(Mo) will be positioned in between two Al(Si) alloys [i.e. Al-xSi/U-7Mo/Al-ySi]. This configuration allows comparison of relative IL

widths minimizing any effect introduced during diffusion couple fabrication. The last one will be used to study the influence of metastable γ U phase decomposition [13] on IL formation.

3. Results and discussion

3.1. U-7Mo/Al-4Si miniplates characterization [11]

As previously mentioned, results presented in this section correspond to part of the investigation of a set of meats of miniplates which has already been presented in more detail in RRFM 2014 meeting. The aim of that study was to obtain an IL, formed by Si-rich phases, that completely surrounds U(Mo) particles. In the following paragraphs more relevant results concerning IL characterization will be shown to ease comparison presented in Section 3.3.

At the end of fabrication process the miniplates U(Mo)/Al-4Si and U(Mo)/Al-4Si_E developed a very narrow IL which showed an important growing during thermal treatment. At the end of fabrication process almost all U(Mo) particles were completely covered by an IL which looks homogenous in thickness (dark gray in Figure 1). The IL developed even between very close particles as shown in detail in Figure 1c. IL thickness measured only on 100 μ m (or higher) particles diameter was estimated in 0.5 - 2 μ m.

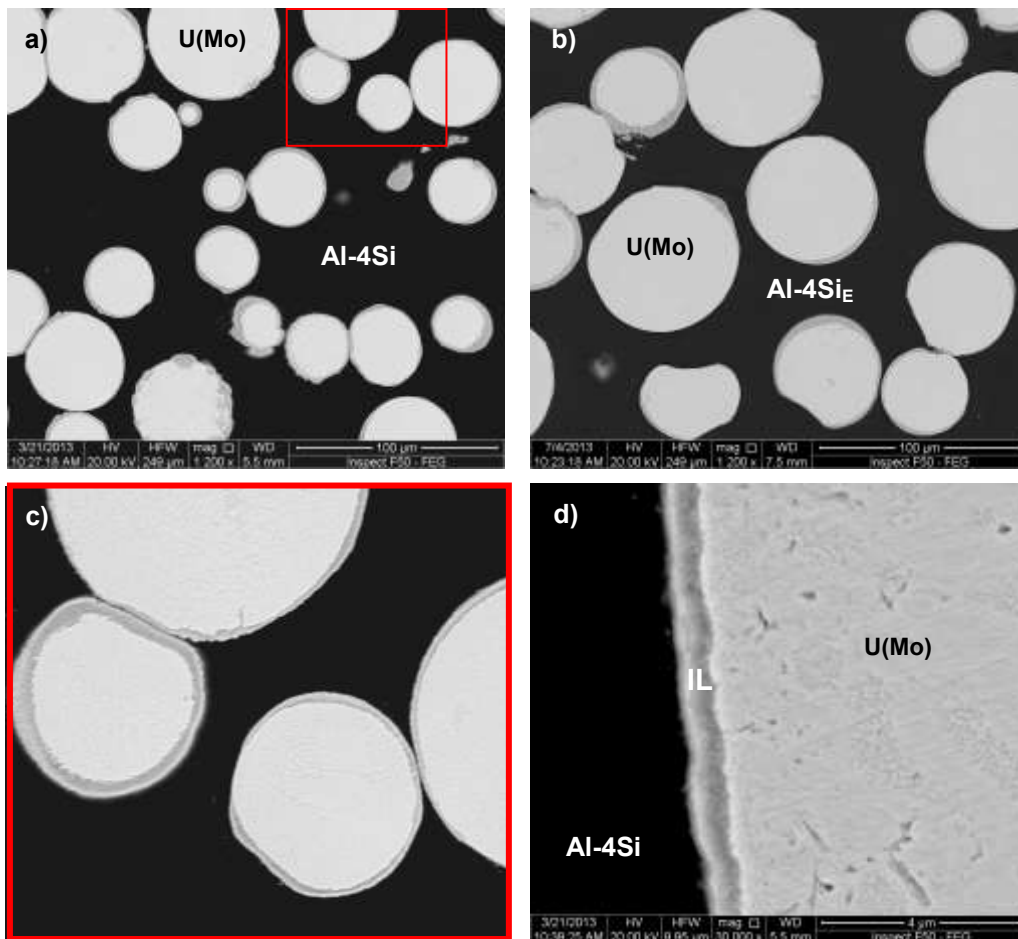


Figure 1. U(Mo) particles completely covered by an IL of homogenous thickness.
a), c) and d) Miniplate U(Mo)/Al-4Si, b) Miniplate U(Mo)/Al-4Si_E. – SEM.

X-ray mapping was performed on both samples using Si $K\alpha$ radiation to evidence IL formation around almost all U(Mo) particles, Figure 2.

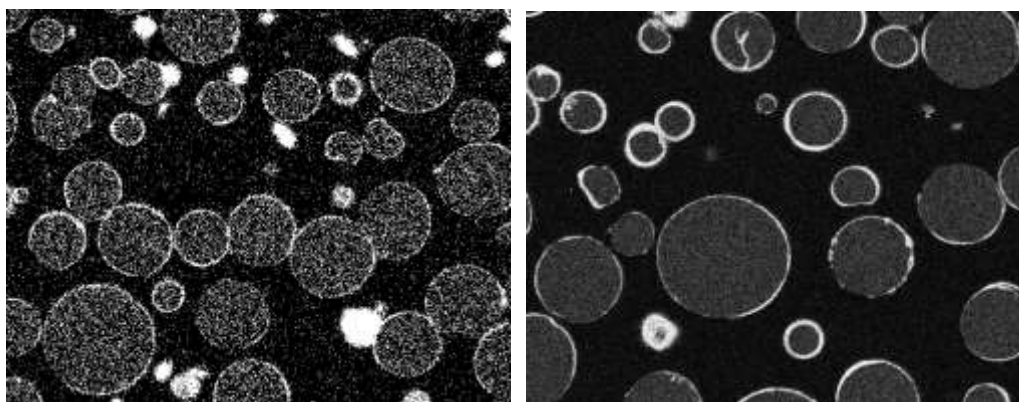
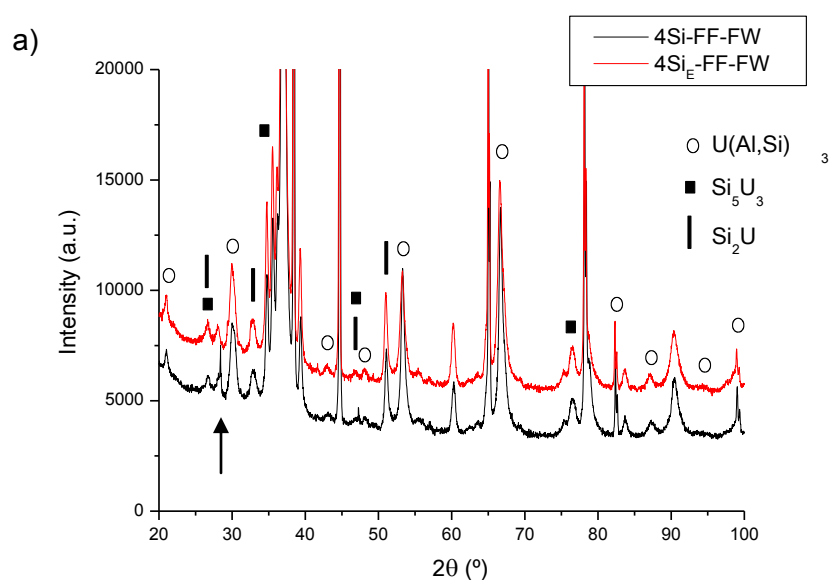


Figure 2. Si X-ray mapping. a) Miniplate U(Mo)/Al-4Si, b) Miniplate U(Mo)/Al-4Si_E. SEM - EDS.

XRD was used to identify crystalline structure of the phases that form the whole meat for both miniplates. The spectra are presented together in Figure 3a for an easy comparison and phases from the IL are only indicated for clarity. Concerning initial components of the meat, γ U, α U and O₂U phases from the U-7Mo particles together with Al phase from the matrices were identified for both miniplates. Si phase was only identified for miniplate U(Mo)/Al-4Si_E (its principal reflection is marked with an arrow in Figure 3a). Concerning IL, U(Al,Si)₃ was clearly identified with lattice parameter $a \sim 4.20 \text{ \AA}$ ($\sim 28 \text{ \%at Si}$ according to Dwyer [14]) meaning that IL is mainly formed by it. A deeper analysis was needed to clarify the possible presence of Si₂U and/ or Si₅U₃. With this objective two new spectra were performed on miniplate U(Mo)/Al-4Si_E. For both of them very narrow angular ranges were selected avoiding reflections from U, Al or Si phases and increasing seventeen times the scan step time. First spectrum, Figure 3b, includes reflection (001) from USi₂ phase and (001) from U₃Si₅ phase and the second one, Figure 3c, includes reflection (200) from USi₂ phase which is very near to reflection (211) from UO₂.



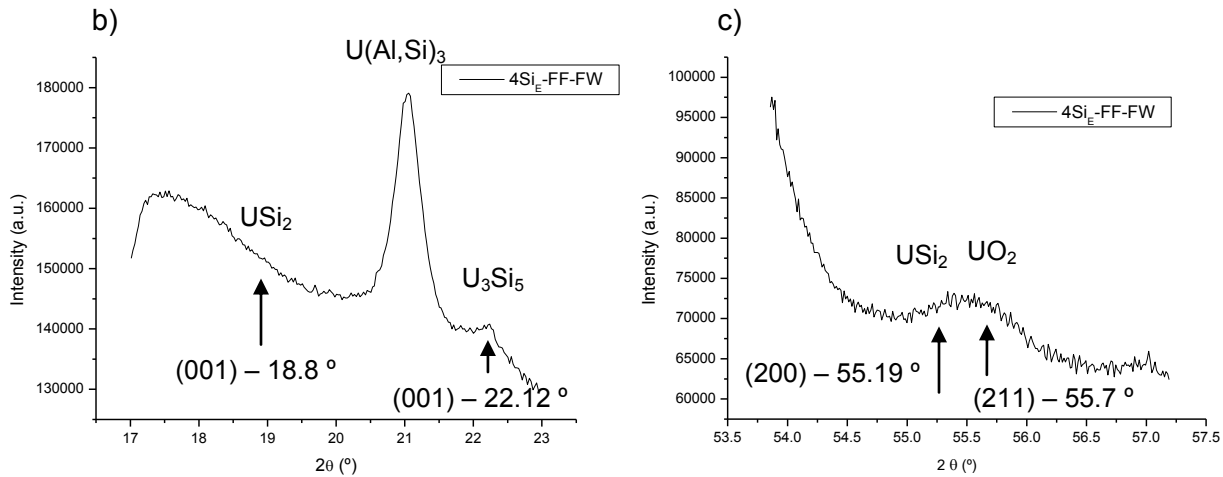


Figure 3. Spectra obtained for miniplates U(Mo)/Al-4Si and U(Mo)/Al-4Si_E.
 a) Phases corresponding to IL, b) and c) Identification of U₃Si₅ in the IL - XRD.

From Figures 3 b) and c) it can be concluded that neither (001) nor (200) reflections from USi₂ are evident in these spectra while reflection (001) from U₃Si₅ is observed. According to this the IL grown during fabrication in miniplates U(Mo)/Al-4Si and U(Mo)/Al-4Si_E is formed by U(Al,Si)₃ and U₃Si₅ phases.

3.2. U₃Si₂/Al plates characterization

XRD was performed on both U₃Si₂ powders in the as cast condition. As shown in Figure 4 only U₃Si₂ crystalline structure was identified in both cases.

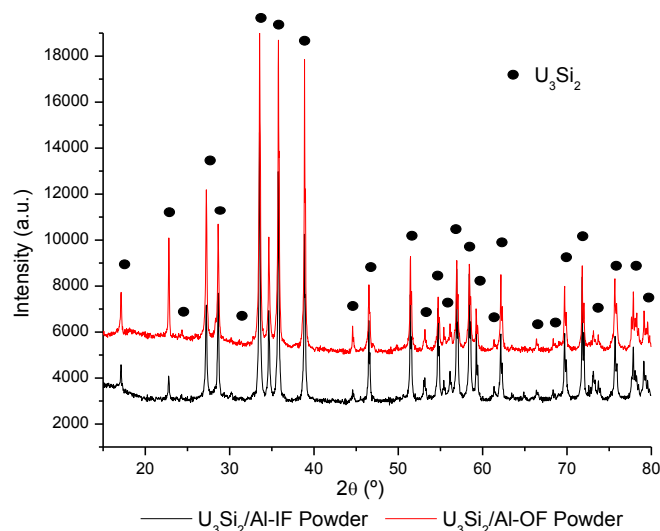


Figure 4. Crystalline structure identification in powders of U₃Si₂ compound in the as cast condition. XRD.

In Figure 5 crystalline structure identification of the meats of the plates U₃Si₂/Al-IF and U₃Si₂/Al-OF after whole fabrication process is shown. Same phases were identified for both samples meaning that different cooling process does not have any significant influence on final product.

Crystalline structure from Al and U_3Si_2 were identified which correspond to meats original components. Forming the IL, $U(Al, Si)_3$ with lattice parameter $a \sim 4.24 \text{ \AA}$ ($\sim 12 \%$ at Si according to Dwigth in [14]) was identified which, according to the low intensity of its reflections, is probably present in very low amount. Besides, a high intensity set of reflections was present in both spectra. From all the known aluminides, silicides and ternary U-Al-Si phases, U_3Si_2 (i.e. $tP10$) theoretical spectrum with modified lattice parameters $a_{modif} \sim 7.56 \text{ \AA}$ and $c_{modif} \sim 4.03 \text{ \AA}$ is the only one that matches this set.

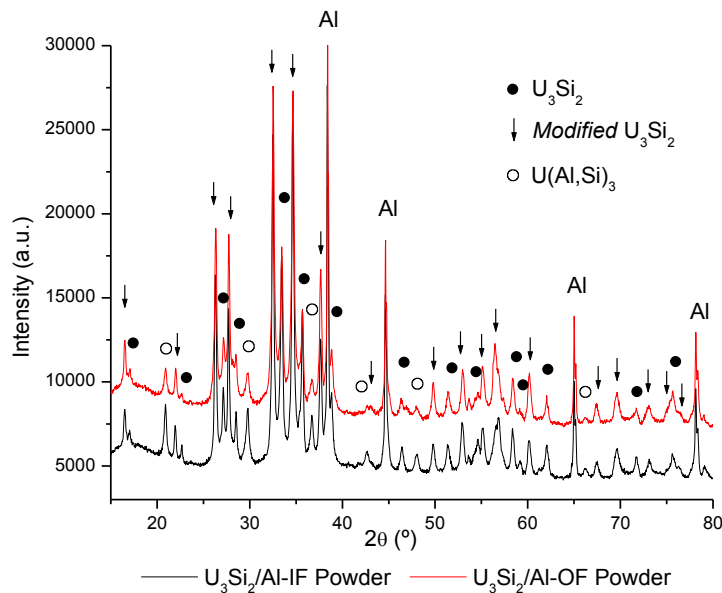


Figure 5. Crystalline structure identification in plates $U_3Si_2/Al-IF$ and $U_3Si_2/Al-OF$. XRD.

High magnification observations in backscatter electron mode revealed zones of dark gray colour (i.e. rich in elements of low atomic weight) as the very narrow layer surrounding particles (more evident in smaller particles), Figure 6a, or regions at the corner of some silicide particles, Figure 6b. EDS determinations on regions as the one shown in Figure 6b evidenced the presence of $\sim 75 \%$ at (Al+Si). These regions would be associated to $U(Al,Si)_3$.

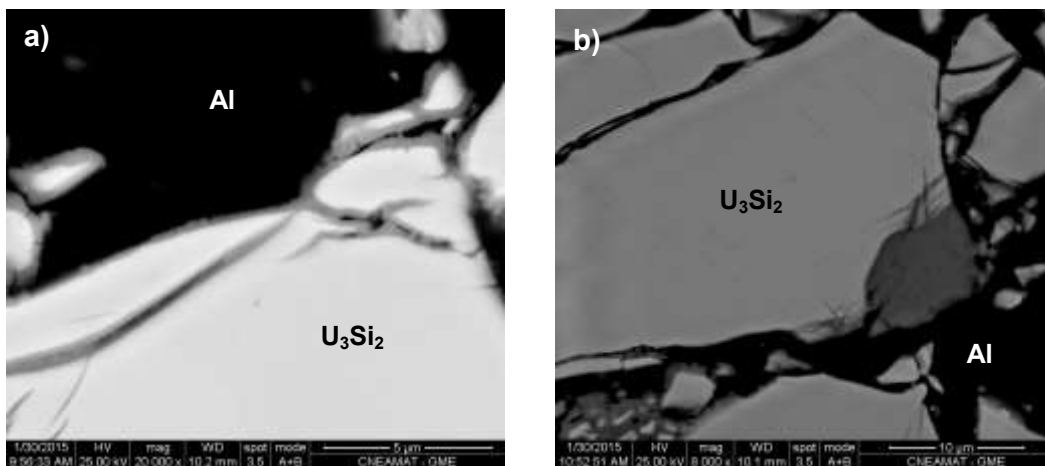


Figure 6. High magnification observations of plates $U_3Si_2/Al-IF$ and $U_3Si_2/Al-OF$ -SEM-BSE.

According to XRD results, fabrication process promotes the formation of a significant amount of another phase which will be called modified U_3Si_2 . Although its high relative participation in the samples, it could neither be observed by OM or SEM nor obtained concentration information that accounts for its location. One possible explanation that could be proposed is that Al incorporation in solution to U_3Si_2 phase can promote an enlargement its cell volume. As Si and Al have very similar atomic weights SEM BSE images are not precise enough to evidence this. Further concentration analysis is mandatory to corroborate this assumption and define its location.

3.3. Influence of the fabrication process in IL formation for U_3Si_2/Al plates and $U(Mo)/Al(Si)$ miniplates. Similarities and differences.

After whole fabrication process both types of fuels (U_3Si_2 and $U(Mo)$) reacted with matrix materials leading to the formation of an interaction layer formed by new phases. For $U(Mo)$ these phases are $U(Al,Si)_3$ and U_3Si_5 meanwhile for U_3Si_2 , $U(Al,Si)_3$ together with *modified* U_3Si_2 were identified.

When comparing relative participation of the IL in each meat, although an accurate calculation would be needed, it can be inferred that it is much more relevant for silicide than for $U(Mo)$.

Crystalline structure corresponding to $U(Al,Si)_3$ was identified for both fuels but with a difference in lattice parameter. As it is well known, lattice parameter variation is correlated with Al (or Si) concentration in the Al-Si sublattice [14]. From results presented in this work Si concentration in this phase is higher for $U(Mo)$ than for U_3Si_2 .

4. Conclusions

In this work two plates fabricated with U_3Si_2 particles dispersed in an Al matrix were analyzed to obtain information about the IL that forms during fabrication process and compares it with the one obtain for the miniplates made with U-7wt%Mo dispersed in Al-4wt%Si matrices.

According to the results presented in this paper, and from the fact that silicide fuels have a good irradiation behavior, an IL formed only by $U(Al,Si)_3$ can be considered “*a proper interaction layer*” to be formed during fabrication process surrounding $U(Mo)$ particles as a protective layer. Diffusion couples presented in section 2.2 will be studied in order to establish if any Si concentration (in Al matrix) favor the formation of this phase over other U-Si phases.

Acknowledgements

The authors want to thank Ricardo Sanabria for his collaboration in sample metallographic preparation together with the technical staff of Gerencia Materiales-GAEN-CNEA and Laboratorio de Difracción de Rayos X-Departamento de Física de la Materia Condensada-GAlyANN-CNEA for their support.

This work was partially financed by Project PICT-2010-1351, Agencia Nacional de Promoción Científica y Tecnológica (Argentina), FONCyT.

References

- 1.- M.K. Meyer, G.L. Hofman, S.L. Hayes, C.R. Clark, T.C. Wiencek, J.L. Snelgrove, R.V. Starin, K.H. Kim, J. Nucl. Mat. 304 (2002) 221-236.
- 2.- J. L. Snelgrove, G. L. Hofman, M. K. Meyer, C. L. Trybus, T. C. Wiencek, Nucl. Eng. Design 178 (1997) 119-126.

-
- 3.- Lundberg, J Nucl Mat. 167 (1989) 64-75.
 - 4 G.L. Hofman, M.R. Finlay, Y.S. Kim, Proceedings of the 26th International Meeting on Reduced Enrichment for Research and Test Reactors (RERTR), Vienna, Austria, 2004.
 - 5 A. Leenaers, S. Van den Berghe, J. Van Eyken, E. Koonen, F. Charollais, P. Lemione, Y. Calzavara, H. Guyon, C. Jarousse, D. Geslin, D. Wachs, D. Keiser, A. Robinson, G. Hofman, Y.S. Kim, J. Nucl. Mater. 441 (2013) 439-448.
 - 6 D.D. Keiser Jr, A.B. Robinson, J-F Jue, P. Medvedev, D.M. Wachs, M.R. Finlay, J. Nucl. Mater. 393 (2009) 311-320.
 - 7 D.D. Keiser Jr, J-F Jue, N.E. Woolstenhulme, E. Ashley, J. Nucl. Mater. 419 (2011) 226-234.
 - 8.- E. Koonen, H. Guyon, P. Lemoine, C. Jarousse, D.M. Wachs, J. Stevens, 31th International Meeting on Reduced Enrichment for Research and Test Reactors, Beijing, China, 2009.
 - 9.- F. Fréry, H. Guyon, E. Koonen, S. Van den Berghe, P. Lemoine, F. Charollais, C. Jarousse, D. Geslin, 32nd International Meeting on Reduced Enrichment for Research and Test Reactors (RERTR), Lisbon, Portugal, 2010.
 - 10.- F. Charollais, P. Lemoine, Y. Calzavara, H. Guyon, E. Koonen, S. Van den Berghe, B. Stepnik, C. Jarousse, D. Geslin, 33rd International Meeting on Reduced Enrichment for Research and Test Reactors (RERTR), Santiago, Chile, 2011.
 - [11] M. Mirandou, S. Aricó, S. Balart and J. Fabro. 18th International Meeting on Research Reactor Fuel Management (RRFM), Ljubljana, Slovenia, 2014.
 - [12] W. Kraus, G. Nolze, U. Müller, Pulverdiffraktogramme aus Einkristalldaten und Anpassung experimenteller Beugungsaufnahmen, PowderCell 2.3., 2000.
 - 13.- D. Blake, R. Hehemann, Transformation in Uranium Base Alloys, Session II, Physical Metallurgy of Uranium Alloys. Burke J. et al., editors. Massachusetts: Brook Hill Publishing Co., Chestnut Hill; 1976: 189-218.
 - 14 A.E. Dwight, Report Specification N° ANL –82-14, 1982, 1-39.

ANALYSIS OF MICROSTRUCTURE AND PRECIPITATIONS IN U-ZR METALLIC FUEL

C. T. LEE and H. L. KIM

Research Reactor Fuel Development, Korea Atomic Energy Research Institute (KAERI)

111 Deadeok-dearo 989 Beon-gil, Yuseong-gu, 305-353, Daejeon, South Korea

ABSTRACT

U-10wt.% Zr metallic fuel for releasing fast fission gas was fabricated using induction melting and sintered methods and the microstructures of the fabricated alloys were then observed through scanning and transmission electron microscopy. In particular, the selected area diffraction pattern and micro-chemical analysis were used to identify the phases. The microstructure of the induction melted U-10wt.% Zr alloy was the lamellar structure consisting of a typical α -U phase and δ -UZr₂ phase. The α -U phase was a orthorhombic crystal structure having compositions of 95.5-99.1 at.% U and 1.2-4.4 at.% Zr, and δ -UZr₂ phase was a hexagonal crystal structure. In addition, the globular precipitates were observed in the induction melted U-10wt.% Zr alloy. While the sintered U-60wt.% Zr alloy showed the inclusions of acicular-type shapes instead of a globular. A globular shape precipitate is a α -Zr with hexagonal structure including O and U elements. Rod and rectangular shape inclusions were identified as a SiZr₂ phase of the tetragonal crystal structure.

1. Introduction

There are renewed interests in metallic fuels for a sodium fast reactor, because of their outstanding properties such as a good breeding performance, high burn-up potential, ease of fabrication and high thermal conductivity [1, 2]. However, metallic fuels have a few serious problems which are the fuel swelling, mechanical and chemical reaction between the cladding and fuel while operating in the reactor. To overcome these problems, the ternary U-Pu-X alloys were suggested by Argonne National Laboratory (ANL). Of the alloying elements which are Mo, Nb, Ti, Zr and fission, the Zr was found to be the most effective [2]. Thus, we examined the U-Zr binary alloy to accumulate the properties prior to irradiation testing related to its characteristics of casting, thermal stability and so on.

Previous studies have dealt only with the thermodynamic properties to understand the irradiation behavior of U-Zr alloys. Studies regarding with the microstructures of matrix and irregular phases, which are affected by impurities, have been rarely carried out. Although a few studies were previously carried out the phase identification on the microstructures of U-Zr alloys, they were mostly conducted by X-ray diffraction technique instead of transmission electron microscopy [3, 4]. However, in the case of an X-ray diffraction technique, it is difficult to determine the effects of impurities on the phase relationship because of the small amounts of impurities.

Therefore, in this study, the microstructures of the U-Zr binary alloy were observed and their phases are identified using energy dispersive spectroscopy (EDS) and a selected area diffraction (SAD) pattern of the TEM. Especially, the impurities were investigated in the microstructure of the U-Zr alloy. In addition, the dominant inclusion shapes were different according to the manufacturing methods such as induction melted and sintered processes. Thus the inclusions of U-Zr alloys were determined using SEM and TEM.

2. Experimental Procedures

The U-10wt.% Zr alloy specimens used in this study were fabricated using vacuum induction melting with depleted uranium(99.9% pure) and zirconium sponge(99.9% pure). To prevent the chemical reaction between the graphite crucible and molten fuel, a graphite

crucible coated with yttrium-stabilized zirconia was used. After holding for 30min at a temperature of 1600 °C, molten alloy was poured into a quartz mold coated with ZrO₂. SiO₂. Meanwhile, in case of the sintered U-60wt.% Zr, the sintering was carried out at 1400 °C during 3hr after atomizing U and Zr powders and compacting mixed powders [5].

A chemical analysis was carried out from samples of the top, center and bottom of the casting rod using inductively coupled plasma atomic emission spectroscopy (ICP-AES). Table 1 shows the results of the chemical analysis.

Metallographic specimens were cut from the transverse section of the center segment of the alloy and then ground to a thickness of below 100 μm. The ground specimens were electropolished using a twin-jet thinner. Scanning electron microscopy (SEM) and transmission electron microscopy (TEM) were used to examine the microstructure. The phases were identified using a selected area diffraction (SAD) pattern and energy dispersive spectrometer (EDS).

3. Results and Discussions

Fig. 1 shows transverse-sectional microstructures of induction melted and sintered U-Zr alloys observed through scanning electron microscopy (SEM). As shown in Fig. 1 (a), the U-10 wt.%Zr alloy consisting of the α-U phase and δ-UZr₂ phase below 617°C has eutectoid lamellar structures and globular precipitates. This lamellar structure is believed as to be the releasing paths of the fission gas during the irradiation because this microstructure has a porous crystal structure [6]. The globular precipitates were α-Zr and different with the acicular-type, which aligned the rectangular precipitates, of sintered U-60wt.% Zr alloy as shown in Fig. 1(b). The U-60wt.% Zr alloy consisted of the δ-UZr₂ matrix with acicular-type α-Zr precipitates. The acicular-type α-Zr shape was different with a globular shape of primary α-Zr formed by eutectoid reaction. It is inferred that the acicular shape inclusion was formed along preferred direction during a sintering process. The detailed characteristics of precipitates in the sintered U-Zr alloy will be studied later.

Fig. 2 shows the bright field TEM image of the lamellar structure and SAD patterns of the dark (α-U) and light (δ-UZr₂) phase in the lamellar. The average thickness of the α-U phase is two or three times larger than that of the δ-UZr₂ phase, which are 40-80 nm and 20-30 nm, respectively (shown in Fig. 2(a)). The α-U phase is showed as an orthorhombic structure from a SAD pattern having a [010] zone axis in Fig. 2(b) and it consists of 95.5-99.1 at.% U and 1.2-4.4 at.% Zr components by EDS. While δ UZr₂ having a [$\bar{1}\bar{1}02$] zone axis in Fig. 2(c) shows a hexagonal structure. The δ-UZr₂ phases are composed of 69.4-78.6 at.% Zr and the other parts of U. Other authors observed that the expansion of the crystal lattice with increasing Zr concentration was larger along the c-axis than along the a-axis [7].

Other irregular phases, which are globular, rod and rectangular shapes, are also founded in the U-10 wt.% Zr alloy. First, a globular shape precipitate was assumed to be α-Zr stabilized by oxygen. Fig. 3 shows micrographs of the globular shape precipitate observed by SEM, TEM and SAD pattern. The size of the α-Zr globular shape is variable to 5-25 μm. The globular phase has a hexagonal structure like pure α-Zr from the analysis of the SAD pattern having a [0001] zone axis. The globular phase was composed of 95-99 at.% Zr concentrations, but as shown in Table 2, the lattice parameter of the globular phase, which was measured from the diffraction patterns, is slightly increased compared to pure α-Zr owing to the impurities such as a O element. The distance between the equivalent planes of the pure α-Zr and measured α-Zr of the specimens are presented in Table 2. In addition, the matrix of globular precipitate exhibited a number of small spots, as shown in Fig. 4. The black spots have a composition of 72 at.% Zr and 28 at.% U. The U elements were precipitated in the globular precipitate because of the decrease of U solubility with decreasing temperature in α-Zr. Thus, it is inferred that the globular α-Zr phase influenced by the oxygen impurity is α-Zr of hexagonal structure including a small spot with U-rich precipitate.

Fig. 5 (a), (b) shows inclusions of a rectangular shape and rod shape, which aligned rectangular inclusions, appearing in the U-Zr alloy. This rectangular shape inclusion had 33 at.% Si and 67 at.% Zr compositions (shown in Table 3). The Si elements were entered from

mold wash. The inclusion size of the rectangular type is about 10 μm . A TEM and SAD pattern of rectangular inclusion is presented in Fig. 5 (c). The rod type also has the same structure and compositions as a rectangular type with a tetragonal structure and SiZr_2 , respectively.

4. Conclusions

The microstructure of the U-10wt.% Zr and U-60wt.% Zr alloy fabricated by induction melting and sintering was studied, respectively. We obtained the following results.

(1) The induction melted U-10wt.% Zr alloy consists of lamellar structure of the α -U phase and δ - UZr_2 phase having the an orthorhombic and hexagonal structure, respectively. The average thickness of the α -U phase is two- or three-times larger than that of the δ - UZr_2 phase. While the sintered U-60wt.% Zr alloy was composed of δ - UZr_2 matrix with acicular-type α -Zr precipitates.

(2) In case of U-10wt.% Zr alloy, the globular shape inclusion is α -Zr having a hexagonal structure and its lattice parameter is larger than pure α -Zr owing to impurity elements such as a O element. In addition, the globular precipitate showed a number of small spots including U-rich precipitate. Whereas the sintered U-60wt.% Zr alloy showed the acicular-type α -Zr phase formed along preferred direction

(3) The rectangular and rod shape inclusions are SiZr_2 with a tetragonal structure in U-10wt.% Zr alloy.

Reference

- [1] J.S.Kim et. al. *Nucl. Eng. Tech.* **38** (2006) 301.
- [2] J. H. Kittel, B. R. T. Frost, J. P. Mustelier, K. Q. Bagley, G. C. Crittenden and J. Van Dievoet, *J. of Nucl. Mater* **204** (1993) 1.
- [3] H. L. Yakel, *Physical Metallurgical of Uranium Alloys*, Brook Hill Pub. Co., Book1 (1976) 259.
- [4] A. E. Dwight and M. H. Mueller, *ANL-5581* (1957).
- [5] T.K.Kim, C.T.Lee and D.S.Sohn, *J. Nucl. Mater.* **372** (2008) 394.
- [6] J. Rest, *J. of Nucl. Mater* **207** (1993) 192.
- [7] A.Landa, P.Soderlind and P.E.A.Turchi, *J. of Alloys Comp.* **478** (2009) 103

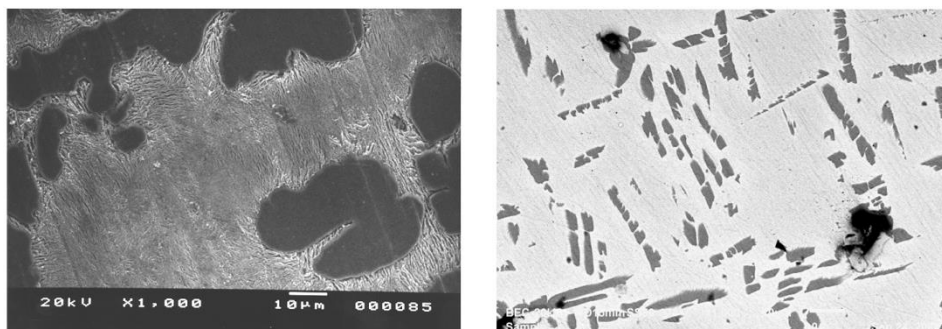


Fig. 1 SEM image of (a) the induction melted U-10 wt.% Zr alloy and (b) sintered U-60 wt.% Zr alloy

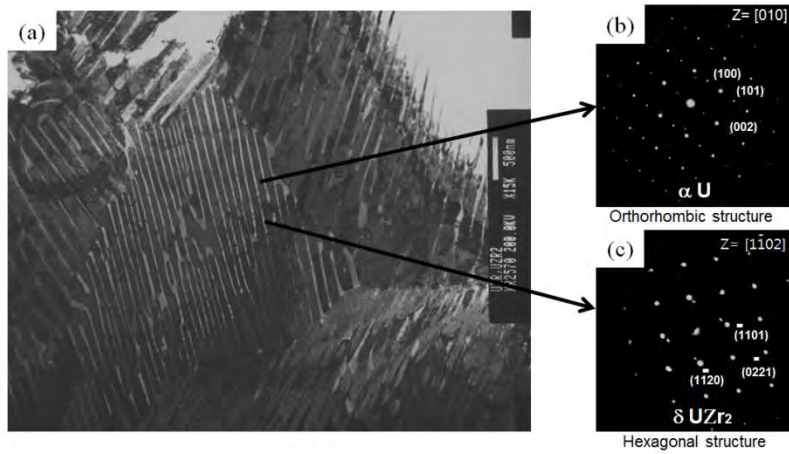


Fig. 2 (a) bright field TEM image and selected area diffraction pattern of (b) the α phase of $[010]$ zone axis and (c) the δ phase of $[1\bar{1}02]$ zone axis in the U-10 wt.% Zr alloy

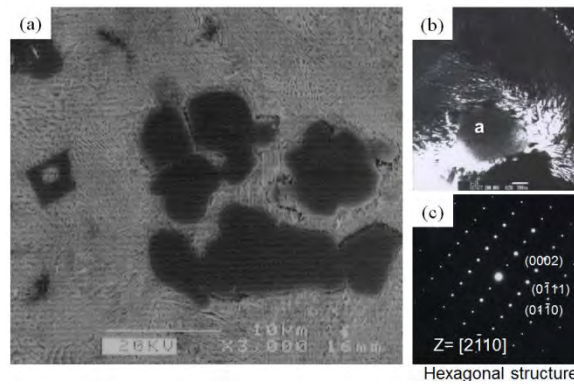


Fig. 3 (a) SEM image, (b) TEM bright field image and (c) selected area diffraction pattern of a globular shape inclusions in the U-10wt.% Zr alloy

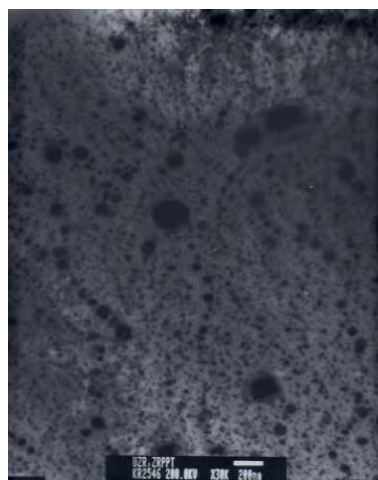


Fig. 4 . TEM bright field image in the globular shape precipitate of the U-10wt.% Zr alloy.

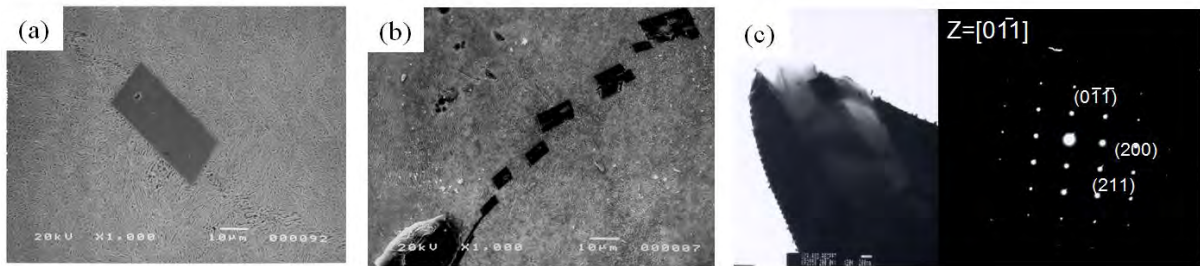


Fig. 5 SEM image of (a) a rectangular shape, (b) a rod shape inclusions and (c) BE image and SAD pattern in the U-10wt.% Zr alloy

Table 1. Chemical compositions of the U-10wt.% Zr alloy (in wt.%)

	Top	Center	Bottom	Average
U	Bal	Bal	Bal	Bal
Zr	9.05	8.95	9.10	9.03
Si	180 ppm	158 ppm	320 ppm	219 ppm
O	1825 ppm	1555 ppm	2341 ppm	1907 ppm
N	32 ppm	23 ppm	38 ppm	31 ppm
C	140 ppm	250 ppm	250 ppm	213 ppm

Table 2. Distance between equivalent planes of the pure α Zr and measured α Zr in the U-10wt.% Zr alloy

	(1010)	(0002)	(1120)	(1121)
pure α Zr	2.799	2.574	1.616	1.542
measured α Zr	2.845	2.583	1.621	1.559

Table 3. Chemical compositions of α , δ phase and precipitations in the U-10 wt.% Zr alloy

	α	δ	globular	rod	rectangular
U	99.16 at.%	30.57 at.%	97.05 at.%		
Zr		69.43 at.%	2.95 at.%	65.51 at.%	67.31 at.%
Si				33.41 at.%	32.69 at.%
O			2000ppm		

NEUTRONIC COMPARISON OF RELAP5-3D AND MCNP5 MODELS FOR THE TRIGA IPR-R1

P. A. F. MESQUITA, A. L. COSTA, C. A. M. SILVA, P. A. L. REIS, C. PEREIRA,
M. A. F. VELOSO, H. V. SOARES

*Departamento de Engenharia Nuclear
Universidade Federal de Minas Gerais
Av. Antônio Carlos Nº 6627, Campus Pampulha, CEP 31270-901
Belo Horizonte, MG, Brazil*

Instituto Nacional de Ciências e Tecnologia de Reatores Nucleares Inovadores/CNPq, Brazil

ABSTRACT

This paper presents two models for the IPR-R1 TRIGA research reactor using the code RELAP5-3D 3.0.0 and the code MCNP5. Such models were verified according with experimental data. Results of radial relative power core distribution, average thermal flux radial core distributions and the effective multiplication factor value, k_{eff} , obtained by RELAP5-3D and MCNP5 codes calculations were compared between them and with available data for power operation of 100 kW.

1. Introduction

The increase of research reactors commercial exploitation commonly directed at neutrons generation for several types of scientific and social purposes has enlarge the interest about safety of these reactors [1]. Power generation is not the main activity of these types of reactors reaching maximum power operation of about 100 MW. In spite of this, specific features are necessary to ensure safe utilization of such installations. Therefore, several codes have been used focusing special attention for research reactors safety analysis and valuation of specific perturbation plant processes. A combination of codes for thermal hydraulic analysis, for assessment of probabilistic risk, fuel investigation and reactor physics studies are fundamental tools for an appropriate reactor behaviour definition [2]. In this work, the codes RELAP5-3D [3] and the MCNP5 [4] were used to simulate the TRIGA IPR-R1 research reactor.

TRIGA (Training, Research, Isotope, General Atomic) research reactors are constructed in a variety of configurations and capabilities, with steady-state power levels ranging from 20 kW up to 16 MW offering true “inherent safety”. In spite of this, some situations may occur disturbing the normal reactor operation. In this work two models of the TRIGA IPR-R1 have been used to simulate the reactor core behaviour. The main aim is to verify the RELAP5-3D model comparing results of k_{eff} and thermal flux distribution with a MCNP5 model, both using a Cartesian geometry. The MCNP5 was used in preceding works to simulate the IPR-R1 using cylindrical geometry model, exactly the same IPR-R1 reactor geometry and good results were obtained [5, 11].

1.1 IPR-R1 Reactor

The IPR-R1 is installed at Nuclear Technology Development Centre (CDTN) of Brazilian Nuclear Energy Commission (CNEN), in Belo Horizonte, Brazil. It is a reactor type TRIGA Mark-I housed in a 6.625 meters deep pool with 1.92 meters of internal diameter and filled with light water which has function of cooling, moderator, neutron reflector and radioactive shielding. IPR-R1 works at 100 kW but it will be briefly licensed to operate at 250 kW.

It works at low power and low pressure being applied in research, training and radioisotopes production. The core presents a radial cylindrical configuration with six concentric rings (A, B, C, D, E, F) with 91 channels able to host either fuel rods or other components like control rods, reflectors and irradiator channels. The 63 fuel elements are constituted by a cylindrical metal cladding filled with a homogeneous mixture of zirconium hydride and Uranium 20% enriched in ^{235}U isotope. There are 59 fuel elements covered with aluminum and 4 fuel elements with stainless steel. In the center of the reactor, there is an aluminum tube (central thimble) to irradiation of experimental samples. This tube is removable and when it is not in use, the reactor pool water fills its volume. The main thermal-hydraulic and kinetic characteristics of the IPR-R1 core are listed in [6, 8]. The radial relative power distribution (Fig. 1) was calculated in preceding works using the WIMSD4C and CITATION codes and also experimental data [7]. The radial factor is defined as the ratio of the average linear power density in the element to the average linear power density in the core. Fig. 1 shows also the six core concentric rings (A, B, C, D, E, F).

Furthermore, the core has an annular graphite reflector with aluminum cladding. Such annular reflector has a radial groove where a rotary rack is assembled for insertion of the samples to irradiation. In such rotary rack is possible to place the samples in 40 different positions around the core. Moreover, tangent to annular reflector, there is a pneumatic tube where the samples also can be inserted to irradiation.

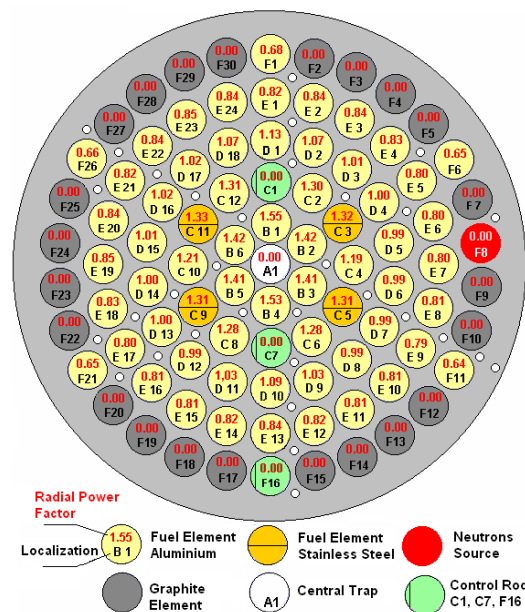


Fig 1. Radial relative power distribution

The reactor cooling occurs predominantly by natural convection governed by the water density differences. To perform the heat removal generated in the core, the water of the pool is pumped through a heat exchanger.

2. RELAP5-3D Model

There are two options for the computation of the reactor power in the RELAP5-3D code [3]. The first option is the point reactor kinetics model that was implemented in previous versions of RELAP5. The second option is a multi-dimensional neutron kinetics model based on the NESTLE code developed at North Carolina State University. RELAP5-3D was modified to call the appropriate NESTLE subroutines depending upon the options chosen by the user and this is the most prominent attribute that distinguishes the RELAP5-3D code from the previous versions. The neutron kinetics model uses the few-group neutron diffusion equations. Two or four energy groups can be utilized, with all groups being thermal groups if

desired. Core geometries modelling include Cartesian and hexagonal. Core symmetry options are available, including quarter, half and full core for Cartesian geometry and one-sixth, one-third and full core for hexagonal geometry.

To perform the IPR-R1 model in the RELAP5-3D, two energy groups were used. The full core has been simulated. As it can be verified in the Fig. 1, the IPR-R1 has circular geometry. To simulate it in the RELAP5-3D, it was chosen the Cartesian geometry. The TH regions and the NK modeling are shown in Fig. 2 for the upper axial plane, which corresponding areas coincide with those from the circular core geometry. As there are 91 nodes for each plane and there are 21 axial planes, then the core has 1911 neutron kinetic nodes. To simplify the model, the 63 fuel elements were collapsed in 13 heat structure (HS) components. These HS components were associated with the 13 corresponding hydrodynamic channels. The neutrons source (F8 in the Fig. 1) was simulated as a reflector element; the control rods (C1, C7, F16 in the Fig. 1) and the central thimble (A1) were simulated as water.

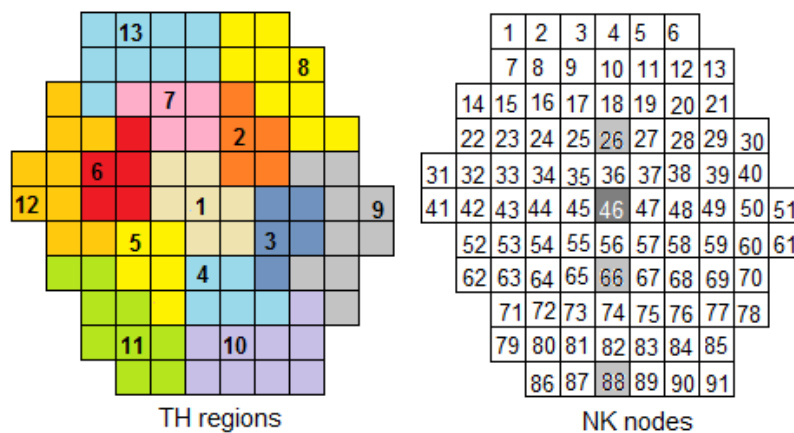


Fig 2. IPR-R1 – TH regions and corresponding NK nodes to RELAP5-3D modelling

To calculate the cross-sections sets, few compositions were considered in the model with six fuel compositions and one reflector composition (graphite element). The cross-section libraries were generated by WIMSD5 code [9] which is a general lattice cell program that uses transport theory to calculate flux as a function of energy and position in the cell. The base cross-sections were calculated according to data of the IPR-R1 exposure in year 2004.

The cross-section sets generated by WIMSD5 code were included in the RELAP5-3D. The tabular form of homogenized cross-section libraries is organized in two energy groups. Data as the scattering, absorption and fission macroscopic cross sections, and assembly discontinuity factors are tabulated for each controlled and uncontrolled composition.

The RELAP5 Mod3.3 has been used to simulate the TH behaviour of the IPR-R1 with good results [6, 8]. Then, the neutron kinetic part was incorporated to the RELAP5-3D to complete the TH-NK coupling. However, as the RELAP5 codes were developed mainly to simulate power reactors with a square geometry, it is necessary to adapt the model to simulate the cylindrical geometry of the IPR-R1.

3. MCNP5 Model

The IPR-R1 core was configured in the MCNP5 code according with neutron kinetic model of RELAP5-3D (NK nodes). This core was modeled by a square lattice with 91 cells able to host either fuel rods or other components like control rods, reflectors and irradiator channels. The

elements are surrounded by water. The control rods and the central thimble were not configured and their corresponding cells are filled with water. The neutron source (F8 in the Fig. 1) was simulated as reflector element. The fuel elements have three axial sections with upper and lower reflector (graphite), and the central portion filled with fuel. The radial reflectors elements are covered with aluminum and filled with graphite having the same dimensions of the fuel elements. Figure 3 illustrates the axial and radial view of simulated modelling and the Table 1 presents the main geometric dimensions.

Parameter	Value (cm)
Fuel radius	1.7900
Gap radius	1.7990
Cladding radius	1.8650
Fuel pitch distance	4.4025
Active length	36.1660
Axial reflector length	13.4170

Tab 1: Dimensions of MCNP5 model

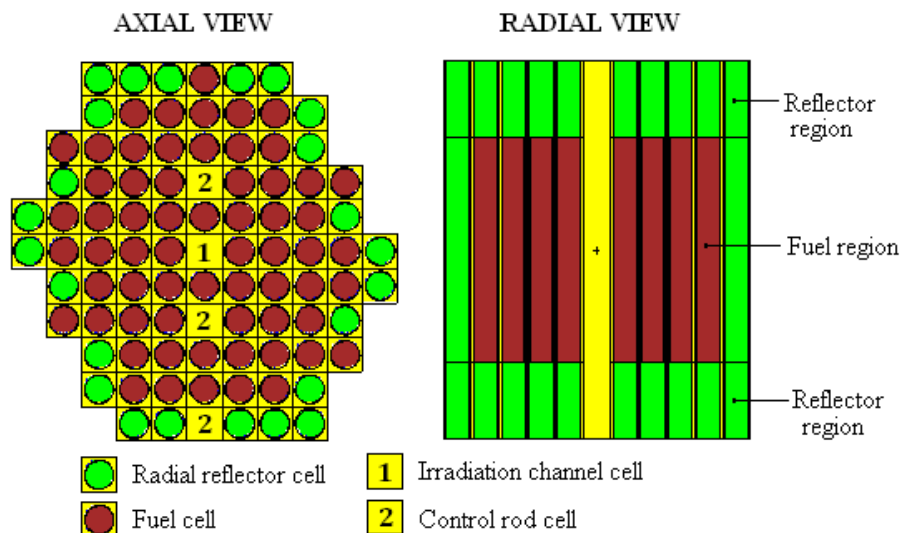


Fig 3. IPR-R1 – Core modelling using the MCNP5

The MCNP5 code apply the Monte Carlo Method that consists of actually following each of many particles from a source throughout its life to its death in some terminal category (absorption, escape, etc.). In the simulation 100 active cycles were calculated with 50000 neutrons per cycle using the ENDF/B-VI continuous neutron energy library.

The MCNP5 calculates k_{eff} values printing the respective standard deviation (sd) in the output file. To perform the neutron flux inside each cell the FMESH card of MCNP5 code was used. This feature allows the user to tally particles on a mesh independent of the problem geometry [4]. The MCNP5 estimates the flux using the source specified by the user. In the model, there are 91 square meshes with the same dimensions of the cell to estimate the neutron flux inside each mesh.

The flux estimation does not match the actual neutron source of the reactor. Thus, it is necessary to normalize the flux values initially calculated by MCNP5. In the simulation, this normalization was performed using the following equation [4]:

$$\phi_N = \phi_{MCNP} \times \left(\frac{P \times \nu}{Q \times k_{eff}} \right)$$

where ϕ_N is the normalized flux; ϕ_{MCNP} is the flux estimated by MCNP5; P is the reactor power level; ν is the average number of fission neutrons and Q is the recoverable energy per fission event. The values of ν , Q and k_{eff} are calculated by MCNP5 and they can be obtained in the output file of the code. The user provides the power level (P). In this case, for IPR-R1 reactor, $P = 100$ kW.

4. RELAP5-3D and MCNP5 Results

Fig. 4 presents the values of the average planar relative power distribution calculated by the RELAP5-3D and the MCNP5 codes; it presents also the data from the reference redistributed according to the Fig. 1 [7] and the difference found between the codes calculations and the reference data. As it can be verified, the main differences for both calculations are in the fuel elements corresponding to the last ring of the core (detached in blue color). These calculated values were considerably underestimated in relation to the reference data. This is probably because the annular graphite reflector surrounding the core was not simulated in both codes.

In fact, the MCNP5 code is capable to simulate in more details the core including the annular reflector [5]. However, as the idea is to verify the RELAP5-3D model using the MCNP5, and the RELAP5-3D is not capable to simulate exactly the same geometry of the core, both models did not consider the reflector surrounding the core. Fig. 5 shows the general result of the average relative power distribution in the core obtained by the RELAP5-3D and MCNP5 for the IPR-R1 simulations considering 100 kW of power operation.

REFERENCE										
0.00	0.00	0.00	0.00	0.00	0.00	0.68	0.00	0.00	0.00	0.00
0.00	0.00	0.00	0.85	0.84	0.82	0.84	0.84	0.00	0.00	0.00
0.00	0.66	0.84	1.02	1.07	1.13	1.07	0.83	0.00	0.00	0.00
0.00	0.00	0.82	1.02	1.31	0.00	1.30	1.01	0.80	0.65	0.00
0.00	0.84	1.01	1.33	1.55	1.42	1.32	1.00	0.80	0.00	0.00
0.00	0.85	1.00	1.21	1.42	0.00	1.41	1.19	0.99	0.80	0.00
0.00	0.00	0.83	1.00	1.31	1.41	1.53	1.31	0.99	0.81	0.00
0.00	0.65	0.80	0.99	1.28	0.00	1.28	0.99	0.79	0.00	0.00
0.00	0.00	0.00	0.81	1.03	1.09	1.03	0.99	0.81	0.64	0.00
0.00	0.00	0.00	0.81	0.82	0.84	0.82	0.81	0.00	0.00	0.00
0.00	0.00	0.00	0.00	0.00	0.00	0.00	0.00	0.00	0.00	0.00

RELAP5-3D										
0.0000	0.0000	0.0000	0.0000	0.0000	0.2730	0.0000	0.0000	0.0000	0.0000	0.0000
0.0000	0.0000	0.0000	0.6570	0.7935	0.7921	0.7524	0.6566	0.0000	0.0000	0.0000
0.0000	0.2847	0.7751	1.0431	1.1333	1.1270	1.0423	0.8157	0.0000	0.0000	0.0000
0.0000	0.0000	0.8355	1.1823	1.3534	0.0000	1.3522	1.1862	0.8336	0.2874	0.0000
0.0000	0.8386	1.2077	1.4451	1.3119	1.3111	1.4428	1.1986	0.7931	0.0000	0.0000
0.0000	0.6878	1.0922	1.4038	1.3227	0.0000	1.3205	1.3996	1.0880	0.6850	0.0000
0.0000	0.0000	0.8019	1.2139	1.4602	1.3239	1.3221	1.4545	1.2133	0.8405	0.0000
0.0000	0.2924	0.8521	1.2177	1.3900	0.0000	1.3811	1.2009	0.8449	0.0000	0.0000
0.0000	0.0000	0.0000	0.8486	1.0975	1.1962	1.1902	1.0775	0.7931	0.2896	0.0000
0.0000	0.0000	0.0000	0.7029	0.8515	0.8945	0.8416	0.6823	0.0000	0.0000	0.0000
0.0000	0.0000	0.0000	0.0000	0.0000	0.0000	0.0000	0.0000	0.0000	0.0000	0.0000

[(RELAP5 - Reference)*100%]/Reference										
0.0	0.0	0.0	0.0	0.0	0.0	-59.9	0.0	0.0	0.0	0.0
0.0	0.0	0.0	-22.7	-5.5	-3.4	-10.4	-21.8	0.0	0.0	0.0
0.0	-56.9	-7.7	2.3	5.9	-0.3	-2.6	-1.7	0.0	0.0	0.0
0.0	0.0	1.9	15.9	3.3	0.0	4.0	17.4	4.2	-55.8	0.0
0.0	-0.2	19.6	8.7	-15.4	-7.7	9.3	19.9	-0.9	0.0	0.0
0.0	-19.1	9.2	16.0	-6.9	0.0	-6.3	17.6	9.9	-14.4	0.0
0.0	0.0	-3.4	21.4	11.5	-6.1	-13.6	11.0	22.6	3.8	0.0
0.0	-55.0	6.5	23.0	8.6	0.0	7.9	21.3	6.9	0.0	0.0
0.0	0.0	0.0	4.8	6.6	9.7	15.6	8.8	-2.1	-54.8	0.0
0.0	0.0	0.0	-13.2	3.8	6.5	2.6	-15.8	0.0	0.0	0.0
0.0	0.0	0.0	0.0	0.0	0.0	0.0	0.0	0.0	0.0	0.0

MCNP5										
0.0000	0.0000	0.0000	0.0000	0.0000	0.3231	0.0000	0.0000	0.0000	0.0000	0.0000
0.0000	0.0000	0.0000	0.5676	0.7007	0.7289	0.6539	0.4541	0.0000	0.0000	0.0000
0.0000	0.2186	0.5838	0.8921	1.1015	1.2517	1.0346	0.7667	0.0000	0.0000	0.0000
0.0000	0.0000	0.8376	1.1727	1.5311	0.0000	1.4713	1.0660	0.6737	0.2392	0.0000
0.0000	0.5443	0.9855	1.3513	1.6349	1.9867	1.5874	1.2833	0.8955	0.0000	0.0000
0.0000	0.5507	1.0153	1.3927	1.8046	0.0000	1.7982	1.3741	1.0026	0.5527	0.0000
0.0000	0.0000	0.9042	1.2838	1.5834	1.9611	1.6149	1.33	0.9709	0.54	0.0000
0.0000	0.2418	0.6780	1.0686	1.4600	0.0000	1.4940	1.1468	0.8198	0.0000	0.0000
0.0000	0.0000	0.0000	0.7673	1.0277	1.2371	1.0828	0.8761	0.5758	0.2163	0.0000
0.0000	0.0000	0.0000	0.4498	0.6391	0.7569	0.69	0.5549	0.0000	0.0000	0.0000
0.0000	0.0000	0.0000	0.0000	0.0000	0.0000	0.0000	0.0000	0.0000	0.0000	0.0000

[(MCNP5 - Reference)*100%]/Reference										
0.0	0.0	0.0	0.0	0.0	0.0	-52.5	0.0	0.0	0.0	0.0
0.0	0.0	0.0	-33.2	-16.6	-11.1	-22.2	-45.9	0.0	0.0	0.0
0.0	-66.9	-30.5	-12.5	2.9	10.8	-3.3	-7.6	0.0	0.0	0.0
0.0	0.0	2.1	15.0	16.9	0.0	13.2	5.5	-15.8	-63.2	0.0
0.0	-35.2	-2.4	1.6	5.5	39.9	20.3	28.3	11.9	0.0	0.0
0.0	-35.2	1.5	15.1	27.1	0.0	27.5	15.5	1.3	-30.9	0.0
0.0	0.0	8.9	28.4	20.9	39.1	5.5	1.7	-1.9	-34.0	0.0
0.0	-62.8	-15.3	7.9	14.1	0.0	16.7	15.8	3.8	0.0	0.0
0.0	0.0	0.0	-5.3	-0.2	13.5	5.1	-11.5	-28.9	-66.2	0.0
0.0	0.0	0.0	-44.5	-22.1	-9.9	-15.5	-31.5	0.0	0.0	0.0
0.0	0.0	0.0	0.0	0.0	0.0	0.0	0.0	0.0	0.0	0.0

Fig 4. Planar average relative power distribution from the reference, the RELAP5-3D and the MCNP5 codes, and the percentage differences in relation to the reference data

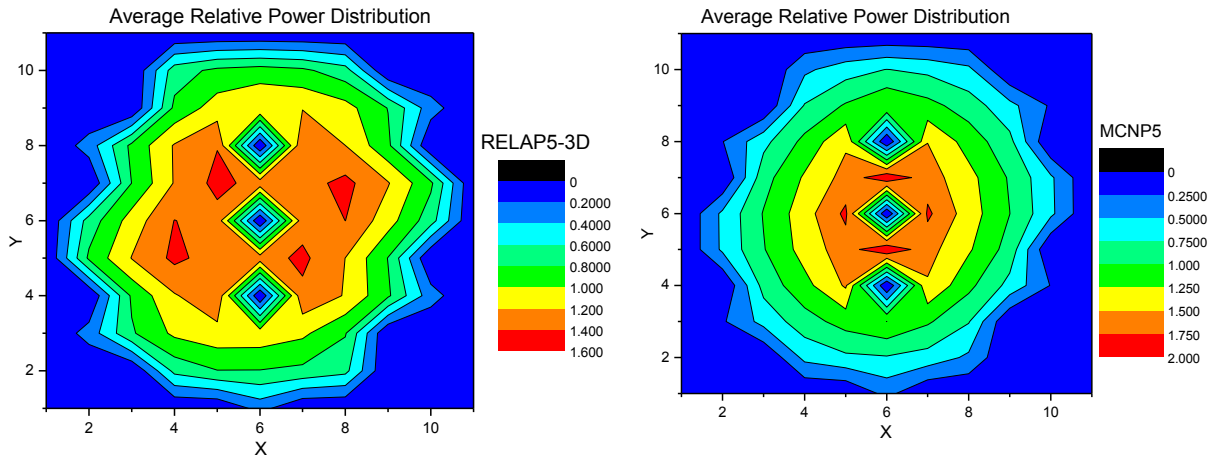


Fig 5. Planar average relative power distribution – RELAP5-3D and MCNP5 models

Fig. 6 presents the radial thermal flux distribution in the center of core (axial level 11) simulated by both codes. As it is demonstrated in Table 2, both calculations are overestimated in relation to reference data, but they are in the same order of magnitude of the experimental available data. For measuring thermal neutron flux at the central thimble it was used cobalt foil irradiated at 27 cm of the bottom of the core that is the position of maximum flux [10].

Type	Thermal neutron flux at 100 kW (neutrons.cm ⁻² .s ⁻¹)
RELAP5-3D	9.81×10^{12}
MCNP5	$(7.11 \pm 0.01) \times 10^{12}$
Experimental [10]	$(4.1 \pm 0.3) \times 10^{12}$

Tab 2: Calculated and experimental thermal fluxes in the central thimble

Finally, the calculated values of the effective neutron multiplication factor, k_{eff} , were compared. The values of k_{eff} given by the MCNP5 and the RELAP5-3D calculations were 0.91351 ($sd = \pm 3.1 \times 10^{-4}$) and 0.91670, respectively, very close each other in spite of the two different ways of neutronic calculation. However, these values are underestimated in relation to the expected value that would be next to 1.0. The explanation to such difference is probably connected to the fact that the reflector surrounding the core was not considered in the models causing a loss of neutrons that could be reflected back to the core. Then, it is necessary to find ways to simulate this part of the core in the RELAP5-3D.

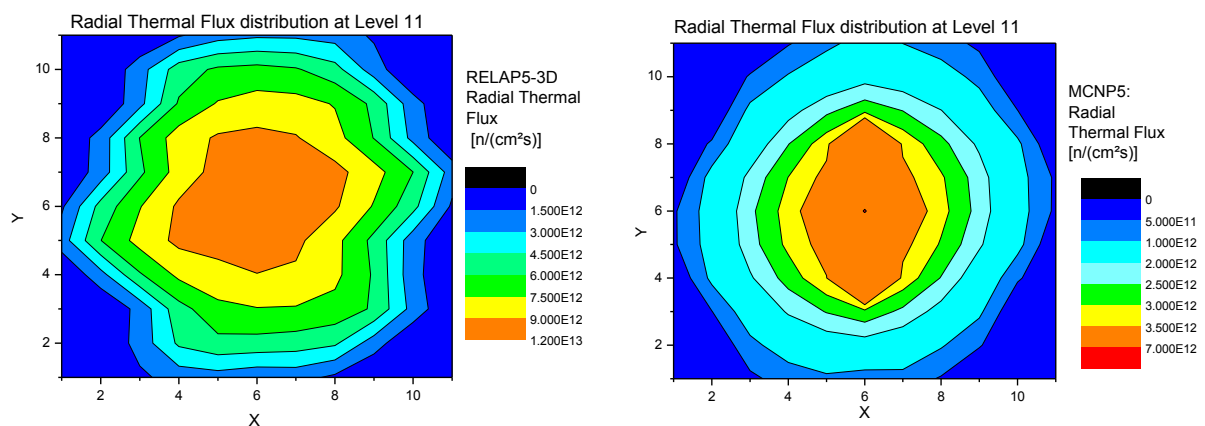


Fig 6. Radial thermal flux distribution in the center of the core (level 11) predicted by RELAP5-3D and MCNP5 models

5. Conclusions

Two models for the IPR-R1 TRIGA research reactor were considered in the RELAP5-3D and MCNP5 codes at 100 kW of power operation. Results of average radial relative power core distribution were compared with the reference data [7]. In a general way, both codes presented values next to the reference data, in spite of the difference presented in the fuel elements localized in the last ring. As the reflector surrounding the core was not considered in both models, this is possibly the cause of the neutrons loss. This also affected the prediction of k_{eff} that presented underestimated value in both models. About the thermal flux radial core distributions, the codes presented values in the same order of magnitude in comparison with the experimental data.

As it was explained, the MCNP5 is more flexible to simulate specific geometries including cylindrical one. However it is not capable to simulate transients with TH variations in nuclear systems mainly because it is not possible to perform the feedback in the cross sections. In the other hand, RELAP5-3D uses a multi-dimensional neutron kinetics model to simulate TH-NK coupled problems as steady state as transient calculations with cross sections feedback. The problem to apply the RELAP5-3D to simulate IPR-R1 TRIGA research reactors is to reproduce cylindrical geometries since it works only with hexagonal or Cartesian types. In this specific case it is necessary to adequate the model to duly simulate the core behaviour and to include also the external circular reflector.

Acknowledgments

The authors are grateful to CAPES, CDTN/CNEN, FAPEMIG and CNPq for the support. Thanks also to Idaho National Laboratory for the permission to use the RELAP5-3D computer software.

References

- [1] IAEA. Safety Analysis for Research Reactors. IAEA Safety Standards Series, N° 55, IAEA, Vienna, Austria, (2008).
- [2] A. L. Costa et al., "Chapter 2: Safety Studies and General Simulations of Research Reactors Using Nuclear Codes", In: Nuclear Power - System Simulations and Operation. Ed. InTech, Rijeka, Croatia, ISBN: 978-953-307-506-8, Vol. 2, p. 21-42, (2011).
- [3] The RELAP5-3D[®] Code Development Team, RELAP5-3D[®] Code Manuals, *INEEL-EXT-98-00834*, (2005).
- [4] T. E. Booth et al., "MCNP – A General Monte Carlo N-Particle Transport Code (version 5)," Tech. Rep. LA-UR-03-1987, Los Alamos National Laboratory, (2003).
- [5] C. A. M. Silva et al., "Sensitivity Analysis of TRIGA IPR-R1 Reactor Models Using the MCNP Code", *International Journal of Nuclear Energy – Vol. 2014*, Article ID 793934, 9 pages (2014).
- [6] P. A. L. Reis et al., "Assessment of a RELAP5 model for the IPR-R1 TRIGA research reactor", *Annals of Nuclear Energy*, 37, pp. 1341-1350, (2010).
- [7] H. M. Dalle, C. Pereira, R. M. G. P., Souza, "Neutronic calculation to the TRIGA IPR-R1 reactor using the WIMSD4 and CITATION codes", *Annals of Nuclear Energy*, 29, pp. 901–912, (2002).
- [8] P. A. L. Reis et al., "Sensitivity analysis to a RELAP5 nodalization developed for a typical TRIGA research reactor", *Nuclear Engineering and Design*, 242, pp. 300-306, (2012).
- [9] RSICC Computer Code Collection WIMSD-5B.12 – Deterministic Code System for Reactor-Lattice Calculations, Oak Ridge National Laboratory (2007).
- [10] R. M. G. P. SOUZA, "Thermal Neutron Flux Measurements in the Irradiation Facilities of the IPR-R1 TRIGA Reactor", In *3rd World TRIGA Users Conference*, Belo Horizonte, Brazil (2006).

- [11] C. A. M. Silva et al., "MCNP5 modeling of the IPR-R1 TRIGA reactor for criticality calculation and reactivity determination", *Nuclear Engineering and Design*, 241, pp. 4989-4993, (2011).

TRANSPORT OF IRRADIATED FUEL RODS AND SEGMENTS OF IRRADIATED FUEL RODS

S. MOESEN, W. BOECKX
Transnubel (TNB)
Zandbergen 1, 2480 Dessel – Belgium

ABSTRACT

The transport of irradiated fuel rods or segments of irradiated fuel rods is essential for the investigation of fuel behaviour after irradiation. The paper will focus on different aspects:

- The return of experience gained during the transport of irradiated fuel rods. More information will be given on the particularities for the loading and unloading sites.
- The return of experience gained during the transport of segments of irradiated fuel rods and identification of specific needs.
- Difficulty regarding the transport of leaking fuel rods. When utilities encounter situations of leaking fuel, it is important to investigate the causes leading to the leak. This requires the transport of leaking fuel rods to laboratories. The difficulty to obtain an approval for the transport of leaking fuel rods will be explained.
- Transport of high burnup fuel rods. The requirement for higher burnup rates in nuclear power plants leads to the need to transport fuel rods with higher burnup. The laboratories need to receive high burnup fuel rods to validate calculation codes. But this validation is needed for the validation of the transport packaging...

1. Introduction

The purpose of this paper is to share the information regarding the transport of irradiated fuel rods, segments of irradiated fuel rods and the difficulties of leaking fuel rods and higher burnup rates in fuel rods.

Until 2011, the transport of full length fuel rods or fuel segments, leaking or not, could be performed using the BG18 transport cask (see Figure 1). Due to the ever increasing demands for packagings to demonstrate compliance with the safety regulations, the older design of the BG18 could no longer guarantee this compliance. The BG18 cask has over 10 years of experience and performed about 40 transport campaigns.

Since 2011, the new R72 transport cask (see Figure 2) is being used as a replacement of the BG18 cask. The R72 packaging is designed for the transport of fuel rods or fuel segments. In this new packaging design the amount of fuel rods transported has been decreased from 30 rods, as for the BG18, to 10 rods. The R72 packaging is owned, designed and constructed by Robatel Industries and managed, operated and maintained by Transnubel. The R72 packaging is also designed but not yet approved for the transport of leaking fuel rods.



Figure 1 – BG18 cask



Figure 2 – R72 cask

2. Return of experience, transport of irradiated fuel rods

Over the years, Transnubel has performed many transports of irradiated fuel rods between research facilities and nuclear power plants in Belgium, Germany, France, Spain, Sweden, Switzerland, etc. For each research facility or power plant, specific constraints, both for the installation itself as for the operational procedures, needed to be taken into account.

Due to the transports performed in the past, Transnubel has acquired a significant experience and knowledge of these facilities. By this way, many particularities could be treated. For instance, the lifting crane may vary which calls for an adapted lifting beam to lift the packaging used for the transport of the fuel rods. Also the loading / unloading zone can have different dimensions which could make it more difficult to load / unload the packaging and ask for specific hoisting equipment or a different size of trailer.

Specific equipment has also been designed for operating the cask, for instance equipment to remove the plug or the basket both in horizontal and vertical positions. A guillotine system has been designed to secure safe working conditions to remove the plug and to guarantee the safe docking of the cask against the hot cell (see Figure 3 and Figure 4).

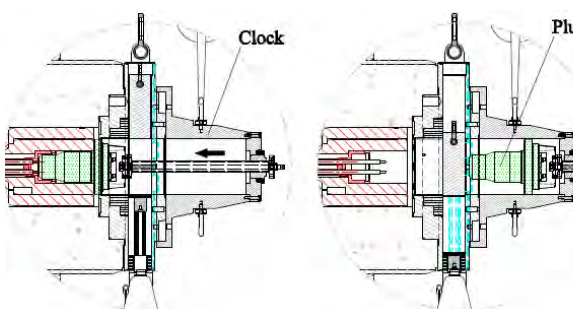


Figure 3 – Principle of guillotine system and clock for plug removal



Figure 4 – Guillotine system and clock for plug removal

A blank test or cold handling is performed by Transnubel at the loading / unloading site when “new” situations occur (other packaging, new site, etc.) to verify and adjust the equipment to perform the loading and unloading operations of the packaging. If necessary, new tools are created and tested.

The R72 packaging is designed to transport the commonly used dimensions of fuel rods. Since the fuel rods that will be transported can also differ in size depending on the loading site,

different baskets are designed to allow these other dimensions. Specific spacers are used to accommodate for different lengths.

For specific loading operations with major dimensional constraints, a Transnubel packaging has been used to act as a lead castle (see Figure 5) to transfer the fuel rods between the loading pool and the transport packaging. For this specific operation, a docking equipment (see Figure 6) was designed to facilitate the transfer of the fuel rods between the lead castle and the transport packaging.

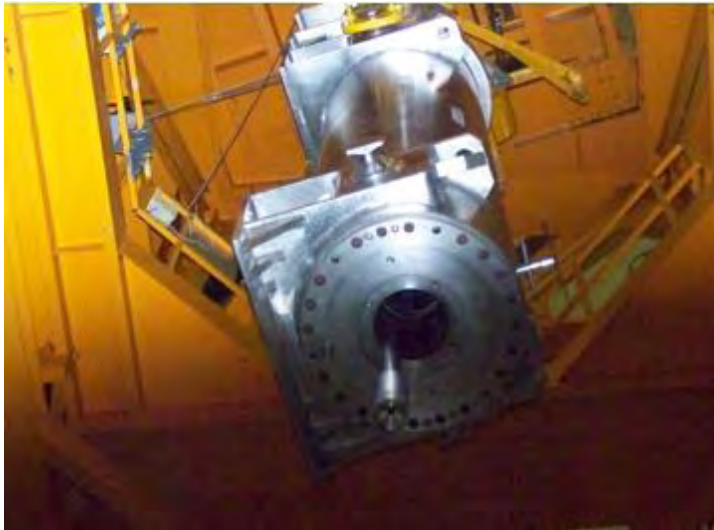


Figure 5 – Packaging serving as lead caste



Figure 6 – Docking of lead castle onto transport packaging

3. Return of experience, transport of irradiated fuel rod segments

Despite the reduced dimensions, the packagings used for the transport of fuel rod segments are subjected to the same issues as those for the transport of irradiated fuel rods. The packaging can be selected depending on the properties of the segments.

For the loading / unloading operations of segments of fuel rods, specific requirements are needed depending on the packaging and the installation. For instance, the docking against the hot cell, the specific basket needed in the packaging or the need to encapsulate the segments which may be required by the safety analysis report of the packaging.



Figure 7 – TNB170

The R72 packaging, as described in paragraph 2, could be used for longer segments of fuel rods if these segments are loaded against a hot cell. A specific spacer has to be foreseen in order to avoid movements of the content during the transport.

For short segments of fuel rods, the TNB170 (see Figure 7) is a promising alternative. The packaging is currently under approval by the authorities and will be available by the end of 2015. Specific equipment has been designed to facilitate the loading and unloading of segments (or other sources) when docked against a hot cell.

A tilting device (see Figure 8) is foreseen to bring the packaging from the vertical to the horizontal position. The docking equipment (see Figure 10) will allow a smooth gliding of the plug when pulled

into the hot cell. In order to have an easy access from inside the hot cell, an extension tool (see Figure 9) is mounted on the plug.



Figure 8 – Tilting device



Figure 9 – Extension tool



Figure 10 – Docking part

4. Difficulty regarding the transport of leaking fuel rods

Most nuclear power plants over the world have been or will be concerned by the presence of leaking irradiated fuel rods in their pool. It is important to understand the reasons of the ruptures or damage in order to be able to take actions and avoid as much as possible the leaking fuel rods in the future. This requires a transport of these leaking fuel rods to specific laboratories for research.

The BG18 packaging was authorized in the past to transport leaking fuel rods but its approval has expired in 2011. The R72 packaging has taken over the transports performed with the BG18. The studies presented in its safety analysis report show that the packaging is able to transport leaking fuel rods, but the certificate of approval does not allow it. At the moment there is no possibility to transport leaking fuel rods as such.

During the preparation of the loaded packaging for transport, the cavity needs to be dried to limit the amount of hydrogen in it. This is done by creating a vacuum to extract the water from the cavity. With leaking fuel rods it could not be fully guaranteed that all water is removed from the fuel rod.

The following two phenomena could occur with leaking fuel rods and explain why the removal of water is not certain:

- Due to the effect of radiation, the pellets inside the fuel rods deform which may result in water trapped inside the fuel rod. One or more pellets deform and could act as a barrier between the hole in the cladding and the remaining water in the rod.
- When a fuel rod cools down after use, an existing hole in the cladding may close during this process. This results also in water trapped inside the fuel rods.

For the approval of leaking fuel rods, a radiolysis analysis is required. This analysis has to demonstrate that the amount of hydrogen remains under 4% (lower explosion limit). The determination of the leak is very difficult and the analysis is practically impossible to carry out because of the deformation of the pellets and the closure of existing holes, especially at nuclear power plants. For these reasons, the amount of hydrogen in the fuel rod could not be shown.

The concern of the authorities deals with the possible presence of water in the packaging during transport. They consider the release of the water out of the fuel rod as possible which could lead to radiolysis and risk of explosion.

5. Transport of high burnup fuel rods

Nuclear power plants ask for higher burnup rates to be able to get more power out of the fuel rods before having to replace them. This demand requires that laboratories need to receive high burnup fuel rods to validate calculation codes. The transport of this high burnup fuel rods however cannot be validated without these calculations.

The currently used calculation codes are validated to a certain limit of burnup for low enriched fuel rods. With these codes it is possible to determine the different characteristics of the irradiated fuel rods such as the thermal power and the isotopic composition. Depending on these characteristics, the operating parameters of the packaging can be determined. These parameters of the packaging are the radiation protection, the thermal analysis and the leak tightness.

With high burnup fuel, more actinides are present in the fuel. This results in lower A_2 -values for the content. The leak tightness of the packaging is also more difficult to show because the limit is more restrictive. Both points reduce the total amount or the total activity to be shipped.

The current calculation codes are valid till a certain limit of burnup. To validate calculation codes for higher burnup of low enriched fuel rods, the laboratories need to receive fuel rods with higher burnup. Before a transport of high burnup fuel may be performed however, it needs validation first.

The evolution of the burnup rates in nuclear power plants leads to a need for transport of fuel rods with higher burnup. The European laboratories need to receive such high burnup fuel rods to evaluate the low enriched fuel's behaviour at high burnup and to collect radiological data in order to obtain a sufficient benchmark for the qualification of calculation codes.

To perform the safety studies on packagings intended for the transport of high burnup low enriched irradiated fuel, designers need to describe the content from the radiological point of view, to be loaded in the packaging; calculation codes need to be used out of the range of their validation.

However, the competent authorities in charge of the approval of packagings request the content to be precisely known; the usual way is to make calculations of the isotopes and activities based on of calculation codes, but these codes need to be validated by the authorities. As the validation is not granted for high burnups, long, hard and expensive discussions start about the way used for the characterization of the content and about the justification of safety margins, without possibility of demonstration.

6. Conclusion

The transports of irradiated fuel rods require in most of the situations a case by case analysis of the loading and unloading possibilities, leading to adapted procedures or specific tooling. These kind of transport campaigns remain in any case punctual operations. Due to the important experience gained by Transnubel over the years, different kinds of solutions have been successfully implemented.

For the transport of irradiated fuel rods or segments of irradiated fuel rods, a specific packaging could be used. For full length fuel rods, the cask R72 is most suited. For segments of irradiated fuel rods, the packaging TNB170 is a promising option.

The transport of leaking fuel rods and high burnup fuel remains a challenge regarding the demonstration to the competent authorities, due to the ever increasing demands for packagings to demonstrate compliance with the safety regulations.

RRFM 2015
EUROPEAN RESEARCH REACTOR CONFERENCE

19 April –23 April 2015
Bucharest, Romania

Y-12 NATIONAL SECURITY COMPLEX U-MO FABRICATION

Amy DeMint
Development Technologies
Y-12 National Security Complex
Oak Ridge, TN 37831 USA

Jim Henkel
Nuclear Material Applications
Y-12 National Security Complex
Oak Ridge, TN 37831 USA

Hollie A. Longmire
Nuclear Material Applications
Y-12 National Security Complex
Oak Ridge, TN 37831 USA

Mike Gambrell
Uranium Metalworking Process Engineering
Y-12 National Security Complex
Oak Ridge, TN 37831 USA

Cary Langham
Uranium Metalworking Process Engineering
Y-12 National Security Complex
Oak Ridge, TN 37831 USA

Alan Moore
Uranium Metalworking Process Engineering
Y-12 National Security Complex
Oak Ridge, TN 37831 USA

ABSTRACT

Y-12 National Security Complex (Y-12 NSC) participates in the Fuel Fabrication Capability (FFC) pillar of the U.S. Department of Energy's (DOE) National Nuclear Security Administration (NNSA) Global Threat Reduction Initiative (GTRI) Convert Pillar system. Y-12 NSC is primarily responsible for developing the fabrication process of a low-enriched uranium-molybdenum (LEU-Mo) feedstock. The baseline LEU-Mo fabrication process included a two-step casting process. Y-12 NSC is examining the feasibility of transitioning to a single step casting process. This presentation will focus on the transition strategy and discuss initial results from the feasibility trials.

DISCLAIMER

This work of authorship and those incorporated herein were prepared by Consolidated Nuclear Security, LLC (CNS) as accounts of work sponsored by an agency of the United States Government under contract DE-NA0001942. Neither the United States Government nor any agency thereof, nor CNS, nor any of their employees, makes any warranty, express or implied, or assumes any legal liability or responsibility for the accuracy, completeness, use made, or usefulness of any information, apparatus, product, or process disclosed, or represents that its use would not infringe privately owned rights. Reference herein to any specific commercial product, process, or service by trade name, trademark, manufacturer, or otherwise, does not necessarily constitute or imply its endorsement, recommendation, or favoring by the United States Government or any agency or contractor thereof, or by CNS. The views and opinions of authors expressed herein do not necessarily state or reflect those of the United States Government or any agency or contractor thereof, or by CNS.

1. Introduction

Y-12 National Security Complex (Y-12 NSC) participates in the Fuel Fabrication Capability (FFC) pillar of the U.S. Department of Energy's (DOE) National Nuclear Security Administration (NNSA) Global Threat Reduction Initiative (GTRI) Convert Pillar system. Y-12 NSC is primarily responsible for developing the fabrication process of a low-enriched uranium-molybdenum (LEU-Mo) feedstock.

The LEU-Mo Baseline Coupon Fabrication Process is a two-step casting process, as depicted in Figure 1. First, HEU is blended with a diluent and molybdenum in an initial cylindrical casting. The cylindrical casting is sampled and analyzed. Based on the analytical results, the feed is adjusted and recast or the alloy is then broken and recast into a single plate form. The LEU-Mo coupons are fabricated from the plate casting. This process has a large molybdenum distribution range, typically from 8% to 12%, resulting in a higher than desired reject rate. One theory is that the initial casting step has too many process variables in a one unit operation to provide a repeatable and predictable casting. Y-12 NSC is experimenting with an Alternate LEU-Mo Casting Process using a pre-alloyed diluent feedstock, labeled as UMoF, and a multi-plate casting form, as depicted in Figure 2.

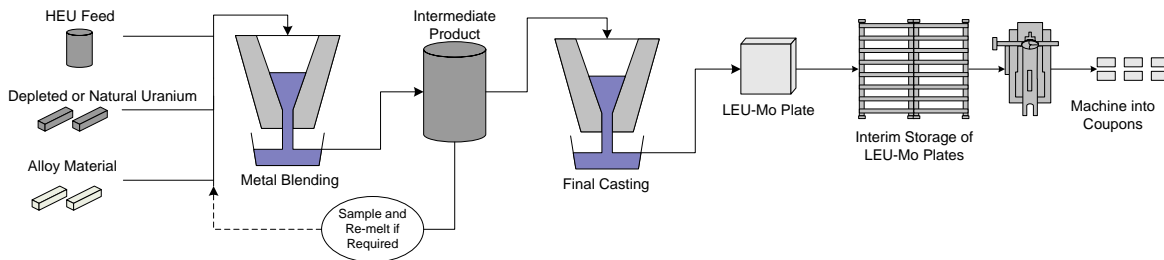


Figure 1: Baseline Coupon Fabrication Process

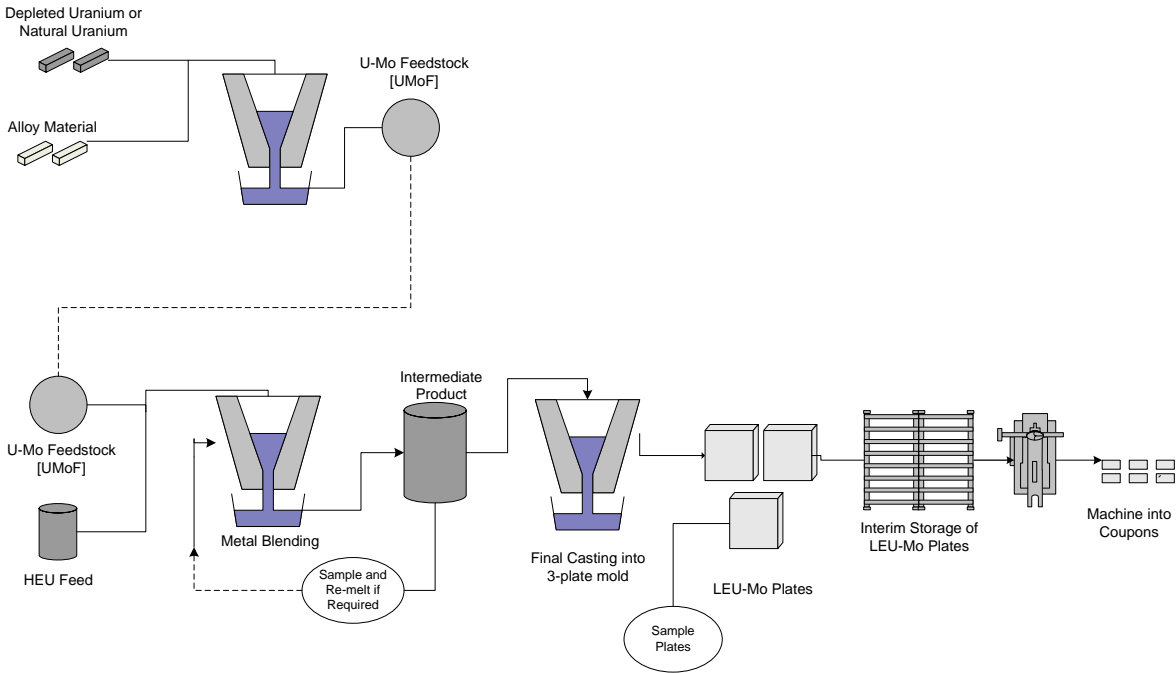


Figure 2: Alternate LEU-Mo Casting Process

Previous trials of the alternate casting process indicated there was a greater control of process parameters by pre-alloying the diluent. The alternate casting process also indicated that the Mo and uranium-235 (U235) distribution throughout the casting were more uniform, indicating a tighter process control of material constituents. In addition to using a pre-alloyed diluent, the alternate casting process indicated that a multi-plate mold could be used to increase material throughput.

In an effort for continuous improvement in both cost reduction and scrap reduction, Y-12 NSC experimented with a Proposed Optimized Casting Process, as shown in Figure 3, based on promising results from the Alternate LEU-Mo Casting Process. A series of castings were performed by eliminating the intermediate cylindrical casting step.

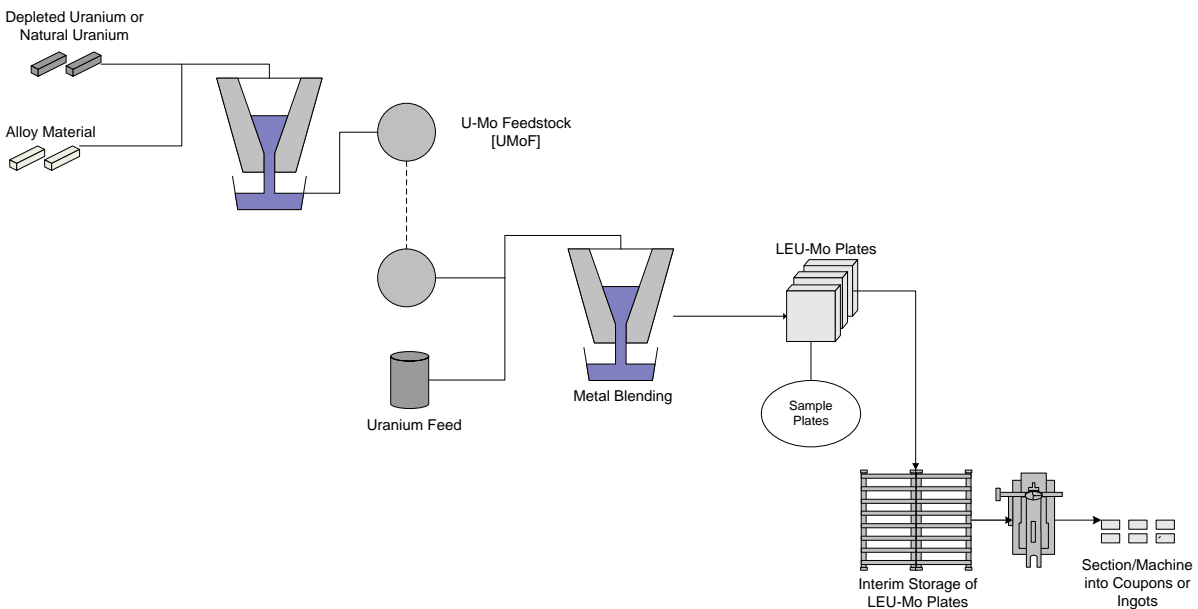


Figure 3: Proposed Optimized Casting Process

2. Description of First Trial Campaign

As part of the trial campaign, Y-12 fabricated DU-Mo plates in accordance with Figure 3. The plates were sectioned and machined into coupons as previously performed in the Baseline Coupon Fabrication Process. The first trial campaign consisted of five castings. A sixth casting was performed to account for fabrication attrition. This trial campaign assumed there was no attrition for cast surface defects. The intent of assuming no attrition was to allow the final fabricator to process all of the coupons and provide feedback to determine if coupon defects lead to foil failures during the fabrication process.

3. Results of First Trial Campaign

Y-12 completed the casting activities as described in Figure 3, which yielded eighteen plates. As the coupons were sectioned from the plates, samples were taken from the milled plate, which is representative of the coupon chemical make-up. Samples were taken from the top, middle and bottom of each plate. The chemical analyses were compared to target. For Molybdenum, the target was $10\% \pm 1\%$. For Uranium, the target was $90\% \pm 1\%$. Results for the castings are shown in Figures 4-5.

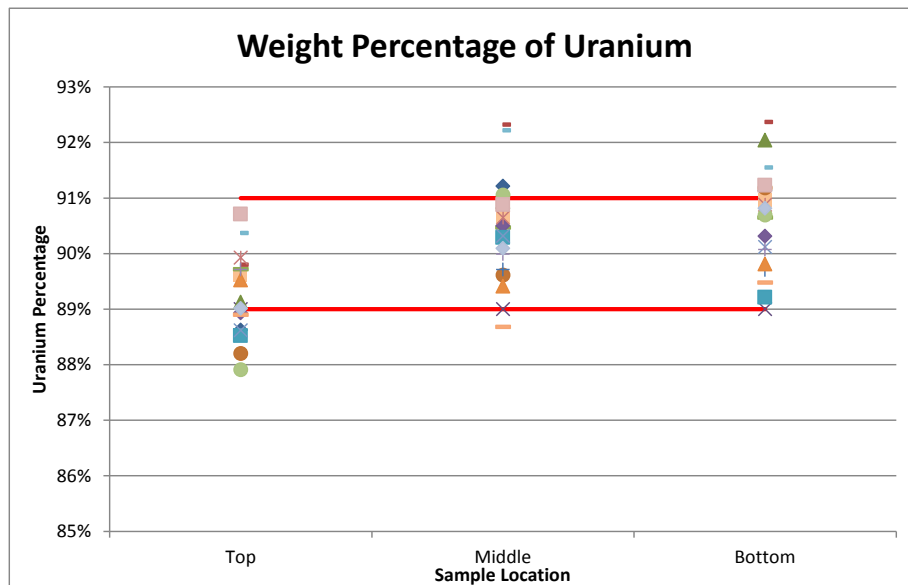


Figure 4: Uranium Weight Percentage Summary

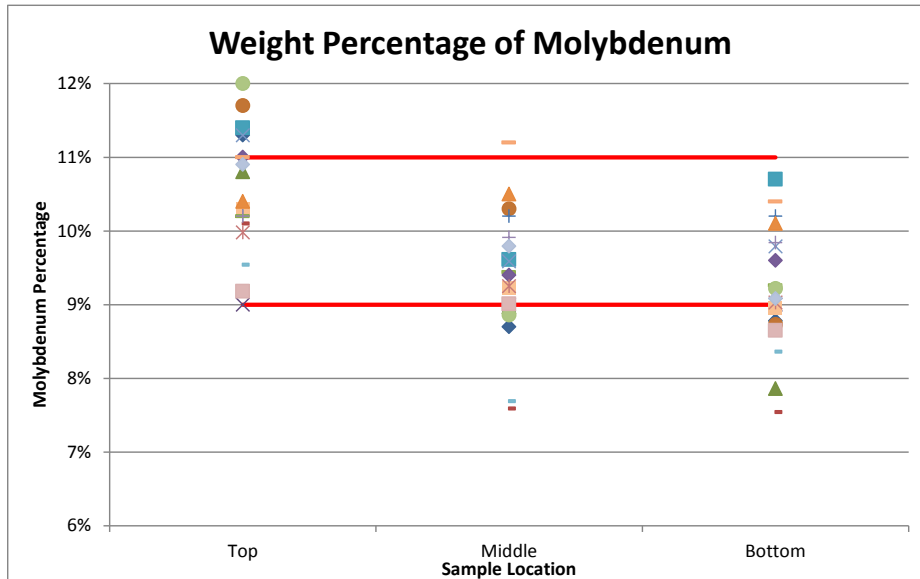


Figure 5: Molybdenum Weight Percentage Summary

The material fabricated in the trial campaign was planned at 10% Molybdenum and 90% Uranium. There were other minor constituents and impurities found in the product. However, as seen in the Figures above, when molybdenum percentages were high, the uranium percentages were lower. On the samples taken, the chemistry was out of the target range 33% of the time. Further analyses indicate that the early castings, performed in August 2013, were out of the target range 44% of the time. The last castings, performed in December 2013, were out of the target range 28% of the time. The decrease may be indicative of proficiency gained in the new process. Since this is the first time the single step casting was tested, achieving the target values for major constituents in over 65% of the trial campaign is promising. This indicates that the single step casting process is viable and may improve with process adjustments.

4. Description of Second Trial Campaign

Y-12 completed a second campaign of casting activities as described in Figure 3. This campaign consisted of nine castings. One casting was discarded, due to a mispour. The remaining castings yielded twenty-four plates. This second campaign included one additional process change. Instead of machining coupons as shown in Figure 6, the process was optimized to reduce scrap and increase material utilization. In an effort to distinguish the final products, the new product was labeled as ingots, as shown in Figure 7.

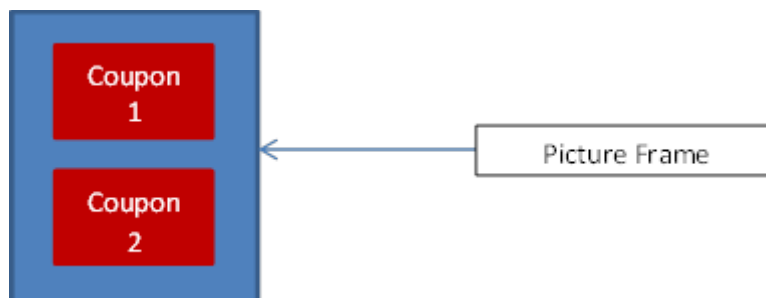


Figure 6: Baseline Machining Process

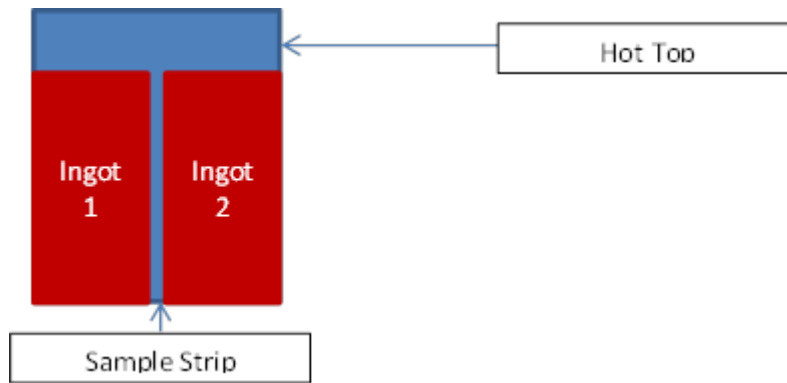


Figure 7: Optimized Machining Process

The twenty four plates were divided into two equal groups of twelve plates. One group of twelve plates (24 ingots) would have skimmed surface (i.e. minimal machining). The second group of twelve plates (24 ingots) would have an as-cast surface (i.e. no machining).

5. Results of Second Trial Campaign

As the DU-Mo ingots were sectioned from the plates, samples were taken, which is representative of the ingot chemical make-up. Samples were taken from the top, middle and bottom of each plate. The chemical analyses were compared to the target specification. For Molybdenum, the target was $10\% \pm 1\%$. For Uranium, the target was $90\% \pm 1\%$. Results for the castings are shown in Figures 8-9.

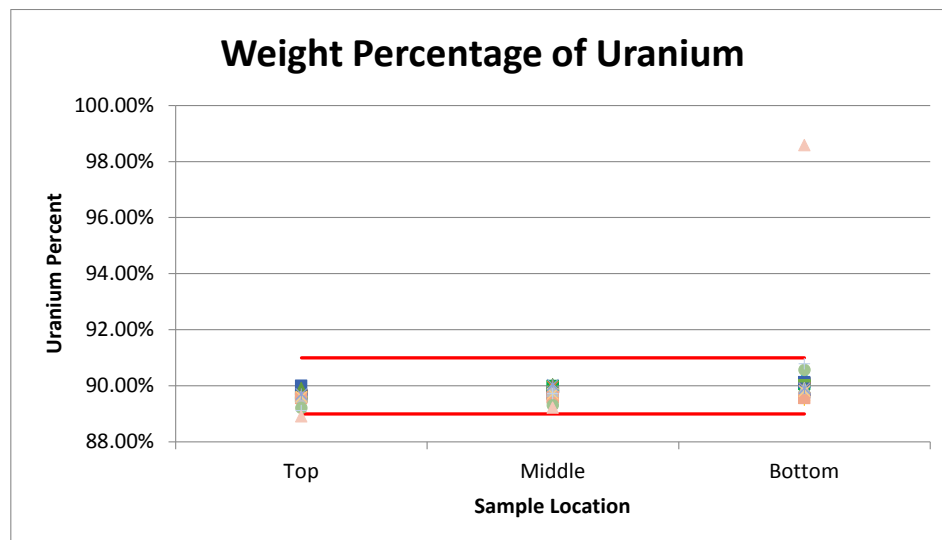


Figure 8: Uranium Weight Percentage Summary

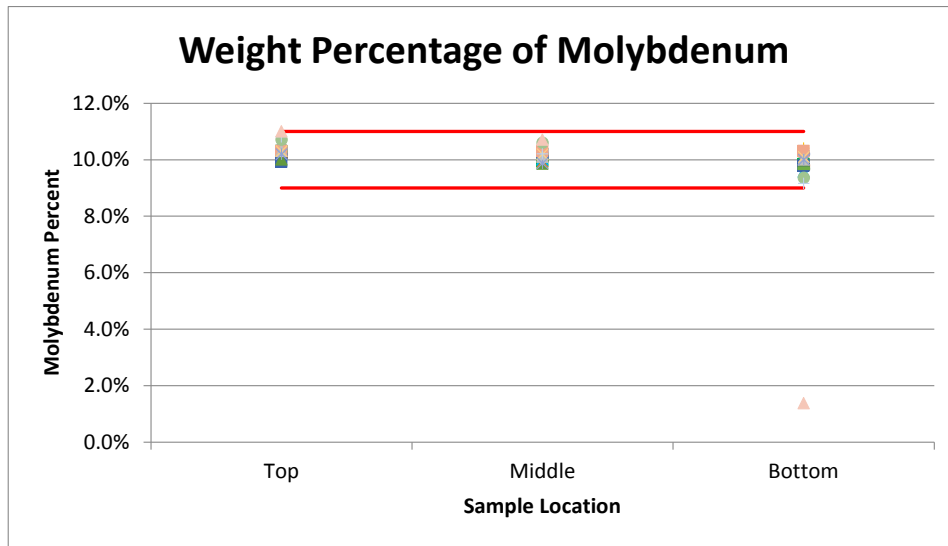


Figure 9: Molybdenum Weight Percentage Summary

The material fabricated in the trial campaign was planned at 10% molybdenum and 90% uranium. As expected, there were other minor constituents and impurities found in the product. However, as seen in the Figures above, the uranium and molybdenum were within specification in all but one sample location which indicates a casting anomaly. Further reviews are being performed on this casting data. However, the chemical analyses results from the second trial campaign further justify the feasibility of the single step casting process.

6. Summary

Y-12 NSC fabricated DU-Mo coupons and ingots using a pre-alloy diluent feedstock and a single step casting process. The trial campaigns also included a multi-plate mold. Based on the chemical analyses results, the single step casting process is a viable process. In the first trial campaign, the chemistry analysis was outside of the target 33% of the time. However, in the second trial, the chemistry analysis indicated only one sample was outside of the target, which is only 4% of the total sample population. Proficiencies were gained and the process was optimized between the first and second trials. The coupons and ingots will be processed at a commercial fuel fabrication vendor. The DU-Mo coupons and ingots will be used to prove-in the fuel fabrication equipment. Data from the fuel fabricator will provide valuable feedback to the front end casting process.



European Nuclear Society
Avenue des Arts 56
1000 Brussels, Belgium
Telephone: +32 2 505 30 50 - FAX: +32 2 502 39 02
rrfm2015@euronuclear.org
www.rrfm2015.org